



Technische Universität München

**Impact of non-conservative force modeling on
GNSS satellite orbits
and global solutions**

Dissertation

von

Carlos Javier Rodríguez Solano

Fachgebiet Satellitengeodäsie

Ingenieurfacultät Bau Geo Umwelt



Ingenieur fakultät Bau Geo Umwelt

Fachgebiet Satellitengeodäsie

**Impact of non-conservative force modeling on
GNSS satellite orbits
and global solutions**

Carlos Javier Rodríguez Solano

Vollständiger Abdruck der von der Ingenieur fakultät Bau Geo Umwelt der Technischen Universität München zur Erlangung des akademischen Grades eines

Doktor - Ingenieurs

genehmigten Dissertation.

Vorsitzender: Univ.-Prof. Dr.-Ing. U. Stilla

Prüfer der Dissertation: 1. Univ.-Prof. Dr. phil. nat. U. Hugentobler
2. Priv.-Doz. Dr. rer. nat. habil. O. Montenbruck
3. Univ.-Prof. Dr. phil. nat. A. Jäggi,
Universität Bern, Schweiz

Die Dissertation wurde am 13.01.2014 bei der Technischen Universität München eingereicht und durch die Ingenieur fakultät Bau Geo Umwelt am 27.06.2014 angenommen.

Abstract

The impact of different non-conservative force modeling approaches on the GNSS (Global Navigation Satellite System) satellite orbits and on the derived global solutions is evaluated in this dissertation. The correct modeling of these forces is a key factor in the precise orbit determination of GNSS satellites. Systematic errors found in the GPS satellite orbits and derived geodetic parameters indicate that radiation pressure orbit modeling deficiencies are still playing an important role. The errors in the orbits show a clear dependency with the Sun elevation above the orbital plane, while the errors in the geodetic parameters appear at harmonics of the GPS draconitic year, the repeat period of the GPS constellation w.r.t. the Sun.

In this dissertation, a new model for the solar radiation pressure impacting GPS and GLONASS satellites has been developed. It is based on a box-wing satellite model and on the physical interaction between solar radiation and satellite surfaces. Furthermore, it can be adjusted to fit the GNSS tracking data. The adjustable box-wing model is an intermediate approach between the physical/analytical models and the empirical models. The box-wing model fits the tracking data by adjusting mainly the optical properties of the satellite's surfaces. In addition, the so called Y -bias and a parameter related to a rotation lag angle of the solar panels around their rotation axis are estimated. This misalignment of the solar panels, not previously identified for GPS or GLONASS satellites, is a key factor for precise orbit determination.

During Sun-Earth eclipse seasons, GPS-IIA satellites perform noon, shadow and post-shadow yaw maneuvers. If the yaw maneuvers are not properly taken into account, the satellite orbits are degraded. In this dissertation the yaw maneuvers have been included in the computation of the solar radiation pressure. Two models are tested for the yaw maneuvers of GPS-IIA satellites, the existing attitude model with nominal yaw rates and an upgraded version based on the real yaw attitude estimated from PPP (Precise Point Positioning) phase residuals.

The new solar radiation pressure and attitude models are mainly compared against the CODE (5-parameter) empirical radiation pressure model, widely used within the International GNSS Service. The following is achieved in the satellite orbits and derived geodetic parameters. The adjustable box-wing model reduces the SLR (Satellite Laser Ranging) - GPS bias and improves the standard deviation outside eclipse seasons. Systematic errors observed in the radial component of the orbit predictions are mitigated. The orbit errors of GPS-IIA satellites during eclipse seasons are largely reduced, however the performance outside eclipse seasons is not yet reached. The draconitic errors in the orbit overlaps are significantly reduced for the GPS satellites, while for GLONASS satellites they are mainly reduced in the cross-track component. All the odd draconitic harmonics found in the geocenter Z -component when the CODE model is used almost disappear with the new radiation pressure models. The draconitic errors in the Earth orientation parameters are reduced for the the X -pole rate and especially for the Y -pole rate. All the draconitic harmonics (except the 2nd harmonic in the North component) found in the station coordinates are significantly reduced.

Zusammenfassung

In dieser Dissertation wird untersucht, wie sich der Einfluss verschiedener Modelle nichtkonservativer Kräfte auf die Bahnen von GNSS (Global Navigation Satellite System) Satelliten sowie auf abgeleitete Parameter globaler Lösungen äußert. Die korrekte Modellierung dieser Kräfte ist ein Schlüsselement zur präzisen Bestimmung der Bahnen von GNSS Satelliten. Systematische Fehler, welche in GPS Satellitenbahnen und abgeleiteten geodätischen Parametern gefunden werden, weisen darauf hin, dass Defizite in der Modellierung des Strahlungsdruckes der Satelliten nach wie vor eine wichtige Rolle spielen. Die Bahnfehler zeigen eine deutliche Abhängigkeit von der Elevation der Sonne über der Bahnebene, während sich die Fehler in den geodätischen Parametern bei harmonischen Frequenzen des sogenannten drakonitischen GPS-Jahres äußern, der Zeitspanne, innerhalb welcher sich die Orientierung der Sonne zur GPS Bahnkonstellation wiederholt.

In dieser Dissertation wird ein neues Modell entwickelt zur Beschreibung des Einflusses der Sonnenstrahlung, welche GPS und GLONASS Satelliten trifft. Dieses beruht auf einem sogenannten box-wing-Satellitenmodell sowie einer physikalischen Beschreibung der Interaktion der Strahlung mit den Oberflächen des Satelliten. Zusätzlich können Parameter dieses Modells an GNSS Beobachtungsdaten angepasst werden. Dieses anpassbare box-wing-Modell ordnet sich zwischen physikalisch-analytischen und empirischen Modellen ein. Das Modell passt sich an Messdaten an durch Schätzung optischer Eigenschaften der Satellitenoberflächen. Zusätzlich wird der sogenannte Y -Bias geschätzt sowie ein "Nachhinkwinkel" der Sonnenpanels zur Richtung zur Sonne. Ein solcher Fehlorientierungswinkel wurde bisher nicht beschrieben, ist aber ein Schlüsselement eines box-wing-Modells für die präzise Bahnbestimmung.

Während der Schattenperioden führen die GPS-IIA Satelliten sogenannte Mittags-, Mitternachts- sowie Sonneneintrittsmanöver aus. Werden diese Giermanöver nicht korrekt berücksichtigt, so wird die Qualität der abgeleiteten Bahnen vermindert. In dieser Dissertation werden diese Manöver in die Berechnung des Strahlungsdruckes einbezogen. Für die GPS-IIA Satelliten werden zwei Giermanöver getestet, nämlich ein existierendes Modell mit nominellen Gierraten sowie ein verbessertes Modell, welches tatsächliche Gierraten verwendet, die mittels präziser Punktpositionierung (PPP) anhand von Phasenbeobachtungen ermittelt wurden.

Die neuen Strahlungsdruck- und Orientierungsmodelle werden in erster Linie mit dem empirischen CODE 5-Parametermodell verglichen, welches innerhalb des International GNSS Services weit genutzt wird. Folgende Resultate werden für Satellitenbahnen und geodätische Parameter erzielt: Das anpassbare box-wing-Modell reduziert den bei SLR (Satellite Laser Ranging) Beobachtungen festgestellten Bias und verbessert die Standardabweichung der SLR Residuen außerhalb der Schattenperioden. Systematische Fehler in der radialen Komponente der Bahnprädiktion werden abgeschwächt. Die Bahnfehler von GPS-IIA Satelliten werden während der Schattenperioden deutlich reduziert, die Bahnqualität erreicht aber noch nicht jene außerhalb der Schattenperiode. Die Fehler mit drakonitischen Perioden in den Sprüngen aufeinanderfolgender Bahnbögen werden bei GPS signifikant reduziert, während sie bei GLONASS vorwiegend in der Komponente quer zur Bahn verbessert werden. Alle Fehler in der Z -Komponente der Geozentrumskoordinaten, welche

beim CODE Modell bei den ungraden Vielfachen der drakonitischen Frequenz gefunden werden, verschwinden für das neue Strahlungsdruckmodell. Die drakonitischen Fehler in den Erdorientierungsparametern werden für die X -Polrate und insbesondere für die Y -Polrate reduziert. Alle Fehler bei drakonitischen Frequenzen (außer der zweiten Harmonischen in der Nordkomponente) in den Stationskoordinaten werden signifikant reduziert.

Contents

Preface	11
1 Introduction	13
1.1 Motivation	13
1.2 State of the art	16
1.3 Scientific questions	26
1.4 Methodology	27
2 Content of publications	29
2.1 P-I: Earth radiation pressure	30
2.2 P-II: Solar radiation pressure	32
2.3 P-III: Non-nominal attitude	36
2.4 P-IV: Impact on global solutions	39
3 Conclusions and outlook	43
3.1 Conclusions	43
3.2 Open questions	46
3.3 Further model improvements	47
4 Appendix: additional results	49
4.1 SLR orbit validation	49
4.2 GLONASS box-wing model	55
5 Appendix: a priori box-wing models	59
5.1 Definitions	59
5.2 GPS-I	61
5.3 GPS-IIA	62
5.4 GPS-IIR	63
5.5 GPS-IIF	64
5.6 GLONASS	65
5.7 GLONASS-M	66
5.8 GLONASS-K	67
6 Bibliography	69
P-I Impact of Earth radiation pressure on GPS position estimates	75
P-II Adjustable box-wing model for solar radiation pressure impacting GPS satellites	85
P-III Improving the orbits of GPS block IIA satellites during eclipse seasons	103
P-IV Reducing the draconitic errors in GNSS geodetic products	125

Preface

This cumulative dissertation is based on the following four publications:

- P-I Rodriguez-Solano C.J., Hugentobler U., Steigenberger P., Lutz S.
Impact of Earth radiation pressure on GPS position estimates.
Journal of Geodesy 86(5):309–317, doi:10.1007/s00190-011-0517-4, 2012.
- P-II Rodriguez-Solano C.J., Hugentobler U., Steigenberger P.
Adjustable box-wing model for solar radiation pressure impacting GPS satellites.
Advances in Space Research 49(7):1113–1128, doi:10.1016/j.asr.2012.01.016, 2012.
- P-III Rodriguez-Solano C.J., Hugentobler U., Steigenberger P., Allende-Alba G.
Improving the orbits of GPS block IIA satellites during eclipse seasons.
Advances in Space Research 52(8):1511–1529, doi:10.1016/j.asr.2013.07.013, 2013.
- P-IV Rodriguez-Solano C.J., Hugentobler U., Steigenberger P., Bloßfeld M., Fritsche M.
Reducing the draconitic errors in GNSS geodetic products.
Journal of Geodesy, submitted, 2013.

The first three are peer-reviewed papers and are already published, the last one was submitted to the journal and is currently under revision. The accepted versions of the first three papers and the submitted version of the last paper are included in full-text at the end of this dissertation. These versions of the papers are the last ones sent to the respective journals. Just minor formatting changes were necessary to include the papers in this dissertation. The four publications are used throughout this dissertation for referencing and quoting purposes. Quotations from these papers (mainly used in Sections 1.1 and 1.2) are indicated with square parentheses, e.g. as [Section 1 of P-I], at the end of the respective paragraphs.

Before the publications a general introduction is given in Chapter 1 including the motivation to start this dissertation, the state of the art of non-conservative force modeling for GNSS satellites, the scientific questions raised and the basic methodology used to address them. In Chapter 2 a summary of the publications is given, including the most important results, the relationship between the publications and the Chapters of the dissertation as well as the individual contribution of the first author to the publications. In Chapter 3 the main conclusions are highlighted, together with remaining open questions and suggestions for further improvements of the non-conservative force models.

Additional relevant results that were not included in the above publications are given in the first Appendix (Chapter 4). In the second Appendix (Chapter 5), the a priori box-wing models for all GPS and GLONASS satellites are given as only the a priori models for GPS-II/IIA and GPS-IIR satellites were included in P-II. These two Appendices would fit best chronologically and thematically between P-II and P-III.

1 Introduction

1.1 Motivation

1.1.1 Errors in GNSS orbits

GNSS (Global Navigation Satellite System) satellites like GPS (Global Positioning System, USA) and GLONASS (Globalnaya Navigatsionnaya Sputnikovaya Sistema, Russia) satellites are at a distance from the Earth where the solar radiation pressure is the main non-gravitational orbit perturbation. The next non-conservative force in importance is the pressure exerted by the radiation reflected and emitted by the Earth, usually called albedo. The correct modeling of these forces is a key factor for the precise orbit determination of GNSS satellites.

The IGS (International GNSS Service, Dow et al, 2009) final orbits have reached an internal precision of around 2.5 cm for GPS and 5 cm for GLONASS satellites¹ from a level about an order of magnitude larger in the mid 1990s. The progress can be attributed to understanding the errors and improving the models affecting the GNSS technique, including those related to precise orbit modeling. Despite the performance attained, however, some problems remain in the orbits but as well as in the position estimates of GPS tracking stations [Section 1 of P-I].

The orbits of the two GPS satellites equipped with laser retro reflector arrays (LRA) show a consistent radial bias of up to several cm, when compared with the Satellite Laser Ranging (SLR) measurements, known as the GPS-SLR orbit anomaly. This bias was observed for the CODE (Center for Orbit Determination in Europe)² final orbits with a magnitude of 3-4 cm by Urschl et al (2007). More recent comparisons between GPS and SLR measurements (for various IGS analysis centers, Bar-Sever et al, 2009) show a smaller bias of 12-22 mm with associated scatters of 16-25 mm. These figures can be used as a measure of the current radial accuracy of IGS final orbits [Section 1 of P-I].

Urschl et al (2007) plotted the GPS-SLR residuals as a function of the position of the Sun with respect to the satellite, more specifically in a $(\beta_0, \Delta u)$ reference frame, where β_0 is the elevation angle of the Sun above the orbital plane and Δu is the argument of latitude of the satellite with respect to the argument of latitude of the Sun (see Fig. 1.1). The plot of Urschl et al (2007) shows a peculiar pattern indicating GPS orbit modeling deficiencies, and the radiation pressure caused by the Earth albedo (not considered at that time in the GPS orbit determination) was mentioned as one of the possible causes to be investigated [Section 1 of P-I].

The a priori solar radiation pressure model was also mentioned by Urschl et al (2007) as a possible cause of the peculiar pattern in the SLR residuals. The orbits showing this problem were generated

¹<http://igscb.jpl.nasa.gov/components/prods.html>, accessed on 25 August 2011.

²CODE is a consortium formed by: the Astronomical Institute of the University of Bern (AIUB, Bern, Switzerland), the Swiss Federal Office of Topography (swisstopo, Wabern, Switzerland), the Federal Agency for Cartography and Geodesy (BKG, Frankfurt am Main, Germany), and the Institut für Astronomische und Physikalische Geodäsie of the Technische Universität München (IAPG, Munich, Germany).

with the ROCK model (more specifically with the T20 model for GPS-II/IIA satellites, Fliegel et al, 1992) while the orbits generated with the a priori CODE radiation pressure model (Springer et al, 1999) did not show this problem. Both models are explained in Section 1.2.4.

The orbits of GPS satellites show a lower performance during Sun-Earth eclipse seasons than during periods outside these seasons. In particular, the orbits of GPS-IIA satellites are worse during eclipses, while GPS-IIR satellite orbits are almost unaffected. The cause of this problem is the yaw attitude of the satellites during eclipses. On the one hand, the yaw attitude of GPS-IIR is simple to model and to predict, being in most cases very close to the nominal yaw-steering attitude (Kouba, 2009). On the other hand, the yaw attitude of GPS-IIA strongly depends on the space vehicle maximum yaw rate. Moreover, the maximum yaw rate may not be constant and in principle it should be estimated for each maneuver as recommended by Bar-Sever (1996). The degradation of the GPS-IIA orbits during eclipse seasons has been observed in different metrics like: 1) errors in the fitting of 10-day arcs of truth orbits (Bar-Sever, 1997; Bar-Sever and Kuang, 2005), 2) prediction errors of GPS II and IIA satellites (Bar-Sever, 1997; Douša, 2010; Leandro et al, 2012; Choi et al, 2012), and 3) GPS minus SLR (satellite laser ranging) residuals to the SVN 35 and SVN 36, the two block IIA spacecraft carrying laser retro-reflector arrays (Urschl et al, 2007). Moreover, the estimated satellite clock corrections are degraded (Kouba, 2009) during yaw maneuvers. This introduces errors for clock prediction or for the combination of clock solutions originating from different IGS (International GNSS Service) analysis centers [Section 1 of P-III].

There are mainly two problems that cause mismodeling of the orbits if the nominal yaw attitude law of the satellites is used: 1) The position of the antenna w.r.t. center of mass of the satellite, more specifically w.r.t. its rotation axis, is wrong, leading to large errors in the observations, as shown by Dilssner et al (2011). 2) The orientation of the satellite w.r.t. the Sun is not well known and consequently the computation of solar radiation pressure will be erroneous if the satellite performs the maneuver in sunlight, which is the case for the post-shadow and the noon maneuvers. Additionally, when the satellite is in the shadow of the Earth a small error results from the infrared Earth radiation impacting the surfaces of the satellite [Section 1 of P-III].

The last examples show that orbit modeling deficiencies, in particular related to non-conservative forces, can still be found in the computed GPS orbits. The orbit mismodeling effects are not only noticeable in the orbits themselves but also in the geodetic parameters (next Section), highlighting the importance of further improvements in our understanding and modeling of the forces acting on GPS satellites, and GNSS satellites in general [Section 1 of P-II].

1.1.2 Errors in GNSS global solutions

Systematic errors at harmonics of the GPS draconitic year have been found in diverse GPS-derived geodetic products. The GPS draconitic year is the repeat period of the GPS constellation w.r.t. the Sun, which is about 351 days or 1.04 cpy (cycles per year). This period results from the secular retrograde motion of the right ascension of the ascending node due to the oblateness of the Earth (i.e. due to the J2 term). The GPS-derived geodetic products in which spurious signals have been found at 1.04 cpy and its harmonics are the following [Section 1 of P-IV]:

- Geocenter Z -component (Hugentobler et al, 2006; Meindl, 2011; Ostini, 2012).
- Station coordinates (Ray et al, 2008; Collilieux et al, 2007; Amiri-Simkooei, 2007; Tregoning and Watson, 2009; King and Watson, 2010; Santamaría-Gómez et al, 2011; Ostini, 2012).

- Y -pole rate (Seitz et al, 2012).
- Orbits (jumps between successive days, Griffiths and Ray, 2013).

For other GNSS constellations similar systematic errors could be expected at harmonics of the respective draconitic years, e.g., for GLONASS the draconitic year is about 353 days or 1.035 cpy. Meindl (2011) found odd harmonics of the GLONASS draconitic year in the time series of the Z -component of the GLONASS-only derived geocenter [Section 1 of P-IV].

Systematic errors in the GNSS data or models are expected to propagate over the whole GNSS solutions introducing these artificial effects on most products. Diverse error sources have been proposed to explain these systematic errors. Hugentobler et al (2006) and Meindl et al (2013) relate the geocenter motion with the orbit modeling parameters, in particular radiation pressure parameters, due to correlations between them. The first paper states that the patterns found in the geocenter Z -component with distinct periods of one GPS draconitic year should be caused by orbit modeling deficiencies and not by geophysical effects. Reischung et al (2013) found that the geocenter coordinates are highly collinear with the satellite clock and troposphere parameters, so that their estimation is very sensitive to GNSS modeling errors, like radiation pressure modeling errors. Ray et al (2008) give two possible coupling mechanisms which could generate the spurious signals at harmonics of 1.04 cpy found in the estimates of station coordinates: 1) Long-period GPS satellite orbit modeling errors, in particular due to the Sun-satellite interactions or during eclipse seasons which happen twice per draconitic year for each orbital plane. 2) Station specific errors that can be aliased due to the repeating geometry of the satellite constellation w.r.t. the tracking network to generate a period of one draconitic year, in particular long-wavelength (i.e. near-field) multipath or errors in the antenna or radome calibrations. King and Watson (2010) demonstrated by using simulated GPS data that multipath errors can produce spurious signals at harmonics of 1.04 cpy on station coordinates time series. Tregoning and Watson (2009) and King and Watson (2010) found that if phase ambiguities are not fixed there is a significant amplification in the expression of the spurious draconitic harmonics. Tregoning and Watson (2009) and Tregoning and Watson (2011) suggest that possible errors in the S1 and S2 tidal models (ocean, atmosphere) which are at diurnal and semidiurnal periods can contribute to the low-frequency draconitic signals seen in the GPS solutions. Griffiths and Ray (2013) introduced errors in the IERS (International Earth Rotation and Reference Systems Service) sub-daily EOP (Earth Orientation Parameters) tide model, which is used as a priori information in the GNSS solutions, and found that those errors can propagate to the GPS orbits at the 1st and 3rd harmonics of 1.04 cpy. Finally, Amiri-Simkooei (2013) focused on the nature of the draconitic errors found in GPS station coordinates and concluded that these errors do not likely depend on station related effects such as multipath but rather on other causes like orbit mismodeling or atmospheric loading effects [Section 1 of P-IV].

1.2 State of the art

1.2.1 Non-conservative forces

Non-conservative or non-gravitational forces play a key role in the precise orbit determination of GNSS satellites, which are at a distance from the Earth where the solar radiation pressure is the main non-conservative force acting on these satellites. As mentioned in Section 1 of P-II, errors in the precise determination of GPS satellite orbits are dominated by solar radiation pressure, and other forces acting on GPS satellites (e.g. gravitational forces) have nowadays a much lower contribution to the orbit error budget. Besides solar radiation pressure, other non-conservative forces like Earth radiation pressure or thermal forces have non-negligible effects on the GPS satellite orbits. In this dissertation Earth and solar radiation pressure have been addressed but not the thermal forces, here relevant work exists in different studies like the ones of Vigue et al (1994), Adhya et al (2005) and Duha et al (2006).

Non-conservative forces act on the surfaces of the satellite and not on its center of mass, therefore the modeling of these forces requires knowledge on:

- The radiation, e.g., from the Sun, reflected or emitted by the Earth, or generated internally by the satellite.
- The dimensions, surface optical properties and mass of the satellite.
- The orientation of the satellite in space, i.e., its attitude.

In Section 1.2.2 the relative geometry of Earth, satellite and Sun is explained together with the nominal attitude of GNSS satellites. Approximate dimensions, surface optical properties and masses of GPS and GLONASS satellites are given in the second Appendix (Chapter 5) of this dissertation. Section 1.2.3 summarizes the previous work done by the author related to the modeling of Earth radiation pressure and its impact on GPS orbits. Section 1.2.4 gives an overview on the current solar radiation pressure models available for GNSS satellites. Finally, Section 1.2.5 describes known deviations of GPS and GLONASS from nominal attitude and the existing approaches to model or to estimate these deviations.

1.2.2 Relative geometry of Earth, satellite and Sun

The relative geometry of Earth, satellite and Sun is depicted in Fig. 1.1, where:

β_0	Sun elevation angle above the orbital plane,
Δu	argument of latitude of the satellite w.r.t. argument of latitude of the Sun,
μ	orbit angle formed between satellite and orbit midnight ($\Delta u = \mu - 180^\circ$),
ϵ	angle formed between Earth, satellite and Sun,
Z	opposite to the radial direction, pointing towards the center of the Earth,
Y	parallel to the rotation axis of solar panels,
X	normal to the surface of the satellite which is always illuminated by the Sun,
D	normal to solar panels, pointing towards the Sun,
B	completes the DYB orthogonal frame, with $B = Y \times D$,
S	along-track direction,
Ψ	yaw angle, formed between the satellite X direction and the along-track S direction.

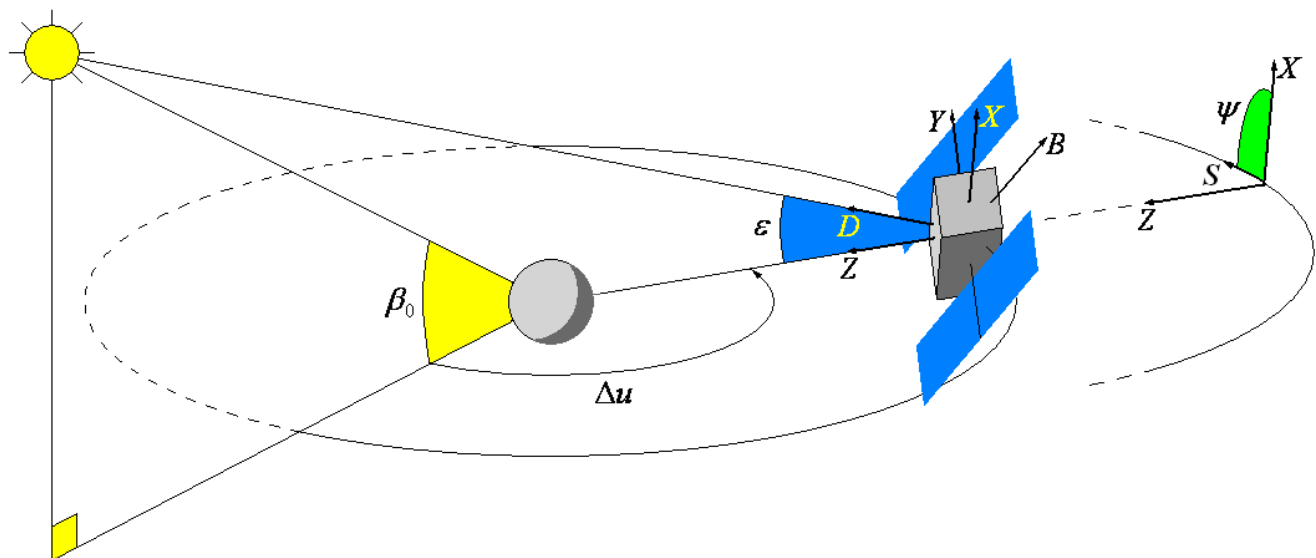


Fig. 1.1: Relative geometry of Earth, satellite and Sun. Nominal yaw-steering attitude as a function of the position of the Sun in the orbital plane. Illustration of DYB (Sun-fixed) and XYZ (body-fixed) orthogonal frames.

The nominal attitude of the GPS and GLONASS satellites is given by accomplishing two conditions at the same time: 1) the antennas should be pointing to the center of the Earth to transmit the navigation signals and 2) the solar panels should be pointing perpendicular to the Sun to keep a maximum power supply. This is done by performing a rotation around the Z axis, such that the solar panels can rotate around the satellite bus to a perpendicular position w.r.t. the Sun. This kind of attitude control is called “yaw-steering”. The angle ϵ together with the XYZ directions contain the full information of the nominal attitude of the satellite and it can be written as:

$$\cos \epsilon = \cos \beta_0 \cos \mu, \quad (1.1)$$

furthermore, the nominal yaw angle is given as:

$$\Psi = \text{ATAN2}(-\tan \beta_0, \sin \mu). \quad (1.2)$$

The last two equations are according to Bar-Sever (1996).

1.2.3 Earth radiation pressure

Relevant work on Earth radiation pressure modeling and its impact on GPS orbits was done by the author previous to the start of this dissertation. This Section summarizes the main results from the two publications listed below, which partially served as starting point and motivation for P-I and P-II.

Rodriguez-Solano C.J.

Impact of albedo modelling on GPS orbits.

Master thesis, Technische Universität München,

<https://mediatum2.ub.tum.de/doc/1083571/1083571.pdf>, 2009.

Rodriguez-Solano C.J., Hugentobler U., Steigenberger P.

Impact of Albedo Radiation on GPS Satellites.

In: Kenyon S., Pacino M.C., Marti U. (Eds) Geodesy for Planet Earth,

IAG Symposia 136, pp. 113–119, doi:10.1007/978-3-642-20338-1_14, 2012.

In these publications, Earth radiation and GPS satellite models of increasing complexity were developed and tested. From those studies the key factors of the models have been identified. For the Earth radiation it was found that the use of an analytical model (based on constant albedo) or one based on numerical integration of Earth's actual reflectivity and emissivity data, give similar results for the irradiance acting on the GPS satellites (difference of up to 10 %), mainly due to the high altitude of these space vehicles. As data from the CERES (Clouds and Earth's Radiant Energy System, Wielicki et al, 1996) satellite mission are available since the beginning of 2000³, the numerical approach was chosen. Concerning the satellite model, use of a box-wing model is a key factor since the variation of the solar panels with respect to the Earth is very important, whereas a simple cannon-ball model is highly inaccurate. The accuracy of the modeled optical properties and the detailed structure of the satellite have a lower impact on the acceleration than the use of a box-wing model, but they are still important enough to be considered [Section 2 of P-I].

The mathematical formulation of the Earth radiation model is the same as the one proposed by Knocke et al (1988) for computing the irradiance received by the satellite due to the Earth's reflected (visible) and emitted (infrared) radiation. It is assumed that the Earth reflects and emits radiation in a purely diffuse way as a Lambertian sphere. The main steps included in the model are: 1) Determine the solar irradiance received by each surface element of the Earth (grid of $2.5^\circ \times 2.5^\circ$). 2) Compute the irradiance received by the satellite based on the reflectivity and emissivity coefficients (from NASA's CERES project, also used by Ziebart et al (2004) but not yet by Knocke et al (1988)) for each Earth's surface element. 3) Compute the Earth radiation pressure caused by the interaction between the irradiance from each surface element of the Earth with the satellite model [Section 2 of P-I].

The physical description of the interaction between radiation and the surfaces of the satellite is provided by Fliegel et al (1992). It is based on the optical properties of the surface, e.g., specularity and reflectivity or equivalently the fraction of reflected, absorbed and diffused photons which should sum up to one (Milani et al, 1987). The dimensions and optical properties are given for block I and block II/IIA GPS satellites in the mentioned paper and for block IIR satellites in Fliegel and Gallini (1996). These two papers are the basis for constructing our box-wing satellite model. They also provide a priori models (ROCK) for solar radiation pressure for precise geodetic applications. However, nowadays no a priori model or purely empirical models are used due to the lower performance of the ROCK models compared to the empirical models. The CODE empirical model for solar radiation pressure (Beutler et al, 1994) was used with no a priori model [Section 2 of P-I].

The Earth radiation and satellite models (assuming nominal attitude) have a main dependency on the elongation angle ψ formed by satellite, Earth and Sun ($\psi = 180^\circ - \epsilon$, see Fig. 1.1), which can

³http://eosweb.larc.nasa.gov/PRODOCS/ceres/level13_es4_table.html, accessed on 29 March 2011.

be simply written as $\cos(\psi) = \cos(\beta_0) \cos(\Delta u)$. The explicit dependency of the Earth radiation and satellite models with the angle ψ is given in Chapters 2 and 3 of the Master thesis. The acceleration acting on GPS satellites has a main radial component which varies from 4×10^{-10} to $20 \times 10^{-10} \text{ m/s}^2$. In the along- and cross-track directions the acceleration is much smaller and varies within $\pm 1 \times 10^{-10} \text{ m/s}^2$. The acceleration as function of β_0 and Δu is shown in Fig. 2 of P-I.

The thrust of the navigation antennas, as reported by Ziebart et al (2004), was also included in the satellite model. An approximate value of 80 Watts of antenna transmission power was used for all GPS satellites (block II/IIA and block IIR)⁴. In previous studies (Ziebart et al, 2004, and the two publications mentioned above), the thrust of the navigation antennas was found to cause a non-negligible effect for GPS satellite orbits. It introduces a constant radial acceleration of around $2.7 \times 10^{-10} \text{ m/s}^2$ for block IIA satellites [Section 2 of P-I].

The most prominent effect of Earth radiation pressure on the GPS orbits is a radial reduction of 1-2 cm. As already mentioned by Ziebart et al (2007) this effect reduces the SLR-GPS range discrepancy by 1-2 cm, from which around 0.5 cm can be attributed to the antenna thrust. The reduction of the SLR-GPS bias obtained in the publications mentioned above was of about 16 mm, i.e., from -23.6 to -6.8 mm for SVN 35 and from -26.1 to -10.1 mm for SVN 36 during the year 2007. These two GPS-IIA satellites are the only ones of the GPS constellation equipped with laser retro reflector arrays. The reason for the radial reduction of orbits is that GPS measurements, being essentially angular measurements due to required clock synchronization, mainly determine the mean motion of the satellite. As a matter of fact, a constant positive radial acceleration (equivalent to a reduction of GM, the product of the gravitational constant and the mass of the Earth) decreases the orbital radius according to Kepler's third law.

The SLR-GPS bias is reduced when introducing Earth radiation pressure and antenna thrust, however, these effects do not reduce (also do not increase) the standard deviation of the SLR residuals. In the two publications mentioned above, tests were also performed with the ROCK model (more specifically with the T20 model for GPS-II/IIA satellites, Fliegel et al, 1992) as a priori solar radiation pressure model. Contrary to expectations, as the T20 model is a physics based model, the use of this model increases the SLR-GPS bias but also the standard deviation from 27.4 to 30.2 mm for SVN 35 and from 32.3 to 35.7 mm for SVN 36. This was an indication that the modeling of solar radiation pressure was still playing an important role in the errors of GPS satellite orbits.

1.2.4 Solar radiation pressure

To compensate the perturbing acceleration due to solar radiation acting on the GPS satellites, two types of models have been employed. 1) Empirical models which fit best the GPS global tracking data and which have led to a precision of 2.5 cm in the IGS final orbits. The main disadvantage of such models resides in the loss of physical understanding of the forces acting on the satellites, which can then result in non physical orbits and potentially introduce undesired systematic errors. 2) Analytical models based on the detailed structure of the satellites and surface properties measured on ground prior to launch. The principal problem of these models is that they cannot compensate accurately enough for the real on-orbit behavior of the satellites,

⁴GPS block specific antenna thrust values have been recently calculated by the IGS analysis center coordinator at NOAA/NGS (available at: <http://acc.igs.org/orbits/thrust-power.txt>). However, these values have not been tested during this dissertation.

e.g., due the change (aging) or uncertainty of the a priori optical properties of the satellite surfaces or deviations from nominal attitude. An interesting discussion of pros and cons between the two types of models is also given by Bar-Sever and Kuang (2004) [Section 1 of P-II].

Sections 2 and 3 of P-II give an extensive review of current empirical and analytical solar radiation pressure (SRP) models for GPS satellites. The following state of the art is solely based on those Sections, with few updates for GLONASS satellites.

Empirical SRP models

One of the first attempts to compensate for non-modeled forces affecting the GPS orbits was done by Colombo (1989) where one finds that:

“Analytical orbit perturbation theory suggests that the errors in the ephemerides of the Global Positioning System (GPS) satellites should be mostly resonant effects that can be corrected by adjusting a few parameters in a simple empirical acceleration formula, despite of the complexity of their causes (mismodeling of gravity, radiation pressure, etc.) at least for arcs free from orbits maneuvers.”

The resonant frequencies of the GPS orbits found by Colombo (1989) are zero and once per revolution. Furthermore, Hill’s equations were used to analytically formulate the orbit perturbations in radial, along- and cross-track directions, denoted by RSW . The nine proposed empirical parameters responsible for absorbing the orbit acceleration errors can be written as:

$$\begin{aligned} R(u) &= R_0 + R_C \cos u + R_S \sin u, \\ S(u) &= S_0 + S_C \cos u + S_S \sin u, \\ W(u) &= W_0 + W_C \cos u + W_S \sin u, \end{aligned} \tag{1.3}$$

where u is the argument of latitude of the satellite. As mentioned by Springer et al (1999) the Colombo model considers the gravity field of the Earth as the major error source in the GPS orbits. Therefore there is not an explicit dependency of the model on the Sun position w.r.t. the satellite.

In Beutler et al (1994) the extended orbit modeling techniques used by the Center for Orbit Determination in Europe (CODE) are described. To compensate the direct solar radiation pressure impacting the satellites, up to nine empirical parameters are estimated in a Sun-Earth oriented frame with directions denoted by DYB (Fig. 1.1). A description of this model is also found in Springer et al (1999) and the estimated parameters are:

$$\begin{aligned} D(u) &= D_0 + D_C \cos u + D_S \sin u, \\ Y(u) &= Y_0 + Y_C \cos u + Y_S \sin u, \\ B(u) &= B_0 + B_C \cos u + B_S \sin u. \end{aligned} \tag{1.4}$$

The D direction gives the orientation of the normal to the solar panels in inertial space, the Y direction points along the solar panel beams and the B direction finally completes the right handed system. However, the B direction does not correspond to the orientation of the satellite bus and varies along the $+Z$, $+X$ and $-Z$ surfaces of the bus as shown in Fig. 1.1. Furthermore the argument of latitude u is not directly related to the attitude of the satellite. Additionally, in the direct radiation pressure model of Beutler et al (1994) the acceleration provided by the SRP

models (sometimes called ROCK models, see next Section) developed by Fliegel et al (1992) and Fliegel and Gallini (1996) can be included as a priori information.

In order to get an adequate a priori model of the real on-orbit solar radiation pressure impacting the satellites, Springer et al (1999) developed a new model:

“The performance of the new model is almost one order of magnitude better than that of the existing ROCK models. It also allows a reduction of the number of orbit parameters that have to be estimated.”

This model was constructed by adjusting several years of CODE final orbits and can be written as:

$$\begin{aligned}
 D &= D_0, \\
 Y &= Y_0, \\
 B &= B_0, \\
 Z(\Delta u) &= Z_1 \sin \Delta u, \\
 X(\Delta u) &= X_1 \sin \Delta u + X_3 \sin 3\Delta u.
 \end{aligned} \tag{1.5}$$

The model has six main parameters, each of them consisting of other parameters with a periodic dependency on β_0 , the elevation angle of the Sun above the orbital plane, in total the model has 18 different parameters. Two additional directions Z and X appear in the model, which correspond to the faces of the satellite illuminated by the Sun. The time argument of the periodic signals is related to Δu , the argument of latitude of the satellite w.r.t. the argument of latitude of the Sun in the orbital plane as shown in Fig. 1.1.

Nowadays CODE uses an updated version⁵ of this last model as a priori information for the generation of its final orbits, additionally this IGS analysis center⁶ estimates five empirical parameters from the model of Beutler et al (1994), more specifically the D_0 , Y_0 , B_0 , B_C and B_S parameters, to obtain a very good fit of the GPS orbits to the tracking data. Moreover, in order to compensate for inaccuracies in the model (a priori plus estimated) of the force field, pseudo-stochastic orbit parameters (instantaneous velocity changes) are estimated every 12 hours in the radial, along- and cross-track directions (Beutler et al, 2006). The approach described in this paragraph has also been applied by CODE for GLONASS satellites but without the use of an a priori solar radiation pressure model.

With an approach similar to the one used by Springer et al (1999) but using a different parametrization, Bar-Sever and Kuang (2004) fitted several years of JPL (Jet Propulsion Laboratory) final orbits to construct an improved GPS Solar Pressure Model (GSPM). The performance of the GSPM model as a priori acceleration plus estimated stochastic parameters was evaluated, against variants of the *DYB* model (without a priori acceleration) of Beutler et al (1994), by Sibthorpe et al (2011). The stochastic parameters used by JPL are: a constant Y -axis bias and a constant scale along the satellite to Sun direction, as well as time varying (stochastic) variations in model scale along the body-fixed spacecraft Z - and X -axes, and small stochastic changes along the Y -axis. This methodology can be regarded as “reduced-dynamic” approach. The evaluation between models (a priori models plus estimated parameters) was done by means of various internal (GIPSY-OASIS Software) and external metrics. Within the metrics favoring the use of the GSPM plus reduced-dynamics approach are: ambiguity resolution statistics, orbit overlaps, SLR

⁵ftp://ftp.unibe.ch/aiub/REPRO_2008/GEN/SATELLIT.I05, accessed on 18 May 2011.

⁶<ftp://igsceb.jpl.nasa.gov/pub/center/analysis/code.acn>, accessed on 15 December 2011.

tracking residuals, station repeatabilities, and GRACE K-band ranging statistics. However, clock overlaps between consecutive days and LOD (Length of Day) differences to IERS (International Earth Rotation and Reference Systems Service) Bulletin A seem to favor the *DYB* approach.

The GSPM model is basically a truncated harmonic expansion in the *XYZ* body-fixed frame:

$$\begin{aligned} X(\epsilon) &= X_1 \sin \epsilon + X_2 \sin 2\epsilon + X_3 \sin 3\epsilon + X_5 \sin 5\epsilon + X_7 \sin 7\epsilon, \\ Y(\epsilon) &= Y_1 \cos \epsilon + Y_2 \cos 2\epsilon, \\ Z(\epsilon) &= Z_1 \cos \epsilon + Z_3 \cos 3\epsilon + X_5 \cos 5\epsilon. \end{aligned} \tag{1.6}$$

The model has 10 parameters and some of them (X_2 and Y_1) also depend on the β_0 angle. It is very interesting to note the selection of the angle ϵ formed by Earth, satellite, and Sun (Fig. 1.1) as the main dependency of the model. The angle ϵ together with the *XYZ* directions contain the full information of the nominal attitude of the satellite, see Section 1.2.2.

Analytical SRP models

Using an analytical approach, a priori solar radiation pressure models have been developed by considering the details of the satellite structure (e.g. small elements and shadowing or re-reflection effects between them), the known optical properties, the physical interaction of radiation with the satellite surfaces (including re-radiated heat effects), and nominal attitude. These models are based on information available on ground provided by the satellite manufactures.

The first available a priori analytical models for the block I and block II/IIA GPS satellites were the ROCK4 and ROCK42 models, developed by the spacecraft manufacturer, Rockwell International, and IBM. These models were improved by Fliegel et al (1992), approximated by a simple Fourier series in the angle ϵ (Eq. (1.1)), and named T10 and T20 respectively. Fliegel and Gallini (1996) used the same approach to develop the T30 model for the block IIR satellite based on a detailed spacecraft model by Martin Marietta, the spacecraft manufacturer. These models are based on the physical characteristics of the GPS satellites, like the optical properties, the dimensions and the interaction between radiation and satellite surfaces, as described in the two mentioned articles. However, these models have gradually lost favor in the IGS analysis centers, which no longer use them as a priori information. A summary of the different strategies to model solar radiation pressure within the IGS can be found in Froideval (2009). In particular Urschl et al (2007) found that these models (at least for block IIA satellites) introduce systematic errors in the SLR-GPS residuals.

In a later work, Marquis and Krier (2000) developed an improved radiation pressure model for the GPS block IIR satellites. A very useful result from this study is the comparison of the different forces acting on the satellite, such that the following force contributions could be identified:

- Solar radiation onto the vehicle surfaces.
- Radiation of thermal blankets.
- Thermal radiation from SV radiators. Includes the effect of radiation onto the solar arrays.
- Solar array thermal radiation.
- Thermal radiation of excess solar array power (shunt).
- Radiation pressure on the nadir surfaces from sunlight reflected off the Earth (albedo).
- Earth Infrared pressure on the nadir surfaces (EIR).

As pointed out by Marquis and Krier (2000):

“The spectral or visible contribution from the Sun is the greatest contributor with nearly 100 percent of the total force.”

“Depending on the orbit position, albedo is the next highest contribution peaking 2.5 percent of the total force. The solar array and shunt thermal radiation forces are the next lowest, representing just under 1 percent of the total each, but provide a nearly constant value about the orbit. Although the magnitudes are similar, these forces are applied in opposite directions and nearly cancel each other out.”

Additionally it is mentioned that the thermal part is small but important for the Y direction of the satellite and EIR is the lowest force acting on the satellite. The resulting model is available as a look up table⁷ but not the dimensions or optical properties used for its construction. However, the dimensions and optical properties for the block I, block II/IIA and block IIR are available from the T10, T20 and T30 models.

More recently Ziebart et al (2005) have developed precise models for dealing with the non-conservative forces acting on different types of low and high orbiting satellites. These models take into account further effects as compared to the T20 and T30 models, e.g., shadowing or re-reflection between surfaces. In the case of GPS satellites, a model was constructed for block IIR considering similar forces as Marquis and Krier (2000). This approach was initially applied to GLONASS satellites by Ziebart (2001); Ziebart and Dare (2001).

The previously mentioned analytical satellite models are very important as a priori information but have the main problem that they cannot easily take into account the deviations of the models from reality. The deviations can be caused by aging of satellite surfaces, inaccurately known optical properties or not nominal attitude. An interesting example is the Y -bias acceleration reported for GPS satellites. For block II/IIA, Fliegel et al (1992) explain the Y -bias by a possible misalignment angle (0.5° to 1°) of the solar panels w.r.t. their nominal position. While for block IIR, Marquis and Krier (2000) explain the Y -bias by internal heat radiated by the Y surfaces.

1.2.5 Non-nominal attitude

Deviations from nominal attitude by the satellites will affect directly the computation of non-conservative forces (as these are surface forces, see Section 1.2.1) producing non-modeled accelerations. Among the known deviations from nominal attitude of GPS and GLONASS satellites are the yaw maneuvers during eclipse seasons and the misalignments of the solar panels, described in the following text. Finally, the solar radiation pressure models which have incorporated these deviations from nominal attitude will be also described in the following.

Yaw attitude

During Sun-Earth eclipse seasons GPS and GLONASS satellites perform yaw maneuvers at orbit noon and orbit midnight, the first one happens in sunlight while the second one occurs in the shadow of the Earth. The reasons for these maneuvers are: 1) the maximum hardware yaw rate of the spacecrafts is exceeded for small β_0 angles such that the satellite can only try to follow the nominal yaw attitude by rotating at this maximum yaw rate, or 2) the Sun sensors are occulted

⁷ftp://sideshow.jpl.nasa.gov/pub/GPS_yaw_attitude/BlockIIR_srp_table, accessed on 20 May 2011.

resulting in a loss of orientation of the satellite (e.g. GPS-II/IIA), alternatively if the satellite can compute on-board the position of the Sun a controlled yaw maneuver can be performed (e.g. GPS-IIR and GLONASS-M). The nominal yaw attitude of GNSS satellites is described in Section 1.2.2 with the nominal yaw angle given by Eq. (1.2). In the following, details are given about the yaw maneuvers performed by GPS-II/IIA, GPS-IIR and GLONASS-M satellites, precisely described by the models of Bar-Sever (1996), Kouba (2009) and Dilssner et al (2011) respectively. GPS-IIF satellites also perform yaw maneuvers as first noted by Dilssner (2010), however this satellite type was not tested during this dissertation.

GPS-II/IIA satellites have a maximum yaw rate of about $0.1^\circ/\text{s}$ (however varying between different spacecrafts, see Section 3 of P-III) which implies that noon maneuvers occur for $|\beta_0| < 4.8^\circ$. During Sun-Earth eclipses, i.e. for $|\beta_0| < 13.9^\circ$, the satellites start to rotate with maximum yaw rate when they enter into the shadow of the Earth with the direction given by the sign of the yaw bias. In these satellites a yaw bias was implemented (starting November 1995 the bias is set to $+0.5^\circ$ on all satellites, Bar-Sever, 1996) in order to make the rotational direction of the shadow maneuvers predictable. After shadow exit the satellites have to perform a post-shadow maneuver in order to recover nominal yaw attitude. As mentioned in Section 1 of P-III, this maneuver is very challenging to model, since the yaw rotational direction depends entirely on the yaw angle at shadow exit and consequently on the yaw rate during the shadow maneuver. The complexity of this maneuver can be avoided for the problem of erroneous position of the antenna w.r.t. the rotation axis of the satellite (Section 1.1.1) by excluding the observation data for 30 minutes after shadow exit (Bar-Sever, 1996; Kouba, 2009). However, for the solar radiation pressure computation, one cannot simply erase the orbit during 30 minutes, and the post-shadow maneuver occurs during full sunlight. In principle, the orbit integration could be restarted after shadow exit, but this would imply 12 hour arcs (for the best cases) instead of 24 hours arcs. This arc splitting alone would imply an important orbit degradation. Finally, as the maximum yaw rate of these satellites varies between different spacecrafts and the maneuvers depend strongly on it, Bar-Sever (1996) recommends to estimate the yaw rate for each maneuver.

GPS-IIR satellites have a maximum yaw rate of about $0.2^\circ/\text{s}$ which implies that noon maneuvers occur for $|\beta_0| < 2.4^\circ$. During Sun-Earth eclipses, i.e. for $|\beta_0| < 13.9^\circ$, the satellites continue to follow nominal yaw attitude until the maximum yaw rate is exceeded such that the shadow maneuver is in fact like a noon maneuver.

GLONASS-M satellites have a maximum yaw rate of about $0.25^\circ/\text{s}$ which implies that noon maneuvers occur for $|\beta_0| < 2.0^\circ$. During Sun-Earth eclipses, i.e. for $|\beta_0| < 14.5^\circ$, the satellites start to rotate with maximum yaw rate when entering into the shadow of the Earth until they reach the nominal yaw angle at shadow exit where rotation stops, such that after shadow exit no post-shadow maneuver is required.

Solar panels attitude

Fliegel et al (1992) explain the causes of the so called *Y*-bias, see also Section 1.2.4, mentioning that alignment requirements of the solar panels of 0.5° to 1° are reported in the Rockwell specifications. More importantly Kuang et al (1996) computed the misalignment angles of the solar panels w.r.t. nominal attitude using a simple SRP model, obtaining also small deviations of 1° to 2° from nominal attitude [Section 4 of P-II]. In general, changes of the nominal attitude of the solar panels will affect the solar and terrestrial radiation pressure computation, producing large

non-modeled accelerations. The solar panels are large structures and the major contributors to the large area-to-mass ratios of the satellites.

Seen in the body-fixed reference frame (Fig. 1.1) the solar panels have only one degree of freedom around the solar panels rotation axis or the $\pm Y$ axis. The motion of the solar panels can be described by the solar panels pitch angle ϵ_{SP} which is measured in the plane formed by the Z and X axes, it grows from $+Z$ to $+X$ and it is defined negative for $-X$ [Section 4 of P-III]. The angle ϵ_{SP} is formed between $+Z$ and the normal to the solar panels. Under nominal attitude conditions (Section 1.2.2) the solar panels pitch angle is equal to the ϵ angle given in Eq. (1.1). Deviations from nominal attitude of the pitch angle will produce non-modeled accelerations in the B direction due to the solar radiation pressure. Indeed, Springer et al (1999) mentions that the periodic terms in the B direction of the CODE model (Eq. (1.4)) most significantly reduce orbit model deficiencies.

During a yaw maneuver it is reasonable to assume that the solar panels are pointed as perpendicular as possible to the Sun (for keeping a maximum power supply). However, according to Bar-Sever (1995) and to personal communication, the solar panels of the block II and IIA satellites do not rotate during a shadow event, being fixed to the ϵ_{SP} angle at shadow entry, i.e., at $\epsilon_{SP} = 13.87^\circ$. This implies that at shadow exit the solar panels have to perform a post-shadow recovery to the best possible pitch angle, in a similar way as the post-shadow yaw maneuver is performed [Section 4 of P-III].

SRP models for non-nominal attitude

The only existing studies, to our knowledge, which developed and tested a solar radiation pressure model for eclipsing GPS II and IIA satellites incorporating the noon and post-shadow yaw maneuvers information are Bar-Sever (1997) and Bar-Sever and Kuang (2005). The first study describes in detail the GSPM.II.97 “split” model used for GPS II and IIA satellites. The second study is an evaluation of the GSPM.II.97 “split” model with more recent data for GPS II and IIA satellites, while for GPS-IIR satellites the GSPM.04a model (created from flight data of non-eclipsing satellites, Bar-Sever and Kuang, 2004) was simply extended into the eclipsing regime. GSPM stands for “GPS Solar Pressure Model” and it is an empirical model based on flight data. By fitting several years of JPL (Jet Propulsion Laboratory) final orbits, the coefficients of a Fourier expansion (as function of the ϵ angle, see Fig. 1.1) could be estimated. This is the basic approach for non-eclipsing satellites. For eclipsing GPS II and IIA satellites, the GSPM.II.97 “split” model was developed, which consist of the T20 model (Fliegel et al, 1992) splitted into two radiation force contributions: the solar array and the main body of the spacecraft. During yaw maneuvers, the main-body-induced radiation force is rotated from its nominal direction around the Z axis by the amount of yaw error. The solar array induced radiation pressure is computed by assuming the optical properties and the orientation of the solar array. The normal vector to the solar array is explicitly modeled following the same principles of the post-shadow yaw maneuver (Bar-Sever, 1996) assuming a pitch rate of $0.25^\circ/\text{s}$. However, no further details are given on the solar array motion model. Overall, with the GSPM.II.97 “split” model, Bar-Sever (1997) and Bar-Sever and Kuang (2005) achieve an improvement of the orbits, but not reaching the same performance as for non-eclipsing satellite orbits [Section 1 of P-III].

1.3 Scientific questions

The errors found in GNSS satellite orbits and global solutions (Section 1.1) as well as the current development of non-conservative force models (Section. 1.2) led to the following general scientific question (answered in Chapter 3):

Q-1 Can new non-conservative force models improve the errors observe in the GNSS satellite orbits and global solutions? In particular when considering new models for Earth radiation pressure, solar radiation pressure and deviations from nominal attitude?

This question can be divided in more specific questions (all answered in Chapter 2):

Q-2 Can Earth radiation pressure reduce the observed draconitic errors in geodetic products?

Q-3 Can new models for solar radiation pressure and deviations from nominal attitude reduce the observed draconitic errors in geodetic products?

Q-4 Why the use of no a priori solar radiation pressure model shows a higher performance in the SLR-GPS residuals than the use of the T20 model (physics based) as a priori?

Q-5 Can the CODE empirical model introduce systematic errors in the GPS satellite orbits?

Q-6 What are the acceleration differences between current solar radiation pressure models?

Q-7 Is it possible to create a new solar radiation pressure model for GPS satellites that combines the advantages from the purely empirical and analytical/physical models?

Q-8 Are the GPS orbits improved with a new solar radiation pressure model?

Q-9 Are there significant deviations from nominal attitude of the solar panels? How these deviations affect the solar radiation pressure computation and the GPS satellite orbits?

Q-10 Is it possible to further reduce the SLR-GPS residuals bias and standard deviation with a new solar radiation pressure model?

Q-11 Can this new modeling approach also be applied to other GNSS satellites, for example GLONASS satellites?

Q-12 How the known yaw maneuvers of GNSS satellites performed during eclipse seasons affect the solar radiation pressure computation?

Q-13 Is it possible to model unambiguously the post-shadow maneuver of GPS-IIA satellites which occurs in full sunlight?

Q-14 What is the attitude of the solar panels of GPS-IIA satellites during yaw maneuvers?

Q-15 Are the observed errors in the GPS-IIA orbits during eclipse seasons reduced by taking into account the yaw maneuvers in the solar radiation pressure computation?

1.4 Methodology

The basic methodology used for this dissertation to answer the scientific questions given in Section 1.3 is the following:

Step 1: development of models

Development of new modeling approaches where deficiencies were identified in the orbits and global solutions (Section 1.1) related to the existing models for non-conservative forces (Section 1.2). During this dissertation the modeling of solar radiation pressure, the most important non-conservative force acting on GNSS satellites, was of central interest. The correct modeling of solar radiation pressure (and non-conservative forces in general) depend strongly on knowing the orientation of the spacecraft surfaces in space. Therefore the study of possible deviations from nominal attitude, and its impact on the solar radiation pressure computation, was also of central interest. The modeling of Earth radiation pressure was addressed during the Master thesis of the author, see Section 1.2.3, and was the starting point of this dissertation. The development of the models was first done in “paper” by studying the physical and mathematical formulations of the models. The models were then implemented in MATLAB, where the optimization of the algorithms and extensive functionality tests were performed.

Step 2: implementation of models

Implementation of the new models for non-conservative forces in a development version of the Bernese GNSS Software (Dach et al, 2007). The implementation was done in FORTRAN 77/90, as the Bernese GNSS Software is written in this programming language. After implementation, extensive tests followed to warrant the proper functionality of the models. At this stage the models were mainly tested in the ORBGEN program of the Bernese GNSS Software, where precise (SP3) orbits can be used as pseudo observations and different orbit models can be employed to adjust them. The resulting orbits can be compared to the initial orbits to test the impact of the new models. Besides studying the impact on the orbits also the impact of the new models on the estimated orbit parameters (e.g. from the CODE radiation pressure model, Section 1.2.4) could be studied at this stage.

Step 3: reprocessing of GNSS data

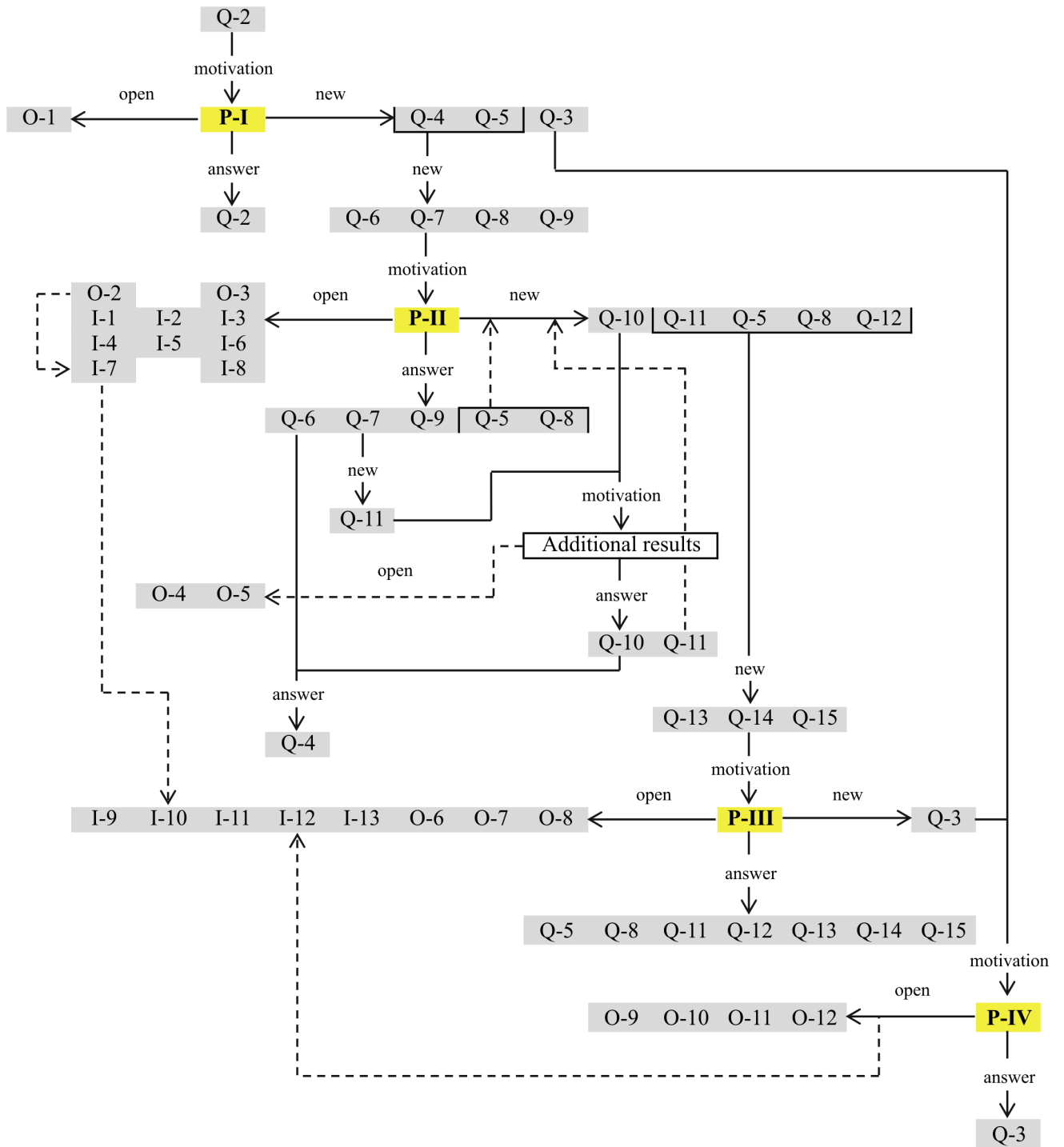
Reprocessing of few to several years of GNSS tracking data from a global network of ground stations. Reprocessing of GNSS data has proven to be an important scientific tool to test different modeling approaches in a consistent way, since solutions can be computed that only differ in the non-conservative force models. Furthermore, the use of GNSS tracking data allows to test the impact of the developed models for non-conservative forces on real GPS and GLONASS orbits using pseudo-range and phase observations, and not only precise orbits as pseudo observations as done in the previous step. Additionally, the impact of the new models on the global solutions can be analyzed as station coordinates, Earth orientation parameters and geocenter motion (within other parameters) can be estimated together with the satellite orbits. For studying the impact on the orbits one or two years of reprocessed orbits are enough, however, to identify the draconitic

errors present in the global solutions (Section 1.1) several years of reprocessed data are needed. The reprocessing of the GNSS orbit solutions was done at the LRZ (Leibniz-Rechenzentrum) Linux-Cluster. During this dissertation two different reprocessing strategies were used: 1) for P-I and P-II, GPS-only solutions were computed with the strategy described by Steigenberger et al (2006, 2011), and 2) for P-III and P-IV, GPS+GLONASS solutions were computed with the strategy described by Fritsche et al (2013).

Step 4: analysis of results

Analysis of results from the reprocessing runs. The satellite orbits were mainly analyzed in terms of orbit differences (computed with and without the new non-conservative models), SLR-GPS residuals, orbit overlap errors and prediction errors. The geodetic products derived from global solutions were mainly analyzed in terms of time series differences (computed with and without the new non-conservative models) and in terms of power spectra (Fast Fourier Transform, Press et al, 1992). The differences between consecutive 1-day orbits at the day boundaries, i.e., the orbit overlap errors, are an indicator of internal orbit consistency. If all orbit models were perfect such differences at the day boundaries should be zero and the orbits continuous. Therefore, an improvement or degradation in the modeling of the orbits should be visible in the orbit overlap errors. Orbit prediction is an important quality measure of the dynamical models used in the orbit determination process. When relying on GNSS tracking data, some orbit modeling deficiencies might be compensated by the strength of the GNSS tracking data. However, when predicting orbits the observations can only contribute to the observed part of the orbit, while the predicted part relies only on the dynamical orbit models. The power spectra of time series of station coordinates, Earth orientation parameters and geocenter motion are very useful to identify systematic periodic errors, e.g. draconitic errors. If systematic errors are successfully reduced also peaks of the power spectra at spurious frequencies should be reduced.

2 Content of publications



This Chapter gives an overview of the publications that form part of this cumulative dissertation, see the Preface. The four papers are included in full-text at the end of the dissertation. In the “Summary” sections, the most important results obtained in the papers are included as well as the individual contribution of the first author to the papers. The relation between the publications is depicted in the diagram of the previous page. This diagram also shows the relation of the publications with the scientific questions (Q) given in Section 1.3, the open questions (O) given in Section 3.2 and the suggested model improvements (I) given in Section 3.3. These relations are explained in the “Introduction” and “Conclusions and outlook” sections of this Chapter. Quotations from the publications are not indicated explicitly in this Chapter as large parts of the text used in Sections 2.1 to 2.4 were obviously taken from the respective publications.

2.1 P-I: Earth radiation pressure

P-I Rodriguez-Solano C.J., Hugentobler U., Steigenberger P., Lutz S.
Impact of Earth radiation pressure on GPS position estimates.
Journal of Geodesy 86(5):309–317, doi:10.1007/s00190-011-0517-4, 2012.

Introduction

Orbit related frequencies have been identified in geodetic time series such as apparent geocenter motion (Z-component) and station displacements derived from GPS tracking data. The spurious frequencies are at harmonics of the GPS draconitic year, the repeat period of the Sun w.r.t. the GPS satellite constellation which is about 351 days or 1.04 cpy (cycles per year), see Section 1.1.2. Since the orbit perturbations caused by Earth radiation pressure depend on the position of Sun, Earth and satellite (see Section 1.2.3), neglecting Earth radiation pressure is a good candidate to be investigated as a cause for the observed anomalous frequencies in the geodetic time series. All this led to Q-2.

In previous studies, it has been shown that Earth radiation pressure has a non-negligible effect on the GPS orbits, mainly a radial reduction of about 1-2 cm. This effect also reduces the SLR-GPS bias accordingly. The Earth radiation pressure model for GPS satellites, for reflected (visible) and emitted (infrared) radiation, was developed during the Master thesis of the first author and the effect on the radial component of GPS satellite orbits was also investigated there, see Section 1.2.3.

Summary

The acceleration, accounting for Earth radiation and satellite models, was introduced in this paper into the computation of a global GPS network (around 200 IGS sites) adopting the analysis strategies from the Center for Orbit Determination in Europe (CODE), described by Steigenberger et al (2006, 2011). Two solutions covering nine years (2000.0 to 2009.0) with and without Earth radiation pressure were computed and form the basis for this study. The computed results were analyzed in terms of differences (between solutions) and power spectra. In this paper the effect of Earth radiation pressure on the along-track and cross-track components of the GPS orbits was studied in detail. The effect on these two orbit components is at the few millimeter level (2-5 mm). When the orbit differences (with and without Earth radiation pressure) are separated

by orbital plane, it becomes evident that when the Earth radiation pressure is zero in the cross-track component for two orbital planes, the other four orbital planes are also unaffected, the mechanism for which is not yet understood and requires further investigation.

If the orbit differences are transformed into North and East, a particular pattern is found in the North component, displacing the orbits towards North at northern latitudes and South at southern latitudes, with a period of one sixth of the GPS draconitic year, see Figs. 3 and 4 of P-I. The same pattern is found in the daily position estimates of GPS ground stations at the sub-millimeter level, see Figs. 5 and 7 of P-I, indicating that a small change in the along-track or cross-track position of the GPS satellites (which can not be absorbed by the clocks like the radial shift) leads to an almost direct effect on the position estimates of GPS ground stations. This “deformation” of the Earth also leads to a reduction in the anomalous spectra of GPS daily position estimates, mainly in the sixth peak of the North component at 6×1.04 cpy. This peak is reduced by about 38% which is an important reduction since as mentioned by Ray et al (2008), the sixth peak in the North component is one of the sharpest and highest, see Fig. 8 of P-I. Moreover, Earth radiation pressure has the effect on the station coordinates that the scale of the solution is reduced by about 0.14 ppb (parts per billion) or about 0.9 mm.

The impact of Earth radiation pressure on the geocenter and length of day (LOD) estimates was also investigated in this paper. The impact on the geocenter is at the 1 mm level while for the LOD it is at the 10 μ s level, see Figs. 9 and 11 of P-I. The power spectrum of the geocenter Z-component shows strong peaks at odd harmonics of 1.04 cpy, see Fig. 10 of P-I. However, the inclusion of Earth radiation pressure in the computation of GPS orbits only minimally reduces the draconitic errors found in the derived geocenter Z-component time series. The power spectrum of the LOD does not show significant peaks at harmonics of 1.04 cpy.

Individual contribution: The idea of testing the impact of Earth radiation pressure on the draconitic errors of GPS geodetic products, especially of station coordinates and geocenter Z-component was of Urs Hugentobler. The reprocessing of the GPS solutions at the LRZ (Leibniz-Rechenzentrum) Linux-Cluster was done by Peter Steigenberger. The reprocessing of the nine years solutions was mainly based on the IGS reprocessing campaign where Simon Lutz was a main contributor. The idea of creating a movie of differences of station coordinates computed with Earth radiation pressure and without it was of Peter Steigenberger, in P-I two “frames” of this movie are shown in Fig. 5. The first author contributions to the paper were: the development of the Earth radiation pressure model for GPS satellites, the implementation of this model into the Bernese GNSS Software, the analysis of the results from the reprocessed solutions, the creation of the figures, the conception of the paper and the writing of the first version. Finally, the co-authors improved the paper through their comments and corrections about content and linguistic issues.

Conclusions and outlook

Earth radiation pressure only reduces the sixth peak of the power spectrum of station coordinates in the North component by 38% (this reduction is important but other peaks and other components did not show a reduction) and just minimal improvements were achieved in the large draconitic errors of the geocenter Z-component. This answers Q-2. Therefore, as only small improvements in the draconitic errors were achieved Q-3 arose. Which was also induced by Q-4 that arose during the Master thesis (see Section 1.2.3) of the author. In this paper O-1 was open but it was not investigated in future papers.

The CODE empirical model was used to compensate the effects of solar radiation pressure on GPS satellites during the Master thesis and during this publication (P-I), and it is also widely used by the IGS analysis centers. Therefore it can not be excluded that also this model introduces

systematic errors in the GPS satellite orbits and derived geodetic parameters, something that can be particularly suspected as it is a purely empirical model. This led to Q-5.

The last questions were the motivation to revise the modeling of the main non-conservative force acting on GPS satellites, the solar radiation pressure, and consequently also the motivation to start P-II. However, Q-3 had to wait until the last publication (P-IV) to find an answer.

2.2 P-II: Solar radiation pressure

P-II Rodriguez-Solano C.J., Hugentobler U., Steigenberger P.
Adjustable box-wing model for solar radiation pressure impacting GPS satellites.
Advances in Space Research 49(7):1113–1128, doi:10.1016/j.asr.2012.01.016, 2012.

Introduction

Global Positioning System (GPS) satellites are at a distance from the Earth where the solar radiation pressure (SRP) is the main non-gravitational orbit perturbation. While the solar radiation impacting the satellites is simple to model, the perturbing acceleration depends on the structure of the satellite and on the optical properties of each surface facing the Sun. Furthermore, the satellite is constantly changing its orientation with respect to the Sun to maintain its nominal attitude, making the modeling of SRP a complex task. To compensate the effects of solar radiation pressure, the International GNSS Service (IGS) analysis centers employ a variety of approaches, ranging from purely empirical models based on in-orbit behavior, to physical models based on pre-launch spacecraft structural analysis, see Section 1.2.4. It has been demonstrated, however, that the physical models fail to predict the real orbit behavior with sufficient accuracy, mainly due to deviations from nominal attitude, inaccurately known optical properties, or aging of the satellite surfaces. All this, and the conclusions from P-I led to: Q-4, Q-5, Q-6, Q-7, Q-8 and Q-9.

Summary

In this paper a new model for the solar radiation pressure impacting GPS satellites was created, using an intermediate approach between the physical/analytical models and the purely empirical models, see Section 1.2.4. The box-wing model is based on the physical interaction between solar radiation and satellite surfaces, simplifying the satellite to a box (satellite bus) and to a wing (solar panels). In addition, nine parameters can be adjusted (estimated) to fit best the GPS tracking data just as the CODE model does, see Section 1.2.4. The nine parameters are:

1. solar panel scaling factor $(1 + \rho + \frac{2}{3}\delta)$,
2. solar panel rotation lag,
3. Y -bias acceleration (Y_0 of CODE model),
4. absorption plus diffusion $(\alpha + \delta)$ of $+X$ bus,
5. absorption plus diffusion $(\alpha + \delta)$ of $+Z$ bus,
6. absorption plus diffusion $(\alpha + \delta)$ of $-Z$ bus,
7. reflection coefficient (ρ) of $+X$ bus,
8. reflection coefficient (ρ) of $+Z$ bus,
9. reflection coefficient (ρ) of $-Z$ bus.

The partial derivatives of the acceleration w.r.t. these parameters are written analytically (for the case of nominal yaw-steering attitude of the GPS satellites, see Section 1.2.2) in Eqs. 10 to 15 of P-II, see also Fig. 2 of P-II. The accelerations point towards the D and B directions for the first two parameters, if nominal yaw attitude is considered, see Fig. 1.1. The scaling factor of the solar panels just differs from D_0 in the units. The solar panel rotation lag is a novel parameter which compensates for a small lag of the solar panels when they follow the Sun, about 1.5 and 0.5 degrees respectively for the GPS-IIA and GPS-IIR satellites. Y_0 is identical to the same parameter of the CODE model. The last six parameters are the optical properties, divided into $\alpha + \delta$ and ρ , of the surfaces of satellite bus which are illuminated by the Sun under nominal yaw attitude conditions, namely the $+Z$, $+X$ and $-Z$ surfaces as shown in Fig. 1.1. The sum of $\alpha + \delta$ is estimated since instantaneous re-radiated heat is approximately taken into account. This approximation is correct for materials that have zero thermal capacity and completely prevent heat transfer toward the satellite interior (Cerri et al, 2010) like multilayer insulation (MLI), a common material in spacecraft design. Due to high correlations within the box-wing model parameters, the $\alpha + \delta$ parameters are estimated with tight constraints while the ρ parameters are estimated with loose constraints, see Section 6 of P-II. Finally, the adjustable box-wing model needs some approximate a priori information of the satellites, namely: mass, surface areas and surface optical properties (given in the second Appendix, Chapter 5).

A similar approach to the adjustable box-wing model was previously applied by Marshall and Luthcke (1994) and Berthias et al (2002) to altimetry satellites (TOPEX/Poseidon and Jason-1, respectively) in order to fulfill the high accuracy orbit requirements of these missions. They adjusted the optical properties of the box-wing models to reproduce as precise as possible the accelerations acting on the satellites.

In this study, GPS orbits were generated based on one year (2007) of tracking data from the global IGS network (around 200 stations). Two solutions were computed, differing only in the solar radiation pressure (SRP) modeling, one with the CODE empirical model and one with the adjustable box-wing model. We have computed 1-day orbits and the SRP model parameters were also estimated once per day. The estimated parameters and formal errors are depicted in Figs. 5 and 6 of P-II. The estimated box-wing parameters are within the range of physically expected a priori values, with some scattering between days and between satellites. Ideally the parameters of the box-wing model should remain constant over time, since the optical properties should not change from day to day or as a function of β_0 . The increase of the scattering as a function of β_0 like, e.g., for $+ZR$ and $-ZR$ for β_0 around 60° (Fig. 5 of P-II), is an indication of the higher correlation of the parameters with others and as a function of β_0 (Fig. 4 of P-II), also visible in the larger a posteriori formal errors (Fig. 6 of P-II). The large scattering for $|\beta_0| < 14^\circ$, in the case of parameters like $+XR$ and SB for block IIA satellites, is most likely associated with the known yaw maneuvers performed during eclipse seasons (Bar-Sever, 1996), which were not yet included in our box-wing model. The estimated absorption plus diffusion parameters for the $\pm Z$ surfaces ($+ZAD$ and $-ZAD$) for the block IIR satellites are very interesting and the results were not expected, see Fig. 5 of P-II. The variation of these parameters with β_0 looks more like a systematic effect (mismodeling problem in the box-wing model), since these two parameters were tightly constrained to the a priori values.

The box-wing model not only fits well the GPS tracking data but also produces orbits with a similar precision as the ones obtained with the CODE empirical model. The precision of the computed orbits was assessed by comparing orbit overlap errors and prediction errors between the CODE and the box-wing model, see Fig. 8 of P-II. This Figure shows that the performance of the box-wing and CODE models is similar, especially in the orbit overlap errors. The orbit

prediction errors are larger for the box-wing model during eclipse season ($|\beta_0| < 14^\circ$) for block II/IIA satellites. This type of satellite performs longer noon and midnight maneuvers than the block IIR satellites, affecting the GPS phase measurements and the dynamical orbit parameters during eclipse seasons.

Another quality measure of the orbits are the estimated pseudo-stochastic pulses, initially introduced to compensate for orbit modeling deficiencies. These pulses show a reduction (mainly in radial direction, Fig. 7 of P-II) when using the box-wing instead of the CODE model. This reduction in the pulses confirms that the box-wing model results in a more physical representation of the GPS orbits than the CODE model. If the solar panel rotation lag (SB) is not estimated, i.e., when using only nominal panel attitude, the pulses in the radial direction show a large increase (note also the different scale in Fig. 7 of P-II). This shows that the solar panel rotation lag parameter, not previously identified for GPS satellites, is a key factor for precise orbit determination.

The quality of the orbits using the two models is very similar, but there are significant and systematic differences between them. Figure 9 of P-II shows the radial differences for block IIA and block IIR satellites in a Sun-fixed reference frame. First of all note the negative radial bias of about 1-2 cm. This bias is in the “correct” direction, i.e., it has the potential to further reduce the bias of SLR minus GPS measurements. Secondly, there are also systematic radial differences between the orbits, which are evident when plotted in a Sun-fixed reference frame, and between the block types. The major dependency for both blocks is on the Δu angle where the partial derivatives (Section 4 of P-II) of the CODE empirical model and the adjustable box-wing model also differ most.

As a final step in this study, we have reconstructed the acceleration due to SRP obtained with the box-wing model for block IIA and block IIR satellites, see Fig. 11 of P-II. Furthermore, the T20 and T30 models (Fliegel et al, 1992; Fliegel and Gallini, 1996), the GSPM.04b model (Bar-Sever and Kuang, 2004), the Lockheed Martin model (LOCK, Marquis and Krier, 2000) for block IIR satellites and an updated version of the CODE empirical model (Springer et al, 1999), were compared with the adjustable box-wing model (BOXW). Figure 11 of P-II shows large differences between the SRP models, with total accelerations of up to $5 \times 10^{-9} \text{ m/s}^2$. Note that the variation of the CODE empirical model is much smaller w.r.t. the other models. The CODE empirical model fits very well the GPS tracking data but the resulting acceleration has poor physical meaning, except for the scale.

Individual contribution: The idea of creating the adjustable box-wing model for solar radiation pressure impacting GPS satellites was of the first author. Nevertheless, the development of the model took many discussions between the first author and Urs Hugentobler, especially concerning the idea of incorporating the solar panel rotation lag parameter to the model. The implementation of the adjustable box-wing model into the Bernese GNSS Software was done by the first author with support of Urs Hugentobler. The reprocessing of the GPS solutions at the LRZ (Leibniz-Rechenzentrum) Linux-Cluster was done by the first author and Peter Steigenberger. The set up of the computation of orbit overlap and prediction errors in the Bernese GNSS Software was done by the first author and Urs Hugentobler. Additionally, the first author contributions to the paper were: the analysis of the results from the reprocessed solutions, the creation of the figures, the conception of the paper and the writing of the first version. Finally, the co-authors improved the paper through their comments and corrections about content and linguistic issues.

Conclusions and outlook

The adjustable box-wing model is an intermediate approach between the physical/analytical models and the purely empirical models. It is a physics based model with parameters that can

be estimated from GPS tracking data to reflect the real on-orbit behavior of the satellites. This answers Q-7 with a yes and led to Q-11 related to other GNSS satellites. Additionally, several possible model improvements were identified, namely I-1, I-2, I-3, I-4, I-5 and I-6. From the estimated box-wing parameters O-2 remains unanswered, but a possible solution is given in I-7.

The importance of the solar panel rotation lag for the precise orbit determination of GPS satellites answers Q-9. This deviation from the nominal attitude of the solar panels has not been previously identified. It is small, about 1.5 and 0.5 degrees respectively for the GPS-IIA and GPS-IIR satellites, but it introduces non-modeled accelerations in the SRP computation which are very important for the precise determination of GPS satellite orbits. Without the solar panel rotation lag in the box-wing model the pseudo-stochastic pulse are largely increased, leading to I-8.

The acceleration differences between current GPS solar radiation pressure models are large, of up to $5 \times 10^{-9} \text{ m/s}^2$, e.g., the maximum acceleration due to Earth radiation pressure is about $2 \times 10^{-9} \text{ m/s}^2$, see Section 1.2.3. This answers Q-6 but a derived question O-3 was not answered. The differences in the reconstructed accelerations and in the orbits (radial component) between the adjustable box-wing model and the CODE empirical model are mainly due to the fact that the first one is based on the physical interaction between solar radiation and satellite, while the second one is not. The bias and pattern in radial orbit differences led to Q-10.

The orbit overlap and prediction errors are similar for the CODE and box-wing models, with some degradation for GPS-IIA satellites during eclipse seasons when using the box-wing model. However, the reconstructed acceleration of the CODE model has a poor physical meaning and it shows large differences w.r.t. other SRP models. Therefore, Q-5 and Q-8 can only be partially answered in this publication. A more detailed study of the orbit overlap and prediction errors was performed in the next publication (P-III) to answer Q-5 and Q-8. The degradation in the GPS satellite orbits introduced by the adjustable box-wing model during eclipse seasons, led to Q-12 which is answered in P-III.

Additional results

Q-10 and Q-11 were not answered in further publications but they are answered in the first Appendix (Chapter 4) of this dissertation. SLR-GPS residuals are reduced when using the adjustable box-wing model instead of the CODE model (Section 4.1), the bias is reduced by 9-10 mm and the standard deviation is reduced but only outside eclipse seasons, inside eclipse seasons the standard deviation was increased. From here O-4 remains open. As the adjustable box-wing model showed a lower performance than the CODE model in the orbit prediction errors and SLR-GPS residuals for eclipsing GPS-IIA satellites, Q-12 was the motivation to start the next publication (P-III).

The adjustable box-wing model was also applied successfully to GLONASS (old type) and GLONASS-M satellites. The main difference w.r.t. the GPS models is that the bus of the GLONASS and GLONASS-M satellites has a cylindrical shape, they are thus actually cylinder-wing models, see Sections 4.2 and 5.1. Otherwise, the parameters and parameter constraints are identical to GPS. For these satellites the solar panel rotation lag is about 4° and 0.5° respectively, see Fig. 4.9. From here O-5 remains open. The impact of the adjustable box-wing model on the GLONASS orbits was investigated in P-III.

Finally, Q-4 can be answered by looking at Fig. 11 of P-II, the T20 model is very different from the adjustable box-wing model for $90^\circ < \Delta u < 270^\circ$. This Δu regime is where the T20 model introduces systematic errors in the SLR-GPS residuals, see Urschl et al (2007). Furthermore, the

adjustable box-wing model reduces the standard deviation of SLR-GPS residuals as demonstrated in Section 4.1. Such that it becomes clear that the T20 model has a modeling error for $90^\circ < \Delta u < 270^\circ$. The exact cause of this modeling error is unclear as the T20 model only provides the total accelerations in the X and Z components.

2.3 P-III: Non-nominal attitude

P-III Rodriguez-Solano C.J., Hugentobler U., Steigenberger P., Allende-Alba G.
Improving the orbits of GPS block IIA satellites during eclipse seasons.
Advances in Space Research 52(8):1511–1529, doi:10.1016/j.asr.2013.07.013, 2013.

Introduction

During Sun-Earth eclipse seasons, GPS-IIA satellites perform noon, shadow and post-shadow yaw maneuvers, see Section 1.2.5. If the yaw maneuvers are not properly taken into account in the orbit determination process, two problems appear: 1) the observations residuals increase since the modeled position of the satellite's navigation antenna differs from the true position, and 2) the non-conservative forces like solar radiation pressure or Earth radiation pressure are mismodeled due to the wrong orientation of the satellite's surfaces in space. Mainly the last problem and the unsolved issues from P-II led to: Q-5, Q-8, Q-11, Q-12, Q-13, Q-14 and Q-15.

Summary

Precise Point Positioning (PPP, Zumberge et al, 1997) phase residuals show a large increase during the noon, shadow and post-shadow yaw maneuvers performed by GPS-IIA satellites (see Figs. 1 and 2 of P-III) if those maneuvers are not properly taken into account. The non-nominal yaw attitude of satellites introduces two main effects on a GNSS clock solution, the phase wind-up effect and the effect to the navigation antenna eccentricity. While the phase wind-up effect (Wu et al, 1993) is completely absorbed by the satellite clock corrections, the effect of the antenna eccentricity will be mainly distributed between the station residuals and the satellite clock corrections. The antenna eccentricity (0.279 m for GPS-IIA satellites) can be exploited to estimate the real yaw attitude of the satellites as previously demonstrated by Bar-Sever (1996) and Dilssner et al (2011). In this study, the PPP phase residuals (result from reprocessing of satellite clocks) were used to estimate the real yaw attitude of GPS-IIA satellites by using Eq. 1 of P-III, see Figs. 4 and 5 of P-III. This method is not as accurate as the reverse kinematic PPP method proposed by Dilssner et al (2011) but it is very fast and it allowed to get epoch-wise (5 min) yaw angle estimates for all the yaw maneuvers and for all GPS-IIA satellites during the years 2007-2008. GPS-IIR and GLONASS (older block) also perform yaw maneuvers during eclipse seasons, however, the antenna offset w.r.t. the satellite rotation axis is zero and consequently the PPP phase residuals do not show any increase during the yaw maneuvers. For GLONASS-M satellites, taking advantage of the non-zero antenna offset (0.545 m), the real yaw angles from PPP phase residuals were also estimated. However, the yaw angle estimates are noisier as compared to the estimates for GPS-IIA satellites, and the few maneuvers that could be observed did not differ from the Dilssner et al (2011) model.

From the estimated yaw angles at 5 min intervals the yaw rates were estimated by evaluating numerically the Bar-Sever (1996) model at different yaw rates. This was done for all the noon, shadow and post-shadow yaw maneuvers. From the estimated yaw rates a β_0 dependent yaw rate model was constructed for each eclipse season and each GPS-IIA satellite, see Figs. 6 and 7 of P-III. These β_0 -dependent yaw rates allowed that the real yaw maneuvers are modeled with high accuracy. In particular, the performance of the noon and post-shadow maneuvers is largely increased compared to the use of nominal yaw rates¹ as shown in Fig. 8 of P-III. The correct modeling of these two maneuvers is very important for this study as these maneuvers occur in full sunlight.

For the computation of solar and terrestrial radiation pressure the orientation of the solar panels is very important. The solar panels are large structures and the major contributors to the large area-to-mass ratios of the satellites. Two models for the attitude of the solar panels have been developed and tested during this study. The first model assumes that the solar panels are pointing as perpendicular as possible to the Sun during a yaw maneuver. The second model is based on Bar-Sever (1995) and on the information provided by the author that the solar panels are fixed during a shadow passage, i.e., they are not rotating w.r.t. the satellite body, implying that the solar panels have to perform a short post-shadow recovery. Both models are analytically described in Section 4 of P-III, see also Fig. 10 of P-III.

Once the yaw attitude of the satellite, i.e., the orientation of the satellite bus in space, and the attitude of the solar panels are known, the information can be used for computing the solar radiation pressure acting on GPS or GLONASS satellites. For this purpose, the adjustable box-wing model described (analytically for nominal yaw-steering attitude) in P-II has been upgraded to incorporate the non-nominal attitude of the body and the solar panels. The main change to the original model is that the partial derivatives of the acceleration due to solar radiation pressure can no longer be described in an analytical way, since the position of the Sun w.r.t. the satellite surfaces is now arbitrary. The partial derivatives, however, can be computed numerically by simply using the angle of incidence between the Sun and the surfaces of the satellite, see Fig. 11 of P-III.

With the different yaw and solar panel attitude models implemented in a development version of the Bernese GNSS Software (Dach et al, 2007, 2008), and with the box-wing model capable of assimilating this information, five different 2-year (2007 and 2008) orbit solutions were computed, see Table 1 of P-III. The computation of 1-day GPS and GLONASS orbits is based on tracking data from the global IGS network, using the strategy described by Fritsche et al (2013). The improvement of the orbits by including these models is quantified in terms of orbit overlap errors (Fig. 12 and Table 2 of P-III), orbit prediction errors during the first 3-9 h (Fig. 13 and Table 3 of P-III) and orbit prediction errors during the 4th day (Fig. 14 and Table 4 of P-III). For the orbit predictions we first computed multi-day arcs (2-day and 4-day arcs, respectively) by stacking 1-day observed arcs (Beutler et al, 1996). While for the 1-day arcs there is a set of radiation pressure parameters (from the CODE or adjustable box-wing models) per day, for the multi-day arcs there is only one set of radiation pressure parameters common to the multi-day solution. As a second step, the multi-day arcs have been used for orbit prediction, using the estimated radiation pressure parameters from the observed part.

From all the attitude models tested in combination with the box-wing model the one that improves the GPS-IIA orbits most (from one solution to the next) is the yaw attitude model with nominal yaw rates. Further small improvements are obtained by using the estimated yaw attitude from

¹ftp://sideshow.jpl.nasa.gov/pub/GPS_yaw_attitude/nominal_yaw_rates

PPP phase residuals and the second attitude model for the solar panels, which result in our best solution. The post-shadow maneuvers whose rotational direction can be ambiguous especially if nominal yaw rates are used, turn out to be no major problem for the solar radiation pressure computation. If the sign of the post-shadow maneuver is mismodeled, the cross-track accelerations acting on the satellite also have an incorrect sign, but the radial and along-track accelerations are almost unaffected, being independent of the sign of the post-shadow maneuver, see Fig. 16 of P-III. This is the reason why the model based on the estimation of the real attitude results in just a small overall improvement in the orbits. Nevertheless, the use of the model based on the estimation of the real attitude is very important, since it allows us to conclude that the remaining errors in the orbits of eclipsing GPS-IIA satellites might not be anymore related to a wrong yaw attitude. Other effects, like improper Earth shadow modeling or thermal effects, might have an important contribution to the remaining errors during eclipse seasons. For GPS-IIR and GLONASS-M satellites, the yaw attitude models of Kouba (2009) and Dilssner et al (2011) with nominal yaw rates, were tested respectively. For both satellite types just a small improvement in the orbits is achieved by using the yaw maneuver models. Errors are still present for the orbits of eclipsing satellites, indicating again that other effects, not related to yaw attitude, might be important to consider during eclipses.

The CODE (5-parameter) radiation pressure model has a better performance than the adjustable box-wing model during eclipse seasons (especially for GPS-IIA satellites) if nominal attitude is used, and this was one of the main motivations to initiate this study. Now with the combination of the box-wing model with the yaw attitude the performance of the box-wing model for GPS-IIA satellites is much better. From the orbit solution including the CODE model with nominal attitude to the one including the adjustable box-wing model with the most refined attitude models, the average improvements in the orbits of GPS-IIA satellites during eclipse seasons are quantified as follows: orbit overlap errors decrease from 0.075 to 0.063 m, orbit prediction errors after the first 3 to 9 hours decrease from 0.141 to 0.095 m, and after four days decrease from 6.49 to 3.28 m. However, small degradations for eclipsing GPS-IIR and GLONASS-M satellites were found when using the box-wing (even if the yaw models are used) instead of the CODE model. The degradations appear mainly in the 4-day orbit predictions while the orbit overlaps show in general an improvement. Finally, in this study it was also found that β_0 (Sun elevation angle above the orbital plane) dependent errors outside eclipse seasons, i.e. with nominal attitude, present in the CODE radiation pressure model are mitigated when using the box-wing model. The errors are mainly visible in the radial component of orbit predictions for GPS-IIA, GPS-IIR and GLONASS-M satellites, see Figs. 15, 17 and 18. The reason for this improvement in regimes with nominal attitude resides in the explicit dependence of the estimated parameters of the adjustable box-wing with the ϵ angle, formed between Earth, satellite and Sun.

Individual contribution: The idea of estimating the yaw attitude of GPS-IIA satellites from PPP phase residuals was of the first author and of Urs Hugentobler, the realization in MATLAB was done by the first author. The implementation of the existing yaw models for GPS-II/IIA, GPS-IIR and GLONASS-M satellites into the Bernese GNSS Software was done by the first author with support of Urs Hugentobler. The set up of the clock and PPP solutions was done by all the authors of the paper. Gerardo Allende-Alba worked as student assistant on the selection of GPS and GLONASS ground stations for the clock solutions and on the effects of the yaw maneuvers on the satellite clocks. The reprocessing of the GPS+GLONASS solutions at the LRZ (Leibniz-Rechenzentrum) Linux-Cluster was done by the first author and Peter Steigenberger. The set up of the computation of orbit overlap and prediction errors in the Bernese GNSS Software was done by the first author with support of Urs Hugentobler. Additionally, the first author contributions to the paper were: the upgrade of the adjustable box-wing model to use non-nominal yaw attitude, the analysis of the results from the reprocessed solutions, the creation of the figures, the conception of the paper and the writing of the first version. Finally, the co-authors improved the paper through their comments and corrections about content and linguistic issues.

Conclusions and outlook

With the more detailed analysis (compared to P-II) of the orbit overlap and prediction errors realized during this paper, Q-5 and Q-8 can be fully answered as well as Q-11. From here O-8 remains open and I-13 is suggested. The CODE (5-parameter) radiation pressure model introduces β_0 systematic errors in the orbits of GPS and GLONASS satellites (mainly visible in the radial component of the prediction errors) during nominal attitude regimes. These errors are mitigated with the use of the adjustable box-wing model. During eclipse seasons the box-wing model introduces larger errors in the orbits than the CODE model, especially for GPS-IIA satellites. These errors are largely reduced for GPS-IIA satellites if the non-nominal yaw attitude is properly incorporated by the adjustable box-wing model, which answers Q-15. The reduction of the β_0 systematic errors with the adjustable box-wing model led again to Q-3 (initially from P-I) and was the main motivation to start P-IV. However, the high performance of the non-eclipsing satellites could not be reached when the yaw maneuvers were used for GPS-IIA, GPS-IIR and GLONASS-M satellites. For these problems some specific model improvements are suggested in I-9, I-10, I-11 and I-12.

The yaw maneuvers performed by GPS-IIA satellites during eclipse seasons affect largely the solar radiation pressure computation, as shown in Figs. 11 and 16 of P-III, which answers Q-12. These yaw maneuvers introduce non-modeled accelerations in the SRP computation which are very important for the precise determination of GPS-IIA satellite orbits.

The post-shadow maneuver of GPS-IIA satellites can be modeled unambiguously using the yaw rate model as a function of the β_0 angle presented in this paper, which answers Q-13. The β_0 yaw rate model also opened O-6 and O-7.

The incorporation of the solar panel attitude model (specific pitch model for shadow and post-shadow maneuvers) for GPS-IIA satellites shows a small but consistent improvement in the orbit predictions. This indicates that the orientation of the solar panels described by this model should be closer to reality than assuming that the panels point as perpendicular as possible to the Sun during a yaw maneuver. This answers Q-14. However, this deviation from nominal attitude only has a small impact on the computed orbits.

2.4 P-IV: Impact on global solutions

P-IV Rodriguez-Solano C.J., Hugentobler U., Steigenberger P., Bloßfeld M., Fritsche M.
Reducing the draconitic errors in GNSS geodetic products.
Journal of Geodesy, submitted, 2013.

Introduction

Systematic errors at harmonics of the GPS draconitic year have been found in diverse GPS-derived geodetic products like the geocenter Z -component, station coordinates, Y -pole rate and orbits (i.e. orbit overlaps). The GPS draconitic year is the repeat period of the GPS constellation w.r.t. the Sun which is about 351 days. Different error sources have been proposed which could generate these spurious signals at the draconitic harmonics. In this study, we focus on one of these error sources, namely the radiation pressure orbit modeling deficiencies in order to answer Q-3.

This last scientific question has originated in P-I. However, only after P-III, where a significant reduction of the β_0 systematic errors in the orbits was obtained, an answer to Q-3 got closer and with it the start of this publication.

Summary

In this study, three GPS+GLONASS solutions of eight years (2004-2011) were computed which differ only in the radiation pressure and satellite attitude models, see Table 1 of P-IV. The models employed in the solutions are: 1) the CODE (5-parameter) radiation pressure model (Beutler et al, 1994) widely used within the IGS (International GNSS Service) community, 2) the adjustable box-wing model for solar radiation pressure impacting GPS (and GLONASS) satellites, developed in P-II, and 3) the adjustable box-wing model upgraded to use non-nominal yaw attitude, developed in P-III. The computation of 1-day GPS and GLONASS orbits was based on tracking data from the global IGS network (with a maximum of 254 ground stations per day), using the strategy described by Fritsche et al (2013). In this study, the draconitic errors of the last three solutions were analyzed mainly in terms of power spectrum (see Section 3.2 of P-IV) for the following geodetic products: orbits (i.e. overlap errors), geocenter Z -component, Earth orientation parameters and station coordinates.

For GPS satellite orbits we find large systematic errors at harmonics of one GPS draconitic year as already reported by Griffiths and Ray (2013). As we have expected from the results of P-III, the draconitic errors in the orbits decrease with the new solar radiation pressure and attitude models, see Fig 2 of P-IV. Moreover, if solutions 1 and 3 are compared directly in Table 2 of P-IV, we find a reduction of the errors for all the draconitic harmonics and for all the components. With an average reduction of 46%, 38% and 57% for the radial, along-track and cross-track components.

For GLONASS satellite orbits we find a mixture of improvements and degradations in the draconitic errors when using the new solar radiation pressure and attitude models, see Table 2 of P-IV. We obtain an average reduction of the errors of 5% and 39% for the along-track and cross-track components, while in the radial component the errors are increased in average by 16%. There are, however, some striking patterns in the power spectra of the GLONASS orbits, like the clusters of peaks around 47 cpy, 94 cpy and 140 cpy, see Fig. 3 of P-IV. The first frequency is close to eight sidereal days or 45.8 cpy, the repeat period of the GLONASS ground tracks. Besides these features, the power spectra are generally decreased when using the adjustable box-wing model, in particular for the cross-track component.

The geocenter Z -component estimated with the CODE (5-parameter) radiation pressure model shows large variations that can be (visually) correlated with the β_0 angle of the different orbital planes as shown in Fig. 4 of P-IV. Moreover, the power spectrum of the geocenter Z -component shows strong draconitic errors at odd harmonics of 1.04 cpy. Exchanging the CODE (5-parameter) radiation pressure model by the adjustable box-wing model results in a significant reduction of the geocenter Z -component variations and of the associated draconitic errors (solutions 1 and 2 in Fig. 4 and Table 3 of P-IV). According to Meindl et al (2013), as soon as radiation pressure parameters produce cross-track accelerations with non-zero means over a revolution there is a danger of generating artifacts in the geocenter Z -component. In this study, we found that the B_C and B_S parameters of the CODE (5-parameter) model and the reflection coefficient of the $+X$ bus surface of the adjustable box-wing model can produce such accelerations. However, with the fundamental difference that the acceleration generated from the once-per-revolution parameters in B -direction is purely empirical while the acceleration due to $+X$ reflection results from the

physical interaction between the Sun and the $+X$ surface. This parametrization difference is, from our point of view, the explanation of the improvement obtained in the geocenter Z -component estimation with the adjustable box-wing model. The largest draconitic error of solution 2 is at the 7th harmonic. This solution has mainly large orbit errors during eclipse seasons (P-III), which happen twice per draconitic year. Fig. 5 of P-IV shows the histograms of differences in days between consecutive GPS orbital planes along the ecliptic (not the equator). The peak of this histogram is at about 50 days which would correspond to the 7th draconitic harmonic. As we would have expected, solution 3, which reduces the orbit errors during eclipse seasons mainly for GPS-IIA satellites, reduces very significantly the 7th draconitic harmonic when compared to the previous solution as shown in Fig. 4 of P-IV. Finally, when comparing solutions 1 and 3 (Fig. 4 and Table 3 of P-IV) it can be observed that the errors of the geocenter Z -component almost disappear for all the draconitic harmonics, with an average reduction of 92%.

The estimated Earth orientation parameters are compared in this study with external sources like the IERS 08 C04² (International Earth Rotation and Reference Systems Service, Bizouard and Gambis, 2009) and the JPL SPACE2011³ (Jet Propulsion Laboratory, Ratcliff and Gross, 2013) time series, as the draconitic harmonics of the solutions themselves were not clearly visible. When subtracting IERS 08 C04 or JPL SPACE2011 the draconitic harmonics become visible. However, the interpretation of the results is difficult as the IERS 08 C04 and JPL SPACE2011 time series contain GPS data which may also include draconitic errors. For the X and Y pole rates the draconitic harmonics are very significant, as shown in Fig. 6 of P-IV. Here the differences between JPL SPACE2011 and IERS 08 C04 are at the level of $10^{-7} \text{ mas}^2/\text{day}^2$, i.e., four orders of magnitude smaller than the differences between our solutions and IERS 08 C04. Previously, Seitz et al (2012) also found draconitic harmonics in the Y -pole rate of GPS minus VLBI (Very Long Baseline Interferometry) time series. For the X and Y pole rates we obtain an average reduction of the draconitic errors between solutions 1 and 3 of 24% and 50% respectively, see Table 4 of P-IV. The draconitic errors for the X and Y pole as well as for the LOD are not that significant as for the pole rates and the results are not conclusive when using the new models.

The power spectra of GPS-derived station coordinates show spurious signals at harmonics of one GPS draconitic year as first noted by Ray et al (2008). At least until the 9th harmonic these spurious signals are visible as shown in the power spectra of our GNSS-derived station coordinates in Fig. 7 of P-IV. In P-I we obtained a reduction of 38% only in the 6th harmonic of the North component. In this study, the 6th harmonic of the North component is reduced by 32% when using the adjustable box-wing model. Another 53% reduction (w.r.t. solution 2) is achieved with the upgraded version of the model based on non-nominal yaw attitude. In total, comparing solutions 1 and 3, a reduction of 68% is achieved for the 6th harmonic in the North component. However, in this study with the new radiation pressure and yaw attitude models not only this peak is reduced but we achieve a general reduction of the draconitic errors in the station coordinates as shown in Fig. 7 of P-IV. In fact, when comparing solutions 1 and 3 in Table 5 of P-IV, it can be observed that all the draconitic harmonics (except the 2nd harmonic in the North component) are reduced in the North, East and Height components. We obtain an average reduction over all the draconitic errors between solutions 1 and 3 of 41%, 39% and 35% for the North, East and Height components.

Individual contribution: The idea of testing the impact of the new solar radiation pressure and attitude models on the draconitic errors of GPS geodetic products, especially of station coordinates and geocenter Z -component was of the first author and of Urs Hugentobler. The idea of creating Fig. 5 was of Urs Hugentobler. The idea of

²<ftp://hpiers.obspm.fr/iers/eop/eopc04>

³<ftp://euler.jpl.nasa.gov/keof/combinations/2011>

testing the impact on the Earth orientation parameters, especially on the Y -pole rates was of Mathis Bloßfeld. The reprocessing of the GPS+GLONASS solutions at the LRZ (Leibniz-Rechenzentrum) Linux-Cluster was done by the first author and Peter Steigenberger. The reprocessing of the eight years solutions was mainly based on a reprocessing project where Mathias Fritsche was a main contributor. Additionally, the first author contributions to the paper were: the analysis of the results from the reprocessed solutions, the creation of the figures, the conception of the paper and the writing of the first version. Finally, the co-authors improved the paper through their comments and corrections about content and linguistic issues.

Conclusions and outlook

Part of the draconitic errors found in GNSS geodetic products are definitely induced by orbit modeling deficiencies, in particular those related to the radiation pressure modeling. Furthermore, the new models for solar radiation pressure and deviations from nominal attitude (developed in P-II and P-III) significantly reduce the draconitic errors found in geodetic products. This answers Q-3. Despite this significant reduction, draconitic errors remain in the geodetic products. In P-III it was shown that there are still β_0 systematic errors present in the GPS and GLONASS orbits, even after using the new models. Therefore, a large potential to further reduce the draconitic errors in the GNSS geodetic products exists if the β_0 systematics in the orbits can be further reduced. This led to the last open question (O-12).

The draconitic errors in the orbit overlaps, as expected from the results of P-III, are significantly reduced with the new models especially for GPS satellites. In the case of GLONASS satellites, mainly the cross-track component is improved while the radial component is slightly degraded regarding the draconitic errors, this points again to I-12. At higher frequencies spurious signals were found related to the ground-track repeating period of the GLONASS orbits, leading to O-9.

The draconitic errors observed in the geocenter Z -component tend to disappear with the new radiation pressure models and it can be concluded that the observed odd harmonics were introduced by the CODE (5-parameter) model, however O-10 remains open.

In the X and Y pole rates the draconitic errors are reduced, however for the X and Y pole as well as for the LOD the results are not conclusive. From here O-11 remains open.

Finally, the draconitic errors of the estimated station coordinates are significantly reduced, in average 41%, 39% and 35% for the North, East and Height components. However, we cannot conclude that only radiation pressure orbit modeling deficiencies contribute to the draconitic errors especially in the station coordinates but also in the other geodetic products. Other error sources like multipath or mismodeling of sub-daily signals (see Section 1.1.2) could be contributing to the remaining draconitic errors. These other error sources cannot be ruled out by the results of this study. Here, an answer to O-12 would be very useful.

3 Conclusions and outlook

3.1 Conclusions

The general scientific question of this dissertation (Q-1, Section 1.3) is answered here.

Q-1 Can new non-conservative force models improve the errors observe in the GNSS satellite orbits and global solutions? In particular when considering new models for Earth radiation pressure, solar radiation pressure and deviations from nominal attitude?

Earth radiation pressure

The acceleration acting on GPS (i.e. box-wing-like) satellites caused by Earth radiation (visible and infrared) depends mainly on the relative position of each satellite, Earth and Sun. This implies a perturbation in the GPS satellite orbits at harmonics of the GPS draconitic year. The main non-negligible effect on the orbits is a reduction of the height by about 1 – 2 cm, see Section 1.2.3. In the other components of the orbits (along-track and cross-track) the effect is about one order of magnitude smaller. In the North component of the orbit differences (with and without Earth radiation pressure) a particular pattern is found, displacing the orbits (few millimeters) towards North at northern latitudes and South at southern latitudes, with a period of one sixth of the GPS draconitic year. The same pattern is found in the daily position estimates of GPS ground stations at the sub-millimeter level, indicating that a small change in the along-track or cross-track position of the GPS satellites (which can not be absorbed by the clocks like the radial shift) leads to an almost direct effect on the position estimates of GPS ground stations. This “deformation” of the Earth also leads to a reduction in the anomalous spectra of GPS daily position estimates, mainly in the sixth peak of the North component by about 38%. The impact of Earth radiation pressure on the geocenter (at the one millimeter level) is less significant. It reduces just slightly some of the anomalous peaks of the geocenter power spectrum and even increases others. For LOD, the impact is of the order of 10 μ s. The small improvement obtained in the draconitic errors was the main motivation to revise the modeling of the main non-conservative force acting on GPS satellites, the solar radiation pressure.

Solar radiation pressure

A new model for the solar radiation pressure on GPS satellites has been developed in this dissertation using an intermediate approach between the physical/analytical models and the empirical models. The model simplifies the satellite to a box (satellite bus) and a wing (solar panels), and assumes an ideal yaw attitude of the satellite, but allows for a misalignment of the solar panels. The model has been derived based on the physical interaction between the solar radiation and the box-wing satellite. The model is capable of fitting the GPS tracking data by adjusting mainly the

optical properties of the satellite surfaces. The adjustable box-wing model has been successfully used for GPS-II/IIA, GPS-IIR, GLONASS (old type) and GLONASS-M satellites.

The computed satellite orbits using the adjustable box-wing model show a similar performance as the ones generated with the CODE empirical model (5-parameter, Beutler et al, 1994), when looking at overlap and prediction errors, and a better performance when looking at the radial pseudo-stochastic pulses which show a reduction. However, systematic differences between the two types of orbits are observed. This indicates that the empirical CODE model fits well the GPS tracking data but cannot totally compensate for the accelerations induced by solar radiation pressure. On the contrary, the box-wing model introduces features in the accelerations and in the orbits due to the physical modeling of solar radiation pressure. It was found that β_0 (Sun elevation angle above the orbital plane) dependent errors outside eclipse seasons, i.e. with nominal attitude, present in the CODE radiation pressure model are mitigated when using the box-wing model. The errors are mainly visible in the radial component of orbit predictions for GPS-IIA, GPS-IIR and GLONASS-M satellites. The reason for this improvement in regimes with nominal attitude resides in the explicit dependence of the estimated parameters of the adjustable box-wing with the ϵ angle (Fig. 1.1) formed between Earth, satellite and Sun.

Furthermore, the adjustable box-wing model reduces the SLR-GPS residuals bias and standard deviation (only outside eclipse seasons) compared to the CODE (5-parameter) radiation pressure model. This last model has a better performance than the adjustable box-wing model especially for GPS-IIA satellites during eclipse seasons if nominal attitude is used. This is visible in the SLR-GPS residuals but also in the orbit overlap and prediction errors.

Non-nominal attitude

The empirical radiation pressure models, like the CODE model, have a high performance as they can adjust to the real orbit behavior. Furthermore, some of the empirical parameters can partially compensate for deviations from nominal attitude. The adjustable box-wing model with purely nominal attitude has a much lower performance than the CODE model. It was very difficult to reach the performance of the CODE empirical model with a different model based on the physical interaction between the solar radiation and satellite surfaces. In fact, it was necessary to take into account a small misalignment of the solar panels w.r.t. their nominal orientation to reach a similar performance as the CODE model. It is therefore a key factor for fitting the real GNSS tracking data and for obtaining highly precise satellite orbits. This deviation from nominal attitude, not previously identified for GPS or GLONASS satellites, is modeled as a rotation lag of the solar panels around their rotation axis. The solar panel rotation lag is about 1.5° for GPS-IIA, 0.5° for GPS-IIR, 4° for GLONASS (old type) and 0.5° for GLONASS-M satellites.

The orbits of GPS-IIA satellites are particularly degraded during Sun-Earth eclipse seasons if the noon, shadow and post-shadow yaw maneuvers are not properly taken into account. Two models for the yaw attitude during maneuvers were tested in this dissertation for GPS-IIA satellites in combination with the adjustable box-wing model. The first model is the existing Bar-Sever (1996) model with nominal yaw rates. The second model is based on the estimation of the real attitude of the satellites from PPP (Precise Point Positioning) phase residuals. Furthermore, two models for the orientation of the solar panels during yaw maneuvers were tested. The first model assumes that the solar panels point as perpendicular as possible to the Sun. The second model assumes that the solar panels are fixed w.r.t. the satellite bus during shadow, implying that a short post-shadow recovery has to be performed. From all the attitude models tested in combination with

the box-wing model the one that improves the orbits most (from one solution to the next) is the yaw attitude model with nominal yaw rates. Further small improvements are obtained by using the estimated yaw attitude from PPP phase residuals and the second attitude model for the solar panels, which resulted in our best solution. The post-shadow maneuvers whose rotational direction can be ambiguous especially if nominal yaw rates are used, turn out to be no major problem for the solar radiation pressure computation. If the sign of the post-shadow maneuver is mismodeled, the cross-track accelerations acting on the satellite also have an incorrect sign, but the radial and along-track accelerations are almost unaffected, being independent of the sign of the post-shadow maneuver. This is the reason why the model based on the estimation of the real attitude results in just a small overall improvement in the orbits. Nevertheless, the use of the model based on the estimation of the real attitude is very important, since it allows us to conclude that the remaining errors in the orbits of eclipsing GPS-IIA satellites might not be anymore related to a wrong yaw attitude. The CODE (5-parameter) radiation pressure model has a better performance than the adjustable box-wing model during eclipse seasons (especially for GPS-IIA satellites) if nominal attitude is used. Now with the combination of the box-wing model with the yaw attitude the performance of the box-wing model for GPS-IIA satellites is much better. However, the performance of non-eclipsing satellites is not yet reached.

For GPS-IIR and GLONASS-M satellites, the yaw attitude models of Kouba (2009) and Dilssner et al (2011) with nominal yaw rates, were tested respectively. For both satellite types just a small improvement in the orbits is achieved by using the yaw maneuver models. Furthermore, small degradations for eclipsing GPS-IIR and GLONASS-M satellites were found when using the box-wing (even if the yaw models are used) instead of the CODE model. The degradations appear mainly in the 4-day orbit predictions while the orbit overlaps show in general an improvement.

Impact on global solutions

The adjustable box-wing model and its upgraded version for non-nominal yaw attitude significantly reduce the draconitic errors in the GNSS-derived geodetic products compared to the use of the CODE (5-parameter) model. The reduction of the draconitic errors is obtained in the orbits (overlap errors), in the geocenter Z -component, in the X and Y pole rates, and in the station coordinates. The draconitic errors for the X and Y pole as well as for the LOD are not that significant as for the pole rates and the results are not conclusive when using the new models. When comparing the solutions computed with the CODE model and with the adjustable box-wing model for non-nominal yaw attitude we achieved the following in the GNSS geodetic products. Orbits: the draconitic errors in the orbit overlaps are reduced for the GPS satellites in all the harmonics on average 46%, 38% and 57% for the radial, along-track and cross-track components, while for GLONASS satellites they are mainly reduced in the cross-track component by 39%. Geocenter Z -component: all the odd draconitic harmonics found when the CODE model is used show a very important reduction (almost disappearing with a 92% average reduction) with the new radiation pressure models and it can be concluded that the observed odd harmonics were introduced by the CODE (5-parameter) model. Earth orientation parameters: the draconitic errors are reduced for the X -pole rate and especially for the Y -pole rate by 24% and 50% respectively. Station coordinates: all the draconitic harmonics (except the 2nd harmonic in the North component) are reduced in the North, East and Height components, with average reductions of 41%, 39% and 35% respectively. This shows, that part of the draconitic errors found in GNSS geodetic products are definitely induced by orbit modeling deficiencies, in particular those related to the radiation pressure modeling.

3.2 Open questions

From this dissertation some questions (given below) remained open. The origin and context of these open questions is described in Chapter 2.

- O-1 Why, when the Earth radiation pressure vanishes in the cross-track component for two orbital planes, the other four orbital planes are also unaffected?
- O-2 Why the $+ZAD$ and $-ZAD$ estimated box-wing parameters ($\alpha + \delta$ of the $\pm Z$ surfaces) for the block IIR satellites show a systematic behavior with β_0 ?
- O-3 What are the specific causes of the large differences between current SRP models (besides the CODE and adjustable box-wing models)?
- O-4 Can the SLR-GPS residuals be reduced during eclipse seasons if the non-nominal yaw attitude is taken into account in the adjustable box-wing model?
- O-5 What is the cause of the behavior of the GLONASS satellites SVN 701 and SVN 713 for $|\beta_0| < 22.5^\circ$ and of SVN 783 for all β_0 regimes?
- O-6 Why do the yaw rates change during an eclipse season as function of β_0 ? Why do some satellites show a β_0 dependency of the shadow yaw rate and others not?
- O-7 Can one generate more general models that are not eclipse season or spacecraft specific? Can one predict the yaw rates for the currently operating GPS-IIA satellites?
- O-8 Why the GPS-IIA satellite orbits are a little worse than the ones of GPS-IIR satellites, independent on whether the CODE (5-parameter) or the adjustable box-wing models are used?
- O-9 Why there are large spurious signals in the power spectra of the GLONASS orbit overlap errors related to the ground-track repeating period of 8 sidereal days?
- O-10 Why the CODE (5-parameter) radiation pressure model generates large draconitic errors in the geocenter Z-component just at odd harmonics?
- O-11 How to detect confidently possible draconitic errors in the GNSS-derived LOD, X-pole and Y-pole?
- O-12 How the draconitic errors of the GNSS-derived geodetic products would look like if all the β_0 systematic errors could be eliminated from the satellite orbits?

3.3 Further model improvements

From this dissertation some specific model improvements (given below) were identified. The origin and context of these model improvements is described in Chapter 2.

- I-1 A reduction of the β_0 dependency of the correlation between the parameters of the adjustable box-wing model (see Figs. 4 and 6 of P-II) would improve the estimation of the box-wing parameters. It could also eliminate β_0 dependencies of the estimated parameters. Some suggestions on how to reduce the correlation between parameters are given in: I-2, I-3 and I-4.
- I-2 β_0 dependent constraints could be introduced for the estimation of the adjustable box-wing parameters, instead of: 1) none for the solar panel scaling factor, the solar panel rotation lag and the Y -bias acceleration, 2) 0.01 for the absorption plus diffusion coefficient of the $+X$, $+Z$ and $-Z$ surfaces, and 3) 0.1 for the reflection coefficient of the $+X$, $+Z$ and $-Z$ surfaces.
- I-3 The constraint implied by Eq. 7 of P-II could be imposed by forcing $\alpha + \rho + \delta$ to be equal to one. In this case a constraint could be applied to the sum of the optical properties, e.g., as 1 ± 0.01 or 1 ± 0.1 . This should strengthen the physical meaning of the estimated optical properties. Originally in P-II this constraint was not applied since it allows to separate between $\alpha + \delta$ and ρ parameters and gives three extra degrees of freedom to the box-wing model.
- I-4 If detailed satellite models would be available, e.g., as the ones developed by Ziebart (2001), the effective area of the satellite surfaces can be computed as function of ϵ , see Fig. 1.1. Then in the Eqs. 10 to 15 of P-II, A can be replaced by $A(\epsilon)$. Other angle dependencies, e.g. an angle in the YZ plane, could also be considered if non-nominal yaw attitude is used. The use of this effective areas implies that shadowing effects would be included in the adjustable box-wing model and an improvement in the computed orbits could be expected.
- I-5 The constant nature of the box-wing parameters opens the possibility of stacking the parameters over several days. The adjustable box-wing model parameters have the advantage that they should in principle remain constant over time, since the optical properties should not change from day to day or as a function of β_0 . Besides a potential orbit improvement, the stacked box-wing parameters can be used to construct an updated set of a priori values of the optical properties. However, if modeling problems exist (like the ones during eclipse seasons due to non-nominal yaw attitude) the stacking of parameters could rather increase the errors, such that the mitigation of modeling problems should be first solved for short (1-day) orbits arcs.
- I-6 The estimated optical properties in the visible could be used for the Earth radiation pressure computation. The possibility to estimate infrared optical properties or the optical properties (visible and infrared) for the back side of the solar panels (all necessary for the computation of Earth radiation pressure) could be also investigated.
- I-7 A possible reason for the problem stated in O-2 are heating or cooling effects, since the bus of block IIR is reported to have very high absorption coefficients (almost like a black

body). The adjustable box-wing model considers instantaneous re-radiated heat but not the heat transfer within the satellite body. Here an analysis of the heating and cooling effects acting on GPS satellites could be performed to try to obtain the key parameter or a small set of parameters driving these forces which could be estimated from GPS tracking data. Alternatively these effects could be considered only as a priori accelerations.

- I-8 The magnitude of the pseudo-stochastic pulses was decreased when using the adjustable box-wing model instead of the CODE model, especially in the radial component as shown in Fig. 7 of P-II. The use of stronger constraints for the pseudo-stochastic pulses (currently 10^{-6} , 10^{-6} , and 10^{-9} m/s respectively for the radial, along- and cross-track components) or the possibility to eliminate them from the orbit determination process could be investigated. This, would allow to have more physical orbits but the errors currently absorbed by the pseudo-stochastic pulses need to be understood and compensated.
- I-9 For GPS-IIR satellites the short yaw maneuvers (which are very close to nominal attitude) only appear when the hardware yaw rate is exceeded, i.e, for $|\beta_0| < 2.4^\circ$ (Kouba, 2009). However, the orbit prediction errors during eclipse seasons for GPS-IIR satellites are not limited to $|\beta_0| < 2.4^\circ$ as shown in Fig. 17 of P-III. Especially the errors at the start and end of the eclipse seasons (with long penumbra passages, $|\beta_0| \approx 13.87^\circ$) could be related to the fact that the shadow of the Earth is currently modeled as a cylinder, which ignores the Earth flattening and the radiation flux during penumbra. Here, the model proposed by Adhya et al (2005) could be used.
- I-10 Just the instantaneous re-radiated heat is approximately taken into account in the adjustable box-wing model (P-II). A more detailed thermal force modeling (see e.g., Vigue et al, 1994; Adhya et al, 2005) could improve the errors observed in days with long eclipses ($\beta_0 \approx 0^\circ$), see Fig. 17 of P-III. This also complements I-7.
- I-11 Besides the possible model improvements mentioned in I-9 and I-10 to reduce orbit errors during eclipse seasons, the specific solar panel orientation of GPS-IIR and GLONASS-M satellites during eclipses (currently unknown) might be a candidate for dedicated investigations.
- I-12 The adjustable box-wing models for GLONASS satellites could be further investigated and if possible refined. For example, the parameter constraints (see Section 6 of P-II) which were initially selected for GPS satellites may not be the best ones for GLONASS satellites.
- I-13 The adjustable box-wing model approach could also be applied to other GNSS satellites like Galileo or BeiDou satellites, see also Section 5.1.5.

4 Appendix: additional results

4.1 SLR orbit validation

Satellite Laser Ranging (SLR) measurements are available for the two GPS satellites SVN 35 and SVN 36 that are equipped with laser retro reflector arrays and for several GLONASS satellites. A SLR orbit validation was done for the years 2004-2010 and for two GNSS orbit solutions, one with the CODE (5-parameter) radiation pressure model and one with the adjustable box-wing model. Some of the results of this Section were already presented in the following poster:

Rodriguez-Solano C.J., Hugentobler U., Steigenberger P., Sosnica K., Fritsche M.
 Non-conservative GNSS satellite modeling: long-term orbit behavior.
 European Geosciences Union General Assembly 2012, Poster, 2012.

The GNSS orbit solutions were computed during this dissertation while the SLR orbit validation was computed by Krzysztof Sosnica of the Astronomisches Institut, Universität Bern. In the above poster, SLR validation results were presented for GPS and GLONASS orbits, however later tests showed that there was a problem in the computation of GLONASS orbits with the CODE model, making the SLR residuals to look much worse as they could actually be when using the CODE model. This problem was identified and corrected before computing the GLONASS orbits for P-III and P-IV. The publications P-I and P-II are unaffected as GPS-only solutions were computed there. Nevertheless in this Section only SLR orbit validation results are presented for GPS satellites.

Satellite Laser Ranging provides an independent accuracy measurement for the computed GNSS orbits, mainly for the radial component. Therefore, it is very useful to do an orbit validation with this technique in order to identify systematic errors in the GNSS orbits. As mentioned in Section 1.2.3, the SLR-GPS bias was reduced by about 16 mm, i.e., from -23.6 to -6.8 mm for SVN 35 and from -26.1 to -10.1 mm for SVN 36 during the year 2007 after including Earth radiation pressure and antenna thrust in the computation of GPS orbits. For obtaining these results the CODE (5-parameter) radiation pressure model was used to compensate the effects

Table 4.1: SLR residuals (mean \pm standard deviation in mm) for the GPS-IIA satellites SVN 35 and SVN 36 during the years 2004-2010.

Satellite	Model	$ \beta_0 > 14^\circ$	All SLR data	$ \beta_0 \leq 14^\circ$
SVN 35	CODE	-14.99 ± 21.72	-14.49 ± 22.36	-10.54 ± 26.55
SVN 35	BOXW	-3.82 ± 21.70	-4.13 ± 23.75	-6.67 ± 35.91
SVN 36	CODE	-15.63 ± 21.90	-15.21 ± 22.05	-12.16 ± 22.83
SVN 36	BOXW	-5.94 ± 21.09	-6.45 ± 24.17	-9.92 ± 39.34

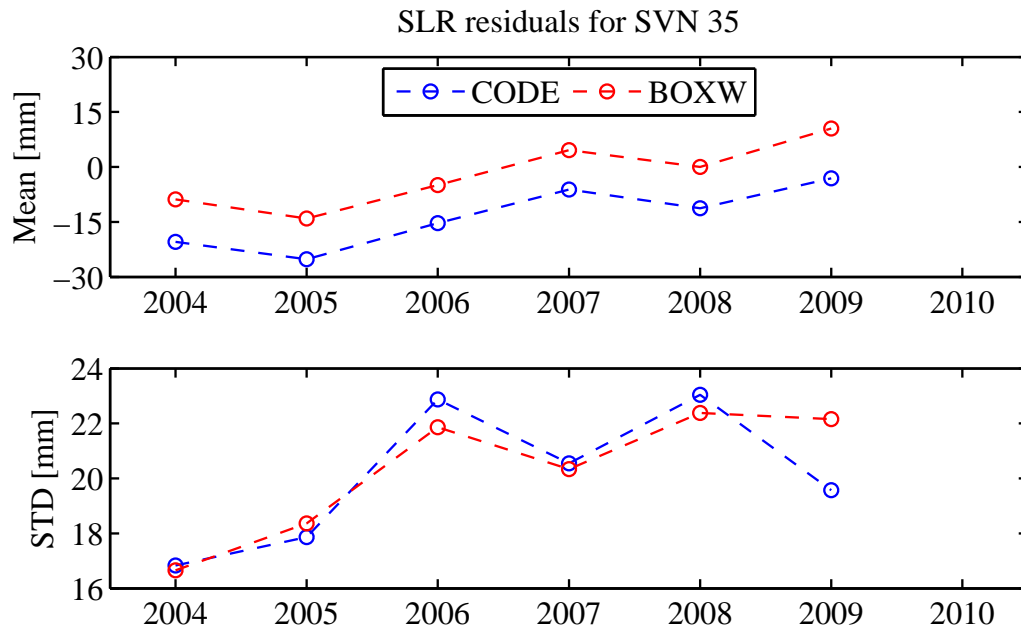


Fig. 4.1: SLR residuals (mean and standard deviation) for SVN 35 as a function of year. Only data outside eclipse seasons ($|\beta_0| > 14^\circ$) has been used.

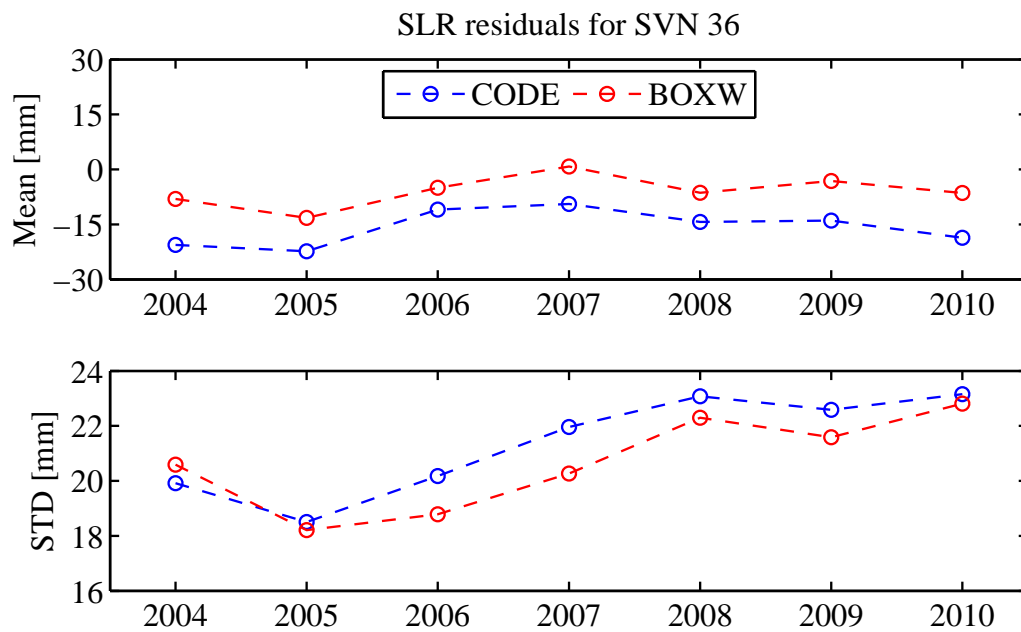


Fig. 4.2: SLR residuals (mean and standard deviation) for SVN 36 as a function of year. Only data outside eclipse seasons ($|\beta_0| > 14^\circ$) has been used.

of solar radiation pressure. If this model is exchanged by the adjustable box-wing mode and considering only the year 2007 the SLR-GPS bias is reduced from -6.3 to +3.8 mm for SVN 35 and from -8.7 to +0.9 mm for SVN 36, including data outside and inside eclipse seasons. There are small differences to the previous remaining SLR-GPS bias of -6.8 and -10.1 mm since different GPS processing strategies were used. For the results of Section 1.2.3 the strategy of Steigenberger et al (2006, 2011) was used while for the results of this Section the strategy of Fritsche et al (2013) was used. The major differences of the second approach w.r.t. the first one are: 1) updated standards, 2) GPS+GLONASS solutions instead of GPS-only, and 3) different and more ground tracking stations. Considering all the years available (2004-2010), the adjustable box-wing model reduces the SLR-GPS bias by 9-10 mm w.r.t. the CODE (5-parameter) radiation pressure model but increases the standard deviation, see Table 4.1. Earth radiation pressure and antenna thrust were included in both orbit solutions as a priori accelerations. In Table 4.1 the mean and standard deviation were also computed for data outside eclipse seasons ($|\beta_0| > 14^\circ$) and for data inside eclipse seasons ($|\beta_0| \leq 14^\circ$). With this separation of the data it can be observed that the standard deviation mainly increases during eclipse seasons when using the adjustable box-wing model with nominal yaw attitude. This problem of the adjustable box-wing model, especially for GPS-IIA satellites, is known and mentioned in P-II and P-III. Both SVN 35 and SVN 36 are GPS-IIA satellites. The orbits generated with the adjustable box-wing model upgraded to use non-nominal yaw attitude (P-III) were not yet compared to SLR measurements, with this upgraded model an improvement can be expected for the SLR residuals during eclipse seasons. Outside eclipse seasons the standard deviation almost does not change for SVN 35 and it even slightly decreases for SVN 36 when using the adjustable box-wing model as shown in Table 4.1. If the mean and standard deviation of the SLR residuals are computed per year (for data outside eclipse seasons) and not for the whole time period 2004-2010, the improvement in the standard deviation with the adjustable box-wing model is more clear as shown in Figures 4.1 and 4.2. For most years the standard deviation decreases, for the year 2009 of SVN 35 the standard deviation has a large increase, this year however has about one third of the number of SLR normal points as the other years since SVN 35 was decommissioned during 2009. It is also interesting to note that for SVN 35 the mean of the SLR residuals tends to increase over the years for both solutions while for SVN 36 there are variations in the mean but not an increase over the years. Moreover, as shown in Figures 4.1 and 4.2 the standard deviation of both satellites tends to increase over the years.

Figures 4.3, 4.4, 4.5 and 4.6 show the SLR residuals plotted as a function of the Sun elevation angle above the orbital plane (β_0) and the argument of latitude of the satellite w.r.t. the argument of latitude of the Sun (Δu), see also Fig. 1.1. In these Figures the larger SLR residuals of the adjustable box-wing model compared to the CODE model can be observed during eclipse seasons ($-14^\circ < \beta_0 < +14^\circ$). Outside eclipse seasons the adjustable box-wing model helps to reduce the dependency that the SLR residuals show w.r.t. Δu for the CODE model. This dependency is much clearer when taking the difference of the SLR residuals between the CODE and box-wing models as shown in Figures 4.7 and 4.8. Of course, this dependency also appears when looking at the differences between orbits generated with the CODE and box-wing models in the radial component as shown in Fig. 9 of P-II. As mentioned in P-II, the Δu variation in the radial orbit differences is a missing feature of the CODE model, as this model fits very well the GPS tracking data but the resulting acceleration (Fig. 11 of P-II) has poor physical meaning.

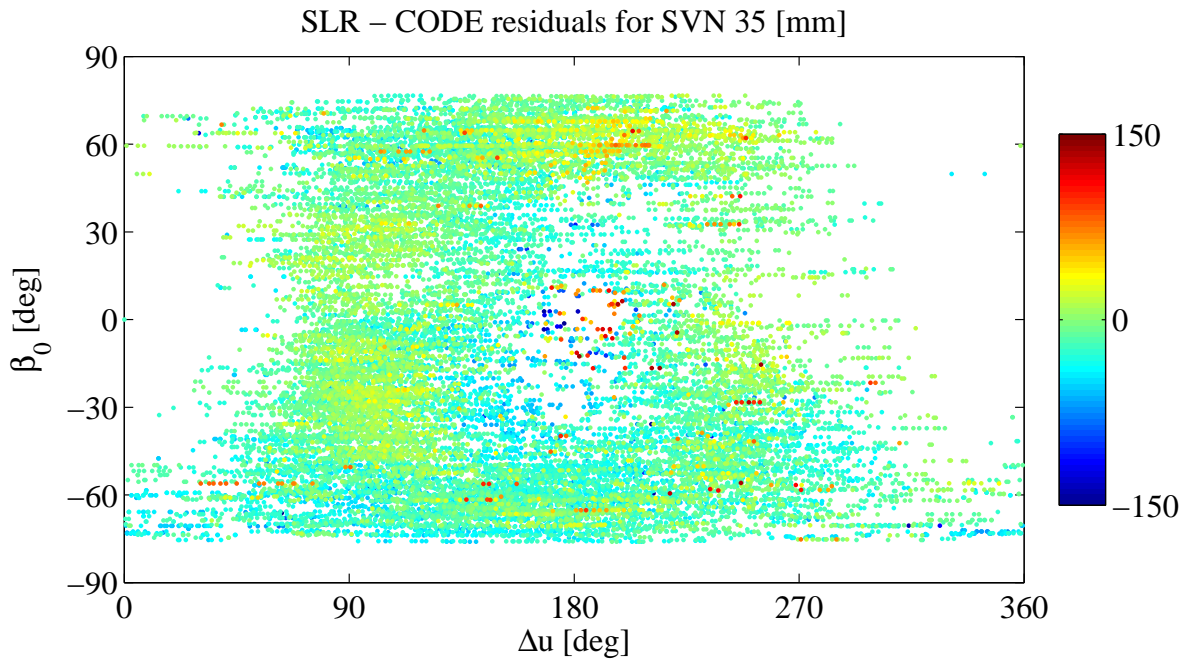


Fig. 4.3: SLR residuals as function of β_0 and Δu for SVN 35 and for the CODE (5-parameter) radiation pressure model during the years 2004-2010.

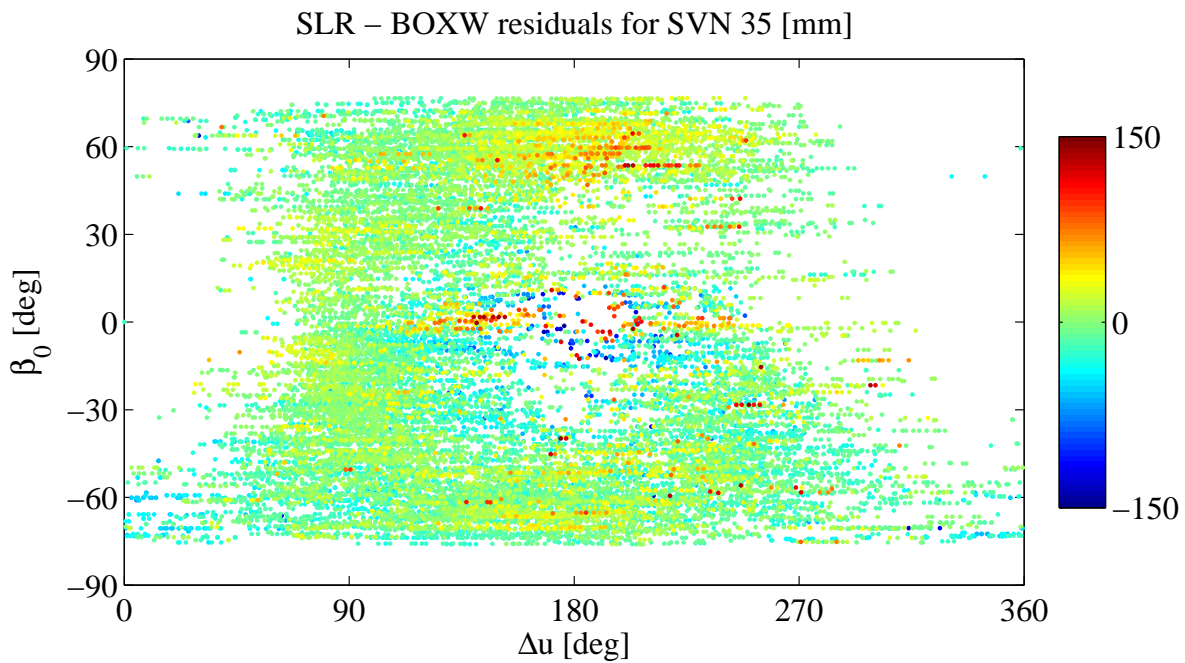


Fig. 4.4: SLR residuals as function of β_0 and Δu for SVN 35 and for the adjustable box-wing model during the years 2004-2010.

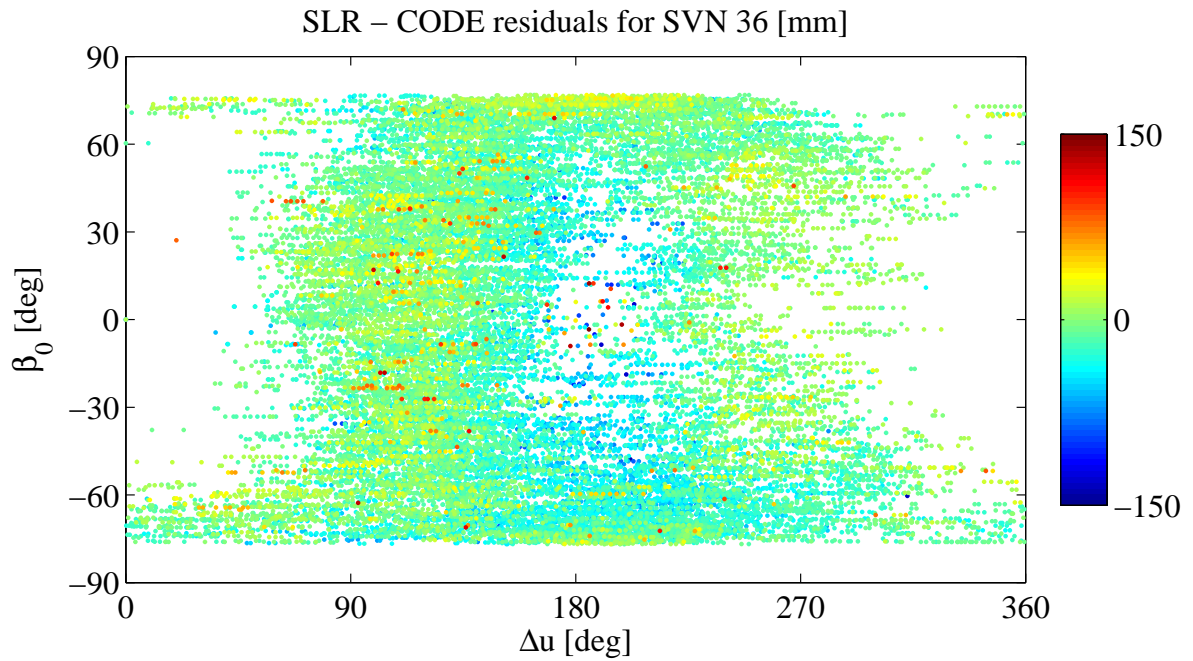


Fig. 4.5: SLR residuals as function of β_0 and Δu for SVN 36 and for the CODE (5-parameter) radiation pressure model during the years 2004-2010.

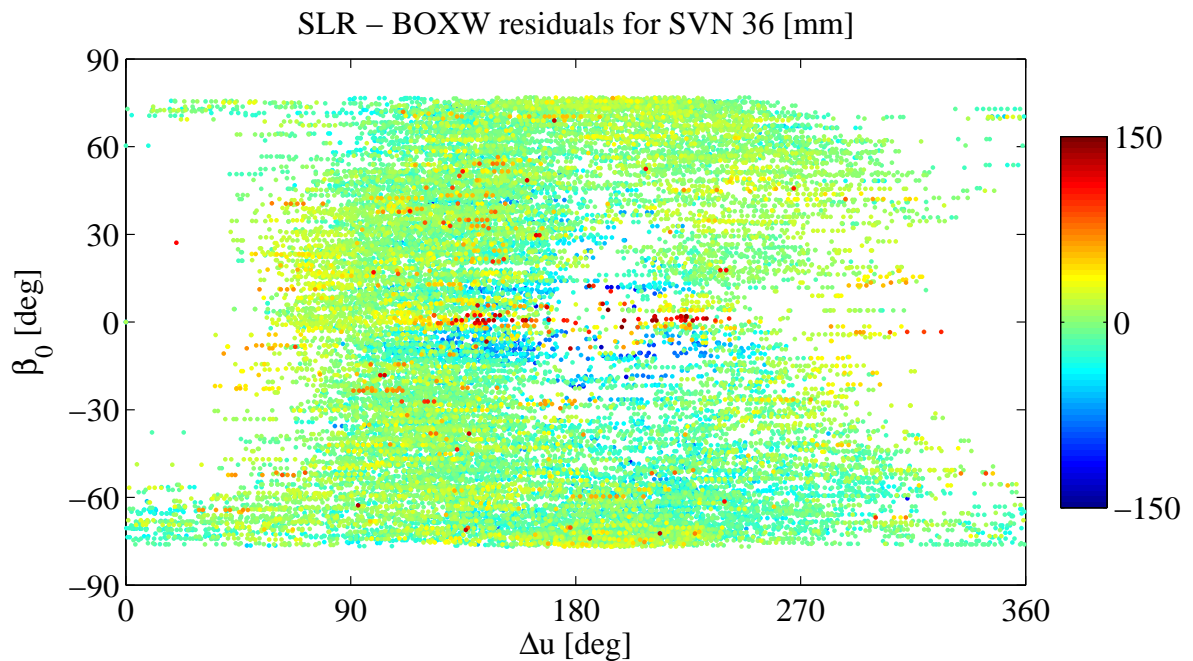


Fig. 4.6: SLR residuals as function of β_0 and Δu for SVN 36 and for the adjustable box-wing model during the years 2004-2010.

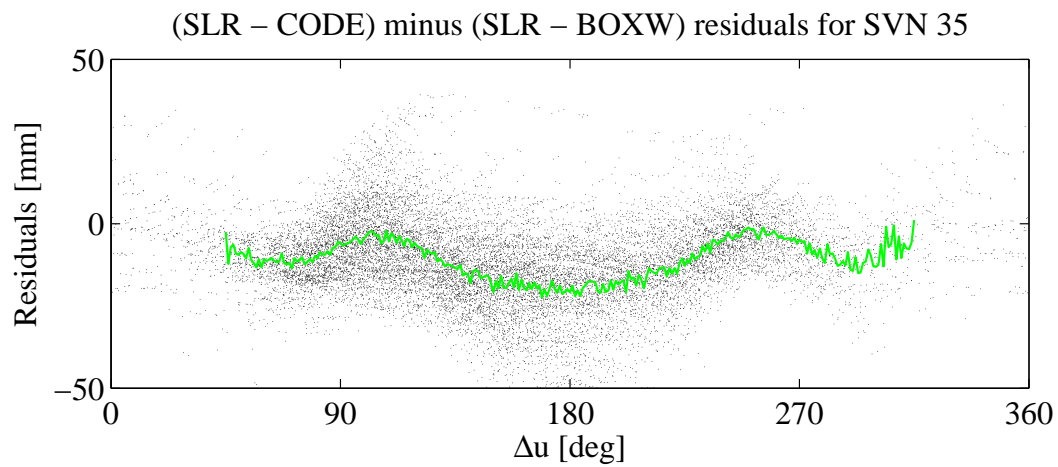


Fig. 4.7: Difference of SLR residuals (between the CODE and box-wing models) as function of Δu for SVN 35 during the years 2004-2010. The green line shows the average at one degree intervals.

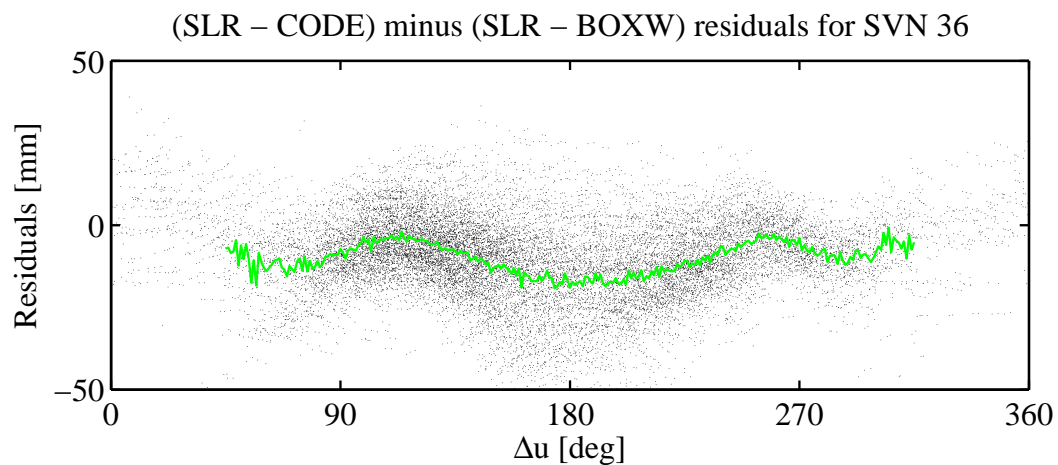


Fig. 4.8: Difference of SLR residuals (between the CODE and box-wing models) as function of Δu for SVN 36 during the years 2004-2010. The green line shows the average at one degree intervals.

4.2 GLONASS box-wing model

The adjustable box-wing model for GPS satellites is described in Section 4 of P-II. This model is valid for satellites whose surfaces can be simplified to be flat. The bus of GLONASS and GLONASS-M satellites have a characteristic cylindrical shape. Therefore for these satellites actually cylinder-wing models were constructed as mentioned in Section 5 of P-III. The explicit formulation of the adjustable cylinder-wing model is given here, following the steps of Section 4 of P-II. The only surfaces of the satellite that are affected by this change are the $\pm Y$ and $\pm X$ surfaces, see Figures 5.6 and 5.7.

The acceleration produced by the physical interaction between the solar radiation and a cylindrical surface of the satellite is formulated by Fliegel et al (1992), and can be written in the following way:

$$\vec{f} = -\frac{A}{M} \frac{S_0}{c} \cos \theta \left[(1 - \rho) \vec{e}_D + \left(\frac{\pi}{6} \delta + \frac{4}{3} \rho \cos \theta \right) \vec{e}_N \right], \quad (4.1)$$

with:

$$\alpha + \rho + \delta = 1, \quad (4.2)$$

where:

- A Cross section area of the cylinder (perpendicular to the cylinder's axis),
- M Mass of the satellite,
- S_0 Solar irradiance at 1 AU ($\approx 1367 \text{ W/m}^2$),
- c Velocity of light in vacuum,
- α Fraction of absorbed photons,
- ρ Fraction of reflected photons,
- δ Fraction of diffusely scattered photons,
- \vec{e}_D Direction of the Sun from the satellite,
- \vec{e}_N Normal to the satellite surface ($\pm Y$ and $\pm X$, perpendicular to the cylinder's axis),
- $\cos \theta = \vec{e}_D \cdot \vec{e}_N$, valid only if $\cos \theta \geq 0$.

Fliegel et al (1992) mention that to a good approximation the energy absorbed by the satellite bus surfaces is instantaneously re-radiated in the form of heat. Considering that this energy is radiated back to space according to Lamberts law, one gets:

$$\vec{f} = -\frac{A}{M} \frac{S_0}{c} \cos \theta \frac{\pi}{6} \alpha \vec{e}_N, \quad (4.3)$$

and by adding the instantaneous re-radiated heat to Eq. (4.1), it can be written in the following way:

$$\vec{f} = -\frac{A}{M} \frac{S_0}{c} \cos \theta \left[(\alpha + \delta) \left(\vec{e}_D + \frac{\pi}{6} \vec{e}_N \right) + \frac{4}{3} \rho \cos \theta \vec{e}_N \right]. \quad (4.4)$$

This last equation is only valid for perfectly cylindrical surfaces. The $\pm Y$ and $\pm X$ surfaces of the GLONASS and GLONASS-M satellites also contain some relevant amount of flat surfaces, see Figures 5.6 and 5.7. For these surfaces the ratio of the sum of cylindrical areas w.r.t. sum of flat areas is given in the "shape" column, where 0 indicates flat and 1 indicates cylindrical, see

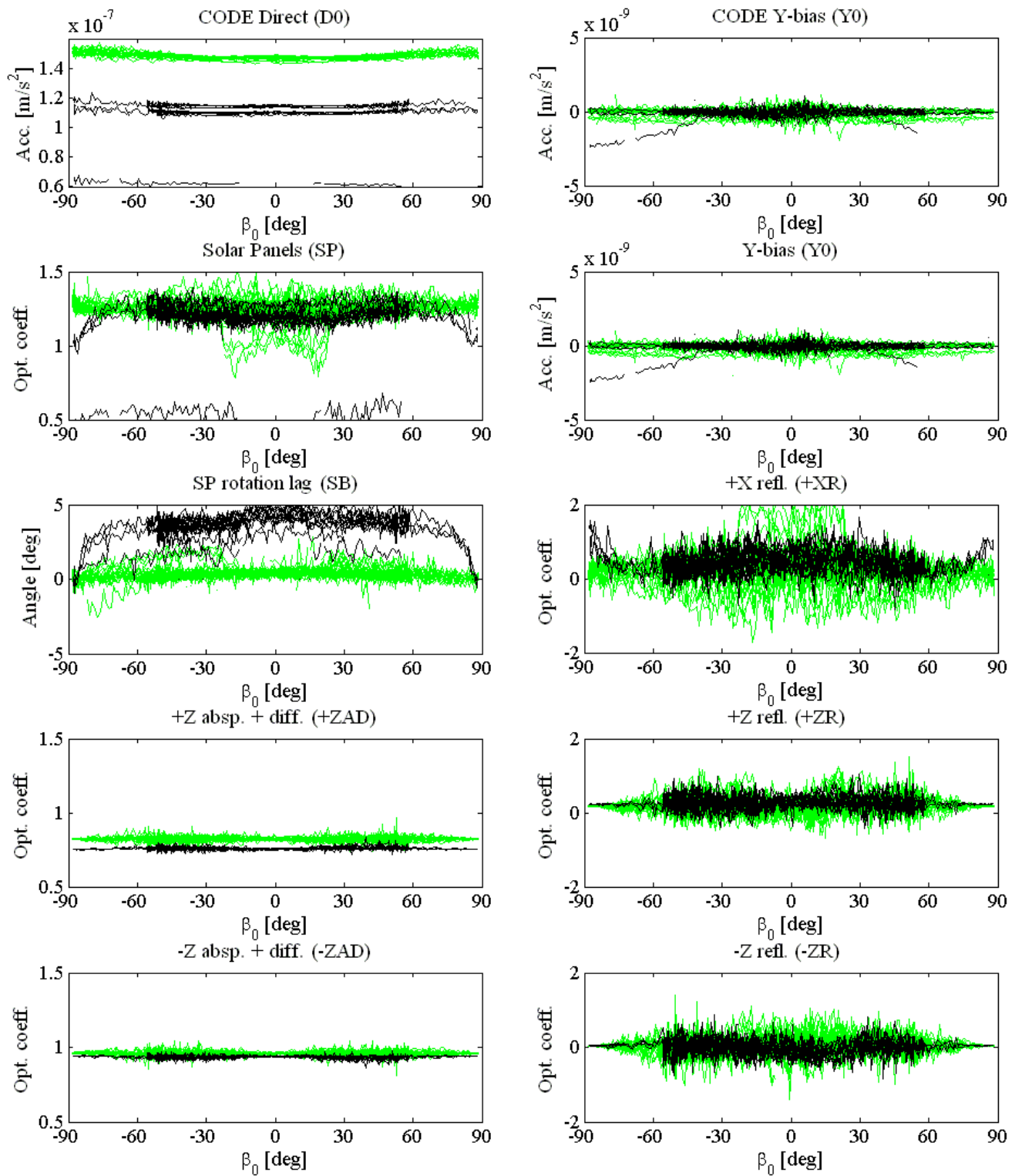


Fig. 4.9: Estimated parameters of the box-wing model for GLONASS satellites in 2007 and 2008, +XAD is not shown since there is not significant variation w.r.t. the a priori value. Estimated D_0 and Y_0 parameters of the CODE empirical model are shown (at the top) for comparison. GLONASS satellites are shown in black and GLONASS-M in green.

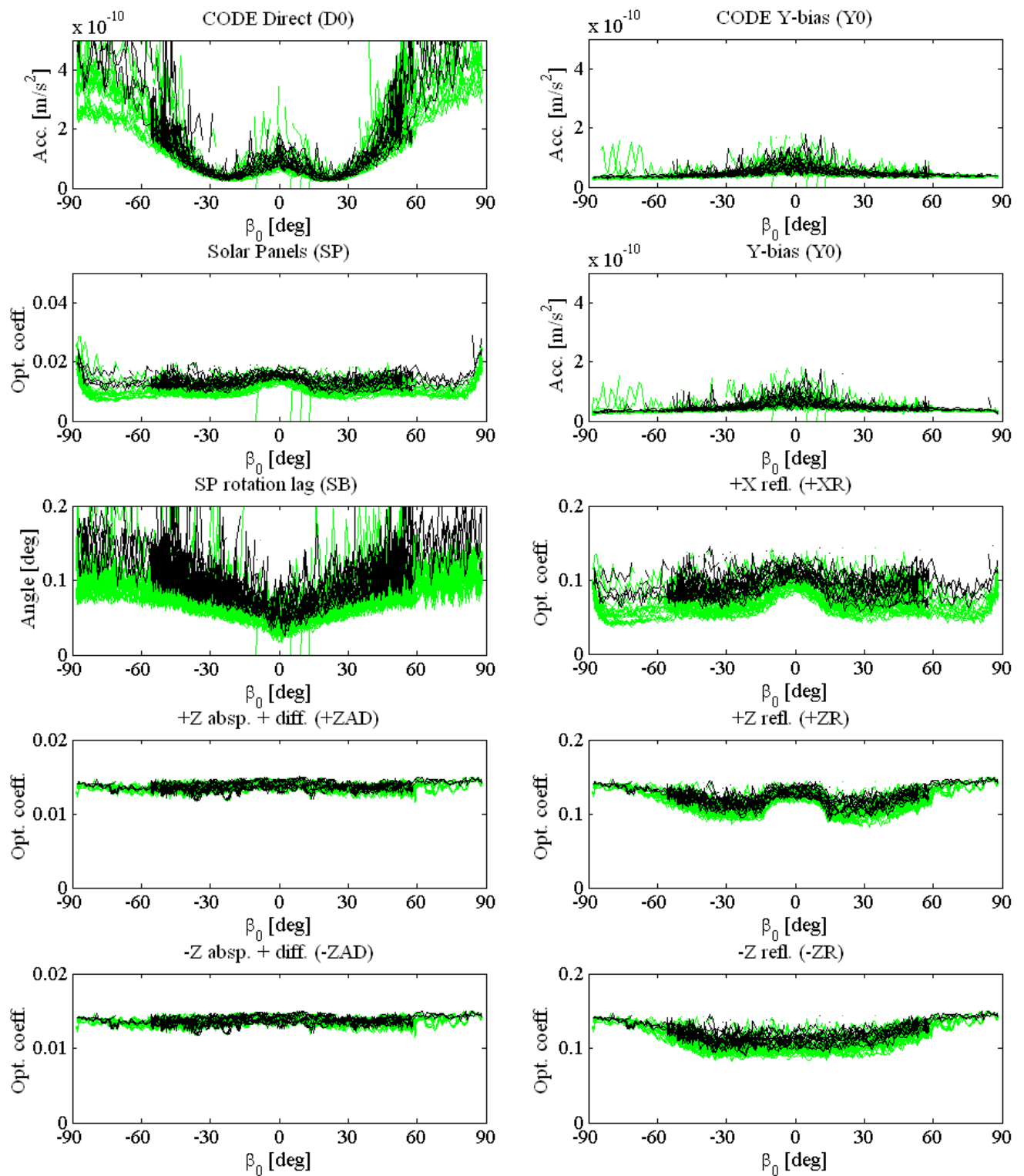


Fig. 4.10: A posteriori formal errors of the estimated parameters of the CODE and box-wing models (see Fig. 4.9). GLONASS satellites are shown in black and GLONASS-M in green.

Tables 5.6 and 5.7. The total acceleration acting on the $\pm Y$ and $\pm X$ surfaces can be written as the sum of the respective accelerations for flat (Eq. 9 of P-II) and cylindrical surfaces (Eq. 4.4) weighted with the “shape” factor (abbreviated here as “s”):

$$\vec{f} = -\frac{A}{M} \frac{S_0}{c} \cos \theta \left[(\alpha + \delta) \left(\vec{e}_D + \left(\frac{\pi}{6}s + \frac{2}{3}(1-s) \right) \vec{e}_N \right) + \left(\frac{4}{3}s + 2(1-s) \right) \rho \cos \theta \vec{e}_N \right]. \quad (4.5)$$

The partial derivatives of the acceleration w.r.t. the optical properties of the $+X$ surface under nominal attitude conditions (when this surface is always illuminated by the Sun) is:

$$\frac{\partial \vec{f}}{\partial (\alpha + \delta)} = -\frac{A_{+X}}{M} \frac{S_0}{c} \sin \epsilon \left(\vec{e}_D + \left(\frac{\pi}{6}s + \frac{2}{3}(1-s) \right) \vec{e}_{+X} \right), \quad (4.6)$$

$$\frac{\partial \vec{f}}{\partial \rho} = -\frac{A_{+X}}{M} \frac{S_0}{c} \sin^2 \epsilon \left(\frac{4}{3}s + 2(1-s) \right) \vec{e}_{+X}. \quad (4.7)$$

where ϵ is angle the formed by Earth, satellite and Sun shown in Fig. 1.1. The a priori mass, dimensions and optical properties for GLONASS and GLONASS-M are given in Tables 5.6 and 5.7 respectively. The constrains used for the parameters of the box-wing model are the same as for GPS satellites, see Section 6 of P-II. The impact on the GLONASS-M orbits by using the adjustable box-wing model was analyzed in terms of orbit overlaps and prediction errors in Sections 7 and 8 of P-III.

The estimated box-wing parameters and a posteriori errors for GLONASS satellites as function of β_0 , the Sun elevation angle above the orbital plane, are given in Figures 4.9 and 4.10. These are the equivalents of Figures 5 and 6 of P-II for GPS satellites. The estimated parameters and formal errors contain strong oscillations, e.g. for the estimated solar panel rotation lag (SB) the signal has a period of about 8 days while for the respective formal errors the period is of about 4 days. This is related to the repeat period of the GLONASS ground tracks which is 8 sidereal days, see also O-9 of Section 3.2.

The solar panel rotation lag angle is about 4° for GLONASS and 0.5° for GLONASS-M. As in the case of GPS satellites where the solar panel rotation lag is about 1.5° for GPS-IIA and 0.5° for GPS-IIR, for GLONASS satellites also the older block type shows a larger rotation lag angle of the solar panels.

Most of the estimated box-wing parameters are very similar for different satellites, however three satellites (SVNs: 701, 713 and 783) show special behaviors during the years 2007-2008. SVN 701 and SVN 713 (both GLONASS-M satellites) show an special behavior for $|\beta_0| < 22.5^\circ$ clearly visible in the the solar panels scaling factor where some values are reduced to about 1. It is interesting to note that this β_0 regime is larger than the one for eclipse seasons ($|\beta_0| < 14.5^\circ$). A different attitude than the nominal could be suspected as the cause of the behavior of SVN 701 and SVN 713 for $|\beta_0| < 22.5^\circ$. SVN 783, a GLONASS (old type) satellite shows a solar panel scaling factor close to 0.5, a rotation lag angle of about 2° and a Y-bias acceleration with a strong dependency on β_0 reaching almost $-2.5 \times 10^{-9} \text{ m/s}^2$ for $\beta_0 = -90^\circ$. Moreover, SVN 783 was turned off during the entire eclipse seasons as it can be seen in lack of estimates for the solar panel scaling factor for $|\beta_0| < 14.5^\circ$. For the strange behavior of SVN 783 a problem related to the solar panels could be suspected, e.g. that only one of the two solar panels was successfully deployed.

5 Appendix: a priori box-wing models

5.1 Definitions

5.1.1 Satellite reference frame

The dimensions and optical properties of the surfaces of the a priori box-wing models are given in the satellite XYZ reference frame shown in the figure below, see also Fig. 1.1. The XYZ frame is orthogonal and right-handed, it is fixed w.r.t. to the bus (body) of the satellite and it is defined as follows:

- Z opposite to the radial direction, pointing towards the center of the Earth,
- Y parallel to the rotation axis of solar panels,
- X normal to the surface of the satellite which is always illuminated by the Sun.

Additionally, the normal to the solar panels points towards the Sun.

Under nominal yaw attitude conditions the Sun only moves in the half-plane formed by the $+Z$, $+X$ and $-Z$ vectors. As the Sun moves, the solar panels rotate around Y to be perpendicular to the Sun. See also Sections 4 and 5 of P-III for a more detail discussion on the nominal yaw attitude and on the implications for the solar radiation pressure computation under non-nominal yaw attitude conditions.

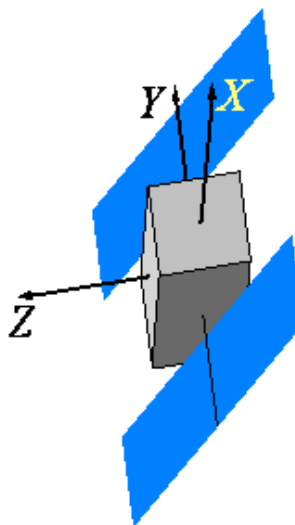


Fig. 5.1: Satellite body-fixed reference frame.

5.1.2 Optical properties

The optical properties of the satellite surfaces are divided into:

- α absorption coefficient, fraction of absorbed photons,
- δ reflection coefficient, fraction of reflected photons,
- ρ diffusion coefficient, fraction of diffusely scattered photons,

according to Milani et al (1987) and with $\alpha + \delta + \rho = 1$.

The optical properties given here are only valid for visible radiation, i.e., the a priori box-wing models are only valid for the computation of solar radiation pressure. For the computation of Earth radiation pressure the optical properties in the infrared as well as for the back of the solar panels (visible and infrared) are required. Approximate values for these optical properties are given in the Master thesis of the author, see Section 1.2.3.

5.1.3 Surfaces shape

The dimensions presented here were obtained by computing a simple average of the area of all elements (flat and cylindrical) contributing to a given surface. The optical properties were weighted according to the area of the respective elements. For most satellite surfaces the contribution of cylindrical surfaces (e.g. antennas) was small enough to simplify the surfaces as purely flat. Just in the case of GLONASS and GLONASS-M satellites, the distinction was made between flat and cylindrical surfaces as the bus of these satellites have a characteristic cylindrical shape. For these satellites the ratio of the sum of cylindrical areas w.r.t. sum of flat areas is given in the “shape” column, where 0 indicates flat and 1 indicates cylindrical. This information was used for the computation of solar radiation pressure as described in Section 4.2.

5.1.4 GPS-I, GPS-IIF and GLONASS-K

During this dissertation box-wing models were created for all GPS and GLONASS satellite types. However, just the GPS-IIA, GPS-IIR, GLONASS and GLONASS-M box-wing models were tested in P-II and P-III, as these satellite types have been the most common ones in the GPS and GLONASS constellations. For older or newer satellite types like GPS-I, GPS-IIF and GLONASS-K box-wing models were created but not tested. These box-wing models are nevertheless included here as they can be useful for future research studies or reprocessing efforts.

5.1.5 Galileo and BeiDou

A priori box-wing models for Galileo and BeiDou satellites are not provided in this Appendix. Nevertheless, they can be simply constructed from approximate dimensions (available at http://igs.org/mgex/Status_GAL.htm and http://igs.org/mgex/Status_BDS.htm) and by using the same assumptions as Section 7.1 of Ziebart (2001) for the optical properties of the satellite surfaces.

5.2 GPS-I

Information sources:

- Dimensions: Fliegel et al (1992), Feltens (1991).
- Optical properties: Fliegel et al (1992).

Table 5.2: A priori box-wing model for GPS-I satellites (mass = 450 kg for SVNs: 03, 04 and 06, mass = 520 kg for SVNs: 08, 09, 10 and 11).

Surface	Area [m ²]	α	δ	ρ
+Z bus	1.510	0.140	0.215	0.645
-Z bus	1.510	0.535	0.093	0.372
+Y bus	2.275	0.393	0.146	0.461
-Y bus	2.275	0.393	0.146	0.461
+X bus	2.047	0.432	0.134	0.434
-X bus	2.047	0.432	0.134	0.434
Solar panels	6.053	0.722	0.042	0.236



Fig. 5.2: GPS-I satellite (Strom, 2002).

5.3 GPS-IIA

Information sources:

- Dimensions: Fliegel et al (1992), Feltens (1991), Wübbena et al (2007), Bar-Sever et al (2009).
- Optical properties: Fliegel et al (1992).
- Section 5 of P-II.

Table 5.3: A priori box-wing model for GPS-II/IIA satellites (mass = 880 kg/975 kg, respectively).

Surface	Area [m ²]	α	δ	ρ
+Z bus	2.881	0.440	0.448	0.112
-Z bus	2.881	0.582	0.335	0.083
+Y bus	3.383	0.511	0.391	0.098
-Y bus	3.383	0.511	0.391	0.098
+X bus	2.719	0.500	0.400	0.100
-X bus	2.719	0.500	0.400	0.100
Solar panels	11.851	0.746	0.057	0.197

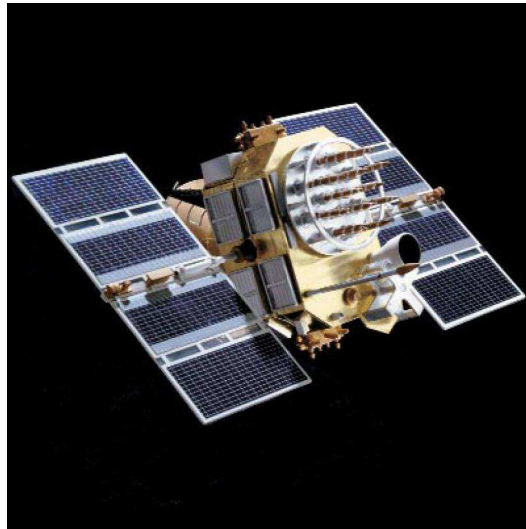


Fig. 5.3: GPS-IIA satellite (Yinger, 2002).

5.4 GPS-IIR

Information sources:

- Dimensions: Fliegel and Gallini (1996).
- Optical properties: Fliegel and Gallini (1996).
- Section 5 of P-II.

Table 5.4: A priori box-wing model for GPS-IIR satellites (mass = 1100 kg).

Surface	Area [m ²]	α	δ	ρ
+Z bus	4.250	0.940	0.060	0.000
-Z bus	4.250	0.940	0.060	0.000
+Y bus	4.460	0.940	0.060	0.000
-Y bus	4.460	0.940	0.060	0.000
+X bus	4.110	0.940	0.060	0.000
-X bus	4.110	0.940	0.060	0.000
Solar panels	13.920	0.707	0.044	0.249



Fig. 5.4: GPS-IIR satellite (Lockheed Martin).

5.5 GPS-IIF

Information sources:

- Dimensions: unpublished document.
- Optical properties: same assumptions as Section 7.1 of Ziebart (2001).

Table 5.5: A priori box-wing model for GPS-IIF satellites (mass = 1555 kg).

Surface	Area [m ²]	α	δ	ρ
+Z bus	5.400	0.440	0.448	0.112
-Z bus	5.400	1.000	0.000	0.000
+Y bus	7.010	0.440	0.448	0.112
-Y bus	7.010	0.440	0.448	0.112
+X bus	5.720	0.440	0.448	0.112
-X bus	5.720	0.440	0.448	0.112
Solar panels	22.250	0.770	0.035	0.195



Fig. 5.5: GPS-IIF satellite (The Boeing Company).

5.6 GLONASS

Information sources:

- Dimensions: Revnivykh and Mitrikas (1998)
- Optical properties: same assumptions as Section 7.1 of Ziebart (2001).
- Section 5 of P-III.

Table 5.6: A priori box-wing model for GLONASS satellites (mass = 1415 kg).

Surface	Shape	Area [m ²]	α	δ	ρ
+Z bus	0.000	1.662	0.374	0.381	0.245
-Z bus	0.000	1.662	0.705	0.236	0.059
+Y bus	0.494	5.123	0.440	0.448	0.112
-Y bus	0.494	5.123	0.440	0.448	0.112
+X bus	0.620	3.310	0.440	0.448	0.112
-X bus	0.620	3.310	0.440	0.448	0.112
Solar panels	0.000	23.616	0.770	0.035	0.195



Fig. 5.6: GLONASS satellite (<http://www.russianspaceweb.com>).

5.7 GLONASS-M

Information sources:

- Dimensions: Mitrikas (2005)
- Optical properties: same assumptions as Section 7.1 of Ziebart (2001).
- Section 5 of P-III.

Table 5.7: A priori box-wing model for GLONASS-M satellites (mass = 1415 kg).

Surface	Shape	Area [m ²]	α	δ	ρ
+Z bus	0.000	2.120	0.409	0.416	0.175
-Z bus	0.000	2.120	0.791	0.167	0.042
+Y bus	0.550	6.000	0.440	0.448	0.112
-Y bus	0.550	6.000	0.440	0.448	0.112
+X bus	0.728	4.530	0.440	0.448	0.112
-X bus	0.728	4.530	0.440	0.448	0.112
Solar panels	0.000	30.850	0.770	0.035	0.195



Fig. 5.7: GLONASS-M satellite (<http://www.russianspaceweb.com>).

5.8 GLONASS-K

Information sources:

- Dimensions: Mitrikas (personal communication, 2011).
- Optical properties: same assumptions as Section 7.1 of Ziebart (2001).

Table 5.8: A priori box-wing model for GLONASS-K satellites (mass = 935 kg).

Surface	Area [m ²]	α	δ	ρ
+Z bus	1.730	0.402	0.409	0.189
-Z bus	1.730	0.540	0.368	0.092
+Y bus	4.350	0.440	0.448	0.112
-Y bus	4.350	0.440	0.448	0.112
+X bus	2.210	0.440	0.448	0.112
-X bus	2.210	0.440	0.448	0.112
Solar panels	16.960	0.770	0.035	0.195



Fig. 5.8: GLONASS-K satellite (<http://www.russianspaceweb.com>).

6 Bibliography

- Adhya S, Ziebart M, Sibthorpe A, Arrowsmith P, Cross P (2005) Thermal Force Modeling for Precise Prediction and Determination of Spacecraft Orbits. *Navig J Inst Navig* 52(3):131–144
- Amiri-Simkooei AR (2007) Least-squares variance component estimation: theory and GPS applications. PhD thesis, Delf University of Technology, Publications on Geodesy 64, Netherlands Geodetic Commission, URL <http://www.ncg.knaw.nl/Publicaties/Geodesy/pdf/64AmiriSimkooei.pdf>
- Amiri-Simkooei AR (2013) On the nature of GPS draconitic year periodic pattern in multivariate position time series. *J Geophys Res* 118(5):2500–2511, DOI 10.1002/jgrb.50199
- Bar-Sever YE (1995) Performance Evaluation of the GPS Yaw Bias Implementation. In: Proceedings of ION GPS 1995, pp 599–611
- Bar-Sever YE (1996) A new model for GPS yaw attitude. *J Geod* 70(11):714–723, DOI 10.1007/BF00867149
- Bar-Sever Y (1997) New and Improved Solar Radiation Models for GPS Satellites Based on Flight Data. Final Report, Jet Propulsion Laboratory, prepared for Air Force Materiel Command SMC/CZSF, URL <http://www.dtic.mil/cgi-bin/GetTRDoc?AD=ADA485820>
- Bar-Sever Y, Kuang D (2004) New Empirically Derived Solar Radiation Pressure Model for GPS Satellites. In: Interplanetary Network Progress Report, vol 42-159, URL http://ipnpr.jpl.nasa.gov/progress_report/42-159/title.htm
- Bar-Sever Y, Kuang D (2005) New Empirically Derived Solar Radiation Pressure Model for GPS Satellites During Eclipse Seasons. In: Interplanetary Network Progress Report, vol 42-160, URL http://ipnpr.jpl.nasa.gov/progress_report/42-160/title.htm
- Bar-Sever Y, Davis JL, Dach R, Flohrer C, Herring T, Ray J, Slater JA, Thaller D (2009) Impact of SLR tracking on GPS. In: Pavlis EC (ed) International Technical Laser Workshop on SLR Tracking of GNSS Constellations. Position Paper, URL http://acc.igs.org/orbits/slr_track_gps_ilrs09-PP.pdf,
- Berthias JP, Broca P, Ferrier C, Guitart A, Houry S, Mercier F, Piuze A, Labbez L (2002) JASON-1: a new reference for precise orbit determination. In: IAF Abstracts, 34th COSPAR Scientific Assembly, The Second World Space Congress
- Beutler G, Brockmann E, Gurtner W, Hugentobler U, Mervart L, Rothacher M, Verdun A (1994) Extended orbit modeling techniques at the CODE processing center of the International GPS Service for Geodynamics (IGS): theory and initial results. *Manuscr Geod* 19(6):367–386
- Beutler G, Brokmann E, Hugentobler U, Mervart L, Rothacher M, Weber R (1996) Combining consecutive short arcs into long arcs for precise and efficient GPS Orbit Determination. *J Geod* 70(5):287–299, DOI 10.1007/BF00867349
- Beutler G, Jäggi A, Hugentobler U, Mervart L (2006) Efficient satellite orbit modelling using pseudo-stochastic parameters. *J Geod* 80(7):353–372, DOI 10.1007/s00190-006-0072-6

- Bizouard C, Gambis D (2009) The Combined Solution C04 for Earth Orientation Parameters Consistent with International Reference Frame 2005. In: Drewes H (ed) Geodetic Reference Frames, IAG Symposia 134, Springer, pp 265–270, DOI 10.1007/978-3-642-00860-3_41
- Cerri L, Berthias JP, Bertiger WI, Haines BJ, Lemoine FG, Mercier F, Ries JC, Willis P, Zelen-sky NP, Ziebart M (2010) Precision Orbit Determination Standards for the Jason Series of Altimeter Missions. *Mar Geod* 33(S1):379–418, DOI 10.1080/01490419.2010.488966
- Choi KK, Ray J, Griffiths J, Bae TS (2012) Evaluation of GPS orbit prediction strategies for the IGS Ultra-rapid products. *GPS Solut* DOI 10.1007/s10291-012-0288-2
- Collilieux X, Altamini Z, Coulot D, Ray J, Sillard P (2007) Comparison of very long baseline interferometry, GPS, and satellite laser ranging height residuals from ITRF2005 using spectral and correlation methods. *J Geophys Res* 112(B12403), DOI 10.1029/2007JB004933
- Colombo OL (1989) The Dynamics of Global Positioning Orbits and the Determination of Precise Ephemerides. *J Geophys Res* 94(B7):9167–9182, DOI 10.1029/JB094iB07p09167
- Dach R, Hugentobler U, Fridez P, Meindl M (2007) Bernese GPS Software, Version 5.0. Astro-nomical Institute, University of Bern
- Dach R, Brockmann E, Schaer S, Beutler G, Meindl M, Prange L, Bock H, Jäggi A, Ostini L (2008) GNSS processing at CODE: status report. *J Geod* 83(3-4):353–365, DOI 10.1007/s00190-008-0281-2
- Dilssner F (2010) GPS IIF-1 Satellite Antenna Phase Center and Attitude Modeling. *Inside GNSS* 5(6):59–64, URL <http://www.insidegnss.com/node/2243>
- Dilssner F, Springer T, Gienger G, Dow J (2011) The GLONASS-M satellite yaw-attitude model. *Adv Space Res* 47(1):160–171, DOI 10.1016/j.asr.2010.09.007
- Douša J (2010) The impact of errors in predicted GPS orbits on zenith troposphere delay esti-mation. *GPS Solut* 14(3):229–239, DOI 10.1007/s10291-009-0138-z
- Dow J, Neilan R, Rizos C (2009) The International GNSS Service in a changing land-scape of Global Navigation Satellite Systems. *J Geod* 83(3-4):191–198, DOI 10.1007/s00190-008-0300-3
- Duha J, Afonso GB, Damasceno Ferreira LD (2006) Thermal re-emission effects on GPS satellites. *J Geod* 80(12):665–674, DOI 10.1007/s00190-006-0060-x
- Feltens J (1991) Nicht-gravitative Störeinflüsse bei der Modellierung von GPS-Erdumlaufbahnen. Deutsche Geodätische Kommission, Reihe C, Heft Nr. 371. (In German)
- Fliegel H, Gallini T, Swift E (1992) Global Positioning System Radiation Force Model for Geodetic Applications. *J Geophys Res* 97(B1):559–568, DOI 10.1029/91JB02564
- Fliegel H, Gallini T (1996) Solar Force Modeling of Block IIR Global Positioning System Satellites. *J Spacecr Rockets* 33(6):863–866, DOI 10.2514/3.26851
- Fritsche M, Sosnica K, Rodriguez-Solano CJ, Steigenberger P, Wang K, Dietrich R, Dach R, Hugentobler U, Rothacher M (2013) Combined Reprocessing of GPS, GLONASS and SLR Observations. *J Geod*, submitted
- Froideval LO (2009) A Study of Solar Radiation Pressure Acting on GPS satellites. PhD thesis, The University of Texas at Austin, URL <http://repositories.lib.utexas.edu/handle/2152/6623>

- Griffiths J, Ray JR (2013) Sub-daily alias and draconitic errors in the IGS orbits. *GPS Solut* 17(3):413–422, DOI 10.1007/s10291-012-0289-1
- Hugentobler U, van der Marel H, Springer T (2006) Identification and mitigation of GNSS errors. In: Springer T, Gendt G, Dow JM (eds) *The International GNSS Service (IGS): "Perspectives and Visions for 2010 and beyond"*, IGS Workshop 2006
- King MA, Watson CS (2010) Long GPS coordinate time series: Multipath and geometry effects. *J Geophys Res* 115(B04403), DOI 10.1029/2009JB006543
- Knocke PC, Ries JC, Tapley BD (1988) Earth radiation pressure effects on satellites. In: *Proceedings of AIAA/AAS Astrodynamics Conference*, pp 577–587
- Kouba J (2009) A simplified yaw-attitude model for eclipsing GPS satellites. *GPS Solut* 13(1):1–12, DOI 10.1007/s10291-008-0092-1
- Kuang D, Rim HJ, Schutz BE, Abusali PAM (1996) Modeling GPS satellite attitude variation for precise orbit determination. *J Geod* 70(9):572–580, DOI 10.1007/BF00867865
- Leandro R, Landau H, Nitschke M, Glocker M, Seeger S, Chen X, Deking A, Tahar MB, Zhang F, Ferguson K, Stolz R, Talbot N, Lu G, Allison T, Brandl M, Gomez V, Kipka A (2012) Real-Time Extended GNSS Positioning: A New Generation of Centimeter Accurate Networks. *GPS World* 23(7):36–42, URL <http://editiondigital.net/publication/?i=119153>
- Marquis W, Krier C (2000) Examination of the GPS Block IIR Solar Pressure Model. In: *Proceedings of ION GPS 2000*, pp 407–415
- Marshall JA, Luthcke SB (1994) Modeling Radiation Forces Acting on Topex/Poseidon for Precision Orbit Determination. *J Spacecr Rockets* 31(1):99–105
- Meindl M (2011) Combined Analysis of Observations from Different Global Navigation Satellite Systems. PhD thesis, Astronomisches Institut der Universität Bern, *Geodätisch-geophysikalische Arbeiten in der Schweiz*, Vol. 83, URL <http://www.sgc.ethz.ch/sgc-volumes/sgk-83.pdf>
- Meindl M, Beutler G, Thaller D, Dach R, Jäggi A (2013) Geocenter coordinates estimated from GNSS data as viewed by perturbation theory. *Adv Space Res* 51(7):1047–1064, DOI 10.1016/j.asr.2012.10.026
- Milani A, Nobili AM, Farinella P (1987) *Non-gravitational perturbations and satellite geodesy*. Adam Hilger, Bristol
- Mitrikas V (2005) GLONASS-M dimensions and center-of-mass correction. IGSMail-5105, URL <http://igscb.jpl.nasa.gov/mail/igsmail/2005/msg00027.html>
- Ostini L (2012) Analysis and Quality Assessment of GNSS-Derived Parameter Time Series. PhD thesis, Astronomisches Institut der Universität Bern, URL http://www.bernese.unibe.ch/publist/2012/phd/diss_lo_4print.pdf
- Press W, Teukolsky S, Vetterling W, Flannery B (1992) *Numerical Recipes in Fortran 77: The Art of Scientific Computing*, 2nd edn. Cambridge University Press
- Ratcliff JT, Gross RS (2013) Combinations of Earth Orientation Measurements: SPACE2011, COMB2011 and POLE2011. JPL Publication 13-5, Jet Propulsion Laboratory, California Institute of Technology, URL <ftp://euler.jpl.nasa.gov/keof/combinations/2011/SpaceCombPole2011.pdf>

- Ray J, Altamini Z, Collilieux X, van Dam T (2008) Anomalous harmonics in the spectra of GPS position estimates. *GPS Solut* 12(1):55–64, DOI 10.1007/s10291-007-0067-7
- Rebischung P, Altamini Z, Springer T (2013) A collinearity diagnosis of the GNSS geocenter determination. *J Geod*, DOI 10.1007/s00190-013-0669-5
- Revnivkykh S, Mitrikas V (1998) GLONASS S/C mass and dimension. IGEXMail-0086, URL <http://igsceb.jpl.nasa.gov/mail/igexmail/1998/msg00085.html>
- Santamaría-Gómez A, Bouin MN, Collilieux X, Wöppelmann G (2011) Correlated errors in GPS position time series: Implications for velocity estimates. *J Geophys Res* 116(B01405), DOI 10.1029/2010JB007701
- Seitz M, Angermann D, Bloßfeld M, Drewes H, Gerstl M (2012) The 2008 DGF realization of the ITRS: DTRF2008. *J Geod* 86(12):1097–1123, DOI 10.1007/s00190-012-0567-2
- Sibthorpe A, Bertiger W, Desai SD, Haines B, Harvey N, Weiss JP (2011) An evaluation of solar radiation pressure strategies for the GPS constellation. *J Geod* 85(8):505–517, DOI 10.1007/s00190-011-0450-6
- Springer T, Beutler G, Rothacher M (1999) A New Solar Radiation Pressure Model for GPS Satellites. *GPS Solut* 2(3):50–62, DOI 10.1007/PL00012757
- Steigenberger P, Rothacher M, Dietrich R, Fritsche M, Rülke A, Vey S (2006) Reprocessing of a global GPS network. *J Geophys Res* 111(B05402), DOI 10.1029/2005JB003747
- Steigenberger P, Hugentobler U, Lutz S, Dach R (2011) CODE Contribution to the First IGS Reprocessing Campaign. Tech. Rep. 1/2011, IAPG/TUM, URL <https://mediatum2.ub.tum.de/doc/1078108/1078108.pdf>
- Strom SR (2002) Charting a Course Toward Global Navigation. *Crosslink - The Aerospace Corporation magazine of advances in aerospace technology* 3(2):6–11, URL <http://www.aerospace.org/wp-content/uploads/crosslink/CrosslinkV3N2.pdf>
- Tregoning P, Watson C (2009) Atmospheric effects and spurious signals in GPS analysis. *J Geophys Res* 114(B09403), DOI 10.1029/2009JB006344
- Tregoning P, Watson C (2011) Correction to “Atmospheric effects and spurious signals in GPS analysis”. *J Geophys Res* 116(B02412), DOI 10.1029/2010JB008157
- Urschl C, Beutler G, Gurtner W, Hugentobler U, Schaer S (2007) Contribution of SLR tracking data to GNSS orbit determination. *Adv Space Res* 39(10):1515–1523, DOI 10.1016/j.asr.2007.01.038
- Vigue Y, Schutz BE, Abusali PAM (1994) Thermal Force Modeling for Global Positioning System Satellites Using the Finite Element Method. *J Spacecr Rockets* 31(5):855–859, DOI 10.2514/3.26523
- Wielicki BA, Barkstrom BR, Harrison EF, Lee III RB, Smith GL, Cooper JE (1996) Clouds and the Earth’s Radiant Energy System (CERES): An Earth Observing System Experiment. *Bull Am Meteorol Soc* 77(5):853–868
- Wu JT, Wu SC, Hajj GA, Bertiger WI, Lichten SM (1993) Effects of antenna orientation on GPS carrier phase. *Manuscr Geod* 18(2):91–98
- Wübbena G, Schmitz M, Mader G, Czopek F (2007) GPS Block II/IIA Satellite Antenna Testing using the Automated Absolute Field Calibration with Robot. In: *Proceedings of ION GNSS 2007*, pp 1236 – 1243

- Yinger CH (2002) Operation and Application of the Global Positioning System. Crosslink - The Aerospace Corporation magazine of advances in aerospace technology 3(2):12–16, URL <http://www.aerospace.org/wp-content/uploads/crosslink/CrosslinkV3N2.pdf>
- Ziebart M (2001) High Precision Analytical Solar Radiation Pressure Modelling for GNSS Spacecraft. PhD thesis, University of East London, URL http://www-research.cege.ucl.ac.uk/gnrg/PhD/Marek_Ziebart%20_PhDThesis.pdf
- Ziebart M, Dare P (2001) Analytical solar radiation pressure modelling for GLONASS using a pixel array. *J Geod* 57(11):587–599, DOI 10.1007/s001900000136
- Ziebart M, Edwards S, Adhya S, Sibthorpe A, Arrowsmith P, Cross P (2004) High Precision GPS IIR Orbit Prediction using Analytical Non-conservative Force Models. In: Proceedings of ION GNSS 2004, pp 1764–1770
- Ziebart M, Adhya S, Sibthorpe A, Edwards S, Cross P (2005) Combined radiation pressure and thermal modelling of complex satellites: Algorithms and on-orbit tests. *Adv Space Res* 36(3):424–430, DOI 10.1016/j.asr.2005.01.014
- Ziebart M, Sibthorpe A, Cross P, Bar-Sever Y, Haines B (2007) Cracking the GPS - SLR Orbit Anomaly. In: Proceedings of ION GNSS 2007, pp 2033–2038
- Zumberge JF, Heflin MB, Jefferson DC, Watkins MM, Webb FH (1997) Precise point positioning for the efficient and robust analysis of GPS data from large networks. *J Geophys Res* 102(B3):5005–5017, DOI 10.1029/96JB03860

Impact of Earth radiation pressure on GPS position estimates

C. J. Rodriguez-Solano^a, U. Hugentobler^a, P. Steigenberger^a, S. Lutz^b

^a Institut für Astronomische und Physikalische Geodäsie, Technische Universität München, 80333 München, Germany

^b Astronomisches Institut, Universität Bern, 3012 Bern, Switzerland

Abstract

GPS satellite orbits available from the International GNSS Service (IGS) show a consistent radial bias of up to several cm and a particular pattern in the Satellite Laser Ranging (SLR) residuals, which are suggested to be related to radiation pressure mismodeling. In addition, orbit related frequencies were identified in geodetic time series such as apparent geocenter motion and station displacements derived from GPS tracking data. A potential solution to these discrepancies is the inclusion of Earth radiation pressure (visible and infrared) modeling in the orbit determination process. This is currently not yet considered by all analysis centers contributing to the IGS final orbits. The acceleration, accounting for Earth radiation and satellite models, is introduced in this paper in the computation of a global GPS network (around 200 IGS sites) adopting the analysis strategies from the Center for Orbit Determination in Europe (CODE). Two solutions covering nine years (2000.0 to 2009.0) with and without Earth radiation pressure were computed and form the basis for this study. In previous studies, it has been shown that Earth radiation pressure has a non-negligible effect on the GPS orbits, mainly in the radial component. In this paper the effect on the along-track and cross-track components is studied in more detail. Also in this paper it is shown that Earth radiation pressure leads to a change in the estimates of GPS ground station positions, which is systematic over large regions of the Earth. This observed “deformation” of the Earth is towards North-South and with large scale patterns that repeat six times per GPS draconitic year (350 days), reaching a magnitude of up to one millimeter. The impact of Earth radiation pressure on the geocenter and length of day estimates was also investigated,

but the effect is found to be less significant as compared to the orbits and position estimates.

Keywords: GPS; albedo; precise orbit modeling; spectra of GPS position estimates.

1 Introduction

The IGS (International GNSS Service, Dow et al, 2009) final orbits have reached an internal precision of around 2.5 cm for GPS and 5 cm for GLONASS satellites¹ from a level about an order of magnitude larger in the mid 1990s. The progress can be attributed to understanding the errors and improving the models affecting the GNSS technique, including those related to precise orbit modeling. Despite the performance attained, however, some problems remain in the orbits but as well as in the position estimates of GPS tracking stations.

The orbits of the two GPS satellites equipped with laser retro reflector arrays (LRA) show a consistent radial bias of up to several cm, when compared with the Satellite Laser Ranging (SLR) measurements, known as the GPS–SLR orbit anomaly. This bias was observed for the CODE (Center for Orbit Determination in Europe)² final orbits with a magnitude of 3–4 cm by Urschl et al (2007). More recent comparisons between GPS and SLR measurements (for various IGS analysis centers, Bar-Sever et al, 2009) show a smaller bias of 12–22 mm

¹<http://igsceb.jpl.nasa.gov/components/prods.html>, accessed on 25 August 2011.

²CODE is a consortium formed by: the Astronomical Institute of the University of Bern (AIUB, Bern, Switzerland), the Swiss Federal Office of Topography (swisstopo, Wabern, Switzerland), the Federal Agency for Cartography and Geodesy (BKG, Frankfurt am Main, Germany), and the Institut für Astronomische und Physikalische Geodäsie of the Technische Universität München (IAPG, Munich, Germany).

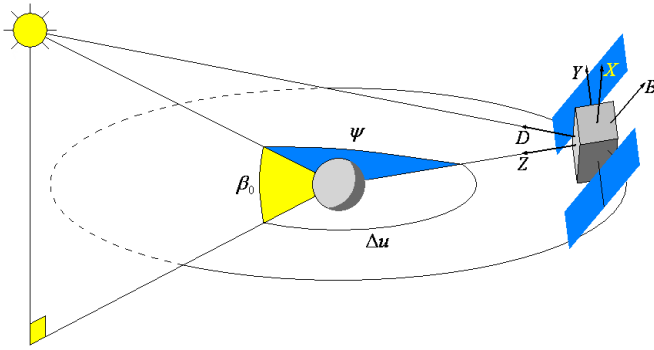


Fig. 1: Relative geometry of Sun, Earth and GPS satellite.

with associated scatters of 16–25 mm. These figures can be used as a measure of the current radial accuracy of IGS final orbits. In addition, orbit related frequencies were identified in geodetic time series such as apparent geocenter motion by Hugentobler et al (2006) and station displacements derived from GPS tracking data by Ray et al (2008). Particularly, an anomalous frequency of 1.04 cpy (cycles per year) was found, corresponding to a period of about 350 days which is very similar to the GPS draconitic year, the repeat period of the Sun with respect to the satellite constellation.

Urschl et al (2007) plotted the GPS–SLR residuals as a function of the position of the Sun with respect to the satellite, more specifically in a $(\beta_0, \Delta u)$ reference frame, where β_0 is the elevation angle of the Sun above the orbital plane and Δu is the argument of latitude of the satellite with respect to the argument of latitude of the Sun (see Fig. 1). The plot of Urschl et al (2007) shows a peculiar pattern indicating GPS orbit modeling deficiencies, and the radiation pressure caused by the Earth albedo (not considered at that time in the GPS orbit determination) was mentioned as one of the possible causes to be investigated. Moreover, since the orbit perturbations caused by Earth radiation pressure depend on the position of Sun, Earth and satellite, neglecting Earth radiation pressure is also a good candidate for causing the observed anomalous frequencies in the geodetic time series.

The mathematical formulation used in our study for the computation of Earth radiation pressure (Sect. 2.2) is based on the model of Knocke et al (1988). The construction of the satellite models for the interaction with Earth radiation (Sect. 2.3) is based on the information contained in Fliegel et al (1992) and Fliegel and Gallini (1996), who developed solar radiation pressure models for GPS satellites. More recently Ziebart et al (2007) and Rodriguez-Solano et al (2010) studied the impact of Earth radiation pressure on GPS orbits (mainly in the radial component) and on GPS–SLR residuals (see also Sect. 4). In the current paper, we include the acceleration due to Earth radiation pressure (visible and

infrared, Sect. 2.4) acting on GPS satellites in the orbit determination process. Two solutions covering nine years (2000.0 to 2009.0) with and without Earth radiation pressure were computed (Sect. 3). This allows to study the impact on the GPS orbits (mainly focussing on the along- and cross-track components, Sect. 4) as well as on GPS derived geodetic parameters like estimated station positions (Sect. 5), geocenter coordinates and length of day (Sect. 6).

2 Models

2.1 Selection of models

In a previous work (Rodriguez-Solano et al, 2010), Earth radiation and GPS satellite models of increasing complexity were developed and tested. From that study the key factors of the models have been identified. For the Earth radiation it was found that the use of an analytical model (based on constant albedo) or one based on numerical integration of Earth’s actual reflectivity and emissivity data, give similar results for the irradiance acting on the GPS satellites (difference of up to 10 %), mainly due to the high altitude of these space vehicles. As data from the CERES (Clouds and Earth’s Radiant Energy System, Wielicki et al, 1996) satellite mission are available since the beginning of 2000³, the numerical approach was chosen (see Sect. 2.2). Concerning the satellite model, use of a box-wing model is a key factor since the variation of the solar panels with respect to the Earth is very important, whereas a simple cannon-ball model is highly inaccurate. The accuracy of the modeled optical properties and the detailed structure of the satellite have a lower impact on the acceleration than the use of a box-wing model, but they are still important enough to be considered (see Sect. 2.3). Further details of the models may be found in Rodriguez-Solano (2009).

2.2 Earth radiation

The mathematical formulation of the Earth radiation model used for this study is the same as the one proposed by Knocke et al (1988) for computing the irradiance received by the satellite due to the Earth’s reflected (visible) and emitted (infrared) radiation. It is assumed that the Earth reflects and emits radiation in a purely diffuse way as a Lambertian sphere. The main steps included in the model are: 1) Determine the solar irradiance received by each surface element of the Earth (grid of $2.5^\circ \times 2.5^\circ$). 2) Compute the irradiance received by the satellite based on the reflectivity and emissivity coefficients (from NASA’s CERES project, also used by Ziebart et al (2004) but not yet by Knocke et al (1988)) for each Earth’s surface element. 3) Compute the Earth

³http://eosweb.larc.nasa.gov/PRODOCS/ceres/level3_es4_table.html, accessed on 29 March 2011.

radiation pressure caused by the interaction between the irradiance from each surface element of the Earth with the satellite model.

2.3 GPS satellites

The physical description of the interaction between radiation and the surfaces of the satellite is provided by Fliegel et al (1992). It is based on the optical properties of the surface, e.g., specularity and reflectivity or equivalently the fraction of reflected, absorbed and diffracted photons which should sum up to one (Milani et al, 1987). The dimensions and optical properties are given for Block I and Block II/IIA GPS satellites in the mentioned paper and for Block IIR satellites in Fliegel and Gallini (1996). These two papers are the basis for constructing our box-wing satellite model. They also provide a priori models (ROCK) for solar radiation pressure for precise geodetic applications. However, nowadays no a priori model or purely empirical models are used due to the lower performance of the ROCK models compared to the empirical models. For this study, the CODE empirical model for solar radiation pressure (see also Sect. 3, Beutler et al, 1994) was used with no a priori model.

To complete the box-wing model, the nominal attitude law of the satellite must be considered, i.e., ensuring that the navigation antennas always point to the geocenter and that the solar panels always point to the Sun. The nominal attitude law is correct in most cases. Only when the satellite is in eclipse season and in the Earth's shadow as at orbit noon, is this no longer true (Bar-Sever, 1996; Kouba, 2009). However, non-nominal orbit noon and midnight maneuvers are not yet considered in our model. With the assumption of nominal attitude, the Earth radiation and satellite models have a main dependency on the angle ψ formed by satellite, Earth and Sun, as shown in Fig. 1, which can be simply written as $\cos(\psi) = \cos(\beta_0) \cos(\Delta u)$.

Finally the thrust of the navigation antennas, as reported by Ziebart et al (2004), was also included in the satellite model. An approximate value of 80 Watts of antenna transmission power was used for all GPS satellites (Block II/IIA and Block IIR). In previous studies (Ziebart et al, 2004; Rodriguez-Solano et al, 2010), the thrust of the navigation antennas was found to cause a non-negligible effect for GPS satellite orbits. It introduces a constant radial acceleration of around $2.7 \times 10^{-10} \text{ m/s}^2$ for Block IIA satellites, a magnitude which is comparable to the minimum radial acceleration due to Earth radiation pressure (around $4 \times 10^{-10} \text{ m/s}^2$).

2.4 Acceleration

By combining the irradiance from each surface element of the Earth with the satellite model, a force acting on the satellite is obtained. By integrating these forces over the part of the Earth visible to the satellite and divid-

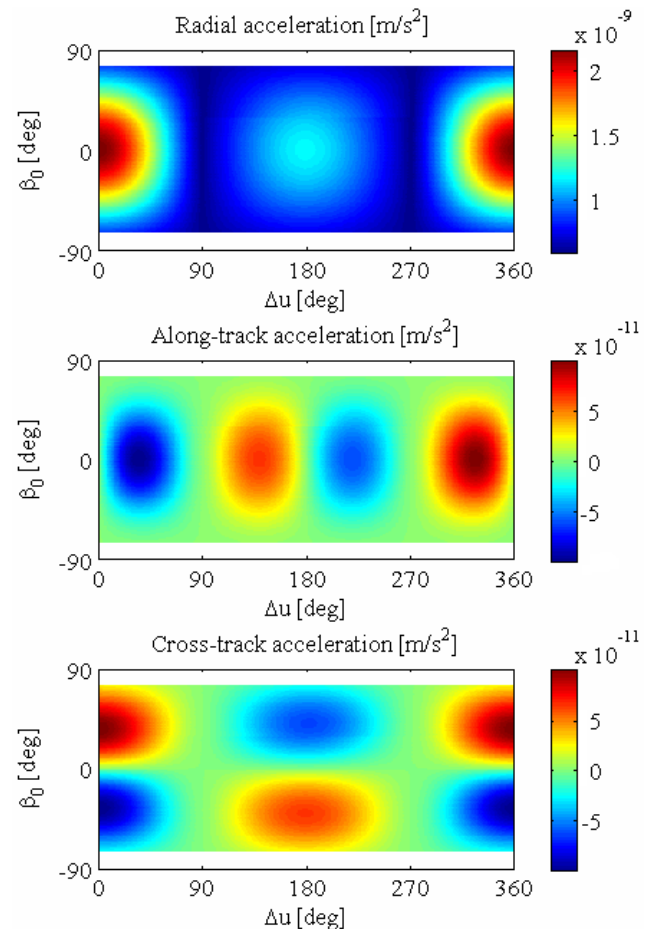


Fig. 2: Acceleration acting on Block IIA satellites due to Earth radiation pressure plus antenna thrust, in a Sun-fixed reference frame. When Δu equals 180° , the satellite is above the shadowed side of the Earth.

ing by the mass of the satellite, the acceleration due to Earth radiation pressure for a specific satellite position is obtained. In Fig. 2 the resulting acceleration is shown for a box-wing GPS Block IIA satellite model in a Sun-fixed reference frame ($\beta_0, \Delta u$) for the radial, along-track and cross-track components. To produce this plot, an analytical Earth radiation model was used assuming a globally constant albedo of 0.3 as well as only a radial impact direction of the irradiance reaching the satellite. This was done for computational efficiency. The acceleration used to calculate the GPS satellite orbits was, however, based on the numerical Earth radiation model (with CERES satellite data, Sect. 2.2).

For the radial component of the acceleration (Fig. 2), the maximum at $\Delta u = 0^\circ$ and $\beta_0 = 0^\circ$ corresponds to the point where Sun, satellite and Earth are exactly aligned, with the spacecraft above the Sun-facing side of the Earth. Note that for $90^\circ < \Delta u < 270^\circ$ the satellite is mainly above the night hemisphere of the Earth. At $\Delta u = 180^\circ$ and $\beta_0 = 0^\circ$ it is in total shadow, where

one finds a secondary maximum of the radial acceleration since the solar panels are maximally exposed to the infrared radiation of the Earth. This last feature would not be present for a cannon-ball model with constant cross-section, since the solar panels change their orientation a lot with respect to the Earth over one revolution. This change of orientation is also responsible for the minima at $\Delta u = 90^\circ$ and $\Delta u = 270^\circ$, where the geocentric directions to the satellite and to the Sun are orthogonal and the exposure of the solar panels to Earth radiation is almost zero.

The acceleration observed in the along-track and cross-track components in Fig. 2 is an effect of the solar panels; i.e., with a cannon-ball model we would not see these particular patterns. Moreover, the along-track acceleration has a period of twice per revolution while the cross-track period is only once per revolution. Also interesting is the change of sign in the cross-track acceleration with the sign of the β_0 angle.

3 Processing strategy

The Earth radiation pressure model as described in Sect. 2.2 and 2.3 was implemented in the Bernese GPS Software (Dach et al, 2007). Adapting the strategy of CODE as described by Steigenberger et al (2006, 2011), nine years (2000.0 to 2009.0) of GPS ground tracking data were processed, using around 200 IGS stations. Two solutions were computed, one including Earth radiation pressure and one without. No net rotation (NNR) and no net translation (NNT) conditions were applied with respect to the IGS05 (Ferland, 2006) reference frame for a subset of up to 125 tracking stations. The last condition is required in order to estimate the offset between the Earth's center of mass, as sensed by the satellites, and the reference frame origin. The resulting orbits and station coordinates are then obtained in the terrestrial reference frame and the respective comparisons (Sect. 4 and 5) are not affected by apparent changes of the geocenter. Moreover, the impact of Earth radiation pressure on the apparent geocenter can be studied independently (Sect. 6).

The solar radiation pressure effect (in both solutions) was modeled by estimating five empirical parameters (per satellite and per day) and with no a priori model. The five empirical parameters were proposed by Beutler et al (1994) and are basically the following: three constants in the D , Y and B directions (see Fig. 1) and two periodic (once per revolution) in the B direction. Additionally, according to the CODE processing strategy, three pseudo-stochastic pulses once per revolution in the radial, along-track and cross-track directions were estimated (individually constrained for each direction). Despite having nine-year solutions, in most of the plots presented in the following sections just the year 2007 is shown in order to keep the figures simple. The full

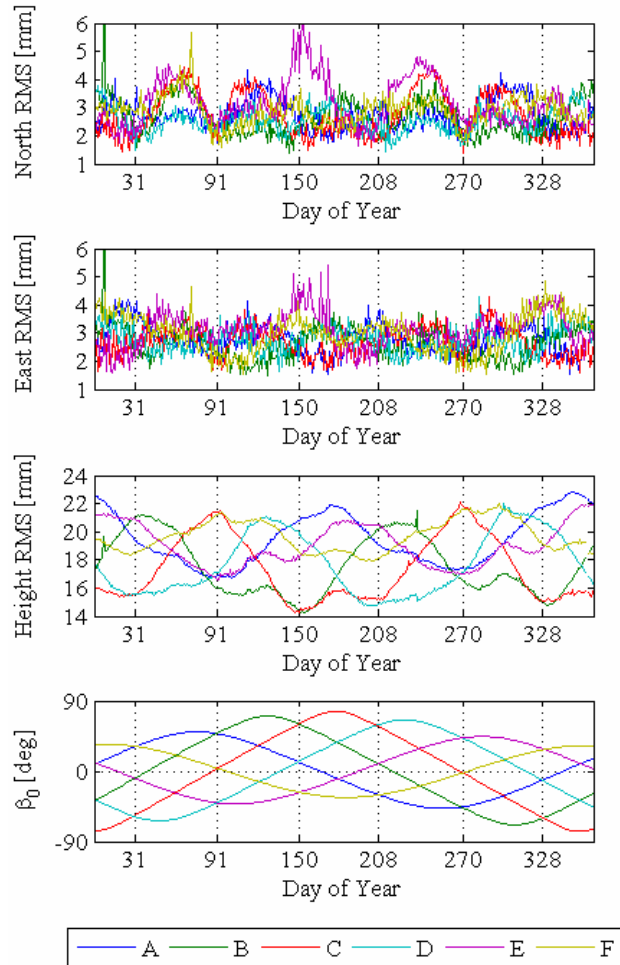


Fig. 3: Top three: RMS of GPS orbit differences per orbital plane (in color) and per day of year for 2007. Bottom: Sun elevation angle above the GPS orbital planes (in color).

nine-year solutions are mainly used for computing the spectra of daily position estimates and geocenter.

4 Impact on GPS orbits

The orbit differences presented in this section were obtained by comparing the orbits of all GPS satellites computed with and without Earth radiation pressure. The results in Fig. 3 and Fig. 4 are plotted in a local Earth-fixed reference frame (North, East, height) rather than in an orbit-fixed reference frame (radial, along-track, cross-track) in order to highlight the relation of the orbit perturbations due to Earth radiation pressure and the position estimates of GPS ground tracking stations (see Sect. 5).

The most prominent effect of Earth radiation pressure on the GPS orbits is a radial offset of 1–2 cm, observable in the height component of Fig. 3 and Fig. 4. As already mentioned by Ziebart et al (2007) this effect

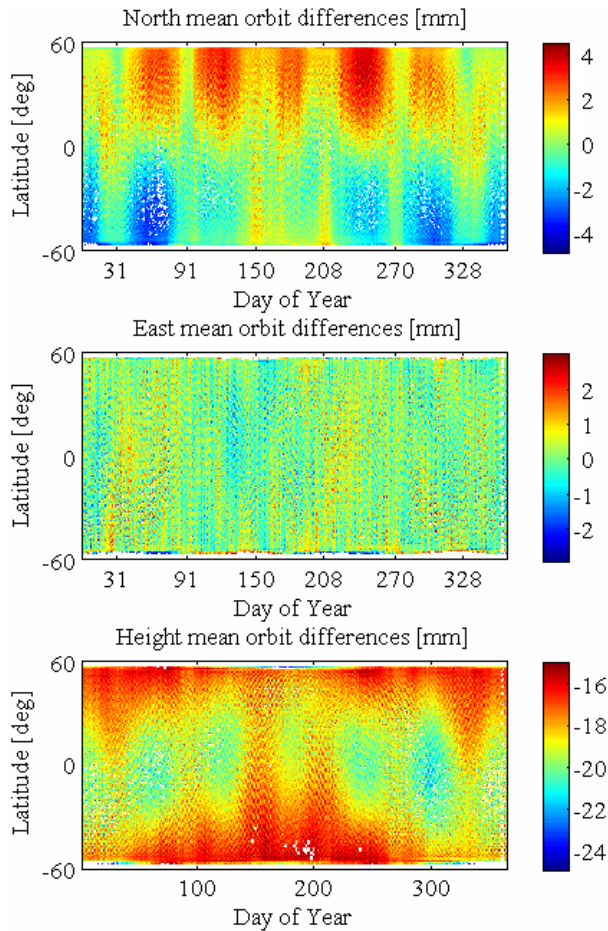


Fig. 4: Mean orbit differences of all GPS satellites plotted as a function of latitude and day of year (2007).

reduces the GPS–SLR range discrepancy by 1–2 cm, from which around 0.5 cm can be attributed to the antenna thrust (Sect. 2.4, Rodriguez-Solano et al, 2010). The reason for this radial reduction of orbits is that GPS measurements, being essentially angular measurements due to required clock synchronization, mainly determine the mean motion of the satellite. As a matter of fact, a constant positive radial acceleration (equivalent to a reduction of GM, the product of the gravitational constant and the mass of the Earth) decreases the orbital radius according to Kepler’s third law (Rodriguez-Solano et al, 2010). From Fig. 3 one can also note the dependency of the height RMS orbit differences with respect to the Sun elevation angle above (or below) the orbital plane (β_0). Consequently, this kind of perturbation should have a main repeat period close to half of the GPS draconitic year, that is about $350/2$ days. The subdaily dependency of the orbit differences on the Δu angle was averaged when Fig. 3 and Fig. 4 were produced, since the differences are presented as RMS and mean values per day for the corresponding figures.

However, the North and East RMS orbit differences

in Fig. 3 do not seem to have a correlation with the β_0 angle of the respective planes, but rather to the combined effect of the β_0 angles of the six orbital planes. More specifically, one finds a minimum in all the orbital planes, repeating six times during one year, for the North component RMS orbit differences (with an exception for day 150 and for the orbital plane E). These minima occur when the β_0 angle of two orbital planes get close to zero degrees (shown with dotted lines in Fig. 3), i.e., when the Sun gets close to the intersection line of the two orbital planes. From the acceleration produced by Earth radiation pressure (Fig. 2), we know that the cross-track acceleration is zero for $\beta_0 = 0^\circ$, therefore one could expect a minimum in the North or East RMS orbit differences for the two orbital planes with a Sun elevation angle close to zero. However, the other four orbital planes with β_0 angles different from zero also seem to be minimally affected by Earth radiation pressure (mainly the North component) and have minima at the same periods. The mechanism for this behavior is not yet understood, but it could be further investigated by e.g. excluding the satellites from one or two orbital planes in the solution computation.

By taking the mean of the orbit differences for all GPS satellites for a given latitude (one degree intervals) and day of year, one gets a very interesting result (Fig. 4). For example the orbit height differences follow the position of the Sun with respect to the Earth over the year, something that is expected since the Earth radiation at the satellite reaches its highest values if there is an alignment of Sun, satellite and Earth. For the East component we find almost no signal (compared to height and North) in the orbit differences. In the North orbit differences we obtain a very similar pattern as the one of Fig. 3, but in addition we observe that the differences are positive for the northern hemisphere and negative for the southern one. This can be interpreted as a change in the inclination of the orbits due to Earth radiation pressure. In fact, the inclination changes by around 1×10^{-8} degrees, which corresponds to 4.6 millimeters in the cross-track orbit positions (Fig. 4).

5 Impact on GPS station position estimates

Earth radiation pressure mismodeling causes a very particular perturbation at the millimeter level in the daily position estimates of GPS ground tracking stations. Figure 5 shows horizontal displacement vectors between solutions with and without modeled Earth radiation pressure. This is shown for two days of 2007, one where the North orbit differences (see Fig. 3) are large (day 61) and one where they are minimal (day 91). For day 61 a “deformation” of the Earth in north- and southwards direction is visible. Moreover, the two characteristic patterns in Fig. 5 alternate six times per GPS draconitic year (350 days). There are also differences in the sta-

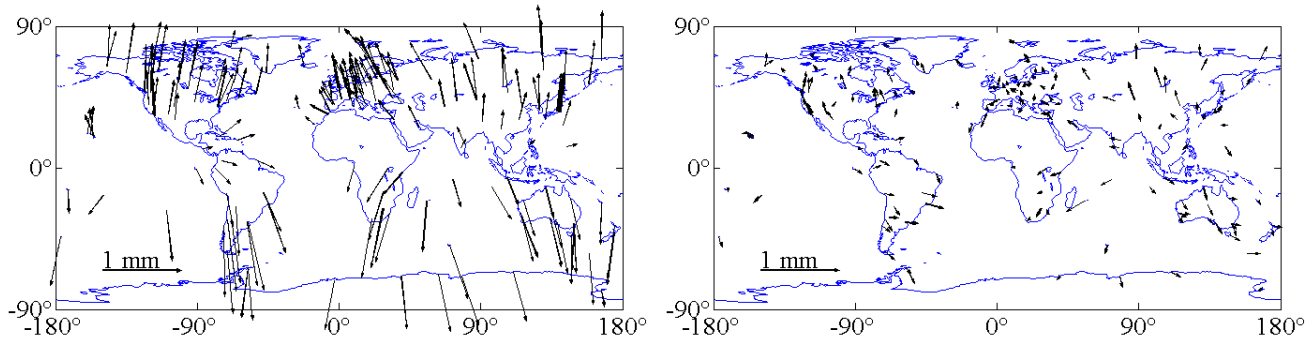


Fig. 5: Change in the estimated horizontal GPS ground station positions (about 200 IGS sites) due to Earth radiation pressure for day 61 (left) and day 91 (right) of year 2007.

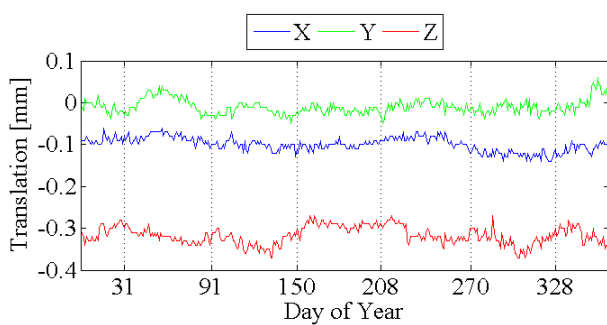


Fig. 6: Helmert translation parameters between GPS position solutions with and without Earth radiation pressure for year 2007.

tion height components (not shown), but their magnitude is smaller than for the North component, which are the most prominent. The comparison of the station positions based on solutions with and without Earth radiation pressure, shown in Fig. 5, was performed using a 7-parameter Helmert transformation. The scale difference is around 0.14 ppb (parts per billion), or a uniform height shift of about 0.9 mm. In Fig. 6 the translation parameters are shown. The shift in the Z-axis is related to the distribution of GPS stations: As more stations are located in the northern hemisphere these dominate the no net translation condition imposed in the solution (see also Sect. 3). Without the Helmert transformation we would observe in Fig. 5 the northern stations almost unchanged and the southern ones largely displaced. The translation in the X-axis is accompanied by a rotation around the same axis of about $-2 \mu\text{as}$, the rotations around Y and Z are both within $\pm 1 \mu\text{as}$.

To demonstrate the correlation between the effects observed in Sect. 4 and the ground station displacements, we plot the mean of the North component differences (of both orbits and stations) as a function of day of year and latitude (one degree intervals). Figure 7 shows basically the same information as Fig. 4 but plot-

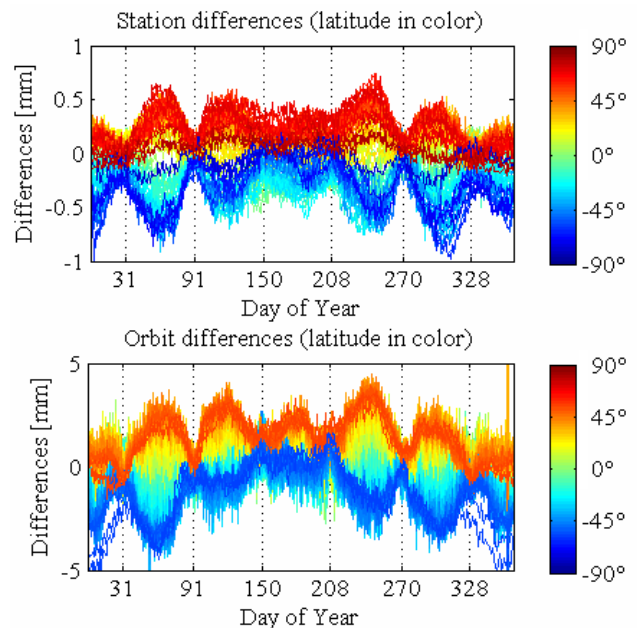


Fig. 7: North component of the mean stations differences (top) and orbit differences (bottom) for year 2007, as a function of day of year and color-coded latitude.

ted in a different way: the differences are shown along the ordinate axis while colors indicate the latitude. This representation is more appropriate to display station displacements as a plot similar to Fig. 4 would leave large gaps in the southern hemisphere. The results show the strong correlation between the orbit perturbations and the station displacements. However, the magnitude of the orbit differences is around 5 times larger than the station differences. If we imagine a GPS satellite placed almost directly over a ground station, both in a middle northern latitude, the satellite would be “pushed” by Earth radiation pressure northwards as well as the station. This relation is almost direct; e.g., if we compute the ratio between the satellite’s semimajor axis and the

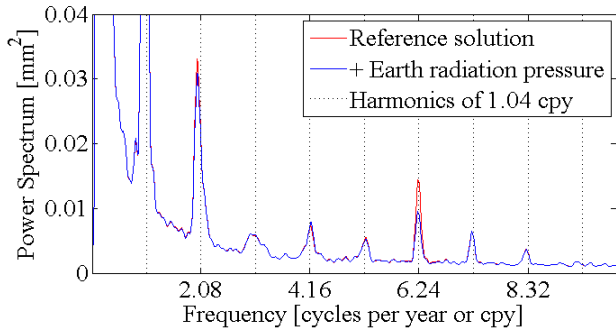


Fig. 8: Power spectrum of the North component of GPS daily position estimates (around 200 IGS sites) from 2000.0 to 2009.0, with (blue) and without (red) Earth radiation pressure.

Earth radius (26560 km/6371 km) we obtain a ratio of 4.17, very close to what we observe in Fig. 7. The situation is of course much more complicated. Nevertheless, we are then in a situation where a small change in the along-track or cross-track position of the GPS satellites (which can not be absorbed by the clocks as in the case of the radial component) leads to an almost direct effect on the position estimates of GPS ground tracking stations.

Furthermore, the observed “deformation” of the Earth changes the power spectrum of the North component of GPS daily position estimates (shown in Fig. 8). This figure is based on nine years of tracking data from around 200 globally distributed IGS stations. By introducing Earth radiation pressure we obtain a reduction mainly in the sixth peak of the power spectrum of the North component, located at approximately 6×1.04 cpy. This frequency is also noticeable in Figs. 3, 4 and 7 (and in Fig. 5 if it would be animated), where we can see a systematic pattern of six cycles over one GPS draconitic year (around 350 days), the repeat period of the Sun with respect to the satellite constellation. As observed in Fig. 8 and also mentioned by Ray et al (2008), the sixth peak in the North component is one of the sharpest and highest. This peak is reduced from 0.01443 mm^2 to 0.00956 mm^2 and after subtracting a noise floor of 0.0016 mm^2 , we obtain a variance reduction of 38 %. This result is very important since it indicates that the solution that includes Earth radiation pressure reduces systematically the anomalous frequency. It also demonstrates that the observed anomalous frequencies in the GPS position time series are related (at least partially) to orbit mismodeling issues. However, the peaks in the East and height power spectrum (not shown) do not exhibit a significant reduction.

The power spectra in this paper were not computed using the Lomb-Scargle Periodogram (Scargle, 1982; Press et al, 1992), as done by other authors (Ray

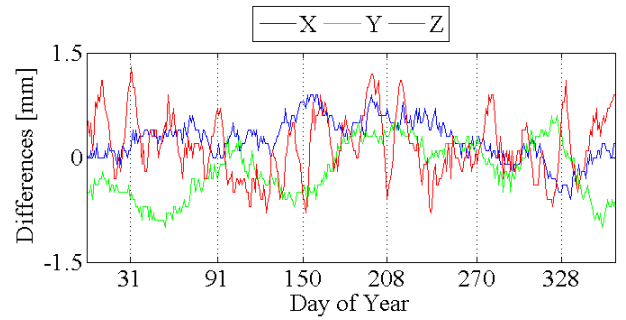


Fig. 9: Geocenter differences between solutions with and without Earth radiation pressure for year 2007.

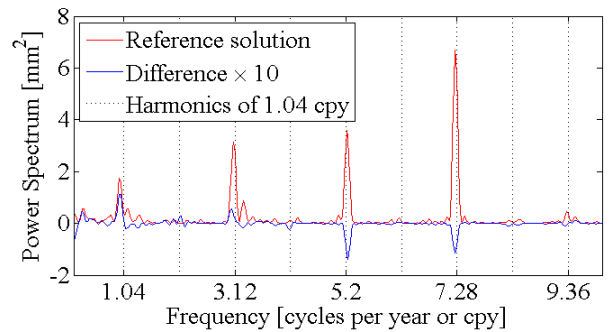


Fig. 10: Power spectrum of the Z-component of the GPS-derived geocenter from 2000.0 to 2009.0. The power spectrum difference between the reference solution minus the one including Earth radiation pressure multiplied by ten is shown in blue.

et al, 2008; Tregoning and Watson, 2009)⁴. Instead, the power spectrum of the Fast Fourier Transform (FFT, Press et al, 1992) was used and where data is missing, zero padding was employed, since GPS-derived daily positions (station coordinates and geocenter) are evenly spaced. The units of the power spectrum are clear (mm^2), while the Lomb-Scargle Periodogram (due to normalization) has no units, and finally, the computation time is largely reduced when employing the FFT. Additionally, to compute the mean power spectrum of the 200 IGS stations (Fig. 8) a weighting according to the inverse of the variance was introduced to ensure that the noisier position time series have a lower contribution.

6 Impact on geocenter and LOD

The impact of Earth radiation pressure on other geodetic parameters, specifically the geocenter position and the length of day (LOD), was also investigated. For the geocenter we find an impact at the one millimeter level

⁴There are also other methods for computing the power spectrum, e.g., a robust estimation method was used by Collilieux et al (2007) for identifying the draconitic harmonics in the individual time series of GPS stations.

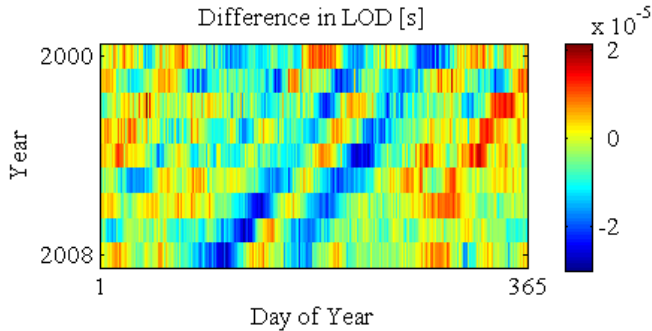


Fig. 11: Difference in length of day (LOD) between the solutions with and without Earth radiation pressure from 2000.0 to 2009.0.

(see Fig. 9), but no clear pattern is visible as for the GPS position estimates (Sect. 5). The geocenter is appropriate for investigation since in the Z-component a period of 350 days, the GPS draconitic year, corresponding to 1.04 cycles per year, was identified by Hugentobler et al (2006). The power spectrum of the geocenter time series (without modeling Earth radiation pressure) is shown in Fig. 10. Note that the main anomalous peaks are found at odd multiples (1, 3, 5, 7) of 1.04 cpy. By including the Earth radiation pressure a small reduction in the 5th and 7th peaks has been achieved, 3.8 % and 1.7 % respectively. Figure 10 shows the difference of the power spectra of the solutions with and without Earth radiation pressure, however multiplied by a factor of 10. A negative sign of the difference, as found for the 5th and 7th peaks, means a reduction of the original power spectrum, while a positive sign means an increase as observed for the 1st and 3rd peaks (by 6.4 % and 1.7 % respectively).

Figure 11, finally, shows the difference in the LOD estimates obtained with and without Earth radiation pressure. The impact is of the order of $10 \mu\text{s}$ with a pattern that has a period close to 350 days, again, the GPS draconitic year. However the LOD power spectrum derived from GPS measurements does not show significant peaks at harmonics of 1.04 cpy. Also the difference of the power spectra of the LOD estimates only shows small variations at harmonics of 1.04 cpy.

7 Conclusions

The acceleration acting on GPS (i.e. box-wing-like) satellites caused by Earth radiation (visible and infrared) depends mainly on the relative position of each satellite, Earth and Sun. This implies a perturbation in the GPS satellite orbits at harmonics of the GPS draconitic year. The main non-negligible effect on the orbits is a reduction of the height by about 1–2 cm, consistent with the findings of Ziebart et al (2007). In the other components of the orbits (along-track and cross-track) the effect is

about one order of magnitude smaller. When the orbit differences (with and without Earth radiation pressure) are separated by orbital plane, it becomes evident that when the Earth radiation pressure is zero in the cross-track component for two orbital planes, the other four orbital planes are also unaffected, the mechanism for which requires further investigation.

Moreover, in the North component of the orbit differences a particular pattern is found, displacing the orbits (few millimeters) towards North at northern latitudes and South at southern latitudes, with a period of one sixth of the GPS draconitic year. The same pattern is found in the daily position estimates of GPS ground stations at the sub-millimeter level, indicating that a small change in the along-track or cross-track position of the GPS satellites (which can not be absorbed by the clocks like the radial shift) leads to an almost direct effect on the position estimates of GPS ground stations. This “deformation” of the Earth also leads to a reduction in the anomalous spectra of GPS daily position estimates, mainly in the sixth peak of the North component at 6×1.04 cpy.

The impact of Earth radiation pressure on the geocenter (at the one millimeter level) is less significant. It reduces just slightly some of the anomalous peaks of the geocenter power spectrum and even increases others. For LOD, the impact is of order $10 \mu\text{s}$. The fact that the impact on geocenter and LOD is low, indicates that other more important problems remain in the orbit modeling, in particular for the geocenter. One of the most likely candidates is the solar radiation pressure, which also has a strong dependency on the GPS draconitic year. It is larger in magnitude than the Earth radiation pressure and currently it is taken into account mainly by applying empirical parameterizations.

Finally, the non-negligible effects of Earth radiation pressure that have been found in the GPS orbits and station position estimates underlines the importance of further improvements in the orbit modeling techniques. Of particular concern is a better understanding and modeling of non-conservative forces affecting the satellites, which involve the modeling of the radiation source, the satellite structure (including its attitude) and surface properties. This also justifies the efforts that are invested in this task by different groups of scientists.

The subroutines to compute the acceleration due to Earth radiation pressure are available at: <http://www.iapg.bv.tum.de/albedo/>. The subroutines contain the Earth radiation models (analytical and numerical with CERES data) as well as the box-wing models for GNSS satellites (GPS and GLONASS).

Acknowledgements

The authors gratefully acknowledge the International GNSS Service (IGS, Dow et al, 2009) for providing the high quality

data needed for this study. The comments and suggestions by Jim Ray (NOAA) and two other reviewers are greatly appreciated. We acknowledge the support of the TUM Graduate School.

References

- Bar-Sever YE (1996) A new model for GPS yaw attitude. *J Geod* 70(11):714–723, DOI 10.1007/BF00867149
- Bar-Sever Y, Davis JL, Dach R, Flohrer C, Herring T, Ray J, Slater JA, Thaller D (2009) Impact of SLR tracking on GPS. In: Pavlis EC (ed) International Technical Laser Workshop on SLR Tracking of GNSS Constellations. Position Paper, URL http://acc.igs.org/orbits/slr_track_gps_ilrs09-PP.pdf,
- Beutler G, Brockmann E, Gurtner W, Hugentobler U, Mervart L, Rothacher M, Verdun A (1994) Extended orbit modeling techniques at the CODE processing center of the international GPS service for geodynamics (IGS): theory and initial results. *Manuscr Geod* 19(6):367–386
- Collilieux X, Altamini Z, Coulot D, Ray J, Sillard P (2007) Comparison of very long baseline interferometry, GPS, and satellite laser ranging height residuals from ITRF2005 using spectral and correlation methods. *J Geophys Res* 112(B12403), DOI 10.1029/2007JB004933
- Dach R, Hugentobler U, Fridez P, Meindl M (2007) Bernese GPS Software, Version 5.0. Astronomical Institute, University of Bern
- Dow J, Neilan R, Rizos C (2009) The International GNSS Service in a changing landscape of Global Navigation Satellite Systems. *J Geod* 83(3-4):191–198, DOI 10.1007/s00190-008-0300-3
- Ferland R (2006) [IGSMail-5455]: IGS05 fine tuning. URL <http://igscb.jpl.nasa.gov/mail/igsmail/2006/msg00178.html>
- Fliegel H, Gallini T, Swift E (1992) Global Positioning System Radiation Force Model for Geodetic Applications. *J Geophys Res* 97(B1):559–568, DOI 10.1029/91JB02564
- Fliegel H, Gallini T (1996) Solar Force Modeling of Block IIR Global Positioning System Satellites. *J Spacecr Rockets* 33(6):863–866, DOI 10.2514/3.26851
- Hugentobler U, van der Marel H, Springer T (2006) Identification and mitigation of GNSS errors. In: Springer T, Gendt G, Dow JM (eds) The International GNSS Service (IGS): "Perspectives and Visions for 2010 and beyond", IGS Workshop 2006
- Knocke PC, Ries JC, Tapley BD (1988) Earth radiation pressure effects on satellites. In: Proceedings of AIAA/AAS Astrodynamics Conference, pp 577–587
- Kouba J (2009) A simplified yaw-attitude model for eclipsing GPS satellites. *GPS Solut* 13(1):1–12, DOI 10.1007/s10291-008-0092-1
- Milani A, Nobili AM, Farinella P (1987) Non-gravitational perturbations and satellite geodesy. Adam Hilger, Bristol
- Press W, Teukolsky S, Vetterling W, Flannery B (1992) *Numerical Recipes in Fortran 77: The Art of Scientific Computing*, 2nd edn. Cambridge University Press
- Ray J, Altamini Z, Collilieux X, van Dam T (2008) Anomalous harmonics in the spectra of GPS position estimates. *GPS Solut* 12(1):55–64, DOI 10.1007/s10291-007-0067-7
- Rodriguez-Solano CJ (2009) Impact of albedo modelling on GPS orbits. Master's thesis, Technische Universität München, URL <https://mediatum2.ub.tum.de/doc/1083571/1083571.pdf>
- Rodriguez-Solano CJ, Hugentobler U, Steigenberger P (2010) Impact of Albedo Radiation on GPS Satellites. In: *Geodesy for Planet Earth*, IAG Symposia 136, Springer, in press
- Scargle J (1982) Studies in astronomical time series analysis. II. statistical aspects of spectral analysis of unevenly spaced data. *Astrophys J* 263:835–853, DOI 10.1086/160554
- Steigenberger P, Rothacher M, Dietrich R, Fritsche M, Rülke A, Vey S (2006) Reprocessing of a global GPS network. *J Geophys Res* 111(B05402), DOI 10.1029/2005JB003747
- Steigenberger P, Hugentobler U, Lutz S, Dach R (2011) CODE Contribution to the First IGS Reprocessing Campaign. Tech. Rep. 1/2011, IAPG/TUM, URL <https://mediatum2.ub.tum.de/doc/1078108/1078108.pdf>
- Tregoning P, Watson C (2009) Atmospheric effects and spurious signals in GPS analysis. *J Geophys Res* 114, B09403, DOI 10.1029/2009JB006344
- Urschl C, Beutler G, Gurtner W, Hugentobler U, Schaer S (2007) Contribution of SLR tracking data to GNSS orbit determination. *Adv Space Res* 39:1515–1523, DOI 10.1016/j.asr.2007.01.038
- Wielicki BA, Barkstrom BR, Harrison EF, Lee III RB, Smith GL, Cooper JE (1996) Clouds and the Earth's Radiant Energy System (CERES): An Earth Observing System Experiment. *Bull Am Meteorol Soc* 77(5):853–868
- Ziebart M, Edwards S, Adhya S, Sibthorpe A, Arrow-smith P, Cross P (2004) High Precision GPS IIR Orbit Prediction using Analytical Non-conservative Force Models. In: *Proceedings of ION-GNSS-2004*, pp 1764–1770
- Ziebart M, Sibthorpe A, Cross P, Bar-Sever Y, Haines B (2007) Cracking the GPS - SLR Orbit Anomaly. In: *Proceedings of ION-GNSS-2007*, pp 2033–2038

Adjustable box-wing model for solar radiation pressure impacting GPS satellites

C. J. Rodriguez-Solano, U. Hugentobler, P. Steigenberger

Institut für Astronomische und Physikalische Geodäsie, Technische Universität München, 80333 München, Germany

Abstract

One of the major uncertainty sources affecting Global Positioning System (GPS) satellite orbits is the direct solar radiation pressure. In this paper a new model for the solar radiation pressure on GPS satellites is presented that is based on a box-wing satellite model, and assumes nominal attitude. The box-wing model is based on the physical interaction between solar radiation and satellite surfaces, and can be adjusted to fit the GPS tracking data.

To compensate the effects of solar radiation pressure, the International GNSS Service (IGS) analysis centers employ a variety of approaches, ranging from purely empirical models based on in-orbit behavior, to physical models based on pre-launch spacecraft structural analysis. It has been demonstrated, however, that the physical models fail to predict the real orbit behavior with sufficient accuracy, mainly due to deviations from nominal attitude, inaccurately known optical properties, or aging of the satellite surfaces.

The adjustable box-wing model presented in this paper is an intermediate approach between the physical/analytical models and the empirical models. The box-wing model fits the tracking data by adjusting mainly the optical properties of the satellite's surfaces. In addition, the so called *Y*-bias and a parameter related to a rotation lag angle of the solar panels around their rotation axis (about 1.5° for Block II/IIA and 0.5° for Block IIR) are estimated. This last parameter, not previously identified for GPS satellites, is a key factor for precise orbit determination.

For this study GPS orbits are generated based on one year (2007) of tracking data, with the processing scheme derived from the Center for Orbit Determina-

tion in Europe (CODE). Two solutions are computed, one using the adjustable box-wing model and one using the CODE empirical model. Using this year of data the estimated parameters and orbits are analyzed. The performance of the models is comparable, when looking at orbit overlap and orbit prediction errors. Nevertheless, the models show important differences between orbits at the 1–2 cm level and total accelerations (up to $5 \times 10^{-9} \text{ m/s}^2$). The differences are mainly due to the fact that the box-wing model is based on the physical interaction between solar radiation and satellite, while the CODE empirical model is not.

Keywords: GPS; box-wing satellite model; precise orbit determination; solar radiation pressure.

1 Introduction

Global Positioning System (GPS) satellites are at a distance from the Earth where the solar radiation pressure (SRP) is the main non-gravitational orbit perturbation. While the solar radiation impacting the satellites is simple to model, the perturbing acceleration depends on the structure of the satellite and on the optical properties of each surface facing the Sun. Furthermore, the satellite is constantly changing its orientation with respect to the Sun to maintain its nominal attitude, making the modeling of SRP a complex task. Several approaches (Sections 2 and 3) have been employed to model the SRP impacting the GPS satellites, both for orbit prediction purposes and for precise orbit determination. The last one is a key issue for geodetic and scientific applications of the Global Positioning System.

Within the IGS (International GNSS Service, Dow et al, 2009) the GPS final orbits have reached a precision of 2.5 cm, where the current SRP models have

played an important role. Despite the high accuracy of the orbits, some orbit modeling deficiencies remain in the Satellite Laser Ranging (SLR) residuals, with a characteristic pattern first noted by Urschl et al (2007). Additionally, orbit related frequencies were identified in geodetic time series, such as apparent geocenter motion by Hugentobler et al (2006), and station displacements derived from GPS tracking data by Ray et al (2008). Recently the impact of including an a priori Earth radiation model on the GPS orbits (Rodriguez-Solano et al, 2012a) and position estimates (Rodriguez-Solano et al, 2012b) was studied. In these works a perturbation in the orbits of 1–2 cm in radial direction (consistent with the findings of Ziebart et al, 2007) and few millimeters in along- and cross-track direction was found, together with a small reduction of the power spectrum at orbit related frequencies of GPS position estimates. The last examples show that orbit modeling deficiencies, in particular related to non-conservative forces, can still be found in the computed GPS orbits. The orbit mis-modeling effects are not only noticeable in the orbits themselves but also in the geodetic parameters, highlighting the importance of further improvements in our understanding and modeling of the forces acting on GPS satellites, and GNSS satellites in general.

Non-conservative force modeling, in particular solar radiation pressure, also plays a key role in the precise orbit determination of other geodetic satellites. For GLONASS satellites, e.g., Ziebart and Dare (2001) have developed and tested a detail solar radiation pressure model. In the case of altimetry satellites (e.g. TOPEX/Poseidon, Jason-1 and Jason-2) several studies have developed and tested models for these forces. Marshall and Luthcke (1994) and Berthias et al (2002) developed box-wing models for TOPEX/Poseidon and Jason-1 respectively. Moreover, they adjusted the optical properties of the box-wing models to reproduce as precise as possible the accelerations acting on the satellites. Further studies (Cerri et al, 2010; Lemoine et al, 2010; Zelensky et al, 2010; Flohrer et al, 2011) compared the performance of different box-wing (macro) models and detail physical satellite models for Jason-1 and Jason-2. In the case of satellites equipped with DORIS receivers (e.g. SPOTs, TOPEX/Poseidon, ENVISAT, Jason-1 and Jason-2), Gobinddass et al (2009) found that different models of solar radiation pressure have a large impact on the geocenter time series derived from DORIS measurements.

To compensate the perturbing acceleration due to solar radiation acting on the GPS satellites, two types of models have been employed. 1) Empirical models which fit best the GPS global tracking data and which have led to a precision of 2.5 cm in the IGS final orbits. The main disadvantage of such models resides in the loss of physical understanding of the forces acting on the satellites, which can then result in non physical orbits and poten-

tially introduce undesired systematic errors. 2) Analytical models based on the detailed structure of the satellites and surface properties measured on ground prior to launch. The principal problem of these models is that they cannot compensate accurately enough for the real on-orbit behavior of the satellites, e.g., due the change (aging) or uncertainty of the a priori optical properties of the satellite surfaces or deviations from nominal attitude. An interesting discussion of pros and cons between the two types of models is also given by Bar-Sever and Kuang (2004).

In Sections 2 and 3 the existing empirical and analytical models found in the literature are described, giving the basis for constructing an analytical box-wing model (satellite bus and solar panels, see Section 4). The box-wing model is based on the physical interaction between the solar radiation and the satellite surfaces, but it is also capable of fitting the GPS tracking data as an empirical model would do. As mentioned before, a similar approach was applied by Marshall and Luthcke (1994) and Berthias et al (2002) to altimetry satellites in order to fulfill the high accuracy orbit requirements of these missions. More recently McMahan and Scheeres (2010) applied an analytical SRP model (described with only seven Fourier coefficients) to study the perturbation effects on the Gravity Recovery and Climate Experiment (GRACE, Tapley et al, 2004) satellites. The idea behind the model of McMahan and Scheeres (2010) is the following:

“A precise, physics-based model of the SRP induced accelerations is combined with a perturbative theory of the accelerations on the orbit to create a system that combines a physical a priori model with a mathematical form that is conducive to studying the orbital effects and estimating the effect of SRP on the orbit.”

In our case, the interest is not to study the effects of SRP on the orbits, but rather to fit the measurements of the orbits (GPS tracking data) with a model capable of compensating the SRP acting on the satellites, which is assumed to be the major error source affecting the GPS satellite orbits. By doing this an improvement in the orbits themselves is also expected. This is achieved by using the analytical box-wing model described in Sections 4 and 5. The estimated SRP box-wing parameters (on-orbit optical properties) and the impact of the model on the GPS orbits are analyzed in Sections 6 and 7. Finally the accelerations obtained with the box-wing model and existing SRP models are compared in Section 8.

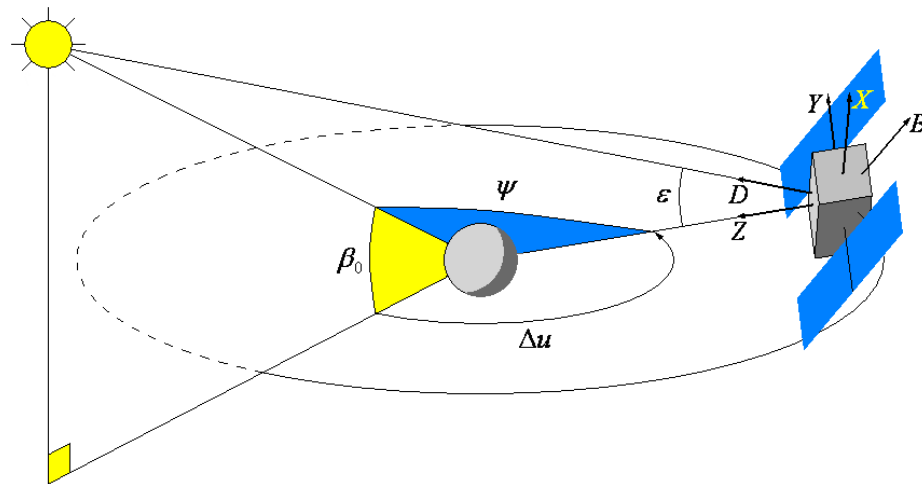


Fig. 1: Nominal attitude of GPS satellites as a function of the position of the Sun in the orbital plane, see also Eq. (5). Illustration of DYB (Sun-fixed) and XYZ (body-fixed) orthogonal frames.

2 Empirical SRP models

One of the first attempts to compensate for non-modeled forces affecting the GPS orbits was done by Colombo (1989) where one finds that:

“Analytical orbit perturbation theory suggests that the errors in the ephemerides of the Global Positioning System (GPS) satellites should be mostly resonant effects that can be corrected by adjusting a few parameters in a simple empirical acceleration formula, despite of the complexity of their causes (mismodeling of gravity, radiation pressure, etc.) at least for arcs free from orbits maneuvers.”

The resonant frequencies of the GPS orbits found by Colombo (1989) are zero and once per revolution. Furthermore, Hill’s equations were used to analytically formulate the orbit perturbations in radial, along- and cross-track directions, denoted by RSW . The nine proposed empirical parameters responsible for absorbing the orbit acceleration errors can be written as:

$$\begin{aligned} R(u) &= R_0 + R_C \cos u + R_S \sin u, \\ S(u) &= S_0 + S_C \cos u + S_S \sin u, \\ W(u) &= W_0 + W_C \cos u + W_S \sin u, \end{aligned} \quad (1)$$

where u is the argument of latitude of the satellite. As mentioned by Springer et al (1999) the Colombo model considers the gravity field of the Earth as the major error source in the GPS orbits. Therefore there is not an explicit dependency of the model on the Sun position w.r.t. the satellite.

In Beutler et al (1994) the extended orbit modeling techniques used by the Center for Orbit Determination

in Europe (CODE) are described. To compensate the direct solar radiation pressure impacting the satellites, up to nine empirical parameters are estimated in a Sun-Earth oriented frame with directions denoted by DYB (Fig. 1). A description of this model is also found in Springer et al (1999) and the estimated parameters are:

$$\begin{aligned} D(u) &= D_0 + D_C \cos u + D_S \sin u, \\ Y(u) &= Y_0 + Y_C \cos u + Y_S \sin u, \\ B(u) &= B_0 + B_C \cos u + B_S \sin u. \end{aligned} \quad (2)$$

The D direction gives the orientation of the normal to the solar panels in inertial space, the Y direction points along the solar panel beams and the B direction finally completes the right handed system. However, the B direction does not correspond to the orientation of the satellite bus and varies along the $+Z$, $+X$ and $-Z$ surfaces of the bus as shown in Fig. 1. Furthermore the argument of latitude u is not directly related to the attitude of the satellite. Additionally, in the direct radiation pressure model of Beutler et al (1994) the acceleration provided by the SRP models (sometimes called ROCK models, see Section 3) developed by Fliegel et al (1992) and Fliegel and Gallini (1996) can be included as a priori information.

In order to get an adequate a priori model of the real on-orbit solar radiation pressure impacting the satellites, Springer et al (1999) developed a new model:

“The performance of the new model is almost one order of magnitude better than that of the existing ROCK models. It also allows a reduction of the number of orbit parameters that have to be estimated.”

This model was constructed by adjusting several years of CODE final orbits and can be written as:

$$\begin{aligned} D &= D_0, \\ Y &= Y_0, \\ B &= B_0, \\ Z(\Delta u) &= Z_1 \sin \Delta u, \\ X(\Delta u) &= X_1 \sin \Delta u + X_3 \sin 3\Delta u. \end{aligned} \quad (3)$$

The model has six main parameters, each of them consisting of other parameters with a periodic dependency on β_0 , the elevation angle of the Sun above the orbital plane, in total the model has 18 different parameters. Two additional directions Z and X appear in the model, which correspond to the faces of the satellite illuminated by the Sun. The time argument of the periodic signals is related to Δu , the argument of latitude of the satellite w.r.t. the argument of latitude of the Sun in the orbital plane as shown in Fig. 1.

Nowadays CODE uses an updated version¹ of this last model as a priori information for the generation of its final orbits, additionally this IGS analysis center² estimates five empirical parameters from the model of Beutler et al (1994), more specifically the D_0 , Y_0 , B_0 , B_C and B_S parameters, to obtain a very good fit of the GPS orbits to the tracking data. Moreover, in order to compensate for inaccuracies in the model (a priori plus estimated) of the force field, pseudo-stochastic orbit parameters (instantaneous velocity changes) are estimated every 12 hours in the radial, along- and cross-track directions (Beutler et al, 2006).

With an approach similar to the one used by Springer et al (1999) but using a different parametrization, Bar-Sever and Kuang (2004) fitted several years of JPL (Jet Propulsion Laboratory) final orbits to construct an improved GPS Solar Pressure Model (GSPM). The performance of the GSPM model as a priori acceleration plus estimated stochastic parameters was evaluated, against variants of the *DYB* model (without a priori acceleration) of Beutler et al (1994), by Sibthorpe et al (2011). The stochastic parameters used by JPL are: a constant Y -axis bias and a constant scale along the satellite to Sun direction, as well as time varying (stochastic) variations in model scale along the body-fixed spacecraft Z - and X -axes, and small stochastic changes along the Y -axis. This methodology can be regarded as “reduced-dynamic” approach. The evaluation between models (a priori models plus estimated parameters) was done by means of various internal (GIPSY-OASIS Software) and external metrics. Within the metrics favoring the use of the GSPM plus reduced-dynamics approach are: ambi-

guity resolution statistics, orbit overlaps, SLR tracking residuals, station repeatabilities, and GRACE K-band ranging statistics. However, clock overlaps between consecutive days and LOD (Length of Day) differences to IERS (International Earth Rotation and Reference Systems Service) Bulletin A seem to favor the *DYB* approach.

The GSPM model is basically a truncated harmonic expansion in the XYZ body-fixed frame:

$$\begin{aligned} X(\epsilon) &= X_1 \sin \epsilon + X_2 \sin 2\epsilon + X_3 \sin 3\epsilon \\ &\quad + X_5 \sin 5\epsilon + X_7 \sin 7\epsilon, \\ Y(\epsilon) &= Y_1 \cos \epsilon + Y_2 \cos 2\epsilon, \\ Z(\epsilon) &= Z_1 \cos \epsilon + Z_3 \cos 3\epsilon + X_5 \cos 5\epsilon. \end{aligned} \quad (4)$$

The model has 10 parameters and some of them (X_2 and Y_1) also depend on the β_0 angle. It is very interesting to note the selection of the angle ϵ formed by Earth, satellite, and Sun (Fig. 1) as the main dependency of the model. The angle ϵ together with the XYZ directions contain the full information of the nominal attitude of the satellite and it can be derived from Fig. 1 as:

$$\cos \epsilon = -\cos \beta_0 \cos \Delta u \quad (5)$$

with $\epsilon = \pi - \psi$. The nominal attitude of GPS satellites is given by accomplishing at any time two conditions: the navigation antennas are pointing to the center of the Earth for transmitting the navigation signals, and the solar panels are pointing to the Sun for keeping the power supply. This is done by performing a rotation around the Z axis, such that the solar panels can rotate around the satellite bus to a perpendicular position w.r.t. the Sun. This kind of attitude control is called “yaw-steering”. However, during eclipse seasons special maneuvers are required for the midnight and noon turns (Bar-Sever, 1996; Kouba, 2009).

Observing the development of the models to compensate for error sources in the GPS satellites orbits, one can note a tendency to create empirical models that can accommodate the solar radiation pressure. It becomes evident that errors in the determination of GPS satellite orbits are dominated by solar radiation pressure and that other forces acting on GPS satellites (e.g. gravitational forces) have nowadays a much lower contribution to the orbit error budget.

3 Analytical SRP models

Using an analytical approach, a priori solar radiation pressure models have been developed by considering the details of the satellite structure (e.g. small elements and shadowing or re-reflection effects between them), the known optical properties, the physical interaction of radiation with the satellite surfaces (including re-radiated heat effects), and nominal attitude. These models are

¹ftp://ftp.unibe.ch/aiub/REPRO_2008/GEN/SATELLIT.I05, accessed on 18 May 2011.

²<ftp://igsceb.jpl.nasa.gov/pub/center/analysis/code.acn>, accessed on 15 December 2011.

based on information available on ground provided by the satellite manufactures.

The first available a priori analytical models for the Block I and Block II/IIA GPS satellites were the ROCK4 and ROCK42 models, developed by the spacecraft manufacturer, Rockwell International, and IBM. These models were improved by Fliegel et al (1992), approximated by a simple Fourier series in the angle ϵ (Eq. (5)), and named T10 and T20 respectively. Fliegel and Gallini (1996) used the same approach to develop the T30 model for the Block IIR satellite based on a detailed spacecraft model by Martin Marietta, the spacecraft manufacturer. These models are based on the physical characteristics of the GPS satellites, like the optical properties, the dimensions and the interaction between radiation and satellite surfaces, as described in the two mentioned articles. However, these models have gradually lost favor in the IGS analysis centers, which no longer use them as a priori information. A summary of the different strategies to model solar radiation pressure within the IGS can be found in Froideval (2009). In particular Urschl et al (2007) found that these models (at least for Block IIA satellites) introduce systematic errors in the SLR-GPS residuals.

In a later work, Marquis and Krier (2000) developed an improved radiation pressure model for the GPS Block IIR satellites. A very useful result from this study is the comparison of the different forces acting on the satellite, such that the following force contributions could be identified:

- Solar radiation onto the vehicle surfaces.
- Radiation of thermal blankets.
- Thermal radiation from SV radiators. Includes the effect of radiation onto the solar arrays.
- Solar array thermal radiation.
- Thermal radiation of excess solar array power (shunt).
- Radiation pressure on the nadir surfaces from sunlight reflected off the Earth (albedo).
- Earth Infrared pressure on the nadir surfaces (EIR).

As pointed out by Marquis and Krier (2000):

“The spectral or visible contribution from the Sun is the greatest contributor with nearly 100 percent of the total force.”

“Depending on the orbit position, albedo is the next highest contribution peaking 2.5 percent of the total force. The solar array and shunt thermal radiation forces are the next lowest, representing just under 1 percent of the total each, but provide a nearly constant value about the orbit. Although the magnitudes are similar, these forces are applied in opposite directions and nearly cancel each other out.”

Additionally it is mentioned that the thermal part is small but important for the Y direction of the satellite and EIR is the lowest force acting on the satellite. The resulting model is available as a look up table³ but not the dimensions or optical properties used for its construction. However, the dimensions and optical properties for the Block I, Block II/IIA and Block IIR are available from the T10, T20 and T30 models, which make them an ideal starting point for constructing the analytical box-wing model (Section 4).

More recently Ziebart et al (2005) have developed precise models for dealing with the non-conservative forces acting on different types of low and high orbiting satellites. These models take into account further effects as compared to the T20 and T30 models, e.g., shadowing or re-reflection between surfaces. In the case of GPS satellites, a model was constructed for Block IIR considering similar forces as Marquis and Krier (2000).

The previously mentioned analytical satellite models are very important as a priori information but have the main problem that they cannot easily take into account the deviations of the models from reality. The deviations can be caused by aging of satellite surfaces, inaccurately known optical properties or not nominal attitude. An interesting example is the Y -bias acceleration reported for GPS satellites. For Block II/IIA, Fliegel et al (1992) explain the Y -bias by a possible misalignment angle (0.5° to 1°) of the solar panels w.r.t. their nominal position. While for Block IIR, Marquis and Krier (2000) explain the Y -bias by internal heat radiated by the Y surfaces.

4 Adjustable box-wing model

Based on the advantages and disadvantages from the previously exposed models, an analytical box-wing model has been derived based on the physical interaction between the direct solar radiation and a satellite consisting of a bus (box shape) and solar panels. Furthermore, some of the parameters of the box-wing model can be adjusted to fit the GNSS tracking data, namely the optical properties of the corresponding satellite surfaces. This kind of model is an intermediate approach between the physically correct analytical satellite models and the purely empirical ones. For constructing the box-wing model the following assumptions were made:

- The satellite structure can be simplified to a box shape bus and flat solar panels.
- Smaller structures (e.g. antennas or engines) contribute to the effective area, but their shape is not considered.
- No shadowing or re-reflection effects from one surface to another are considered.
- The forces due to internal heat generation cancel from opposite surfaces.

³ftp://sideshow.jpl.nasa.gov/pub/GPS_yaw_attitude/BlockIIR_srp_table, accessed on 20 May 2011.

- Absorbed radiation is assumed to be re-radiated immediately back to space, therefore heating or cooling effects are not considered.
- The irradiance from the Sun, the dimensions, and the mass of the satellite are known.

In future work, the following a priori models are planned to be included: Earth radiation pressure (Rodriguez-Solano et al, 2012a) and yaw attitude during eclipse seasons for Block II/IIA (Bar-Sever, 1996) and Block IIR (Kouba, 2009). These effects are not included in the current study in order to test only a simple box-wing model (with nominal attitude) interacting only with the solar radiation pressure.

The acceleration produced by the physical interaction between the solar radiation and a flat surface of the satellite is formulated by Milani et al (1987) in the following way:

$$\vec{f} = -\frac{A}{M} \frac{S_0}{c} \cos \theta \left[(1 - \rho) \vec{e}_D + 2 \left(\frac{\delta}{3} + \rho \cos \theta \right) \vec{e}_N \right], \quad (6)$$

with:

$$\alpha + \rho + \delta = 1, \quad (7)$$

where:

- A Area of the surface,
- M Mass of the satellite,
- S_0 Solar irradiance at 1 AU ($\approx 1367 \text{ W/m}^2$),
- c Velocity of light in vacuum,
- α Fraction of absorbed photons,
- ρ Fraction of reflected photons,
- δ Fraction of diffusely scattered photons,
- \vec{e}_D Direction of the Sun from the satellite,
- \vec{e}_N Normal to the satellite surface,
- $\cos \theta = \vec{e}_D \cdot \vec{e}_N$, valid only if $\cos \theta \geq 0$.

Fliegel et al (1992) use a different notation to describe the same physical phenomenon, in particular just two optical properties are used: reflectivity (ν) ranging from 0 (black) to 1 (white) and specularity (μ) ranging from 0 (diffuse) to 1 (specular). Additionally the distinction between flat and cylindrical surfaces is made. The relation between both notations is direct by writing the optical properties as: $\alpha = 1 - \nu$, $\rho = \mu \nu$ and $\delta = \nu(1 - \mu)$, which also satisfies Eq. (7). Furthermore, Fliegel et al (1992) mention that to a good approximation the energy absorbed by the satellite bus surfaces is instantaneously re-radiated in the form of heat. Considering that this energy is radiated back to space according to Lambert's law, one gets:

$$\vec{f} = -\frac{A}{M} \frac{S_0}{c} \cos \theta \frac{2}{3} \alpha \vec{e}_N, \quad (8)$$

and by adding the instantaneous re-radiated heat to Eq. (6), it can be written in the following way:

$$\vec{f} = -\frac{A}{M} \frac{S_0}{c} \cos \theta \left[(\alpha + \delta) \left(\vec{e}_D + \frac{2}{3} \vec{e}_N \right) + 2\rho \cos \theta \vec{e}_N \right], \quad (9)$$

which is only valid for the satellite bus. This assumption is correct for materials that have zero thermal capacity and completely prevent heat transfer toward the satellite interior (Cerri et al, 2010) like multilayer insulation (MLI), a common material in spacecraft design. However, using Eq. 9 for all the surfaces of the bus means to constrain the box to be completely covered by MLI, which is not true for GPS satellites. This assumption also implies that heating or cooling effects are neglected, but specially during eclipse seasons (where the satellites are up to 55 minutes in shadow) these effects can be significant. The adjustable box-wing model is only appropriate for solar radiation pressure and other smaller effects (like heating or cooling effects) may lead to systematic errors in the orbits or may be aliased in the box-wing parameters, but they are out of the scope of this paper.

For the solar panels we use Eq. (6). Adhya et al (2005) have shown that the thermal force acting on the solar panels of GPS IIR satellites is roughly 1 % of the SRP force on the panels. More important, according to Adhya et al (2005), is the thermal force acting on the satellite bus with the main force component in the D direction. Both thermal effects, on the solar panels and on the bus (D component), can be accommodated in the solar panels (SP) scaling factor (Eq. 10).

From Eqs. (6) and (9) one can get the partial derivatives of the acceleration w.r.t. the optical properties of the satellite surfaces. Using the assumption of nominal attitude the main dependency is then on the angle ϵ formed by Earth, satellite and Sun (see Fig. 1). A total of seven partial derivatives of the acceleration are obtained:

Solar panels (SP) with $\cos \theta = 1$:

$$\frac{\partial \vec{f}}{\partial (1 + \rho + \frac{2}{3}\delta)} = -\frac{A_{SP}}{M} \frac{S_0}{c} \vec{e}_D. \quad (10)$$

+ X bus surface (+ XAD , + XR) with $\cos \theta = \sin \epsilon$:

$$\frac{\partial \vec{f}}{\partial (\alpha + \delta)} = -\frac{A_{+X}}{M} \frac{S_0}{c} \sin \epsilon \left(\vec{e}_D + \frac{2}{3} \vec{e}_{+X} \right), \quad (11)$$

$$\frac{\partial \vec{f}}{\partial \rho} = -\frac{A_{+X}}{M} \frac{S_0}{c} 2 \sin^2 \epsilon \vec{e}_{+X}. \quad (12)$$

+Z bus surface (+ZAD, +ZR) with $\cos \theta = \cos \epsilon$:

$$\frac{\partial \vec{f}}{\partial (\alpha + \delta)} = -\frac{A_{+Z}}{M} \frac{S_0}{c} \cos \epsilon \left(\vec{e}_D + \frac{2}{3} \vec{e}_{+Z} \right), \quad (13)$$

$$\frac{\partial \vec{f}}{\partial \rho} = -\frac{A_{+Z}}{M} \frac{S_0}{c} 2 \cos^2 \epsilon \vec{e}_{+Z}. \quad (14)$$

The $-Z$ partial derivatives ($-ZAD$, $-ZR$) are constructed in the same way as for $+Z$, with the appropriate sign changes. The partial derivatives are plotted in Fig. 2.

In addition to the seven parameters of the solar radiation pressure box-wing model with nominal attitude, two more parameters have been included to fit the GPS tracking data: 1) the Y -bias parameter ($Y0$) to compensate a constant acceleration acting on the Y -axis of the satellite, and 2) a rotation lag of the solar panels around their rotation axis.

Fliegel et al (1992) explain the causes of the so called Y -bias, mentioning that alignment requirements of the solar panels of 0.5° to 1° are reported in the Rockwell specifications. More importantly Kuang et al (1996) computed the misalignment angles of the solar panels w.r.t. nominal attitude using a simple SRP model, obtaining also small deviations of 1° to 2° from nominal attitude. In general, changes of the nominal attitude of the satellite will affect the SRP, producing non-modeled accelerations. Assuming that there might be small misalignment biases in the nominal rotations around X , Y and Z (Fig. 1), how can they be taken into account by our box-wing model? There are known changes in the yaw attitude (rotation around Z) of the satellites (Bar-Sever, 1996; Kouba, 2009) specially during eclipse seasons, but other smaller misalignment biases in the yaw angle are assumed to be partially absorbed by the box-wing and Y -bias parameters. A simple calculation shows that the deviation from nominal yaw attitude introduced by the yaw bias for GPS II/IIA satellites (Bar-Sever, 1996) will manifest in a constant acceleration acting along the Y -axis. A change in the rotation angle around the X -axis will lead directly to small accelerations in the Y -axis which again can be absorbed by the Y -bias.

For the rotation angle around the Y -axis we distinguish between a misalignment bias of the satellite bus and of the solar panels. The acceleration produced by a non-nominal angle in the satellite bus can be partially absorbed by the parameters of the box part of the box-wing model. For the solar panels a misalignment bias around the Y -axis causes a constant acceleration in the B direction (Fig. 1), which cannot be compensated by the box-wing model. In fact the box-wing model (seven parameters and Y -bias) adjusted to the GPS tracking data results in a much lower performance w.r.t. the purely empirical CODE model, see Fig. 7. Indeed, Springer et al (1999) mentioned that the periodic

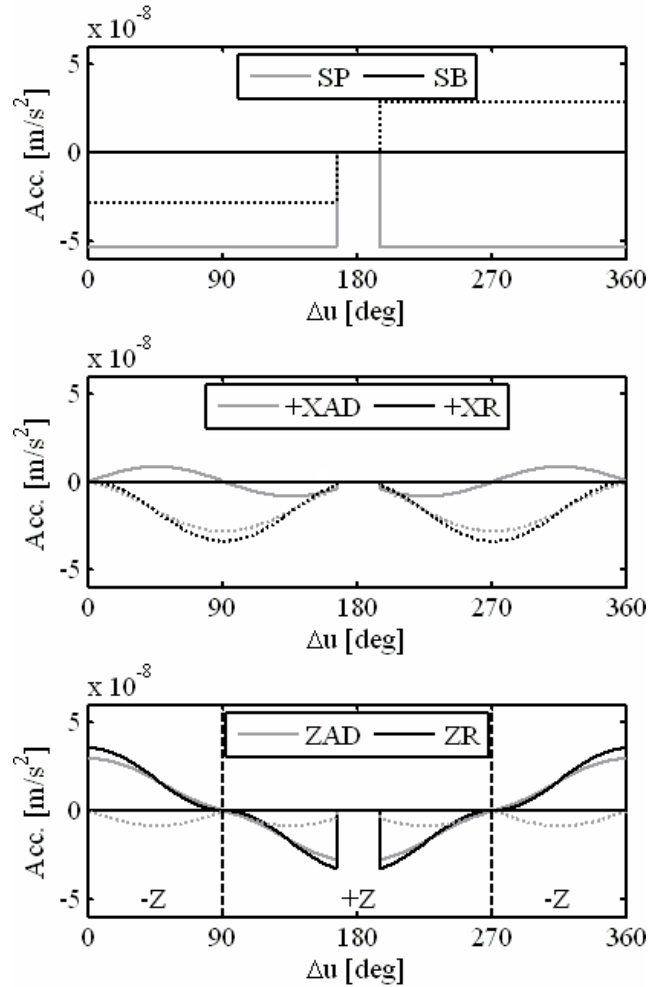


Fig. 2: Partial derivatives of the box-wing model (defined in Eqs. (10) to (15)) for a Block IIR satellite and $\beta_0 = 0^\circ$: top in DB Sun-fixed reference frame, middle and bottom in ZX body-fixed reference frame. D and Z are shown in solid lines, B and X are shown with dotted lines. The Sun is eclipsed for $|\Delta u - 180^\circ| < 14^\circ$.

terms in the B direction most significantly reduce orbit model deficiencies. For modeling the missing parameter of the box-wing model there are basically two possibilities: 1) a B -bias, assuming that the misalignment bias around the Y -axis is constant and does not depend on the direction of rotation of the solar panels, or 2) the misalignment bias around the Y -axis depends on the direction of rotation of the panels or more specifically on the sign of $\dot{\epsilon}$ (time derivative of Eq. (5)) which changes once per revolution. The second option has proven to be the one that fits better the GPS tracking data, with the interpretation that the solar panels follow the Sun with a small lag, therefore we have called this parameter “solar panel rotation lag” (θ_{SB}) and its partial derivative can be written (for nominal yaw attitude) as:

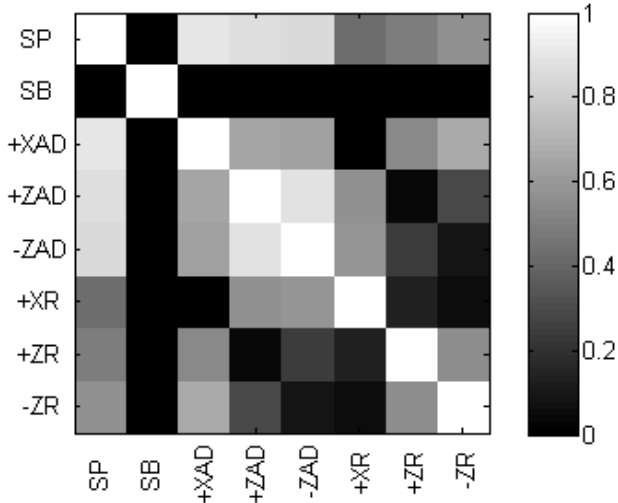


Fig. 3: Correlation between unconstrained parameters of the box-wing model for a Block IIR satellite and $\beta_0 = 0^\circ$. The Y -bias is not shown since its correlations w.r.t. all other parameters are zero.

$$\frac{\partial \vec{f}}{\partial \theta_{SB}} = -\frac{A_{SP} S_0}{M c} 2 \left(\frac{\delta_{SP}}{3} + \rho_{SP} \right) \text{sign}(\dot{\epsilon}) \vec{e}_B, \quad (15)$$

using the small angle approximation ($\sin \theta_{SB} = \theta_{SB}$ and $\cos \theta_{SB} = 1$) and with δ_{SP} and ρ_{SP} being the a priori optical properties of the solar panels (Tables 1 and 2). With this last parameter the analytical box-wing model is complete. In summary we have nine parameters:

- SP : solar panel scaling factor ($1 + \rho + \frac{2}{3}\delta$)
- SB : solar panel rotation lag
- $Y0$: Y -bias acceleration
- $+XAD$: absorption plus diffusion of $+X$ bus ($\alpha + \delta$)
- $+ZAD$: absorption plus diffusion of $+Z$ bus ($\alpha + \delta$)
- $-ZAD$: absorption plus diffusion of $-Z$ bus ($\alpha + \delta$)
- $+XR$: reflection coefficient of $+X$ bus (ρ)
- $+ZR$: reflection coefficient of $+Z$ bus (ρ)
- $-ZR$: reflection coefficient of $-Z$ bus (ρ).

The constraint implied by Eq. 7 has not been imposed, i.e., $\alpha + \rho + \delta$ need not be equal to one. This allows to separate between $\alpha + \delta$ and ρ parameters and gives three extra degrees of freedom to the box-wing model.

The partial derivatives of the box-wing model (except for the Y -bias) are plotted in Fig. 2, for $\beta_0 = 0^\circ$, when the Sun is in the orbital plane of the satellite. Note that all partial derivatives but SB are even functions over one revolution (they can be reflected w.r.t. $\Delta u = 180^\circ$). Moreover for the satellite bus ($+X$, $+Z$ and $-Z$) there are even and odd partial derivatives over half a revolution (w.r.t. $\Delta u = 90^\circ$ or $\Delta u = 270^\circ$). The situation is very different, e.g., for the CODE empirical model

(Eqs. (2) and (3)) where the short term (one revolution) dependency is mainly on $\cos u$ and $\sin u$. However one of the main disadvantages of the box-wing model is the high correlation between the partial derivatives (Fig. 3). In particular the absorption plus diffusion terms (AD) are highly correlated w.r.t. the solar panel scaling factor (SP). The correlation is in general lower for the reflection terms (R). The solar panel rotation lag (SB) is uncorrelated w.r.t. all other parameters, since it is the only one with an odd partial derivative over one revolution. Due to the high correlation of the absorption plus diffusion terms, additional constraints w.r.t. the a priori values (Section 5) are applied to these three terms, when the box-wing model is used to fit the GPS tracking data (Section 6).

5 A priori box-wing model

The box-wing model needs certain a priori information of the satellite. Mandatory are realistic values of mass and dimensions and helpful are the optical properties of the satellite surfaces. The main source for the a priori information are the papers of Fliegel et al (1992) for Block II/IIA and Fliegel and Gallini (1996) for Block IIR. The dimensions presented in Tables 1 and 2 were obtained by computing a simple average of the area of all elements (flat and cylindrical) contributing to a given surface. The optical properties were weighted according to the area of the respective elements.

Applying this simple procedure to the Block IIA, the cylindrical elements of the $+X$ surface sum to 3.331 m^2 ($\alpha = 0.579, \delta = 0.337, \rho = 0.084$), additionally the flat $+X$ surface is 1.553 m^2 , meaning that the $+X$ surface would have an effective area of 4.884 m^2 . In Fliegel et al (1992) the area of each navigation antenna adapter is given as 0.181 m^2 (there are 12 antennas in total). We have computed an approximate value of 0.032 m^2 , derived from pictures and dimensions of the Block II/IIA antenna array (Wübbena et al, 2007), which is more than five times smaller than 0.181 m^2 . We have also considered that just 9 antennas (instead of 12) contribute to the $+X$ effective area, due to shadowing between antennas. Additionally in Fliegel et al (1992) a plume shield is reported, which also contributes to the effective $+X$ surface (diameter 1.84 m, thickness 0.22 m). In satellite bus drawings (Bar-Sever et al, 2009) the diameter seems to be about 0.57 m. Wübbena et al (2007) reports a diameter of 1.34 m for the navigation antenna array, but the diameter of the plume shield cannot be much larger than the one of the antenna array. As no better information was available a diameter of 0.57 m was used for the plume shield, if this value is incorrect it should have just a small impact on the scale of the box-wing parameters (Section 6). Considering 9 antennas of 0.032 m^2 and a plume shield of 0.57 m, we obtain a cylindrical surface of around 35 % of 3.331 m^2 , by adding 1.553 m^2 we get the

Table 1: Dimensions and optical properties of GPS Block II/IIA satellites (mass = 880 kg / 975 kg, respectively).

Surface	Area [m^2]	α	δ	ρ
Solar panels	11.851	0.746	0.057	0.197
+X bus	2.719	0.500	0.400	0.100
+Z bus	2.881	0.440	0.448	0.112
-Z bus	2.881	0.582	0.335	0.083

Table 2: Dimensions and optical properties of GPS Block IIR satellites (mass = 1100 kg).

Surface	Area [m^2]	α	δ	ρ
Solar panels	13.920	0.707	0.044	0.249
+X bus	4.110	0.940	0.060	0
+Z bus	4.250	0.940	0.060	0
-Z bus	4.250	0.940	0.060	0

value of Table 1. The rest of the dimensions provided by Fliegel et al (1992) seem to be correct and are in accordance with other satellite drawings (e.g. Feltens, 1991). For the Block IIR satellite dimensions no conflicts were found. However, these satellites have large antenna arrays (W-sensor, low- and high-band) which are reported by Fliegel and Gallini (1996) to contribute $0.5 m^2$ in the $\pm Z$ directions, therefore this value was added to the $\pm Z$ areas in Table 2.

The a priori information collected here is appropriate for the use with a box-wing model. If better a priori information is available, e.g., by constructing a 3-D model of the satellite and computing shadowing effects (Ziebart et al, 2005), this also may improve the quality of the estimated parameters and the computed orbits. This last step is, however, out of the scope of this paper, where just a simple (but capable of fitting the GPS tracking data) box-wing model accounting for SRP is tested.

6 On-orbit GPS optical properties

GPS orbits were generated based on one year (2007) of tracking data from the global IGS network (around 200 stations). Two solutions were computed, differing only in the solar radiation pressure modeling, one with the CODE empirical model and one with the adjustable box-wing model. We have computed 1-day orbits and the SRP model parameters were also estimated once per day. This was done with the Bernese GPS Software (Dach et al, 2007), where the box-wing model has been implemented in a development version, and using the processing scheme derived from the one used at CODE (Steigenberger et al, 2006, 2011). The a priori weight for the GPS phase measurements corresponds to 1 mm

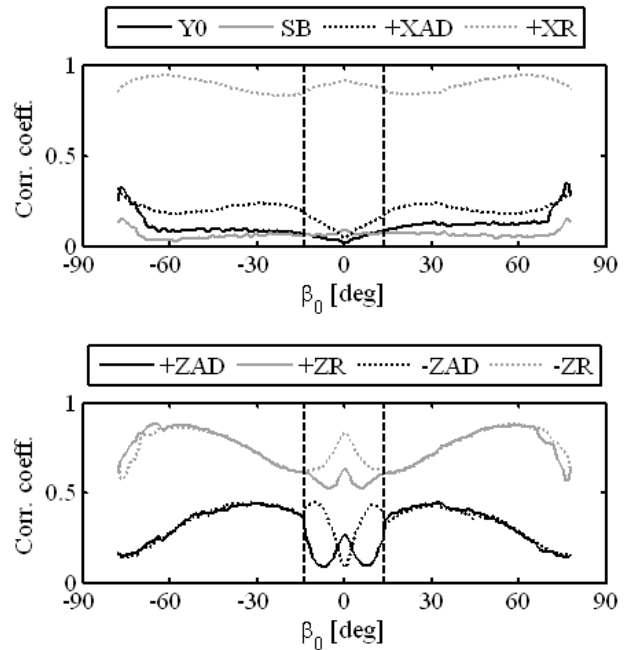


Fig. 4: Correlation of the parameters (constrained) of the box-wing model w.r.t. the solar panel parameter (SP) as a function of β_0 , average over all satellites. Eclipse season for $|\beta_0| < 14^\circ$.

at the zenith of ground stations (elevation dependent weighting was used). The year 2007 has the advantage that the number of Block IIA and IIR satellites is similar: 15 Block IIA and 15 Block IIR satellites (transition of PRN 15 and PRN 29 from II/IIA to IIR, see Table 3), in total 32 satellites.

The CODE empirical model consists of five unconstrained parameters (Eq. (2)): $D0$, $Y0$, $B0$, BC and BS . Additionally, for most satellites (all except PRN 12, 15 (SVN 55), 29 (SVN 57) and 31, see also Table 3) an updated version of the CODE a priori model (Eq. (3), Springer et al, 1999) was applied as a priori acceleration. The CODE a priori model does not consider Earth radiation pressure or antenna thrust explicitly but these effects were partially absorbed in the estimated parameters of the model. Although models for these effects are available (Rodriguez-Solano et al, 2012a), they have not been included in the box-wing model allowing for a clearer comparison w.r.t. the CODE model. Consequently, both models are only well suited for solar radiation pressure and smaller effects will be aliased into the estimated parameters. For the adjustable box-wing model its nine parameters (Section 4) were estimated with different constraints: 1) SP , SB and $Y0$ unconstrained, 2) $+XAD$, $+ZAD$ and $-ZAD$ tightly constrained to 0.01 (around 1 % of the a priori value) and 3) $+XR$, $+ZR$ and $-ZR$ loosely constrained to 0.1 (similar to the a priori value). Additionally for both SRP

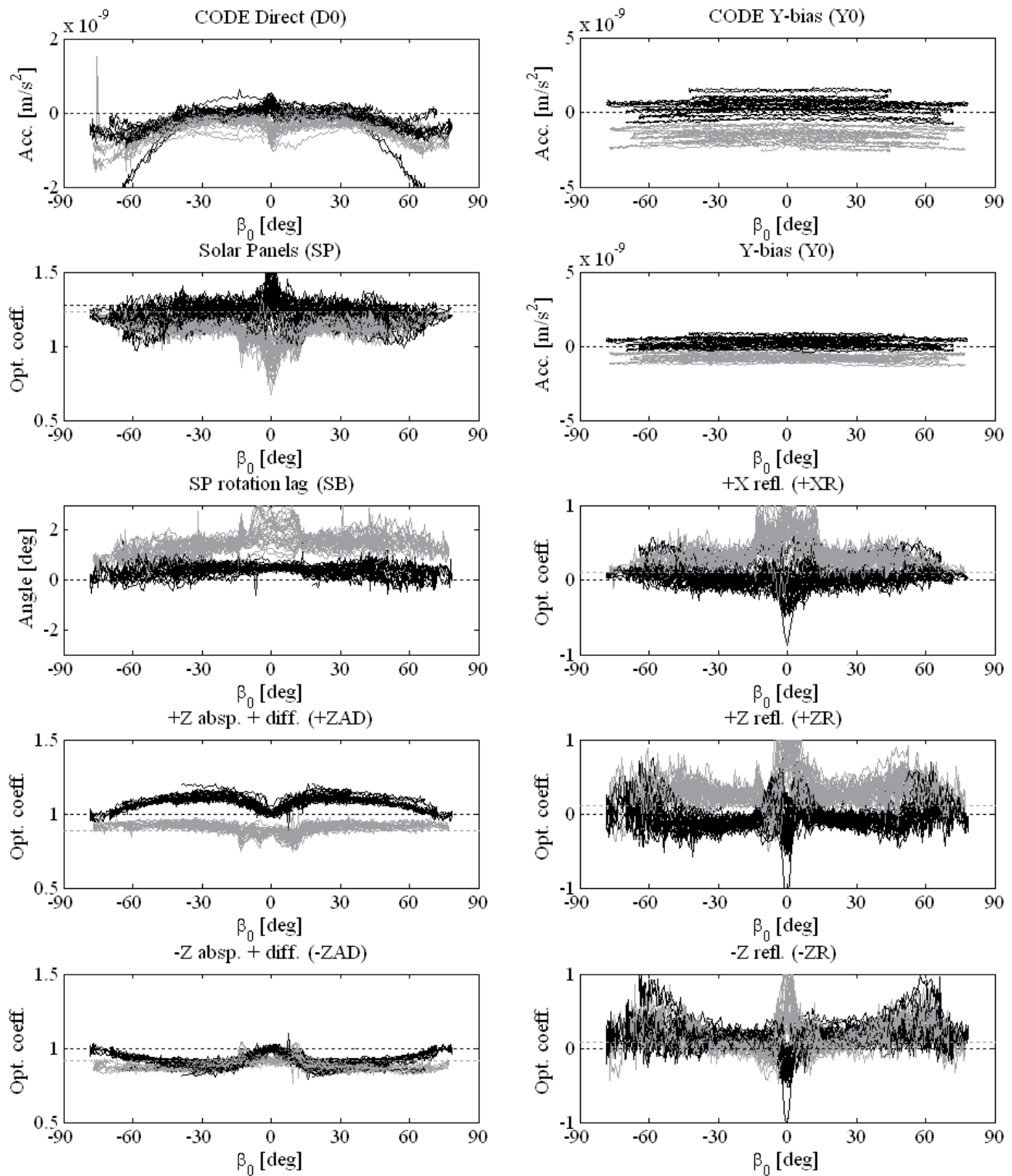


Fig. 5: Estimated parameters of the box-wing model for most GPS satellites in 2007, +XAD is not shown since there is not significant variation w.r.t. the a priori value. Estimated $D0$ and $Y0$ parameters of the CODE empirical model are shown (at the top) for comparison. Block II/IIA satellites are shown in gray and Block IIR in black. A priori values are shown with dashed lines.

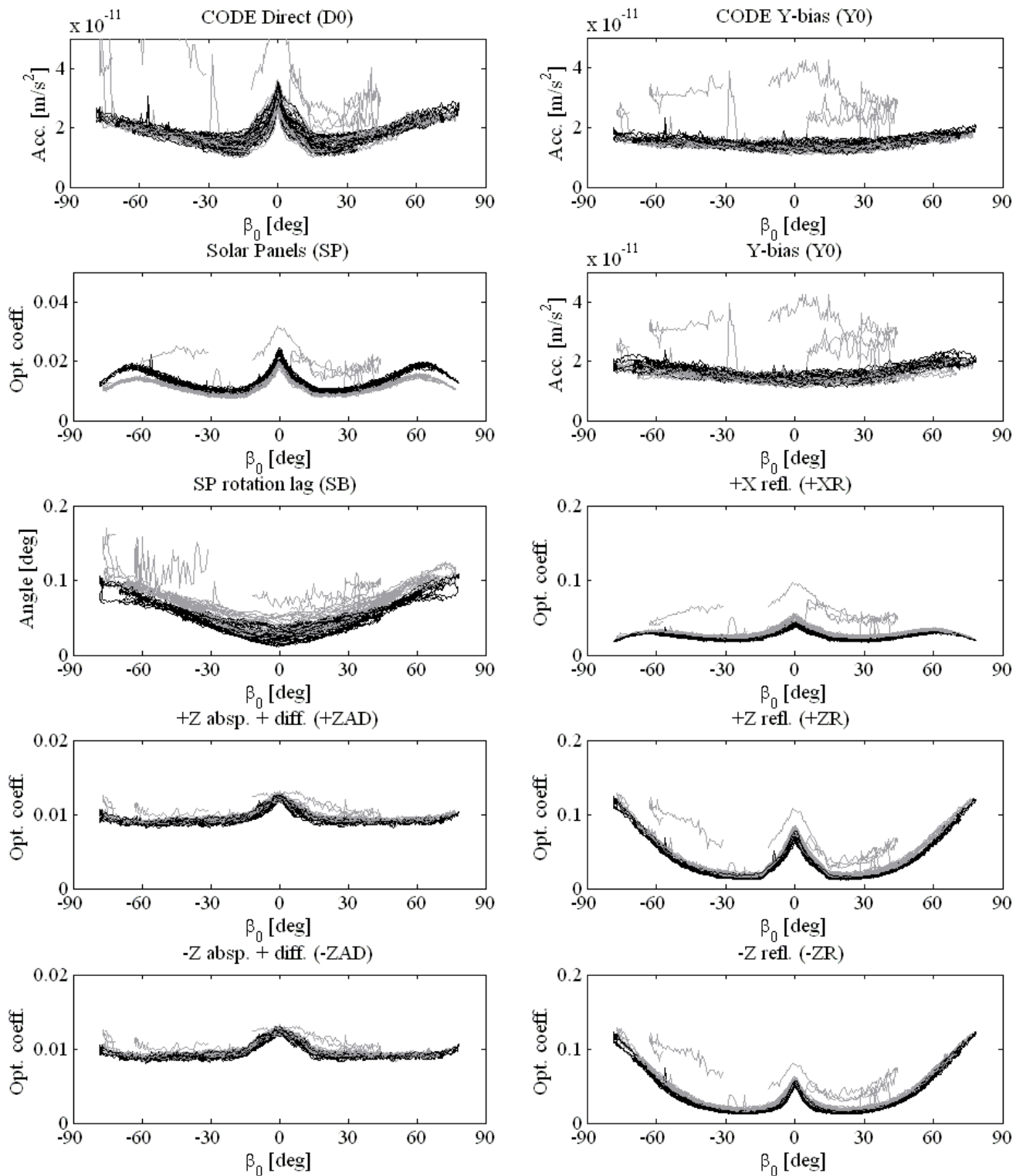


Fig. 6: A posteriori formal errors of the estimated parameters of the CODE and box-wing models (see Fig. 5). Block II/IIA satellites are shown in gray and Block IIR in black.

models, pseudo-stochastic pulses (Beutler et al, 2006) were estimated once per day in the radial, along- and cross-track directions, constrained to 10^{-6} , 10^{-6} , and 10^{-9} m/s respectively.

The constraining of the parameters of the box-wing model has as consequence that the correlation between the absorption plus diffusion terms (AD) decreases w.r.t. the other parameters. In Fig. 4 the correlation of the parameters w.r.t. the solar panel parameter (SP) is shown as a function of β_0 (note that for Fig. 3 the parameters were unconstrained), where the correlation coefficients across all satellites are averaged. The β_0 dependency is a result of the changing incidence radiation angles and exposure times of the bus surfaces as the nominal attitude of the satellite changes with β_0 . Note also that the correlation coefficients, specially for the $+Z$ and $-Z$ surfaces, change when the satellite is in eclipse season ($|\beta_0| < 14^\circ$), since the Sun radiation impacts the $+Z$ surface during less time (see also Fig. 2). The high correlation between the box-wing parameters and the dependency with β_0 are issues that should be further investigated and if possible improved in the future.

Despite the above-mentioned problems, the parameters of the box-wing model (optical properties, solar panel rotation lag and Y -bias) have been successfully estimated from GPS tracking data. The results are presented in Fig. 5 (estimated parameters) and Fig. 6 (a posteriori formal errors) as a function of β_0 for most GPS satellites in 2007. The a posteriori formal errors (Fig. 6) show some outliers mostly for Block II/IIA satellites, related to satellites with less observations than others. Some satellites like PRN 29, or specific days were excluded from the presented results for both models, see Table 3, due to large outliers in the estimated parameters of the box-wing model (Fig. 5). Moreover, for the same reason, satellites performing maintenance maneuvers⁴ have been excluded for the complete day where the maneuver occurred. As expected the box-wing model is only suited for well behaving satellites.

The estimated box-wing parameters are within the range of physically expected a priori values, with some scattering between days and between satellites. Ideally the parameters of the box-wing model should remain constant over time, since the optical properties should not change from day to day or as a function of β_0 . There may be, however, different scales between the parameters of different satellites, for example due to different on-orbit mass values (assumed to be the same for all satellites of the same type, see Tables 1 and 2). The increase of the scattering as a function of β_0 like, e.g., for $+ZR$ and $-ZR$ for β_0 around 60° (Fig. 5), is an indication of the higher correlation of the parameters with others and as a function of β_0 (Fig. 4), also visible in the

Table 3: Manual removal of specific satellites and doy (day of year) intervals, due to large outliers in the estimated parameters of the box-wing model. SVN = Space Vehicle Number.

Satellite	1 st doy	2 nd doy	Reason
PRN 14	296	296	Unknown
PRN 28	48	48	Unknown
PRN 04	39	51	Unknown
PRN 31	39	51	Unknown
PRN 15	72	72	End of life SVN 15
PRN 15	298	304	Start of life SVN 55
PRN 29	1	296	End of life SVN 29
PRN 29	360	365	Start of life SVN 57
PRN 32	93	179	Start of life SVN 23

larger a posteriori formal errors (Fig. 6). The large scattering for $|\beta_0| < 14^\circ$, in the case of parameters like $+XR$ and SB for Block IIA satellites, is most likely associated with the known yaw maneuvers performed during eclipse seasons (Bar-Sever, 1996), which were not yet included in our box-wing model.

The estimated absorption plus diffusion parameters for the $\pm Z$ surfaces ($+ZAD$ and $-ZAD$) for the Block IIR satellites are very interesting and the results were not expected. The variation of these parameters with β_0 looks more like a systematic effect (mismodeling problem in the box-wing model), since these two parameters were tightly constrained to the a priori values. For $+XAD$ (not shown in Fig. 5) no variation with β_0 is observed, however the correlation is also lower w.r.t. the solar panel parameter (Fig. 4). A possible reason for the variation in $+ZAD$ and $-ZAD$ are heating or cooling effects (not considered in the box-wing model), since the bus of Block IIR is reported to have very high absorption coefficients (almost like a black body). Another possibility is that the optical properties of the $+Z$ and $-Z$ surfaces are not equal (Table 2) as reported by Fliegel and Gallini (1996). However, these possibilities have to be further investigated.

For comparison, the $D0$ (direct solar radiation) and $Y0$ (Y -bias) estimated parameters of the CODE empirical model are also shown in Fig. 5 and their a posteriori formal errors in Fig. 6. Firstly, note the significant reduction of the Y -bias when using the box-wing model for both satellite types, indicating that the more physical box-wing model helps to reduce the not fully understood Y -bias (see Section 3). This is consistent with the observation that the correlation of the Y -bias w.r.t. the rest of parameters (including Keplerian elements and pseudo-stochastic pulses) is significantly reduced when introducing the box-wing model. For comparing the $D0$ and SP parameters, we should first consider that an

⁴GPS satellite maneuvers detected by CODE: ftp://ftp.unibe.ch/aiub/REPRO_2008/GEN/SAT_2007.CRX, accessed on 11 August 2011.

error of 0.1 (observed scatter) w.r.t. the a priori value is equivalent to $4.2 \times 10^{-9} \text{ m/s}^2$ for Block IIR satellites ($1 + \rho + \frac{2}{3}\delta = 1.278$). So, in fact, the variation of the CODE empirical parameter is lower than the one of the box-wing model. We should nevertheless consider that the first one uses the CODE a priori model which is based on few years of GPS tracking data, while the box-wing model is just based on one day.

7 Quality of GPS orbits

The box-wing model not only fits well the GPS tracking data but also produces orbits with a similar precision as the ones obtained with the CODE empirical model. The metrics used here to quantify the precision of the computed orbits are not exhaustive, i.e., other metrics are also important, e.g., SLR validation, but can give a first insight into the performance of the adjustable box-wing model.

One quality measure of the orbits are the estimated pseudo-stochastic pulses, initially introduced to compensate for orbit modeling deficiencies. These pulses show a reduction (mainly in radial direction, Fig. 7) when using the box-wing instead of the CODE model. This reduction in the pulses confirms that the box-wing model results in a more physical representation of the GPS orbits than the CODE model. If the solar panel rotation lag (SB) is not estimated, i.e., when using only nominal attitude, the pulses in the radial direction show a large increase (note also the different scale in Fig. 7). Note also that the radial pulses without the SB parameter are larger for Block II/IIA than for Block IIR satellites, corresponding to the larger solar panel rotation lag observed in Fig. 5.

The precision of the computed orbits can also be assessed by comparing orbit overlap errors and prediction errors between the CODE and the box-wing model (Fig. 8). The orbit overlap errors are computed as the magnitude of the vector (radial, along- and cross-track) obtained by taking the difference between consecutive 1-day orbits at the day boundaries. For the prediction errors, the magnitude of the difference vector between predicted 7-day and estimated 1-day orbits is taken, then the RMS (over one day) is taken as prediction error. In addition, for computing the errors shown in Fig. 8, the RMS values for all satellites of the same type (Block II/IIA and IIR) are averaged as a function of the β_0 angle. Figure 8 shows that the performance of the box-wing and CODE models is similar, specially in the orbit overlap errors. The orbit prediction errors are larger for the box-wing model during eclipse season ($|\beta_0| < 14^\circ$) for Block II/IIA satellites. This type of satellite performs longer noon and midnight maneuvers than the Block IIR satellites, affecting the GPS phase measurements and the dynamical orbit parameters during eclipse seasons. Therefore, as the box-wing

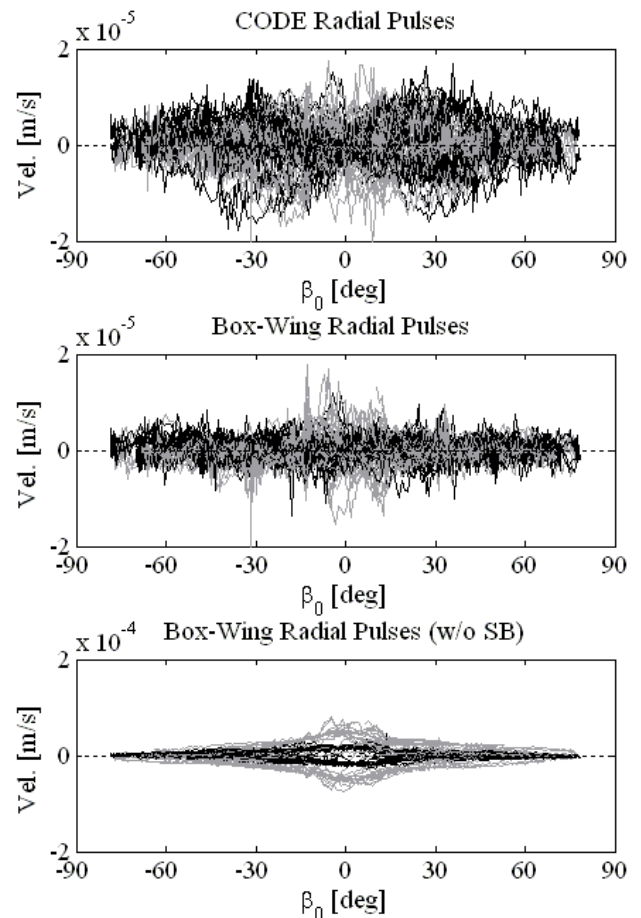


Fig. 7: Estimated pseudo-stochastic pulses in the radial direction for the CODE empirical, box-wing, and box-wing without SB models, for most GPS satellites in 2007. Block II/IIA satellites are shown in gray and Block IIR in black. Please note the different scale of the lowest figure.

model adopts nominal yaw attitude, the effect of the not modeled yaw attitude impacts the box-wing derived orbits more than those obtained with the CODE empirical model, where the parameters in the B direction are capable of partially absorbing the effects caused by non-nominal attitude. A small reduction in the prediction errors is observed for the box-wing model around $\beta_0 = \pm 60^\circ$. Although the prediction performance of the CODE and box-wing models is similar, it should be taken into account that the first one uses the CODE a priori model, derived from several years of data, while the prediction with the box-wing model is based on adjusting one day of GPS tracking data, making this result indeed remarkable.

The quality of the orbits using the two models is very similar, but there are significant and systematic differences between them. Figure 9 shows the radial differ-

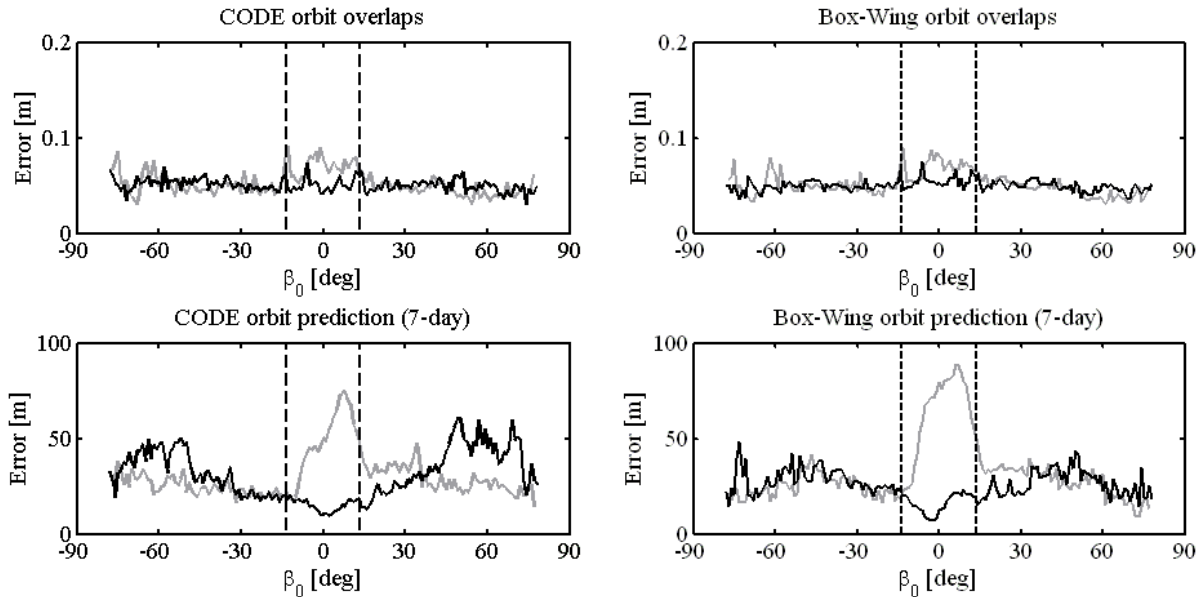


Fig. 8: Orbit overlap and prediction (after 7 days) errors for the CODE empirical (left) and the box-wing (right) models. Average over all satellites of the same type, Block II/IIA (gray) and Block IIR (black). Eclipse season for $|\beta_0| < 14^\circ$.

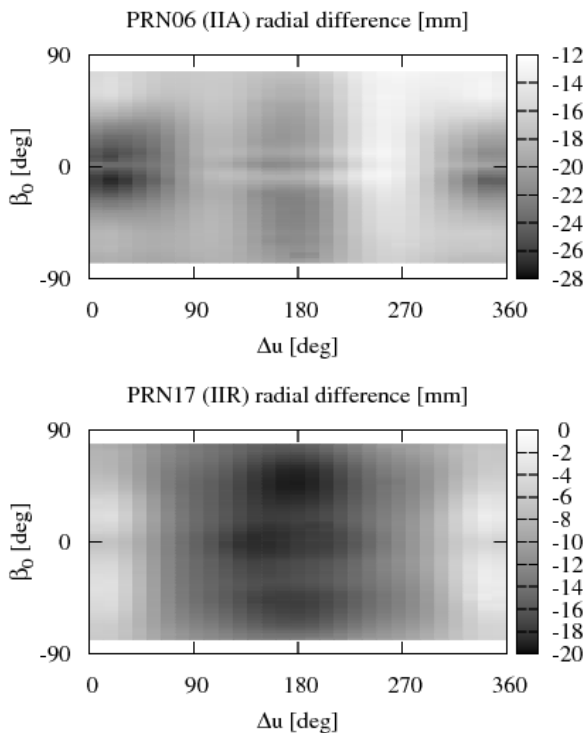


Fig. 9: Orbit differences (box-wing minus CODE empirical) in the radial direction for PRN06 (Block IIA) and PRN17 (Block IIR).

ences for two specific satellites (PRN 06 and PRN 17) in a Sun-fixed reference frame. The along- and cross-track orbit differences are of smaller magnitude and therefore not shown. First of all note the negative radial bias of about 1–2 cm. This bias is in the “correct” direction, i.e., it has the potential to further reduce the bias of SLR minus GPS measurements. Recent comparisons of SLR minus GPS measurements (Bar-Sever et al, 2009) show a negative bias of 1.2–2.2 cm with associated scatters of 1.6–2.5 cm. Secondly, there are also systematic radial differences between the orbits, which are evident when plotted in a Sun-fixed reference frame, and between the block types. Similar patterns are observed when plotting the acceleration differences due to SRP in the radial direction between the box-wing and the CODE empirical model, see also Section 8. There is a β_0 dependency in the radial differences specially for Block IIA satellites, but the major dependency for both blocks is on the Δu angle (the argument of latitude of the satellite w.r.t. the argument of latitude of the Sun) where the partial derivatives (Section 4) of the CODE empirical model and the adjustable box-wing model also differ most. The acceleration caused by the solar panel rotation lag is shown in Fig. 10 for Block IIA and for a specific β_0 angle, for Block IIR (not shown) the acceleration is of smaller magnitude since the rotation lag angle is also smaller (Fig. 5). Note that the radial acceleration shows a shift at $\Delta u = 0^\circ$ and $\Delta u = 180^\circ$. A similar asymmetry can also be seen in Fig. 9 in the radial orbit differences between the box-wing and CODE models.

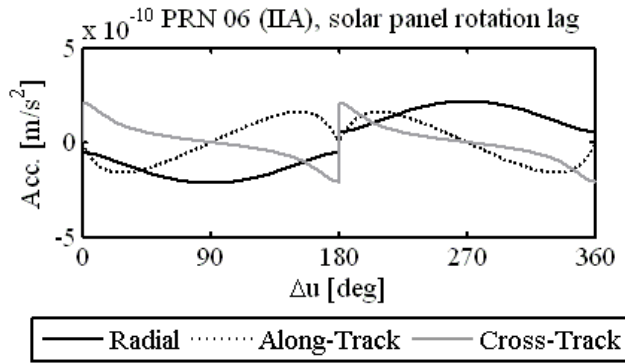


Fig. 10: Acceleration caused by the solar panel rotation lag for $\beta_0 \approx 15^\circ$ and PRN 06 (Block IIA, doy 102).

8 Reconstruction of SRP acceleration

As a final step in this study, we have reconstructed the acceleration due to SRP obtained with the box-wing model. For this purpose the partial derivatives (Section 4), the a priori dimensions (Section 5) and the estimated box-wing parameters using GPS tracking data (Section 6) were combined. The resulting acceleration is plotted in Fig. 11 for PRN 06 and PRN 17. $\beta_0 \approx 15^\circ$ was chosen since the satellites are outside of eclipse season (without yaw attitude problems) and because a small β_0 allows better comparison with other models. Specifically the T20 and T30 models (Fliegel et al, 1992; Fliegel and Gallini, 1996), the GSPM.04b model (Bar-Sever and Kuang, 2004), the Lockheed Martin model (LOCK, Marquis and Krier, 2000) for Block IIR satellites and an updated version of the CODE empirical model (Springer et al, 1999), were compared with the adjustable box-wing model (BOXW).

Figure 11 shows large differences between the SRP models. Note that the variation of the CODE empirical model is much smaller w.r.t. the other models. The CODE empirical model fits very well the GPS tracking data but the resulting acceleration has poor physical meaning, except for the scale. This low variation of the CODE model would indicate that the features observed in the radial orbit differences (Fig. 9), correspond to features in the acceleration introduced mainly by the box-wing model.

In the case of the Block IIR satellites the other four models, two based just on a priori information (T30 and LOCK) and two based on GPS tracking data (GSPM and box-wing) behave very similar, with only small differences. For Block IIA the situation is more interesting, T20 and GSPM are similar and both differ from BOXW, in particular for $90^\circ < \Delta u < 270^\circ$, i.e., when the $+Z$ surface of the satellite bus is illuminated by the Sun (Fig. 1). This difference between the models for Block IIA is not only present for a particular β_0 angle but it

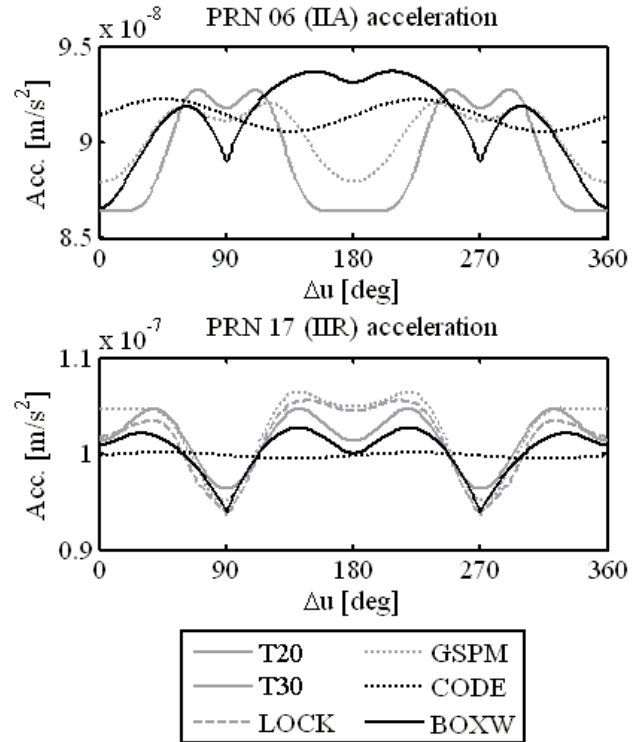


Fig. 11: Reconstructed total acceleration due to SRP for the box-wing model and comparison with existing models, for $\beta_0 \approx 15^\circ$ and PRN 06 (Block IIA, doy 102) and PRN 17 (Block IIR, doy 104).

is systematic. When plotting the total acceleration of the T20 and box-wing models in a Sun-fixed reference frame (β_0 vs. Δu), the T20 model shows a minimum for $90^\circ < \Delta u < 270^\circ$ while the box-wing model shows a maximum. It seems as if there would be an important difference in the construction of the T20 and the box-wing model. It is interesting that the T20 and GSPM models are mainly symmetric for the $+Z$ and $-Z$ surfaces, considering that the reported optical properties by Fliegel et al (1992) are not equal for the $+Z$ and $-Z$ surfaces. The GSPM model is symmetric around $\Delta u = 180^\circ$, just like the box-wing model, but no differences can be seen when the Sun illuminates the $+Z$ or $-Z$ bus surfaces (different than for Block IIR). However, the differences in the optical properties for Block II/IIA would lead to much smaller acceleration differences between the $+Z$ and $-Z$ as the ones observed by the box-wing model. Furthermore, as Earth radiation pressure and antenna thrust were not considered in the box-wing model they may also contribute to the discrepancy between models for Block II/IIA satellites. This problem requires further investigation to decide which model is “correct”, however when computing SLR-GPS residuals (Urschl et al, 2007) the T20 model has shown problems while the adjustable box-wing model could rather re-

duce the SLR-GPS bias (Fig. 9), favoring probably the adjustable box-wing model.

9 Conclusions

A new model for the solar radiation pressure on GPS satellites has been developed. The model simplifies the satellite to a box (satellite bus) and a wing (solar panels), and assumes an ideal yaw attitude of the satellite, but allows for a misalignment of the solar panels. The model has been derived based on the physical interaction between the solar radiation and the box-wing satellite. The model is capable of fitting the GPS tracking data by adjusting mainly the optical properties of the satellite surfaces. The misalignment of the solar panels w.r.t. their nominal orientation is modeled as a rotation lag of the solar panels around their rotation axis. In particular this last parameter of the box-wing model, not previously identified for GPS satellites, is a key factor for fitting the tracking data and obtaining highly precise GPS orbits.

The nine parameters of the box-wing model, optical properties of the surfaces, solar panels rotation lag and Y-bias, together with the satellite orbits have been estimated by fitting one year of GPS tracking data from the IGS network (around 200 global stations). The estimated parameters show a main dependency on the β_0 angle, the Sun elevation angle above the orbital plane, mainly due to correlations of box-wing parameters. However, other effects are also visible, like the not nominal yaw attitude of the Block II/IIA satellites during eclipse seasons or not modeled surface forces specially for Block IIR satellites. Smaller effects than SRP like Earth radiation pressure, antenna thrust and heating or cooling effects have not been considered in this study making the box-wing model only appropriate for solar radiation pressure.

The computed GPS orbits using the adjustable box-wing model show a similar performance as the ones generated with the CODE empirical model, when looking at overlap and prediction errors, and a better performance when looking at the radial pseudo-stochastic pulses which show a reduction. However, systematic differences between the two types of orbits are observed. This indicates that the empirical CODE model fits well the GPS tracking data but cannot totally compensate for the accelerations induced by solar radiation pressure. On the contrary, the box-wing model introduces features in the accelerations and in the orbits due to the physical modeling of solar radiation pressure.

From the estimated parameters of the box-wing model the acceleration due to solar radiation pressure was reconstructed. The acceleration was also compared to the one provided by the available analytical and empirical models. The differences between models are large, in particular for the Block II/IIA satellites. This indicates

that further work should be invested in understanding the differences between the models.

This paper highlights that there are still open issues in the modeling of solar radiation pressure, in particular for GPS satellites (but also for other satellites like GLONASS). The further modeling and understanding of the non-conservative forces impacting the GNSS satellites is very important. This cannot only improve the satellite orbits but also the geodetic parameters derived from them.

GPS satellites are very good to test developments in the modeling of non-conservative forces affecting the satellites due to: 1) the high quality of GPS data provided by the IGS network and 2) the availability of a priori information concerning the satellite structure and optical properties. Improvement in the orbits of these satellites is, however, limited. Once the non-conservative forces acting on GPS satellites are well modeled, the adjustable box-wing model can be applied to satellites where the optical properties are not available or not known, like GLONASS. The orbit improvement there could be higher. Finally, reprocessing of GPS data has proven to be an important scientific tool to test different modeling approaches in a consistent way.

Acknowledgements

This work is funded by the DFG project “LEO orbit modeling improvement and application for GNSS and DORIS LEO satellites”, performed in cooperation with VUGTK (Štěpánek et al, 2010).

The authors gratefully acknowledge the International GNSS Service (IGS, Dow et al, 2009) for providing the high quality data needed for this study. The comments and suggestions of three reviewers and the editor Pascal Willis are greatly appreciated. We acknowledge the support of the TUM Graduate School’s Faculty Graduate Center Bau-Geo-Umwelt at the Technische Universität München.

References

- Adhya S, Ziebart M, Sibthorpe A, Arrowsmith P, Cross P (2005) Thermal Force Modeling for Precise Prediction and Determination of Spacecraft Orbits. *Navig J Inst Navig* 52(3):131–144
- Bar-Sever YE (1996) A new model for GPS yaw attitude. *J Geod* 70(11):714–723, DOI 10.1007/BF00867149
- Bar-Sever Y, Kuang D (2004) New Empirically Derived Solar Radiation Pressure Model for GPS Satellites. In: *Interplanetary Network Progress Report*, vol 42-159, URL http://ipnpr.jpl.nasa.gov/progress_report/42-159/title.htm
- Bar-Sever Y, Davis JL, Dach R, Flohrer C, Herring T, Ray J, Slater JA, Thaller D (2009) Impact of SLR tracking on GPS. In: Pavlis EC (ed) *International Technical Laser Workshop on SLR Tracking of GNSS*

- Constellations. Position Paper, URL http://acc.igs.org/orbits/slr_track_gps_ilrs09-PP.pdf
- Berthias JP, Broca P, Ferrier C, Guitart A, Houry S, Mercier F, Piuze A, Labbez L (2002) JASON-1: a new reference for precise orbit determination. In: IAF Abstracts, 34th COSPAR Scientific Assembly, The Second World Space Congress
- Beutler G, Brockmann E, Gurtner W, Hugentobler U, Mervart L, Rothacher M, Verdun A (1994) Extended orbit modeling techniques at the CODE processing center of the International GPS Service for Geodynamics (IGS): theory and initial results. *Manuscr Geod* 19(6):367–386
- Beutler G, Jäggi A, Hugentobler U, Mervart L (2006) Efficient satellite orbit modelling using pseudo-stochastic parameters. *J Geod* 80(7):353–372, DOI 10.1007/s00190-006-0072-6
- Cerri L, Berthias JP, Bertiger WI, Haines BJ, Lemoine FG, Mercier F, Ries JC, Willis P, Zelensky NP, Ziebart M (2010) Precision Orbit Determination Standards for the Jason Series of Altimeter Missions. *Mar Geod* 33(S1):379–418, DOI 10.1080/01490419.2010.488966
- Colombo OL (1989) The Dynamics of Global Positioning Orbits and the Determination of Precise Ephemerides. *J Geophys Res* 94(B7):9167–9182, DOI 10.1029/JB094iB07p09167
- Dach R, Hugentobler U, Fridez P, Meindl M (2007) Bernese GPS Software, Version 5.0. Astronomical Institute, University of Bern
- Dow J, Neilan R, Rizos C (2009) The International GNSS Service in a changing landscape of Global Navigation Satellite Systems. *J Geod* 83(3-4):191–198, DOI 10.1007/s00190-008-0300-3
- Feltens J (1991) Nicht-gravitative Störeinflüsse bei der Modellierung von GPS-Erdumlaufbahnen. Deutsche Geodätische Kommission, Reihe C, Heft Nr. 371. (In German)
- Fliegel H, Gallini T, Swift E (1992) Global Positioning System Radiation Force Model for Geodetic Applications. *J Geophys Res* 97(B1):559–568, DOI 10.1029/91JB02564
- Fliegel H, Gallini T (1996) Solar Force Modeling of Block IIR Global Positioning System Satellites. *J Spacecr Rockets* 33(6):863–866, DOI 10.2514/3.26851
- Flohrer C, Otten M, Springer T, Dow J (2011) Generating precise and homogeneous orbits for Jason-1 and Jason-2. *Adv Space Res* 48(1):152–172, DOI 10.1016/j.asr.2011.02.017
- Froideval LO (2009) A Study of Solar Radiation Pressure Acting on GPS satellites. PhD thesis, The University of Texas at Austin
- Gobinddass P M L Willis, de Viron O, Sibthorpe A, Zelensky NP, Ries JC, Ferland R, Bar-Sever Y, Dament M, Lemoine FG (2009) Improving DORIS geocenter time series using an empirical rescaling of solar radiation pressure models. *Adv Space Res* 44(11):1279–1287, DOI 10.1016/j.asr.2009.08.004
- Hugentobler U, van der Marel H, Springer T (2006) Identification and mitigation of GNSS errors. In: Springer T, Gendt G, Dow JM (eds) *The International GNSS Service (IGS): "Perspectives and Visions for 2010 and beyond"*, IGS Workshop 2006
- Kouba J (2009) A simplified yaw-attitude model for eclipsing GPS satellites. *GPS Solut* 13(1):1–12, DOI 10.1007/s10291-008-0092-1
- Kuang D, Rim HJ, Schutz BE, Abusali PAM (1996) Modeling GPS satellite attitude variation for precise orbit determination. *J Geod* 70(9):572–580, DOI 10.1007/BF00867865
- Lemoine FG, Zelensky NP, Chinn DS, Pavlis DE, Rowlands DD, Beckley BD, Luthcke SB, Willis P, Ziebart M, Sibthorpe A, Boy JP, Luceri V (2010) Towards development of a consistent orbit series for TOPEX, Jason-1, and Jason-2. *Adv Space Res* 46(12):1513–1540, DOI 10.1016/j.asr.2010.05.007
- Marquis W, Krier C (2000) Examination of the GPS Block IIR Solar Pressure Model. In: *Proceedings of ION GPS 2000*, pp 407–415
- Marshall JA, Luthcke SB (1994) Modeling Radiation Forces Acting on Topex/Poseidon for Precision Orbit Determination. *J Spacecr Rockets* 31(1):99–105
- McMahon JW, Scheeres DJ (2010) New Solar Radiation Pressure Force Model for Navigation. *J Guid Contr Dynam* 33(5):1418–1428, DOI 10.2514/1.48434
- Milani A, Nobili AM, Farinella P (1987) Non-gravitational perturbations and satellite geodesy. Adam Hilger, Bristol
- Ray J, Altamini Z, Collilieux X, van Dam T (2008) Anomalous harmonics in the spectra of GPS position estimates. *GPS Solut* 12(1):55–64, DOI 10.1007/s10291-007-0067-7
- Rodriguez-Solano CJ, Hugentobler U, Steigenberger P (2012a) Impact of Albedo Radiation on GPS Satellites. In: Kenyon S, Pacino MC, Marti U (Eds) *Geodesy for Planet Earth*, IAG Symposia 136, Springer, pp 113–119, DOI 10.1007/978-3-642-20338-1_14
- Rodriguez-Solano CJ, Hugentobler U, Steigenberger P, Lutz S (2012b) Impact of Earth radiation pressure on GPS position estimates. *J Geod* 86(5):309–317, DOI 10.1007/s00190-011-0517-4
- Sibthorpe A, Bertiger W, Desai SD, Haines B, Harvey N, Weiss JP (2011) An evaluation of solar radiation pressure strategies for the GPS constellation. *J Geod* 85(8):505–517, DOI 10.1007/s00190-011-0450-6
- Springer T, Beutler G, Rothacher M (1999) A New Solar Radiation Pressure Model for GPS Satellites. *GPS Solut* 2(3):50–62, DOI 10.1007/PL00012757
- Steigenberger P, Rothacher M, Dietrich R, Fritsche M, Rülke A, Vey S (2006) Reprocessing of a global GPS

- network. *J Geophys Res* 111(B05402), DOI 10.1029/2005JB003747
- Steigenberger P, Hugentobler U, Lutz S, Dach R (2011) CODE Contribution to the First IGS Reprocessing Campaign. Tech. Rep. 1/2011, IAPG/TUM, URL <https://mediatum2.ub.tum.de/doc/1078108/1078108.pdf>
- Štěpánek P, Douša J, Filler V, Hugentobler U (2010) DORIS data analysis at Geodetic Observatory Pecný using single-satellite and multi-satellite geodetic solutions. *Adv Space Res* 46(12):1578–1592, DOI 10.1016/j.asr.2010.04.015
- Tapley BD, Bettadpur S, Watkins M, Reigber C (2004) The gravity recovery and climate experiment: Mission overview and early results. *Geophys Res Lett* 31(L09607), DOI 10.1029/2004GL019920
- Urschl C, Beutler G, Gurtner W, Hugentobler U, Schaer S (2007) Contribution of SLR tracking data to GNSS orbit determination. *Adv Space Res* 39(10):1515–1523, DOI 10.1016/j.asr.2007.01.038
- Wübbena G, Schmitz M, Mader G, Czopek F (2007) GPS Block II/IIA Satellite Antenna Testing using the Automated Absolute Field Calibration with Robot. In: *Proceedings of ION GNSS 2007*, pp 1236 – 1243
- Zelensky NP, Lemoine FG, Ziebart M, Sibthorpe A, Willis P, Beckley BD, Klosko SM, Chinn DS, Rowlands DD, Luthcke SB, Pavlis DE, Luceri V (2010) DORIS/SLR POD modeling improvements for Jason-1 and Jason-2. *Adv Space Res* 46(12):1541–1558, DOI 10.1016/j.asr.2010.05.008
- Ziebart M, Dare P (2001) Analytical solar radiation pressure modelling for GLONASS using a pixel array. *J Geod* 57(11):587–599, DOI 10.1007/s001900000136
- Ziebart M, Adhya S, Sibthorpe A, Edwards S, Cross P (2005) Combined radiation pressure and thermal modelling of complex satellites: Algorithms and on-orbit tests. *Adv Space Res* 36(3):424–430, DOI 10.1016/j.asr.2005.01.014
- Ziebart M, Sibthorpe A, Cross P, Bar-Sever Y, Haines B (2007) Cracking the GPS - SLR Orbit Anomaly. In: *Proceedings of ION GNSS 2007*, pp 2033–2038

Improving the orbits of GPS block IIA satellites during eclipse seasons

C. J. Rodriguez-Solano, U. Hugentobler, P. Steigenberger, G. Allende-Alba

Institut für Astronomische und Physikalische Geodäsie, Technische Universität München, 80333 München, Germany

Abstract

During Sun-Earth eclipse seasons, GPS-IIA satellites perform noon, shadow and post-shadow yaw maneuvers. If the yaw maneuvers are not properly taken into account in the orbit determination process, two problems appear: 1) the observations residuals increase since the modeled position of the satellite's navigation antenna differs from the true position, and 2) the non-conservative forces like solar radiation pressure or Earth radiation pressure are mismodeled due to the wrong orientation of the satellite's surfaces in space.

In this study we consider the yaw maneuvers for the computation of solar radiation pressure and Earth radiation pressure acting on a box-wing like satellite. Also the computation of the satellite's navigation antenna position takes into account the yaw maneuvers. Two models are tested for the yaw maneuvers of GPS-IIA satellites, the existing attitude model with nominal yaw rates and an upgraded version based on the real yaw attitude estimated from PPP (Precise Point Positioning) phase residuals. Additionally, for GPS-IIR and GLONASS-M the existing yaw attitude models with nominal yaw rates are tested. Moreover, two models are tested for the orientation of the solar panels of GPS-IIA satellites during yaw maneuvers, one assuming that the panels point as perpendicular as possible to the Sun and the other assuming a specific pitch attitude during the shadow and post-shadow turns.

The attitude models of increasing complexity are introduced into the computation of daily orbits based on real GPS+GLONASS tracking data for the years 2007 and 2008. From the solutions including the box-wing model with nominal attitude to the one with the most refined attitude models, the average improvements in

the orbits of GPS-IIA satellites during eclipse seasons are quantified as follows: orbit overlap errors decrease from 0.075 to 0.063 m, orbit prediction errors after the first 3 to 9 hours decrease from 0.155 to 0.095 m, and after four days decrease from 6.77 to 3.28 m.

Keywords: GNSS; box-wing satellite model; precise orbit determination; solar radiation pressure; yaw attitude.

1 Introduction

The orbits of GPS satellites show a lower performance during Sun-Earth eclipse seasons than during periods outside these seasons. In particular, the orbits of GPS-IIA satellites are worse during eclipses, while GPS-IIR satellite orbits are almost unaffected. The cause of this problem is the yaw attitude of the satellites during eclipses. On the one hand, the yaw attitude of GPS-IIR is simple to model and to predict, being in most cases very close to the nominal yaw-steering attitude (Kouba, 2009). On the other hand, the yaw attitude of GPS-IIA strongly depends on the space vehicle maximum yaw rate. Moreover, the maximum yaw rate may not be constant and in principle it should be estimated for each maneuver as recommended by Bar-Sever (1996). During eclipse seasons the GPS-IIA satellites perform noon, shadow and post-shadow yaw maneuvers. Additionally, in these satellites a yaw bias was implemented (starting November 1995 the bias is set to $+0.5^\circ$ on all satellites, Bar-Sever, 1996) in order to make the rotational direction of the shadow maneuvers predictable, which then corresponds to the sign of the yaw bias. The complete model for the GPS-IIA satellites is provided by Bar-Sever (1996).

In this paper, the real yaw attitude of the satellites

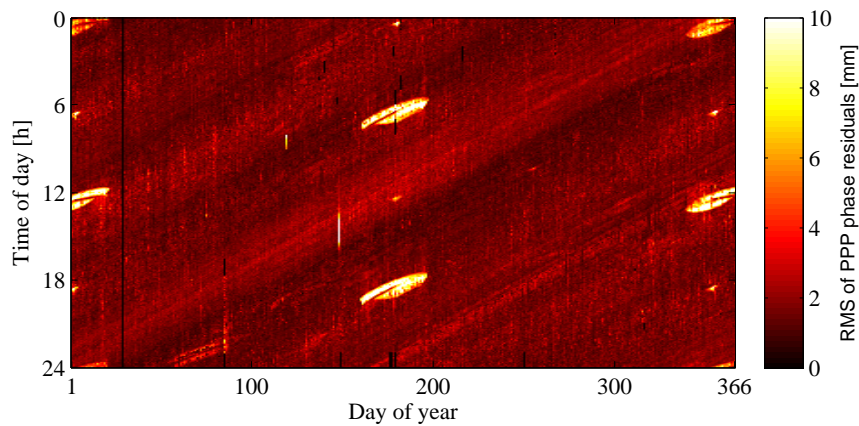


Fig. 1: RMS of elevation weighted PPP phase residuals over all stations visible to the GPS-IIA satellite SVN 40, shown as function of time of day and day of year (2008). The ellipse-shaped white areas reveal the satellite's shadow and post-shadow maneuver periods.

is estimated from PPP residuals (see Fig. 1) exploiting the offset of the navigation antenna w.r.t. the satellite rotation axis. This method is less precise than other approaches, like the inverse PPP method, applied to GPS-IIF (Dilssner, 2010) and GLONASS-M (Dilssner et al, 2011) satellites. However, the estimation of the yaw angle starting from PPP residuals is very fast, making possible to compute the real yaw attitude for long periods as shown in Section 2. Furthermore, from the epoch-wise yaw angle estimates the best fitting maximum yaw rate was estimated, and an empirical model of the yaw rate as function of β_0 , the Sun elevation angle above the orbital plane, was created (Section 3).

The degradation of the GPS-IIA orbits during eclipse seasons has been observed in different metrics like: 1) errors in the fitting of 10-day arcs of truth orbits (Bar-Sever, 1997; Bar-Sever and Kuang, 2005), 2) prediction errors of GPS II and IIA satellites (Bar-Sever, 1997; Douša, 2010; Rodriguez-Solano et al, 2012c; Leandro et al, 2012; Choi et al, 2012), and 3) GPS minus SLR (satellite laser ranging) residuals to the SVN 35 and SVN 36, the two block IIA spacecraft carrying laser retro-reflector arrays (Urschl et al, 2007). Moreover, the estimated satellite clock corrections are degraded (Kouba, 2009) during yaw maneuvers. This introduces errors for clock prediction or for the combination of clock solutions originating from different IGS (International GNSS Service) Analysis Centers.

There are mainly two problems that cause mismodeling of the orbits if the nominal yaw attitude law of the satellites is used: 1) The position of the antenna w.r.t. center of mass of the satellite, more specifically w.r.t. its rotation axis, is wrong, leading to large errors in the observations, as shown by Dilssner et al (2011). Fig. 1 also shows how the PPP phase residuals increase during noon, shadow and post-shadow yaw maneuvers.

2) The orientation of the satellite w.r.t. the Sun is not well known and consequently the computation of solar radiation pressure will be erroneous if the satellite performs the maneuver in sunlight, which is the case for the post-shadow and the noon maneuvers. Additionally, when the satellite is in the shadow of the Earth a small error results from the infrared Earth radiation impacting the surfaces of the satellite.

One of the major motivations for this study is the post-shadow maneuver of GPS-IIA satellites. This maneuver is very challenging to model, since the yaw rotational direction depends entirely on the yaw angle at shadow exit and consequently on the yaw rate during the shadow maneuver. The complexity of this maneuver can be avoided for the problem of erroneous position of the antenna w.r.t. the rotation axis of the satellite by erasing the observation data for 30 minutes after shadow exit (Bar-Sever, 1996; Kouba, 2009). However, for the solar radiation pressure computation, one cannot simply erase the orbit during 30 minutes, and as mentioned above, the post-shadow maneuver occurs during full sunlight. In principle, the orbit integration could be restarted after shadow exit, but this would imply 12 hour arcs (for the best cases) instead of 24 hours arcs. This arc splitting alone would imply an important orbit degradation.

For the computation of the solar and the terrestrial radiation pressure, not only the orientation of the satellite bus in space is important, but clearly also the orientation of the large solar panels arrays should be well known. In this paper we explore two different models for the attitude of the solar panels. The first model simply assumes that the panels are pointed as perpendicular as possible to the Sun (for keeping a maximum power supply) for a given yaw angle. The second model is based on Bar-Sever (1995) and on the information provided by the author that the solar panels are fixed during a shadow

passage, i.e., they are not rotating w.r.t. the satellite body, implying that the solar panels have to perform a short post-shadow recovery. Both models are analytically described in Section 4. Furthermore, the solar radiation pressure is computed using the adjustable box-wing model presented in Rodriguez-Solano et al (2012c), while the Earth radiation pressure is computed using the model presented in Rodriguez-Solano et al (2012a). In Section 5, the changes needed in the box-wing model to include the non-nominal yaw and solar panels attitude are explained in detail.

In this study we also analyzed the GPS-IIR and GLO-NASS-M satellites. For these satellites, besides the nominal attitude model, we have implemented the corresponding models of Kouba (2009) and Dilssner et al (2011) for the noon and shadow yaw maneuvers. No attempt has been made to estimate the real yaw attitude of those satellites, and just the nominal yaw rates of $0.2^\circ/\text{s}$ and $0.25^\circ/\text{s}$ were used respectively. With the different yaw and solar panel attitude models implemented in a development version of the Bernese GNSS Software (Dach et al, 2007, 2008), and with the box-wing model capable of assimilating this information, five different 2-year (2007 and 2008) orbit solutions were computed, see Section 6. The improvement of the orbits by including these models is quantified in terms of orbit overlap errors (Section 7) and orbit prediction errors (Section 8).

The only existing studies, to our knowledge, which developed and tested a solar radiation pressure model for eclipsing GPS II and IIA satellites incorporating the noon and post-shadow yaw maneuvers information are Bar-Sever (1997) and Bar-Sever and Kuang (2005). The first study describes in detail the GSPM.II.97 “split” model used for GPS II and IIA satellites. The second study is an evaluation of the GSPM.II.97 “split” model with more recent data for GPS II and IIA satellites, while for GPS-IIR satellites the GSPM.04a model (created from flight data of non-eclipsing satellites, Bar-Sever and Kuang, 2004) was simply extended into the eclipsing regime. GSPM stands for “GPS Solar Pressure Model” and it is an empirical model based on flight data. By fitting several years of JPL (Jet Propulsion Laboratory) final orbits, the coefficients of a Fourier expansion (as function of the ϵ angle, see Fig. 1) could be estimated. This is the basic approach for non-eclipsing satellites. For eclipsing GPS II and IIA satellites, the GSPM.II.97 “split” model was developed, which consist of the T20 model (Fliegel et al, 1992) splitted into two radiation force contributions: the solar array and the main body of the spacecraft. During yaw maneuvers, the main-body-induced radiation force is rotated from its nominal direction around the Z axis by the amount of yaw error. The solar array induced radiation pressure is computed by assuming the optical properties and the orientation of the solar array. The normal vector to the solar array is explicitly modeled following the same

principles of the post-shadow yaw maneuver (Bar-Sever, 1996) assuming a pitch rate of $0.25^\circ/\text{s}$. However, no further details are given on the solar array motion model. Overall, with the GSPM.II.97 “split” model, Bar-Sever (1997) and Bar-Sever and Kuang (2005) achieve an improvement of the orbits, but not reaching the same performance as for non-eclipsing satellite orbits. Bar-Sever (1997) provides orbit predictions errors, but these results look in general worse (6.057 m) than ours (3.281 m, Section 8) after applying the corrective models for eclipsing satellites. However, as these results are based on data from July, 1995 to May, 1996, they cannot be compared directly, since the quality of GPS orbits (e.g. IGS final orbits, Dow et al, 2009) has increased greatly since the early years due the better ground tracking network and algorithms used in the data processing. Unfortunately, in the latest study of eclipsing satellites (Bar-Sever and Kuang, 2005) no updated orbit prediction errors are provided as done for non-eclipsing satellites (Bar-Sever and Kuang, 2004), which are compared directly in Section 8.

2 Yaw angle from PPP residuals

Precise Point Positioning (PPP) can be performed if satellite clocks and orbits are well known (Zumberge et al, 1997). This technique is mainly used to compute the position (with a precision of up to few centimeters) of individual GNSS receivers. We have used the PPP technique to evaluate the quality of a global satellite phase-only clock solution (Fritsche et al, 2013), where satellite clocks and orbits are introduced as known when estimating daily ground stations positions and two-hourly troposphere parameters. The residuals of the PPP solution were then used to study the quality of the satellite clock solution. While a high-rate clock solution (30 seconds) was computed, the PPP residuals are given every 5 minutes. The reason is simply related to the current data storage capabilities which

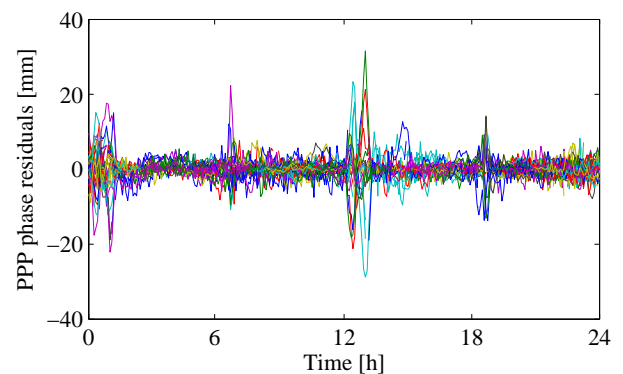


Fig. 2: Elevation weighted PPP phase residuals for all stations visible (each line) by the GPS-IIA satellite SVN 40 during 1st of January 2008.

does not allow us to store 30 seconds PPP residuals for several years, with up to 90 stations and up to 32+24 (GPS+GLONASS) satellites. For most satellites and days the elevation weighted PPP phase residuals were between one and two millimeter (see Fig. 1), i.e., the noise of phase microwave measurements at zenith. This is an indication of the high fidelity of the models used in the clock and PPP solutions. However, for the GPS-IIA satellites large phase residuals appear when the satellites are in eclipse seasons, more specifically the residuals are larger when the satellites are performing a yaw maneuver, as shown in Figures 1 and 2. At the moment of computing the satellite clock solution only the nominal yaw-steering attitude was used for all satellites. Although GPS-IIR satellites are also performing maneuvers during eclipse seasons, the effect is not visible in the residuals since the antenna offset w.r.t. the rotation axis is zero for these satellites. The only effect that remains for GPS-IIR satellites is the phase wind-up (Wu et al, 1993) which can be largely absorbed by the satellite clock corrections. In the case of GLONASS-M satellites the PPP residuals are particularly large during the yaw maneuvers due to a navigation antenna eccentricity of 0.545 m, while for GLONASS (older block) satellites there is no antenna eccentricity and the situation is similar to GPS-IIR satellites. For GLONASS-M satellites, taking advantage of the non-zero antenna offset, we have estimated the real yaw angles from PPP phase residuals. However, the yaw angle estimates are noisier as compared to the estimates for GPS-IIA satellites. Furthermore, the few maneuvers we could observe for GLONASS-M satellites did not differ from the Dilssner et al (2011) model.

The large PPP phase residuals during eclipse seasons for a GPS-IIA satellite are evident in Fig. 1, where the RMS (over all visible stations) of elevation weighted residuals is shown as a function of epoch of the day (vertical axis) and day of year (horizontal axis) for SVN 40 during 2008. Similar phase residuals during yaw maneuvers were also observed for GPS-II and GLONASS-M satellites by Kouba (2009) and Dilssner et al (2011), respectively. Note that not only the shadow and post-shadow maneuvers are visible in Fig. 1, but also the noon maneuvers. Figure 2 shows the elevation weighted PPP residuals for 1st of January 2008, where each line represents a different station visible by the satellite.

Looking at the clear signal of the station residuals shown in Fig. 2 during the yaw maneuvers, the estimation of the real yaw angle from the residuals seemed as something worth to try. In fact, the estimation of the yaw angle is straightforward and can be written for one satellite, one receiver and one specific epoch as:

$$\Delta\rho = x_0 \vec{e} \cdot \vec{e}_X - x_0 (\vec{e} \cdot \vec{e}_X \cos \Delta\Psi + \vec{e} \cdot \vec{e}_Y \sin \Delta\Psi) + \vec{e} \cdot \vec{e}_R \Delta T, \quad (1)$$

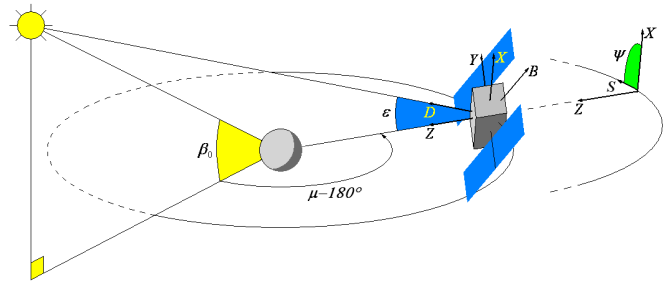


Fig. 3: Nominal yaw-steering attitude of GPS satellites as a function of the position of the Sun in the orbital plane. Illustration of *DYB* (Sun-fixed) and *XYZ* (body-fixed) orthogonal frames. The Earth-satellite-Sun angle ϵ it is identical to the solar panels pitch angle ϵ_{SP} (Section 4) for nominal attitude.

with:

$$\begin{aligned} \vec{e}_X &= \vec{e}_S \cos \Psi_n - \vec{e}_W \sin \Psi_n, \\ \vec{e}_Y &= -\vec{e}_S \sin \Psi_n - \vec{e}_W \cos \Psi_n, \end{aligned} \quad (2)$$

$$\Psi_n = \text{ATAN2}(-\tan \beta_0, \sin \mu), \quad (3)$$

where:

$\Delta\rho$	range residuals between receiver and satellite
x_0	GPS-IIA antenna offset in \vec{X} direction
\vec{e}	unit vector between receiver and satellite
\vec{e}_X	unit vector in body-fixed \vec{X} direction, Fig. 1
\vec{e}_Y	unit vector in body-fixed \vec{Y} direction, Fig. 1
\vec{e}_R	unit vector in radial direction
\vec{e}_S	unit vector in along-track direction
\vec{e}_W	unit vector in cross-track direction
Ψ_n	nominal yaw angle (Bar-Sever, 1996), Fig. 1
β_0	Sun elevation angle above the orbital plane, Fig. 1
μ	angle formed between spacecraft position vector and orbit midnight, Fig. 1
$\Delta\Psi$	yaw angle correction
ΔT	satellite clock correction

Equation (1) can be read as follows: the range residuals between a satellite and a receiver for a given epoch are equal to the difference of the computed minus observed antenna position, plus a satellite clock correction in radial direction. The main assumption made in Eq. (1) is that the errors in the yaw angle map directly into the range residuals. The non-nominal yaw attitude of satellites introduces two main effects on a GNSS clock solution, the phase wind-up effect and the effect to the navigation antenna eccentricity. While the phase wind-up effect is completely absorbed by the satellite clock corrections, the effect of the antenna eccentricity will be mainly distributed between the station residuals and the satellite clock corrections. This is the reason why the last term in Eq. (1) is needed.

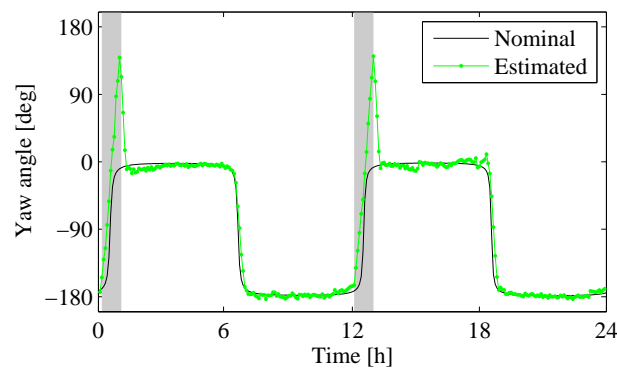


Fig. 4: Yaw angle estimation from PPP phase residuals for GPS-IIA satellite SVN 40 during 1st of January 2008. The formal errors (not shown) are around 7.5 degrees.

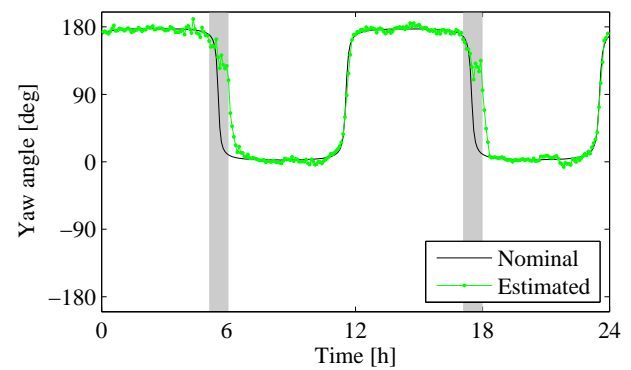


Fig. 5: Yaw angle estimation from PPP phase residuals for GPS-IIA satellite SVN 38 during 7th of June 2008 (day 159, $\beta_0 = -2.58^\circ$). The formal errors (not shown) are around 9.5 degrees.

The yaw angle can then be computed by using the residuals from different stations visible by the satellite at a given epoch. At least three stations are required for solving for the cosine, sine and clock terms as linear parameters of Eq. (1). If more than three stations are available the information can be used to estimate the yaw angle using least squares, with $\Delta\rho - x_0 \vec{e} \cdot \vec{e}_X$ as the observation vector and $\cos\Psi$, $\sin\Psi$ and ΔT as the unknown parameters, where

$$\Psi = \Psi_n + \Delta\Psi, \quad (4)$$

the full yaw angle is obtained by introducing Eq. (2) into Eq. (1). Finally, the full yaw angle is obtained as:

$$\Psi = \text{ATAN2}(\sin\Psi, \cos\Psi). \quad (5)$$

The estimation of the yaw angle can be improved by: 1) down weighting the low elevation observations, 2) applying the condition $\cos^2\Psi + \sin^2\Psi = 1$, which is equivalent to constrain the measurements to a circle of radius $x_0 = 0.279\text{ m}$, namely the antenna offset w.r.t. the rotation axis for GPS-IIA satellites, but converts the estimation problem to a non-linear problem.

Figure 4 depicts the estimated yaw angle for 1st of January 2008 together with the nominal yaw angle and the formal errors of the estimated yaw angle. Note that the shadow and post-shadow maneuvers are clearly visible in Fig. 4. The noon maneuver is not as visible as the previous ones but it can be still detected. The formal errors are around 7.5 degrees. Strictly mapping the residuals of the PPP solution to the yaw angle may not be the best strategy regarding precision since other error sources in the solution, e.g., orbits, troposphere etc. are assumed to not contribute. If the highest accuracy in the estimation of the yaw angle is required, the reverse kinematic precise point positioning method proposed by Dilssner et al (2011) is probably more appropriate. However, as mentioned in the Introduction, the method pro-

posed here is very fast and allows to analyze all eclipsing satellites over long time spans, using residuals from analysis runs that were not specifically set up for investigation of attitude. The estimation of the yaw angle from PPP residuals was realized in MATLAB. Once the PPP residuals and precise orbits are read in MATLAB format the processing time for one satellite during one day was around 5 seconds, making it possible to process all satellites during one year in only one hour using a personal computer.

Once the real yaw attitude of the satellite is known, the next step is to use this information for precise orbit determination, where the information has to be available for computing the antenna position and, in combination with the box-wing satellite model, the solar and the terrestrial radiation pressure. The estimated yaw angles could be used epoch wise, but this implies that for every single epoch the yaw angle should be correctly estimated. This is of course not the case and the yaw angle estimates show in some cases outliers or data gaps. Moreover, the yaw angle does not follow a stochastic behavior but rather a deterministic behavior described by the model of Bar-Sever (1996) for GPS-IIA satellites. The key parameter of the model is the maximum yaw rate, which can be estimated from the yaw angle measurements as shown in Section 3. This single parameter then makes it possible to precisely describe a specific maneuver of a satellite.

3 Yaw rate as function of the β_0 angle

The maximum hardware yaw rate has been estimated from the real yaw angles obtained from PPP residuals. This has been done for every single yaw maneuver for all GPS-IIA satellites during 2007 and 2008, see Fig. 6. The model of Bar-Sever (1996) depends mainly on the maximum yaw rate of the satellite to compute the yaw angle

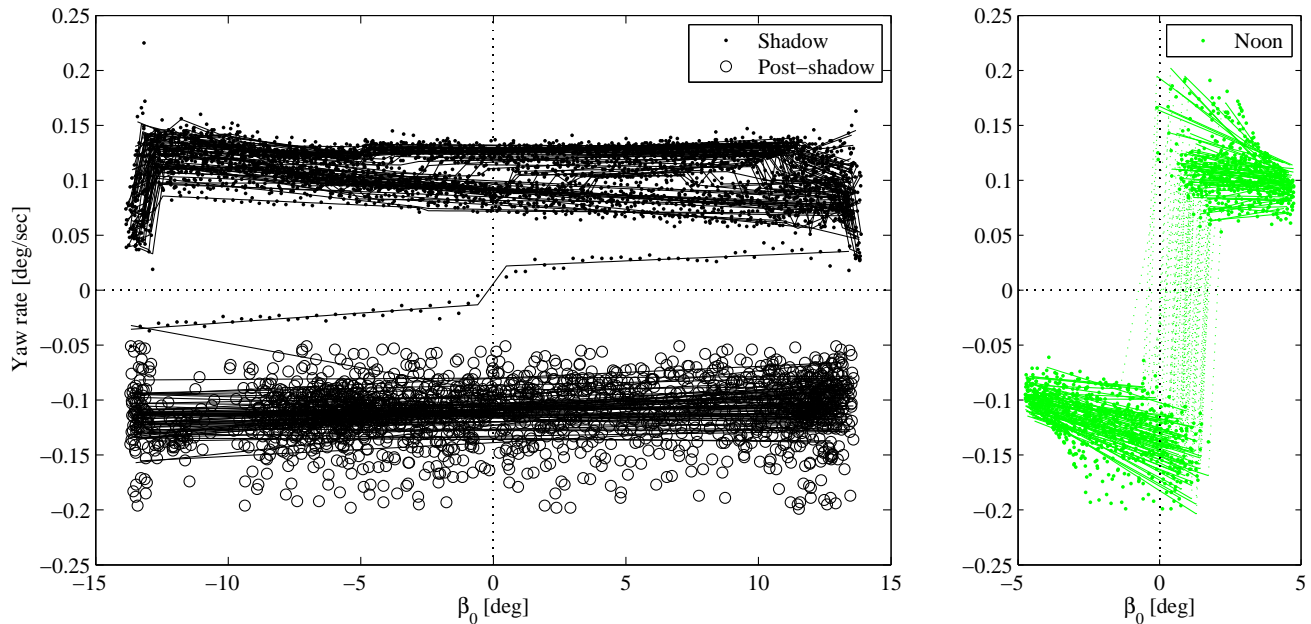


Fig. 6: Yaw rate estimates for shadow, post-shadow (with yaw reversal) and noon maneuvers, together with the corresponding β_0 models (lines) for all GPS-IIA satellites and for all eclipse seasons during 2007 and 2008.

during a specific maneuver. However, the dependency on the yaw rate is non-linear, making its estimation an iterative process as described by Bar-Sever (1996). Nevertheless it is possible to estimate the yaw rates at least for the shadow and noon maneuvers. The post-shadow maneuver is more complex since its rotational direction after shadow depends on the yaw angle at shadow exit, which makes it also ambiguous if the difference between the yaw angle at shadow exit and the nominal yaw angle is close to $\pm 180^\circ$. In fact, Bar-Sever (1996) recommends not to use the data 30 minutes after shadow due to the inherent ambiguity in the post-shadow maneuver. Moreover, if the yaw rate is estimated for the shadow and post-shadow maneuvers together, the estimation becomes highly non-linear due to the possible sign change at shadow exit. For this study, the correct direction of the post-shadow maneuver is crucial since, as mentioned in Section 1, the orbit integration and the solar radiation pressure computation cannot be stopped during 30 minutes after shadow exit. Consequently, the maximum yaw rates have been estimated per maneuver in a numerical way, i.e., by evaluating the model of Bar-Sever (1996) at different yaw rates and comparing it to the measured yaw angles. The full model of Bar-Sever (1996) is considered, i.e., no approximations are done regarding the yaw bias of the satellites ($+0.5^\circ$) or the yaw acceleration (different for block II and IIA). The simplified model proposed by Kouba (2009) includes these approximations which is the main reason why we do not use it. The numerical evaluation of the Bar-Sever (1996) yaw model allows to identify the best fitting yaw rate to

any maneuver. The procedure is described in detail for each type of maneuver in the following paragraphs.

3.1 The shadow maneuver

The yaw rate during the shadow maneuver is estimated from the yaw measurements that fall within shadow. The shadow of the Earth is approximated as a cylinder, i.e., the satellite is in shadow when the angle between Earth, satellite and Sun (ϵ , see Fig. 1) is below 13.87° . No further considerations are done regarding the penumbra passage. For β_0 angles of few degrees the penumbra passage is short and consequently the error by assuming a cylindrical shadow is small. However, for β_0 angles close to $\pm 13.87^\circ$ the penumbra passage is longer and a possible error is introduced in the shadow entry or exit time. From the real yaw angle measurements the shadow entry and exit times, more precisely the start and end of shadow maneuvers, can be observed. However, by analyzing few shadow maneuvers of different spacecraft for β_0 angles close to $\pm 13.87^\circ$, no clear rule was found whether the satellites start or stop to rotate at the beginning of umbra or penumbra. Additionally, the yaw angles are estimated every 5 minutes, which makes it difficult to precisely determine the start and end times of the maneuvers. Consequently the middle time between penumbra and umbra was considered as a good compromise.

For the estimation of the yaw rate during shadow, also the post-shadow maneuver was considered, i.e., by using 30 minutes of data after shadow exit. This is cru-

cial since it allows the determination of the correct rotational direction during the post-shadow maneuver. Most of the yaw rates during shadow are within $+0.06^\circ/\text{s}$ and $+0.15^\circ/\text{s}$ as shown in Fig. 6. However, during the years 2007 and 2008, one spacecraft (SVN 38) was showing a completely different behavior during an entire eclipse season. The shadow yaw rate of SVN 38 was smaller than $|0.05^\circ/\text{s}|$ during the eclipse season from day 136 until 175 of 2008. This special yaw behavior is shown in Fig. 5 for day 159. Additionally, for negative β_0 angles the estimated yaw rates were also negative, see Fig. 6, pointing to a temporarily negative yaw bias. By enabling the use of negative shadow rates the special eclipse season of SVN 38 can be correctly modeled.

3.2 The post-shadow maneuver

If a yaw reversal is detected after shadow exit, the yaw rate is estimated again during the post-shadow maneuver. Otherwise one yaw rate for the shadow plus post-shadow maneuver is estimated from the data of both maneuvers. These positive post-shadow yaw rates are not shown in Fig. 6 to make it simpler. It was observed that for some post-shadow maneuvers the yaw rate was higher than the shadow maneuver with opposite direction. Therefore, the yaw model was upgraded to be able to use different rate values for shadow and post-shadow in case of yaw reversal. The yaw rate during the post-shadow maneuver was estimated only if the approximate duration of the maneuver was large enough to be observed in the yaw angle data. A threshold of 45° has been used for the difference between the yaw angle at shadow exit and the nominal yaw angle at the same time, i.e., only for yaw differences higher than 45° the post-shadow rates were estimated. This ensures that at least 1–2 yaw angle measurements are available to perform the estimation. Besides the higher yaw rate detected for some maneuvers, the post-shadow maneuver follows the Bar-Sever (1996) model.

3.3 The noon maneuver

The yaw rate during the noon maneuvers is estimated when the maximum yaw rate during the turn exceeds $0.1^\circ/\text{s}$. Only one deviation from the Bar-Sever (1996) model was found. In the model, the yaw rate sign is given by $-\text{sign}(\beta_0)$, but the change of sign does not occur exactly at $\beta_0 = 0^\circ$ but rather close to $+1^\circ$, see Fig. 6. To deal with this mismodeling issue, the yaw rates during the noon maneuvers were allowed to be positive and negative, replacing $-\text{sign}(\beta_0)$ by -1 in the model of Bar-Sever (1996).

3.4 The β_0 dependency

The estimated yaw rates for each yaw maneuver for all GPS-IIA satellites during 2007 and 2008 are shown in

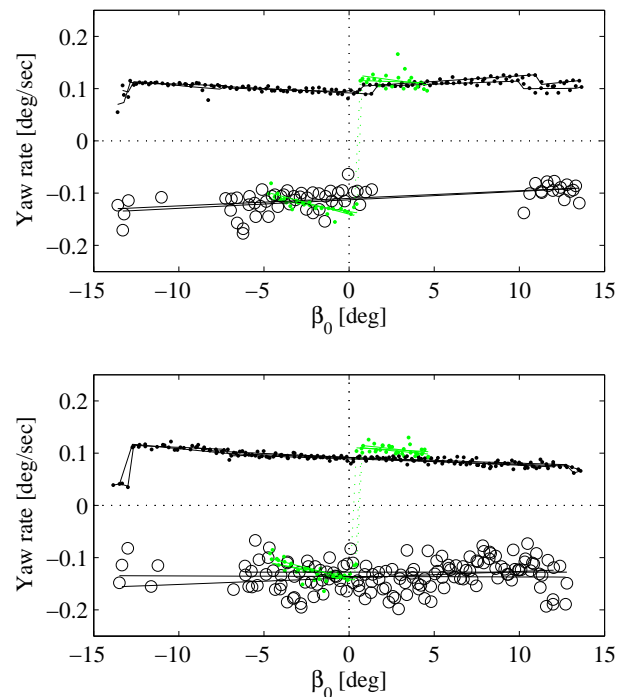


Fig. 7: Yaw rate estimates for GPS-IIA satellite SVN 40 and for all eclipse seasons during 2007 and 2008. Eclipse seasons are separated between increasing β_0 (top, two eclipse seasons, start at -13.87° and end at $+13.87^\circ$) and decreasing β_0 (bottom, three eclipse seasons). The meaning of the symbols is the same as for Fig. 6.

Fig. 6. The yaw rates during shadow are almost constant over β_0 for a group of spacecraft (SVNs: 23, 26, 33, 34, 36 and 39), while for another group they show a clear linear dependency with β_0 (SVNs: 25, 29 and 35). For a third group of spacecraft (SVNs: 24, 27, 30, 32, 37, 38 and 40) the shadow yaw rates show different behaviors for eclipse seasons with increasing or decreasing β_0 angles (SVN 40 is shown in Fig. 7 as an example). In addition to the previous complexity, the yaw rate estimates are not perfect for all maneuvers and may contain outliers. Therefore a β_0 -dependent yaw rate model, specific for each eclipse season and spacecraft, is more convenient to use in the orbit determination process than the individual yaw rates. Summarizing, we perform two fits. First we obtain the best fitting yaw rates for each maneuver from the real yaw angle estimates, and second we fit those yaw rates over an entire eclipse season with a β_0 -dependent model.

The shadow yaw rates were fitted for different β_0 intervals with a first order polynomial for which the corresponding post-shadow maneuvers had the same sign, i.e., when a change in the sign of the post-shadow maneuver was detected a new β_0 linear fit of the shadow yaw rates was performed. In particular it is very challenging to model the change of the post-shadow maneuvers sign

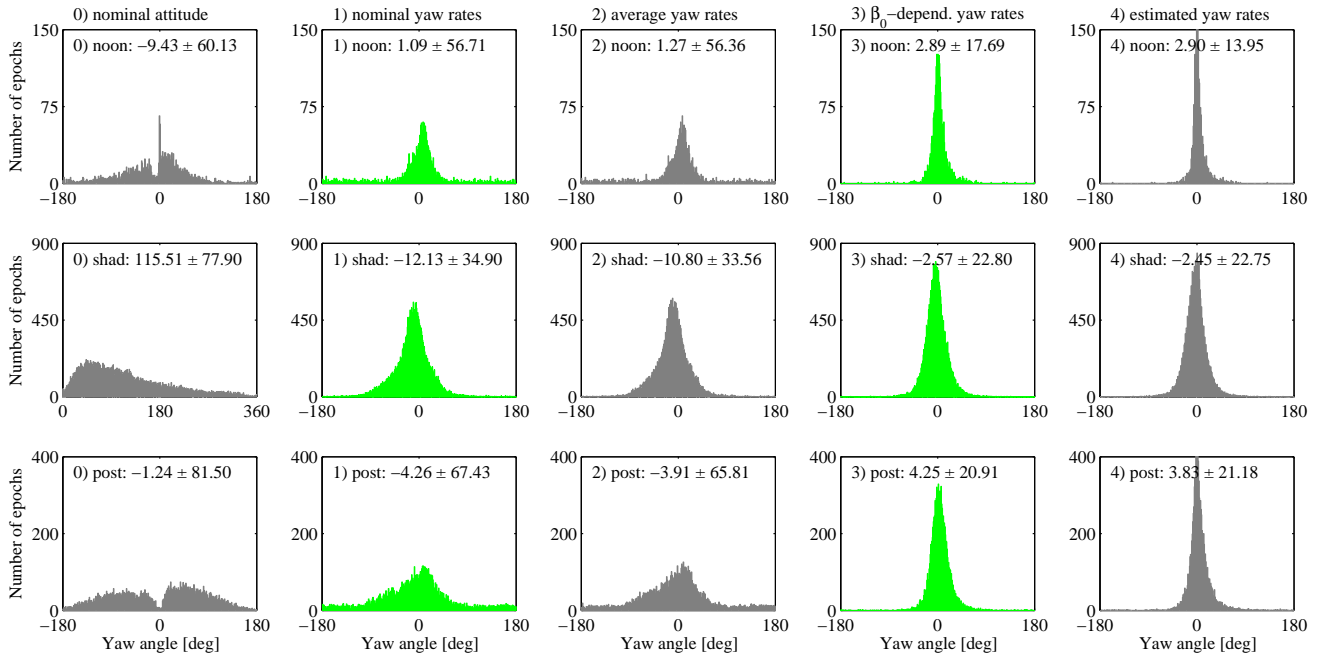


Fig. 8: Histograms of yaw angle differences between yaw angle estimates from PPP residuals and yaw angles obtained from four different yaw rates models (see Section 3.5). The figure includes all noon, shadow and post-shadow maneuvers of all GPS-IIA satellites during 2007 and 2008.

if the difference of the yaw angle at shadow exit w.r.t. the nominal yaw angle $\Delta\Psi_{exit}$ is close to $\pm 180^\circ$, e.g., for β_0 angles close to $+1^\circ$ or to $+10.5^\circ$ in Fig. 7(top). Around $\beta_0 = -7.5^\circ$ in Fig. 7 the change of the post-shadow sign occurs when $\Delta\Psi_{exit}$ is close to 0° and the short post-shadow maneuvers are well modeled with the corresponding shadow yaw rates. Due to the possible ambiguity for the long post-shadow maneuvers where $\Delta\Psi_{exit}$ is close to $\pm 180^\circ$, the decision of whether a yaw reversal is performed or not is based on the sign of the post-shadow maneuvers for the individual β_0 intervals. This is what allows the β_0 -dependent model to reach a high performance during the post-shadow maneuvers, as shown in Section 3.5. The β_0 intervals are visible in Figures 6 and 7, where one can also observe that close to the start or end of the eclipse seasons (e.g. close to $\beta_0 = -13^\circ$ in Fig. 7) the post-shadow maneuver may change the sign, indicating long post-shadow maneuvers although the eclipses are short. The smaller magnitude of the yaw rates at the start or end of the eclipse seasons are because the satellite does not start to rotate at exactly $\epsilon = 13.87^\circ$ as indicated in Section 3.1. This mismodeling is compensated by smaller estimated yaw rates. Finally, the post-shadow yaw rates (of those maneuvers where a yaw reversal was detected) are more noisy than the shadow yaw rates, which can be expected since they are based on less data than the shadow yaw rates. The measured post-shadow yaw rates were fitted using a single β_0 linear model for each eclipse season.

The noon yaw rates show a different behavior for positive and negative β_0 angles, see Figures 6 and 7, consequently a separate linear fit was used for each regime. In order to model precisely the noon yaw rates, the β_0 angle at which the change of rate sign occurs has been estimated.

The yaw rate model as a function of the β_0 angle presented here is a first attempt to model the yaw rates for GPS-IIA satellites. This first attempt, however, shows a great improvement in the yaw maneuvers (Section 3.5) compared to the use of constant nominal yaw rates. The estimated yaw rates and the modeled β_0 dependency open new questions, not addressed in this paper, which can be worth to answer in future studies. Some of these questions are: 1) Why do the yaw rates change during an eclipse season as function of β_0 ? 2) Why do some satellites show a β_0 dependency of the shadow yaw rate and others not? 3) Can one generate more general models that are not eclipse season or spacecraft specific? 4) Can one predict the yaw rates for the currently operating GPS-IIA satellites?

3.5 Performance evaluation

The performance of the model with β_0 -dependent yaw rates has been evaluated by computing the yaw angles for all satellites and all yaw maneuvers during 2007 and 2008. These yaw angles have been compared with the yaw angles obtained from PPP residuals (Section 2).

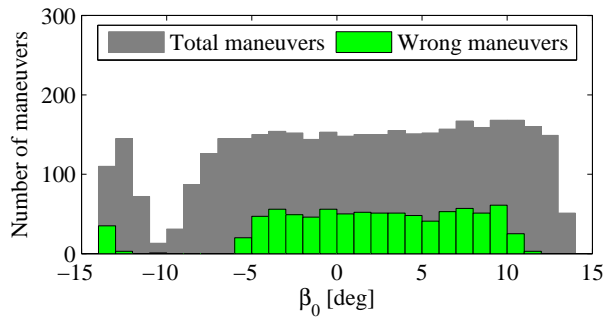


Fig. 9: Total number of post-shadow maneuvers during 2007 and 2008 as function of β_0 (in black). Also shown is the number of post-shadow maneuvers with wrong yaw rate sign if the yaw model with nominal yaw rates is used (in green).

The computation of the yaw maneuvers has been performed using the Bar-Sever (1996) model with five different yaw rate models: 0) no model, i.e., nominal attitude, 1) nominal yaw rates¹ provided by JPL, 2) weighted averages of estimated JPL yaw rates² (Kouba, 2009), 3) our model with β_0 -dependent yaw rates, and 4) our estimated yaw rates for each maneuver. The yaw angle differences (observed minus computed) of the five different yaw rates models are depicted in Fig. 8. The use of nominal or averaged yaw rates (models 1 and 2) shows a great improvement w.r.t. the use of nominal attitude (model 0). The error behavior of the shadow maneuver (resulting only in positive yaw errors) for nominal attitude is a consequence of the positive yaw bias of 0.5° , see also Section 1. Moreover, models 1 and 2 show a very similar error behavior with only a minimal improvement when using averaged yaw rates (model 2). Especially for the noon and post-shadow maneuvers the errors introduced by using constant yaw rates are much larger as compared to estimating yaw rates for each maneuver (models 3 and 4). In particular many noon and post-shadow maneuvers (about 12% and 23% respectively) are modeled with wrong signs if constant rates are used, underlining the importance of estimating yaw rates for each maneuver as it was first proposed by Bar-Sever (1996). Figure 9 shows the number of post-shadow maneuvers with wrong yaw rate sign as function of β_0 if the nominal yaw rates are used. For β_0 angles between -11° and -7° the post-shadow maneuvers are short and well modeled since the yaw angle at shadow exit is very close to the nominal yaw angle. However for β_0 angles below -13° or between -5° and $+10^\circ$ the post-shadow maneuvers are long and the probability of a wrong sign of the post-shadow maneuvers is about 33%. The noon maneuvers (not shown) have a probability of wrong sign

¹ftp://sideshow.jpl.nasa.gov/pub/GPS_yaw_attitude/nominal_yaw_rates

²<http://acc.igs.org/orbits/yrates.pdf>

of about 54% if the β_0 angle is between 0° and $+1^\circ$, see also Fig. 6. Finally, the comparison of performance of our model with β_0 -dependent yaw rates (model 3) with the estimated yaw rates (model 4) shows only a small degradation, and as shown in Fig. 8 the distribution of the errors are close to Gaussian for the three maneuvers.

4 Solar panel attitude model

The nominal yaw-steering attitude of the GPS and GLONASS satellites is given by accomplishing two conditions at the same time: 1) the antennas should be pointing to the center of the Earth to transmit the navigation signals and 2) the solar panels should be pointing perpendicular to the Sun to keep a maximum power supply. When a yaw maneuver is performed, i.e., a rotation around the vector formed between satellite and Earth, the first condition is obviously accomplished but this is no longer the case for the second condition. For the computation of solar and terrestrial radiation pressure the orientation of the solar panels is very important. The solar panels in general and those of the GLONASS-M satellites in particular are large structures and the major contributors to the large area-to-mass ratios of the satellites. The question arises, what is the orientation of the solar panels in space when the spacecraft performs a yaw maneuver?

Two models for the attitude of the solar panels have been developed and tested during this study. The first model assumes that the solar panels are pointing as perpendicular as possible to the Sun during a yaw maneuver. The second model (explained below in detail) assumes a specific pitch orientation of the solar panels of GPS-IIA satellites during shadow and post-shadow maneuvers. Figure 10 shows typical shadow and post-shadow yaw maneuvers and the corresponding solar panel pitch angle for the two models described in this section.

Seen in the body-fixed reference frame (Fig. 1) the solar panels have only one degree of freedom around the solar panels rotation axis or the $\pm Y$ axis. The motion of the solar panels can be described by the solar panels pitch angle ϵ_{SP} which is measured in the plane formed by the Z and X axes, it grows from $+Z$ to $+X$ and it is defined negative for $-X$. During nominal yaw-steering attitude, the solar panels pitch angle ϵ_{SP} is identical to the ϵ angle between Earth, satellite and Sun, see Fig. 1. The normal vector to the solar panels (\vec{e}_{SP}) pointing as perpendicular as possible to the Sun can be obtained as:

$$\begin{aligned}\vec{e}_Y &= -\vec{e}_S \sin \Psi - \vec{e}_W \cos \Psi, \\ \vec{e}_B &= \frac{\vec{e}_Y \times \vec{e}_D}{|\vec{e}_Y \times \vec{e}_D|}, \\ \vec{e}_{SP} &= \vec{e}_B \times \vec{e}_Y,\end{aligned}\tag{6}$$

valid for any given yaw angle Ψ . The directions of the

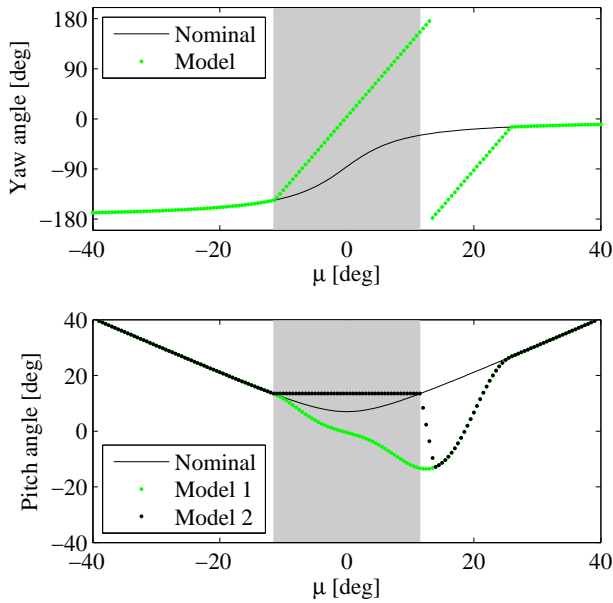


Fig. 10: Solar panels pitch angle for typical shadow and post-shadow yaw maneuvers, at $\beta_0 = 7^\circ$ with a yaw rotation rate of $0.11^\circ/\text{s}$ and with a solar panels rotation rate of $0.1^\circ/\text{s}$.

unit vectors \vec{e}_Y , \vec{e}_B and the unit vector from the satellite to the Sun \vec{e}_D are shown in Fig. 1, whereas the unit vectors \vec{e}_S and \vec{e}_W point in the along- and cross-track directions. Moreover, if the previous steps are performed analytically by writing each vector only as function of the angles μ , β_0 and Ψ (see Section 2 and Fig. 1 for definitions), an analytical expression for the solar panels pitch angle ϵ_{SP} (see Fig. 10, model 1), can be found as follows:

$$\begin{aligned} \kappa^2 &= (\cos \mu \sin \Psi)^2 + (\sin \mu \sin \Psi \sin \beta_0 - \cos \Psi \cos \beta_0)^2, \\ \cos \epsilon_{SP} &= \frac{\cos \mu \cos \beta_0}{\kappa}, \\ \sin \epsilon_{SP} &= \frac{\sin \mu \cos \beta_0 \cos \Psi - \sin \beta_0 \sin \Psi}{\kappa}, \\ \epsilon_{SP} &= \text{ATAN2}(\sin \epsilon_{SP}, \cos \epsilon_{SP}). \end{aligned} \quad (7)$$

According to Bar-Sever (1995) and to personal communication, the solar panels of the block II and IIA satellites do not rotate during a shadow event, being fixed to the ϵ_{SP} angle at shadow entry, i.e., at $\epsilon_{SP} = 13.87^\circ$. This implies that at shadow exit the solar panels have to perform a post-shadow recovery to the best possible pitch angle, in a similar way as the post-shadow yaw maneuver as shown in Fig. 10. In fact, the implementation of the model was done in the same way as the post-shadow yaw maneuver model described in Bar-Sever (1996) for which Eq. 7, the ϵ_{SP} angle as func-

tion of μ , β_0 and Ψ , is needed. The model needs the pitch rotation rate of the solar panels, for which Bar-Sever (1995) reports a value of $0.1^\circ/\text{s}$. However, Bar-Sever (1997) assumes a value of $0.25^\circ/\text{s}$ for the pitch rate which is used for computing the normal vector to the solar array during yaw maneuvers. In this study, the value of $0.1^\circ/\text{s}$ has been used, since it was first known. Nevertheless, considering the lower value of $0.1^\circ/\text{s}$ and the extreme case when the yaw angle at shadow exit differs 180° from the nominal yaw angle, where the post-shadow yaw maneuver can take up to 30 minutes, the solar panels post-shadow recovery can take up to $(2 \times 13.87)/(0.1 \times 60) \approx 4.6$ minutes. This means that the solar panels are misoriented in sunlight for a very short time. In fact, the small improvement obtained in the orbit predictions (Section 8), shows that the choice of the pitch rate value is not critical.

5 SRP box-wing model for non-nominal attitude

Once the yaw attitude of the satellite (Sections 2 and 3), i.e., the orientation of the satellite bus in space, and the attitude of the solar panels are known (Section 4), the information can be used for computing the solar radiation pressure acting on GPS or GLONASS satellites. For this purpose, the adjustable box-wing model described (analytically for nominal yaw-steering attitude) in Rodriguez-Solano et al (2012c) has been upgraded to incorporate the non-nominal attitude of the body and the solar panels. The necessary changes to the adjustable box-wing model are described in this section.

The main change to the original model is that the partial derivatives of the acceleration due to solar radiation pressure can no longer be described in an analytical way, since the position of the Sun w.r.t. the satellite surfaces is now arbitrary. The partial derivatives, however, can be computed numerically by simply using the angle of incidence between the Sun and the surfaces of the satellite. In the case of the satellite body, the separation of the estimated parameters between reflection coefficients and absorption plus diffusion coefficients is still valid. When the satellites are in nominal yaw-steering attitude the only surfaces of the bus illuminated by the Sun are $+Z$, $+X$ and $-Z$, see Fig. 1. However, during a yaw maneuver any of the surfaces of the bus can be illuminated. This requires special handling of the box-wing surfaces and related parameters as follows.

- The $+Z$ and $-Z$ parameters are identical to the ones described in Rodriguez-Solano et al (2012c).
- The $+Y$ and $-Y$ surfaces are only illuminated when a satellite is performing a yaw maneuver. The acceleration induced by these surfaces during the yaw maneuvers and due to the yaw bias of 0.5° (constant acceleration) is only included as a priori acceleration.

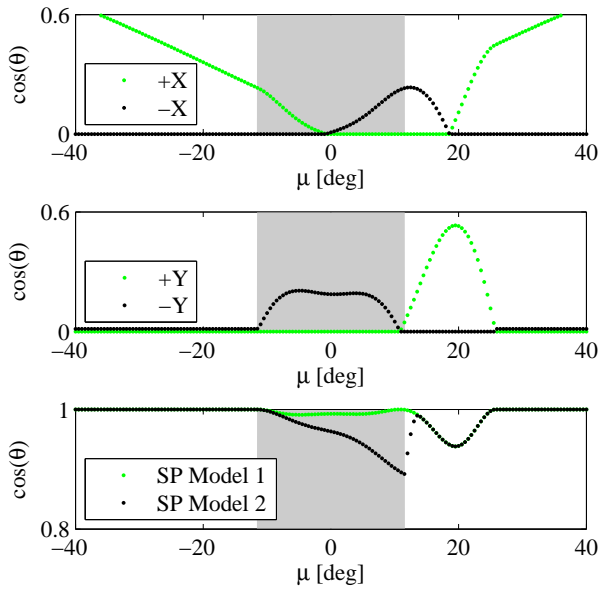


Fig. 11: Cosine of incidence angle for the $\pm X$, $\pm Y$ and solar panels (*SP*) surfaces of the box-wing model for $\beta_0 = 7^\circ$, corresponding to the yaw and solar panels pitch angles shown in Fig. 10.

The *Y*-bias acceleration, present also outside eclipse seasons, still has to be estimated.

- The $+X$ parameters of the original model now include also the $-X$ surface, i.e., it is assumed that the optical properties of $+X$ and $-X$ are identical. We do not include a new pair of parameters for $-X$ since this surface is only shortly illuminated during yaw maneuvers.
- The solar panel scaling factor ($1 + \rho + \frac{2}{3}\delta$, with the reflection and diffusion coefficients ρ and δ) has to be changed since the Sun is no longer perpendicular to the panels during the yaw maneuvers. The partial derivative of the acceleration w.r.t. the solar panels scaling factor S_{SP} is simply Eq. (6) of Rodriguez-Solano et al (2012c), however, now with θ being the actual incidence angle of the Sun w.r.t. the solar panels. Furthermore, we divided that equation by $1 + \rho + \frac{2}{3}\delta$, for backward compatibility to the box-wing model with nominal attitude.
- The solar panel rotation lag parameter is unchanged, i.e., we use the time derivative of the nominal Earth-satellite-Sun angle ϵ . This is done to avoid having a function with frequent jumps during yaw maneuvers.

In Fig. 11 the cosines of the sunlight incidence angles on the surfaces of a GPS-IIA satellite are plotted during a yaw maneuver, the same maneuver as shown in Fig. 10. Moreover, the accelerations are plotted for different attitude models: 1) yaw maneuvers with the solar panels pointing as perpendicular as possible to the

Sun, and 2) yaw maneuvers with the attitude model for the solar panels described in Section 4.

In this paper, also box-wing models of GLONASS and GLONASS-M satellites have been used since we are computing GPS+GLONASS solutions. The main difference w.r.t. the GPS models is that the bus of the GLONASS and GLONASS-M satellites has a cylindrical shape, so they are actually cylinder-wing models. Otherwise, the parameters and parameter constraints are identical to GPS. For the construction of the GLONASS cylinder-wing models approximate dimensions from satellite manufacturer drawings have been used (Revnivykh and Mitrikas, 1998; Mitrikas, 2005). No information is available on the surface optical properties for these satellites, consequently rough assumptions have been made on the optical properties as done by Ziebart (2001); Ziebart and Dare (2001). One of the main advantages of the adjustable box-wing model (Rodriguez-Solano et al, 2012c) is that it does not need accurate information of the satellite (e.g. mass, surface areas or optical properties). It only needs good first approximations, such that the lack of accurate information is not a severe disadvantage, since it can be compensated in the estimation of the adjustable box-wing model parameters.

6 Reprocessing experiments

The models presented in Sections 3, 4 and 5 have been used in the computation of GPS and GLONASS satellite orbits based on global tracking data. Five different solutions, of increasing complexity, have been computed changing only one of the models for each solution. Table 1 lists the models used for each solution. The first two are our reference solutions for the CODE (5-parameters: D_0 , Y_0 , B_0 , B_C and B_S , Beutler et al, 1994) and for the adjustable box-wing solar radiation pressure models with results already presented in Rodriguez-Solano et al (2012c). For this study, we computed three new solutions to evaluate our adjustable box-wing model with two different yaw rate models (nominal and β_0 -dependent, Table 1) and with two different models for the attitude of the solar panels.

The generation of 1-day precise GPS and GLONASS orbits is based on tracking data from the global IGS network, using the processing scheme of the combined reprocessing of GPS and GLONASS observations project (Fritsche et al, 2013), realized by four universities: Technische Universität Dresden, Technische Universität München, Universität Bern and Eidgenössische Technische Hochschule Zürich. The only changes to the processing scheme used in the project are the following: 1) Pseudostochastic orbit parameters (instantaneous velocity changes) are estimated every 12 hours in the radial, along- and cross-track directions (Beutler et al, 2006). We constrained them to 10^{-6} , 10^{-6} and 10^{-9} m/s, respectively,

Table 1: Solar radiation pressure, yaw attitude and solar panels attitude models selected for the reprocessing experiments.

# sol.	Solar radiation pressure	Yaw attitude	Solar panels attitude
1	CODE 5-parameters	Nominal attitude law	Towards the Sun
2	Adjustable box-wing	Nominal attitude law	Towards the Sun
3	Adjustable box-wing	GPS-IIA: nominal yaw rates, Bar-Sever (1996) GPS-IIR: 0.20°/s, Kouba (2009) GLONASS-M: 0.25°/s, Dilssner et al (2011)	Towards the Sun
4	Adjustable box-wing	GPS-IIA: β_0 -dependent yaw rates	Towards the Sun
5	Adjustable box-wing	GPS-IIA: β_0 -dependent yaw rates	Shadow and post-shadow model

as done in Rodriguez-Solano et al (2012c) instead of 10^{-6} , 10^{-5} and 10^{-8} m/s. 2) We estimate, together with the satellite orbits, the apparent geocenter coordinates, i.e., the offset between the instantaneous Earth's center of mass, as sensed by the satellites, and the reference frame origin (applying a no-net-translation condition) as done in Rodriguez-Solano et al (2012b) instead of constraining it to zero. 3) For the solutions that include a yaw maneuver model (3, 4 and 5 in Table 1), we reduced the integration step size to about one minute. This was done to incorporate in the orbit integration the details from short yaw maneuvers or from the short post-shadow recovery of the solar panels. 4) We start from screened observations, generated within the project, to compute the 1-day orbits. The observation residuals were cleaned using the CODE (5-parameter) radiation pressure model and the nominal attitude law, i.e, no yaw maneuvers were considered. These are not optimal initial conditions, ideally the observations should be clean using the specific models of each solution (Table 1), and this approach has the disadvantage that the observations could favor the models used for cleaning them. Nevertheless, starting from clean observations is in fact what allows us, in terms of computational effort, to reprocess several yearly solutions in order to investigate the effects of different orbit models, as the data cleaning requires a significant computing effort. Despite the mentioned disadvantages of starting from cleaned observations, the improvements in the orbits by using different models are well visible and can be quantified by investigating orbit overlap and prediction errors (Sections 7 and 8).

The years 2007 and 2008 were selected for the reprocessing experiments since for these years a similar number of GPS-IIA and GPS-IIR satellites is present. However, just a few GLONASS (first block) satellites were present during those years, restricting our analysis to GLONASS-M satellites. Nevertheless, the last block type is more interesting since it has observable noon and shadow yaw maneuvers that have been modeled by Dilssner et al (2011). Moreover, using two years implies

that around four eclipse seasons occur for each satellite, making our results and conclusions more general. Finally, regarding non-conservative force modeling, in accordance with Fritsche et al (2013), Earth radiation pressure and antenna thrust were included as a priori accelerations in all solutions using the models described in Rodriguez-Solano et al (2012a). The only difference is that we have enabled the capability of the satellite box-wing model to use non-nominal attitude, such that it can accommodate any direction of the radiation source. This is important since we consider visible (reflected) and infrared (emitted) Earth radiation with the last one also present during Sun-Earth eclipses. The orientation of the solar panels is particularly important for the Earth radiation pressure computation since the solar panels show large variations w.r.t. the Earth. Finally, the resulting a priori acceleration was taken into account in the determination of GPS and GLONASS satellite orbits.

7 Orbit overlap errors

The differences between consecutive 1-day orbits at the day boundaries, i.e., the orbit overlap errors, are an indicator of internal orbit consistency. If all orbit models were perfect such differences at the day boundaries should be zero and the orbits continuous. Therefore, an improvement or degradation in the modeling of the orbits should be visible in the orbit overlap errors. Figure 12 shows the differences in position at the day boundaries for GPS-IIA, GPS-IIR and GLONASS-M satellites and for the computed solutions (Table 1). GLONASS satellites are not shown since much less data were available during 2007 and 2008 as compared to GLONASS-M satellites, but the tendency in the orbit overlap errors (solutions 1 and 2) is similar as for the GLONASS-M satellites. For generating Fig. 12, we first computed the position differences in radial, along-track and cross-track for each day and each satellite in 2007 and 2008, and then classify them according to the block types and β_0 angles, to compute the averages shown in

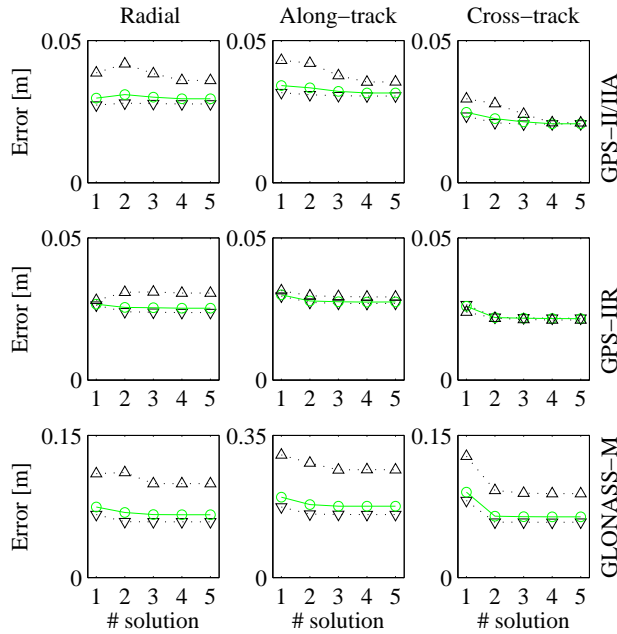


Fig. 12: Average of orbit overlap errors for all GPS-IIA, GPS-IIR and GLONASS-M satellites present during 2007 and 2008, and for the solutions in Table 1. The averages were performed separately for data out of eclipse seasons ($|\beta_0| > 15^\circ$, ∇), data in and out of eclipse seasons (\circ) and data in eclipse seasons ($|\beta_0| \leq 15^\circ$, \triangle).

Table 2: Average of 3-dimensional orbit overlap errors (in meters) for different solutions (Table 1) and for all GPS-IIA, GPS-IIR and GLONASS-M satellites present during 2007 and 2008.

Sat. type	#	$ \beta_0 > 15^\circ$	All data	$ \beta_0 \leq 15^\circ$
GPS-IIA	1	0.0556	0.0597	0.0747
GPS-IIA	2	0.0543	0.0588	0.0751
GPS-IIA	3	0.0536	0.0567	0.0679
GPS-IIA	4	0.0535	0.0555	0.0628
GPS-IIA	5	0.0535	0.0555	0.0627
GPS-IIR	1	0.0551	0.0553	0.0561
GPS-IIR	2	0.0493	0.0507	0.0554
GPS-IIR	3	0.0488	0.0502	0.0550
GLO-M	1	0.2274	0.2566	0.3831
GLO-M	2	0.1966	0.2250	0.3481
GLO-M	3	0.1959	0.2204	0.3270

Fig. 12. For computing Fig. 12 and the figures in Section 8, a simple removal of gross outliers was performed by eliminating the highest errors common to the five solutions, the highest 1% for GPS and the highest 3% for GLONASS. The 3-dimensional overlap position errors were computed and averaged, as done for Fig. 12, to write the overlap errors in Table 2.

For GPS-IIA satellites there is a small improvement in and out of eclipse seasons by exchanging the CODE by the box-wing solar radiation pressure model (solutions 1 to 2, except for the radial component). The use of the yaw maneuver model with nominal yaw rates (solution 3) and the use of the β_0 -dependent yaw rates (solution 4) bring both similar improvements during eclipse seasons. In particular in the cross-track component the difference of orbit overlap errors between in and out eclipse seasons tends to disappear. Finally, the use of the solar panel model is not visible in the orbit overlap errors, just small improvements are visible in the orbit prediction errors (Section 8).

For GPS-IIR satellites the most important improvement comes with the adjustable box-wing model. With exception of the radial component during eclipse seasons, there is a general improvement from solution 1 to 2. Just small improvements are visible in the orbit overlap errors by including a yaw attitude model (solution 3) for the short noon and shadow yaw maneuvers. The situation is almost the same for GLONASS-M satellites, however, for these satellites the use of the yaw attitude model (solution 3) does show a larger improvement w.r.t. the previous solutions.

8 Orbit prediction errors

The prediction of satellite orbits is very important in real time applications, ranging from very precise applications like real-time precise positioning (Caissy et al, 2012; Leandro et al, 2012) or real-time zenith troposphere delay estimation (Douša, 2010; Choi et al, 2012), to the broadcast of orbits for stand-alone receivers. Orbit prediction is also an important quality measure of the dynamical models used in the orbit determination process. When relying on GNSS tracking data, some orbit modeling deficiencies might be compensated by the strength of the GNSS tracking data. In particular the data and the coverage (global and dense) of the IGS network of GPS ground stations is of very high quality. However, when predicting orbits the observations can only contribute to the observed part of the orbit, while the predicted part relies only on the dynamical orbit models.

For this study we first computed multi-day arcs by stacking 1-day observed arcs (Beutler et al, 1996). While for the 1-day arcs there is a set of radiation pressure parameters (from the CODE or adjustable box-wing models) per day, for the multi-day arcs there is only one set of radiation pressure parameters common to the multi-day solution. As a second step, the multi-day arcs have been used for orbit prediction, using the estimated radiation pressure parameters from the observed part.

Two types of orbit prediction errors are presented in this study. The first type of prediction errors are computed as the RMS of the orbit differences (predicted minus observed 1-day orbits) during the first day, more

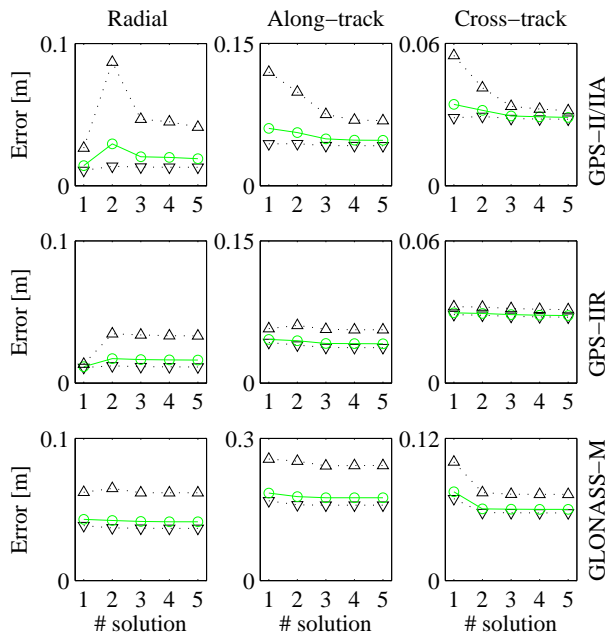


Fig. 13: Average RMS of orbit prediction errors (3 to 9 hours) for all GPS-IIA, GPS-IIR and GLONASS-M satellites present during 2007 and 2008, and for the solutions in Table 1. The averages were performed separately for data out of eclipse seasons ($|\beta_0| > 15^\circ$, ∇), data in and out of eclipse seasons (\circ) and data in eclipse seasons ($|\beta_0| \leq 15^\circ$, \triangle).

Table 3: Average RMS of 3-dimensional orbit prediction errors (3 to 9 hours) for different solutions (Table 1) and for all GPS-IIA, GPS-IIR and GLONASS-M satellites present during 2007 and 2008. The errors are given in meters.

Sat. type	#	$ \beta_0 > 15^\circ$	All data	$ \beta_0 \leq 15^\circ$
GPS-IIA	1	0.0574	0.0755	0.1413
GPS-IIA	2	0.0587	0.0793	0.1545
GPS-IIA	3	0.0563	0.0667	0.1046
GPS-IIA	4	0.0561	0.0652	0.0985
GPS-IIA	5	0.0560	0.0644	0.0953
GPS-IIR	1	0.0558	0.0593	0.0715
GPS-IIR	2	0.0538	0.0606	0.0844
GPS-IIR	3	0.0514	0.0579	0.0805
GLO-M	1	0.1968	0.2155	0.2963
GLO-M	2	0.1833	0.2020	0.2829
GLO-M	3	0.1825	0.1994	0.2725

specifically the RMS is computed only during the first 3 to 9 hours. This is similar to what is done by the IGS ultra-rapid orbits (Springer and Hugentobler, 2001), where orbit predictions are computed every 6 hours but the results are released with a latency of 3 hours. For

this type of prediction, 2-day arcs have been first formed and later used for prediction. The choice of 2-day arcs is according to the results of Choi et al (2012), where observed arc lengths between 40 and 45 hours were found to be optimal for the IGS ultra-rapid orbits. We first compute 1-day solutions such that the length of the observed arcs could only be increased in steps of one day. In addition, we perform tests with 1-day, 2-day and 4-day arc lengths, finding in accordance to Choi et al (2012) an arc length of 48 hours as the best option.

The second type of prediction errors are computed as the RMS of the orbit differences (predicted minus observed 1-day orbits) during the fourth complete day. For this type of prediction, 4-day arcs have been first formed and later used for prediction. The reasons behind using 4-day arcs are the following: 1) by using long arcs the mean motion of the satellite is well determined, having a positive impact on the along-track component and consequently on the radial component, 2) the same approach (4-day observed orbits and 4-day predicted orbits) was used by Bar-Sever and Kuang (2004), making our results directly comparable with that study.

In this study, our main focus is on the predictive power of the non-conservative force models, solar radiation pressure and Earth radiation pressure. Thus, we have made simplifications, making our orbit prediction tests not a real-world or real-time tests, but rather controlled prediction tests to evaluate different non-conservative force models. The two main simplifications are: 1) we do not predict the yaw rates, in the case of nominal yaw rates there is no need for prediction. However for the β_0 -dependent yaw rates there is a need, for the last case we used the complete β_0 yaw rate model, and 2) we do not predict the Earth orientation parameters (EOP), but we use the information available from the IERS EOP 08 C04 (International Earth Rotation Service, Bizouard and Gambis, 2009) files, attaching 1 or 4 days to the estimated Earth orientation parameters of the first 2- or 4-day solutions. As described by Bar-Sever and Kuang (2004), the propagation of the orbit force models in time is more conveniently done in a inertial system but the representation of the orbits is more precise in an Earth-fixed system, such that the Earth orientation parameters are needed to transform one system to the other. In fact, the prediction errors shown in this section were computed by comparing precise orbits (no Helmert parameter transformations were applied), represented in an Earth-fixed system.

Figures 13 and 14 were computed in a similar way as Fig. 12, except that the RMS of orbit differences (predicted minus observed 1-day orbits) was used instead of the orbit overlap errors. The same is valid for Tables 3 and 4 w.r.t. Table 2. To show the details of the orbit prediction errors, we provide the Figures 15, 17 and 18 respectively for the GPS-IIA, GPS-IIR and GLONASS-M satellites. In these figures we show the RMS of orbit

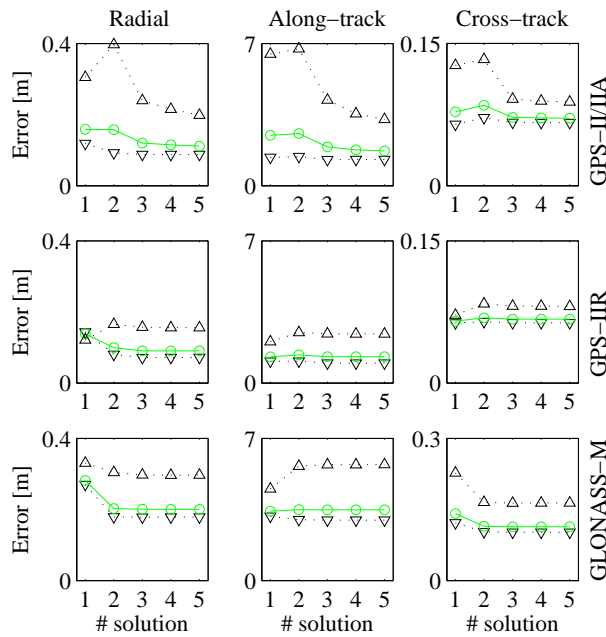


Fig. 14: Average RMS of orbit prediction errors (during 4th day) for all GPS-IIA, GPS-IIR and GLONASS-M satellites present during 2007 and 2008, and for the solutions in Table 1. The averages were performed separately for data out of eclipse seasons ($|\beta_0| > 15^\circ$, ∇), data in and out of eclipse seasons (\circ) and data in eclipse seasons ($|\beta_0| \leq 15^\circ$, \triangle).

Table 4: Average RMS of 3-dimensional orbit prediction errors (during 4th day) for different solutions (Table 1) and for all GPS-IIA, GPS-IIR and GLONASS-M satellites present during 2007 and 2008. The errors are given in meters.

Sat. type	#	$ \beta_0 > 15^\circ$	All data	$ \beta_0 \leq 15^\circ$
GPS-IIA	1	1.409	2.495	6.494
GPS-IIA	2	1.445	2.581	6.765
GPS-IIA	3	1.295	1.923	4.233
GPS-IIA	4	1.297	1.780	3.561
GPS-IIA	5	1.296	1.720	3.281
GPS-IIR	1	1.100	1.309	2.043
GPS-IIR	2	1.084	1.399	2.505
GPS-IIR	3	0.990	1.311	2.439
GLO-M	1	3.190	3.446	4.555
GLO-M	2	3.013	3.508	5.654
GLO-M	3	2.988	3.501	5.725

prediction errors during the fourth day, the prediction errors of 3 to 9 hours show a similar behavior. Each black dot in the figures represents the RMS prediction error for one day and one satellite. Moreover, the results are shown as a function of β_0 , the Sun elevation angle

above the orbital plane, together with the mean (computed at one degree intervals) as green line to highlight the specific behavior of the prediction errors.

The average RMS prediction errors during the 4th day (Table 4) can be directly compared with the results reported by Bar-Sever and Kuang (2004) of 1.02 and 0.99 meters, for GPS-II/IIA and GPS-IIR satellites outside the eclipse seasons. These results were obtained by using the GSPM.04a solar radiation pressure model. Our results of 1.30 and 0.99 meters for GPS-IIA and GPS-IIR satellites show a great coincidence for the latter satellite type, but are larger for GPS-IIA satellites. From the orbit quality measures we presented in this paper (orbit overlaps and prediction errors) the GPS-IIA satellite orbits are always a little worse than the ones of GPS-IIR satellites, independently if the CODE 5-parameter or the adjustable box-wing models were used. For this small degradation of the GPS-IIA satellite orbits we have at the moment no explanation.

For the orbit prediction errors during the first 3 to 9 hours (Table 3) we cannot do a one to one comparison to the existing studies. Leandro et al (2012) provides a figure of 0.04 m for the 3D prediction error accuracy (for eclipsing and non-eclipsing GPS-IIA and GPS-IIR satellites) of their orbit processing approach which includes very frequent updates (few minutes) of the orbit predictions. Douša (2010) reports accuracies during the first predicted 9 hours of 0.04-0.05 m and 0.08-0.12 m respectively for non-eclipsing and eclipsing GPS-IIA satellites, after estimating Helmert transformation parameters (3 rotations). Choi et al (2012) obtained weighted RMS residuals, median and rotation scatter of 0.013, 0.011 and 0.023 m over the first 6 hours of predicted orbits, after applying a 7-parameter Helmert transformation and excluding eclipsing GPS-IIA satellites. In comparison to the results of the previous studies, our results (Table 3) look worse, including the non-eclipsing satellites. However, our results may be too pessimistic since we do not apply any Helmert transformation when comparing predicted and observed orbits and due to the simple outlier removal that we applied to the data. Nevertheless, our reference solutions (1 and 2) with nominal yaw attitude allows us to evaluate the impact of different attitude models on the orbits, and to affirm that the tested models bring an important improvement for short (3 to 9 hours) orbit predictions.

For GPS-IIA satellites, one of the most visible features in Figures 13 and 14 is the degradation, especially visible in the radial component, of the orbits during eclipse seasons when exchanging the CODE 5-parameter model by the adjustable box-wing model. This degradation during eclipse seasons is also visible in Fig. 15. This was in fact one of the main motivations to start this study and to include the yaw attitude models in the box-wing model. During eclipse seasons, the largest improvement in orbit prediction results from incorpo-

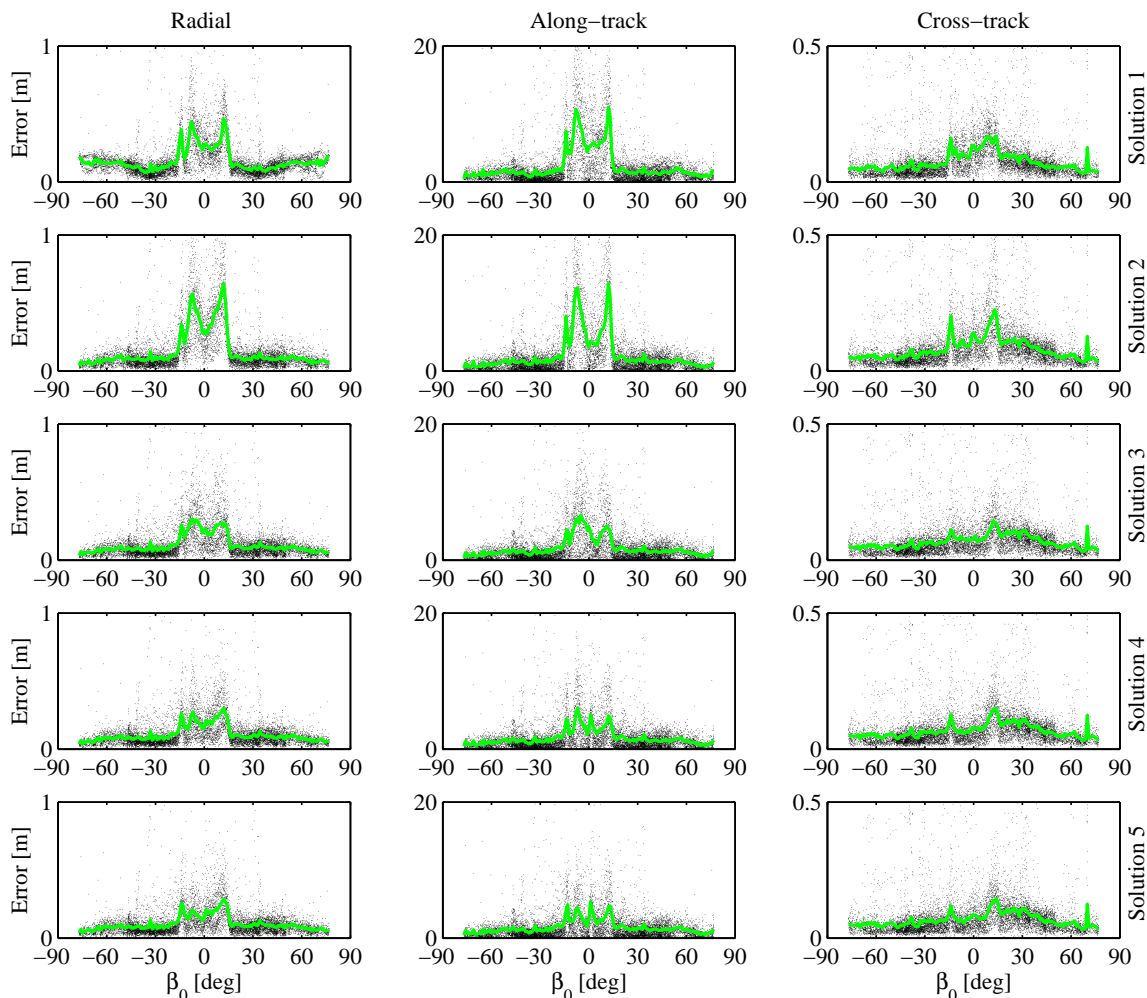


Fig. 15: RMS of orbit prediction errors (during 4th day) for all GPS-IIA satellites present during 2007 and 2008, and for all the solutions in Table 1. The prediction errors are shown as function of β_0 , the Sun elevation angle above the orbital plane, together with the average line in green.

ration of the yaw attitude model with nominal rates. Smaller but consistent improvements result from the use of the β_0 -dependent yaw rates and the solar panel attitude model. This was not expected but it is very interesting. We would have expected that the largest improvement would result from the β_0 -dependent yaw rates and the solar panel attitude model. The fact that the yaw model with nominal yaw rates brings the largest improvement shows that the use of any yaw model (even one with known errors, see Fig. 8) is much better than ignoring the yaw maneuvers of the satellites. Nevertheless, the use of the β_0 -dependent yaw rates is very important for the understanding of the problem, since it shows that other mismodeling problems (and not the wrong yaw attitude during maneuvers) are still affecting the GPS-IIA satellite orbits.

Figure 16 helps to explain why the largest improve-

ment in the GPS-IIA orbits (from one solution to the next) is obtained when using the yaw attitude model with nominal rates (solution 3). Nevertheless, the best GPS-IIA orbits are obtain with the β_0 -dependent rates and the dedicated solar panel attitude model (solution 5). Figure 16 shows that the direction of the post-shadow maneuver has little influence on the radial and along-track acceleration components, only the cross-track acceleration changes sign if the sign of the post-shadow maneuver changes. This means that a possible ambiguity in the sign of the post-shadow maneuver due the use of an incorrect yaw rate has mainly a mismodeling effect on the cross-track component. The radial and along-track components are affected by the incorrect use of the yaw attitude but they do not show a sign change in the acceleration. This is demonstrated by the fact that there are small improvements in the three components

of the orbit overlap and prediction errors by using the yaw attitude model with β_0 -dependent yaw rates (solution 4). The large differences between the accelerations obtained when using the nominal attitude law and the yaw maneuvers show the importance of using any yaw maneuver model.

The incorporation of the solar panel attitude model for GPS-IIA satellites shows a small but consistent improvement in the orbit predictions (3 to 9 hours and during the 4th day). This indicates that the orientation of the solar panels described by our model should be closer to reality than assuming that the panels point as perpendicular as possible to the Sun during a yaw maneuver.

Outside eclipse seasons, the orbit predictions (during 4th day) of GPS-IIA satellites show a small degradation in the cross-track component when exchanging the CODE by the box-wing model, see Fig. 14. This is partially compensated by using the yaw model with nominal rates (Figures 14 and 15), which shows that the use of the yaw model has a positive impact also outside eclipse seasons, because of the small improvement of the whole solution. Also the use of the β_0 -dependent yaw rates and the dedicated solar panel attitude model improves the whole solution. These small improvements are visible for the solutions 2 to 5 ($|\beta_0| > 15^\circ$) in the Tables 2, 3 and 4. An interesting feature of the orbit predictions outside eclipse seasons is observed for the radial component (Fig. 15) when exchanging the CODE by the box-wing model. As one can see the adjustable box-wing contributes to mitigate β_0 -dependent systematic errors. This can be explained by the explicit dependency of the box-wing parameters on the Earth-satellite-Sun angle (ϵ , Fig. 1) which is a function of the μ and β_0 angles (Rodriguez-Solano et al, 2012c).

For GPS-IIR satellites, one of the most visible features in Figures 13 and 14 is the degradation of the orbits during eclipse seasons when exchanging the CODE by the box-wing model. There is only a very small improvement when including the yaw model (solution 3). The yaw maneuvers for this type of satellite are short and very close to the nominal attitude. Moreover, yaw maneuvers only appear when the hardware yaw rate is exceeded, i.e, for $|\beta_0| < 2.4^\circ$ (Kouba, 2009). However, the errors during eclipse seasons are not limited to $|\beta_0| < 2.4^\circ$ as shown in Fig. 17. The remaining errors during the eclipse seasons ($|\beta_0| < 13.87^\circ$) could be related to the two following reasons: 1) The shadow of the Earth is currently modeled as a cylinder, which ignores the Earth flattening and the radiation flux during penumbra (Adhya et al, 2005). Especially the errors at the start and end of the eclipse seasons (with long penumbra passages, $|\beta_0| \approx 13.87^\circ$) could be related to these two approximations, 2) Just the instantaneous re-radiated heat is approximately taken into account in the adjustable box-wing model (Rodriguez-Solano et al,

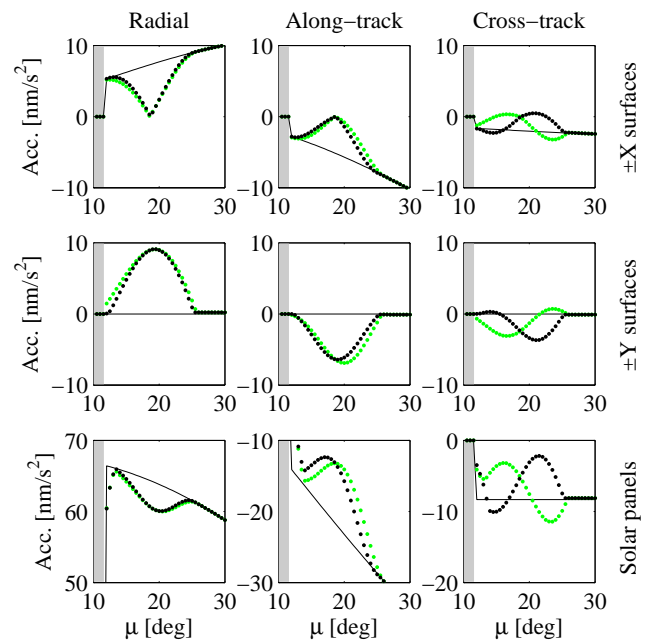


Fig. 16: A priori accelerations acting on the $\pm X$ and $\pm Y$ surfaces of the satellite bus and on the solar panels, represented in radial, along- and cross-track. The accelerations correspond to the yaw angles depicted in Fig 10 and the model 2 for the solar panels attitude (black line for nominal attitude and green dots for the post-shadow maneuver). In addition, by using a yaw rotation rate of $0.106^\circ/\text{s}$ (black dots), the yaw post-shadow maneuver was reversed.

2012c). A more detailed thermal force modeling (see e.g., Vigue et al, 1994; Adhya et al, 2005) could improve the errors observed in days with long eclipses ($\beta_0 \approx 0^\circ$). Outside eclipse seasons, the GPS-IIR orbit predictions show a very interesting feature especially for the radial component of the CODE model (Fig. 17). This systematic error is mitigated by using the adjustable box-wing model. The reason is the same as for the GPS-IIA satellites, the explicit dependency of the box-wing parameters on the Earth-satellite-Sun angle.

For GLONASS-M satellites, the main change in the prediction errors occurs by exchanging the CODE for the box-wing model (Figures 13 and 14). This has a positive impact especially for the cross-track component, but also a large negative impact on the along-track component (Fig. 14) during eclipse seasons. Both error changes (along- and cross-track) are also visible in Fig. 18. As in the case of non-eclipsing GPS-IIA and GPS-IIR satellites, systematic errors in the radial component (Fig. 18) are reduced when introducing the adjustable box-wing model. The use of the yaw maneuver model just brings a very small improvement, mainly visible for the radial component, in the orbit predictions (during 4th day, Fig. 18) but accompanied of a degradation in the along-

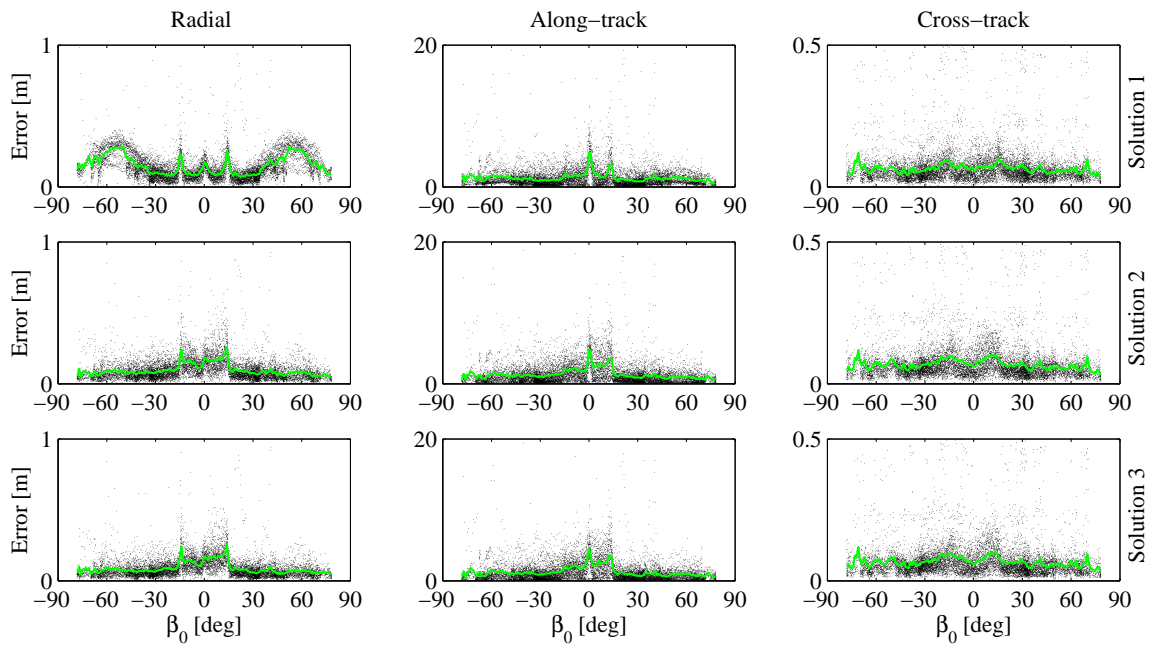


Fig. 17: RMS of orbit prediction errors (during 4th day) for all GPS-IIR satellites present during 2007 and 2008, and for the first three solutions in Table 1. The prediction errors are shown as function of β_0 , the Sun elevation angle above the orbital plane, together with the average line in green.

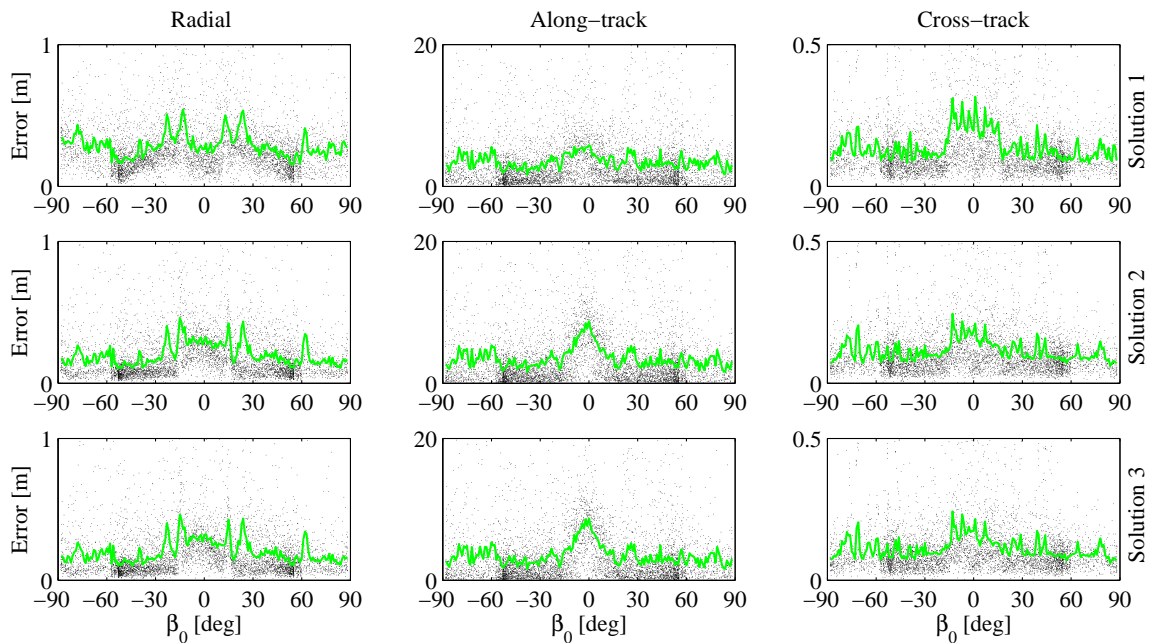


Fig. 18: RMS of orbit prediction errors (during 4th day) for all GLONASS-M satellites present during 2007 and 2008, and for the first three solutions in Table 1. The prediction errors are shown as function of β_0 , the Sun elevation angle above the orbital plane, together with the average line in green.

track component. The GLONASS-M orbit predictions errors show in general during eclipse seasons an improvement for short predictions (3 to 9 hours, Table 3) but a degradation for long predictions (during 4th day, Table 4), when including the adjustable box-wing and the yaw attitude models.

9 Conclusions

The orbits of GPS-IIA satellites are degraded during Sun-Earth eclipse seasons if the noon, shadow and post-shadow yaw maneuvers are not properly taken into account. Besides the incorrect position of the navigation antenna during the maneuvers, the non-conservative forces acting on the satellite, like solar radiation pressure and Earth radiation pressure, are mismodeled due to the misorientation of the satellite's surfaces in space. The combination of our box-wing models, adjustable for solar radiation pressure and a priori for Earth radiation pressure (Rodriguez-Solano et al, 2012c,a), with the yaw attitude information during maneuvers shows a significant improvement for the orbits of eclipsing GPS-IIA satellites w.r.t. the orbits computed with the nominal attitude law. However, the performance of non-eclipsing satellites is not yet reached.

Two models for the yaw attitude during maneuvers were tested in this study for GPS-IIA satellites. The first model is the existing Bar-Sever (1996) model with nominal yaw rates. The second model is based on the estimation of the real attitude of the satellites from PPP (Precise Point Positioning) phase residuals. Furthermore, two models for the orientation of the solar panels during yaw maneuvers were tested. The first model assumes that the solar panels point as perpendicular as possible to the Sun. The second model assumes that the solar panels are fixed w.r.t. the satellite bus during shadow, implying that a short post-shadow recovery has to be performed. From all the attitude models tested in combination with the box-wing model the one that improves the orbits most (from one solution to the next) is the yaw attitude model with nominal yaw rates. Further small improvements are obtained by using the estimated yaw attitude from PPP phase residuals and the second attitude model for the solar panels, which result in our best solution. The post-shadow maneuvers whose rotational direction can be ambiguous especially if nominal yaw rates are used, turn out to be no major problem for the solar radiation pressure computation. If the sign of the post-shadow maneuver is mismodeled, the cross-track accelerations acting on the satellite also have an incorrect sign, but the radial and along-track accelerations are almost unaffected, being independent of the sign of the post-shadow maneuver. This is the reason why the model based on the estimation of the real attitude results in just a small overall improvement in the orbits. Nevertheless, the use of the model based

on the estimation of the real attitude is very important, since it allows us to conclude that the remaining errors in the orbits of eclipsing GPS-IIA satellites might not be anymore related to a wrong yaw attitude. Other effects, like improper Earth shadow modeling or thermal effects, might have an important contribution to the remaining errors during eclipse seasons.

For GPS-IIR and GLONASS-M satellites, the yaw attitude models of Kouba (2009) and Dilssner et al (2011) with nominal yaw rates, were tested respectively. For both satellite types just a small improvement in the orbits is achieved by using the yaw maneuver models. Errors are still present for the orbits of eclipsing satellites, indicating again that other effects, not related to yaw attitude, might be important to consider during eclipses. Besides the possible errors mentioned in the previous paragraph, the specific solar panel orientation of GPS-IIR and GLONASS-M satellites during eclipses (currently unknown) might be a candidate for dedicated investigations.

The CODE 5-parameter radiation pressure model has a better performance than the adjustable box-wing model during eclipse seasons (especially for GPS-IIA satellites) if nominal attitude is used, and this was one of the main motivations to initiate this study. Now with the combination of the box-wing model with the yaw attitude the performance of the box-wing model for GPS-IIA satellites is much better. However, small degradations for eclipsing GPS-IIR and GLONASS-M satellites were found when using the box-wing (even if the yaw models are used) instead of the CODE model. The degradations appear mainly in the 4-day orbit predictions while the orbit overlaps show in general an improvement. Finally, in this study it was also found that β_0 (Sun elevation angle above the orbital plane) dependent errors outside eclipse seasons, i.e. with nominal attitude, present in the CODE radiation pressure model are mitigated when using the box-wing model. The errors are mainly visible in the radial component of orbit predictions for GPS-IIA, GPS-IIR and GLONASS-M satellites. The reason for this improvement in regimes with nominal attitude resides in the explicit dependence of the estimated parameters of the adjustable box-wing with the ϵ angle, formed between Earth, satellite and Sun.

Acknowledgements

This work has been funded by the DFG projects "LEO orbit modeling improvement and application for GNSS and DORIS LEO satellites" and "Geodätische und geodynamische Nutzung reprozessierter GPS-, GLONASS- und SLR-Daten". The comments and suggestions of three reviewers and the editor Pascal Willis are greatly appreciated.

References

- Adhya S, Ziebart M, Sibthorpe A, Arrowsmith P, Cross P (2005) Thermal Force Modeling for Precise Prediction and Determination of Spacecraft Orbits. *Navig J Inst Navig* 52(3):131–144
- Bar-Sever YE (1995) Performance Evaluation of the GPS Yaw Bias Implementation. In: *Proceedings of ION GPS 1995*, pp 599–611
- Bar-Sever YE (1996) A new model for GPS yaw attitude. *J Geod* 70(11):714–723, DOI 10.1007/BF00867149
- Bar-Sever Y (1997) New and Improved Solar Radiation Models for GPS Satellites Based on Flight Data. Final Report, Jet Propulsion Laboratory, prepared for Air Force Materiel Command SMC/CZSF
- Bar-Sever Y, Kuang D (2004) New Empirically Derived Solar Radiation Pressure Model for GPS Satellites. In: *Interplanetary Network Progress Report*, vol 42-159, URL http://ipnpr.jpl.nasa.gov/progress_report/42-159/title.htm
- Bar-Sever Y, Kuang D (2005) New Empirically Derived Solar Radiation Pressure Model for GPS Satellites During Eclipse Seasons. In: *Interplanetary Network Progress Report*, vol 42-160, URL http://ipnpr.jpl.nasa.gov/progress_report/42-160/title.htm
- Beutler G, Brockmann E, Gurtner W, Hugentobler U, Mervart L, Rothacher M, Verdun A (1994) Extended orbit modeling techniques at the CODE processing center of the International GPS Service for Geodynamics (IGS): theory and initial results. *Manuscr Geod* 19(6):367–386
- Beutler G, Brockmann E, Hugentobler U, Mervart L, Rothacher M, Weber R (1996) Combining consecutive short arcs into long arcs for precise and efficient GPS Orbit Determination. *J Geod* 70(5):287–299, DOI 10.1007/BF00867349
- Beutler G, Jäggi A, Hugentobler U, Mervart L (2006) Efficient satellite orbit modelling using pseudo-stochastic parameters. *J Geod* 80(7):353–372, DOI 10.1007/s00190-006-0072-6
- Bizouard C, Gambis D (2009) The Combined Solution C04 for Earth Orientation Parameters Consistent with International Reference Frame 2005. In: *Drewes H (ed) Geodetic Reference Frames, IAG Symposia 134*, Springer, pp 265–270, DOI 10.1007/978-3-642-00860-3_41
- Caissy M, Agrotis L, Weber G, Hernandez-Pajares M, Hugentobler U (2012) The International GNSS Real-Time Service. *GPS World* 23(6):52–58
- Choi KK, Ray J, Griffiths J, Bae TS (2012) Evaluation of GPS orbit prediction strategies for the IGS Ultra-rapid products. *GPS Solut* DOI 10.1007/s10291-012-0288-2
- Dach R, Hugentobler U, Fridez P, Meindl M (2007) Bernese GPS Software, Version 5.0. Astronomical Institute, University of Bern
- Dach R, Brockmann E, Schaer S, Beutler G, Meindl M, Prange L, Bock H, Jäggi A, Ostini L (2008) GNSS processing at CODE: status report. *J Geod* 83(3-4):353–365, DOI 10.1007/s00190-008-0281-2
- Dilssner F (2010) GPS IIF-1 Satellite Antenna Phase Center and Attitude Modeling. *Inside GNSS* 5(6):59–64
- Dilssner F, Springer T, Gienger G, Dow J (2011) The GLONASS-M satellite yaw-attitude model. *Adv Space Res* 47(1):160–171, DOI 10.1016/j.asr.2010.09.007
- Douša J (2010) The impact of errors in predicted GPS orbits on zenith troposphere delay estimation. *GPS Solut* 14(3):229–239, DOI 10.1007/s10291-009-0138-z
- Dow J, Neilan R, Rizos C (2009) The International GNSS Service in a changing landscape of Global Navigation Satellite Systems. *J Geod* 83(3-4):191–198, DOI 10.1007/s00190-008-0300-3
- Fliegel H, Gallini T, Swift E (1992) Global Positioning System Radiation Force Model for Geodetic Applications. *J Geophys Res* 97(B1):559–568, DOI 10.1029/91JB02564
- Fritsche M, Sosnica K, Rodriguez-Solano CJ, Steigenberger P, Wang K, Dietrich R, Dach R, Hugentobler U, Rothacher M (2013) Combined Reprocessing of GPS, GLONASS and SLR Observations. *J Geod*, submitted
- Kouba J (2009) A simplified yaw-attitude model for eclipsing GPS satellites. *GPS Solut* 13(1):1–12, DOI 10.1007/s10291-008-0092-1
- Leandro R, Landau H, Nitschke M, Glocker M, Seeger S, Chen X, Deking A, Tahar MB, Zhang F, Ferguson K, Stolz R, Talbot N, Lu G, Allison T, Brandl M, Gomez V, Kipka A (2012) Real-Time Extended GNSS Positioning: A New Generation of Centimeter Accurate Networks. *GPS World* 23(7):36–42
- Mitrikas V (2005) GLONASS-M dimensions and center-of-mass correction. *IGSMail-5105*, URL <http://igs.cb.jpl.nasa.gov/mail/igsmail/2005/msg00027.html>
- Revnivykh S, Mitrikas V (1998) GLONASS S/C mass and dimension. *IGEXMail-0086*, URL <http://igs.cb.jpl.nasa.gov/mail/igexmail/1998/msg00085.html>
- Rodriguez-Solano CJ, Hugentobler U, Steigenberger P (2012a) Impact of Albedo Radiation on GPS Satellites. In: *Kenyon S, Pacino MC, Marti U (Eds) Geodesy for Planet Earth, IAG Symposia 136*, Springer, pp 113–119, DOI 10.1007/978-3-642-20338-1_14
- Rodriguez-Solano CJ, Hugentobler U, Steigenberger P, Lutz S (2012b) Impact of Earth radiation pressure on GPS position estimates. *J Geod* 86(5):309–317,

- DOI 10.1007/s00190-011-0517-4
- Rodriguez-Solano CJ, Hugentobler U, Steigenberger P (2012c) Adjustable box-wing model for solar radiation pressure impacting GPS satellites. *Adv Space Res* 49(7):1113–1128, DOI 10.1016/j.asr.2012.01.016
- Springer T, Hugentobler U (2001) IGS ultra rapid products for (near-) and real-time applications. *Phys Chem Earth* 26(6-8):623–628, DOI 10.1016/S1464-1895(01)00111-9
- Urschl C, Beutler G, Gurtner W, Hugentobler U, Schaer S (2007) Contribution of SLR tracking data to GNSS orbit determination. *Adv Space Res* 39(10):1515–1523, DOI 10.1016/j.asr.2007.01.038
- Vigue Y, Schutz BE, Abusali PAM (1994) Thermal Force Modeling for Global Positioning System Satellites Using the Finite Element Method. *J Spacecr Rockets* 31(5):855–859, DOI 10.2514/3.26523
- Wu JT, Wu SC, Hajj GA, Bertiger WI, Lichten SM (1993) Effects of antenna orientation on GPS carrier phase. *Manuscr Geod* 18(2):91–98
- Ziebart M (2001) High Precision Analytical Solar Radiation Pressure Modelling for GNSS Spacecraft. Ph.D. thesis, University of East London
- Ziebart M, Dare P (2001) Analytical solar radiation pressure modelling for GLONASS using a pixel array. *J Geod* 57(11):587–599, DOI 10.1007/s001900000136
- Zumberge JF, Heflin MB, Jefferson DC, Watkins MM, Webb FH (1997) Precise point positioning for the efficient and robust analysis of GPS data from large networks. *J Geophys Res* 102(B3):5005–5017, DOI 10.1029/96JB03860

Reducing the draconitic errors in GNSS geodetic products

C. J. Rodriguez-Solano^a, U. Hugentobler^a, P. Steigenberger^a, M. Bloßfeld^b, M. Fritsche^c

^a Institut für Astronomische und Physikalische Geodäsie, Technische Universität München, 80333 München, Germany

^b Deutsches Geodätisches Forschungsinstitut, 80539 München, Germany

^c Institut für Planetare Geodäsie, Technische Universität Dresden, 01069 Dresden, Germany

Abstract

Systematic errors at harmonics of the GPS draconitic year have been found in diverse GPS-derived geodetic products like the geocenter Z -component, station coordinates, Y -pole rate and orbits (i.e. orbit overlaps). The GPS draconitic year is the repeat period of the GPS constellation w.r.t. the Sun which is about 351 days. Different error sources have been proposed which could generate these spurious signals at the draconitic harmonics. In this study, we focus on one of these error sources, namely the radiation pressure orbit modeling deficiencies. For this purpose, three GPS+GLONASS solutions of eight years (2004-2011) were computed which differ only in the radiation pressure and satellite attitude models. The models employed in the solutions are: 1) the CODE (5-parameter) radiation pressure model widely used within the IGS (International GNSS Service) community, 2) the adjustable box-wing model for solar radiation pressure impacting GPS (and GLONASS) satellites, and 3) the adjustable box-wing model upgraded to use non-nominal yaw attitude. When comparing the first solution with the third one we achieved the following in the GNSS geodetic products. Orbits: the draconitic errors in the orbit overlaps are reduced for the GPS satellites in all the harmonics on average 46%, 38% and 57% for the radial, along-track and cross-track components, while for GLONASS satellites they are mainly reduced in the cross-track component by 39%. Geocenter Z -component: all the odd draconitic harmonics found when the CODE model is used show a very important reduction (almost disappearing with a 92% average reduction) with the new radiation pressure models. Earth orientation parameters: the draconitic errors are reduced for the X -pole rate and especially for the Y -pole

rate by 24% and 50% respectively. Station coordinates: all the draconitic harmonics (except the 2nd harmonic in the North component) are reduced in the North, East and Height components, with average reductions of 41%, 39% and 35% respectively. This shows, that part of the draconitic errors found in GNSS geodetic products are definitely induced by radiation pressure orbit modeling deficiencies.

Keywords: GPS; GLONASS; solar radiation pressure; yaw attitude; draconitic harmonics.

1 Introduction

Systematic errors at harmonics of the GPS draconitic year have been found in diverse GPS-derived geodetic products. The GPS draconitic year is the repeat period of the GPS constellation w.r.t. the Sun, which is about 351 days or 1.04 cpy (cycles per year). This period results from the secular retrograde motion of the right ascension of the ascending node due to the oblateness of the Earth (i.e. due to the J_2 term). The GPS-derived geodetic products in which spurious signals have been found at 1.04 cpy and its harmonics are the following:

- Geocenter Z -component (Hugentobler et al, 2006; Meindl, 2011; Rodriguez-Solano et al, 2012a; Ostini, 2012).
- Station coordinates (Ray et al, 2008; Collilieux et al, 2007; Amiri-Simkoei, 2007; Tregoning and Watson, 2009; King and Watson, 2010; Santamaría-Gómez et al, 2011; Rodriguez-Solano et al, 2012a; Ostini, 2012).
- Y -pole rate (Seitz et al, 2012).
- Orbits (jumps between successive days, Griffiths and Ray, 2013).

For other GNSS constellations similar systematic errors could be expected at harmonics of the respective draconitic years, e.g., for GLONASS the draconitic year is about 353 days or 1.035 cpy. Meindl (2011) found odd harmonics of the GLONASS draconitic year in the time series of the Z -component of the GLONASS-only derived geocenter. For combined GPS+GLONASS products (like the ones generated in this study) the system-specific systematic errors are difficult to distinguish from the low harmonics of the draconitic years, as the fundamental frequencies are very close to each other.

Systematic errors in the GNSS data or models are expected to propagate over the whole GNSS solutions introducing these artificial effects on most products. Diverse error sources have been proposed to explain these systematic errors. Hugentobler et al (2006) and Meindl et al (2013) relate the geocenter motion with the orbit modeling parameters, in particular radiation pressure parameters, due to correlations between them. The first paper states that the patterns found in the geocenter Z -component with distinct periods of one GPS draconitic year should be caused by orbit modeling deficiencies and not by geophysical effects. Reischung et al (2013) found that the geocenter coordinates are highly collinear with the satellite clock and troposphere parameters, so that their estimation is very sensitive to GNSS modeling errors, like radiation pressure modeling errors. Ray et al (2008) give two possible coupling mechanisms which could generate the spurious signals at harmonics of 1.04 cpy found in the estimates of station coordinates: 1) Long-period GPS satellite orbit modeling errors, in particular due to the Sun-satellite interactions or during eclipse seasons which happen twice per draconitic year for each orbital plane. 2) Station specific errors that can be aliased due to the repeating geometry of the satellite constellation w.r.t. the tracking network to generate a period of one draconitic year, in particular long-wavelength (i.e. near-field) multipath or errors in the antenna or radome calibrations. King and Watson (2010) demonstrated by using simulated GPS data that multipath errors can produce spurious signals at harmonics of 1.04 cpy on station coordinates time series. Tregoning and Watson (2009) and King and Watson (2010) found that if phase ambiguities are not fixed there is a significant amplification in the expression of the spurious draconitic harmonics. Tregoning and Watson (2009) and Tregoning and Watson (2011) suggest that possible errors in the S1 and S2 tidal models (ocean, atmosphere) which are at diurnal and semidiurnal periods can contribute to the low-frequency draconitic signals seen in the GPS solutions. Griffiths and Ray (2013) introduced errors in the IERS (International Earth Rotation and Reference Systems Service) sub-daily EOP (Earth Orientation Parameters) tide model, which is used as a priori information in the GNSS solutions, and found that those errors can propagate to the GPS orbits at the 1st

and 3rd harmonics of 1.04 cpy. Finally, Amiri-Simkooei (2013) focused on the nature of the draconitic errors found in GPS station coordinates and concluded that these errors do not likely depend on station related effects such as multipath but rather on other causes like orbit mismodeling or atmospheric loading effects.

In this study, we focus only on one of the error sources proposed by previous authors, namely the radiation pressure orbit modeling deficiencies. In Rodriguez-Solano et al (2012a) we tested the impact of Earth radiation pressure on the draconitic errors present in station coordinates and geocenter Z -component, obtaining only a reduction (about 38%) in the 6th harmonic of the North component of the station coordinates and just a minimal reduction for the harmonics of the geocenter Z -component. From that study it became clear that the modeling of the main non-conservative force acting on GPS satellites, the solar radiation pressure, should also be revised as we used the CODE radiation pressure model (Beutler et al, 1994). In Rodriguez-Solano et al (2012b) we developed a new approach to model the solar radiation pressure impacting GPS satellites which we called the adjustable box-wing model. This new model could reduce β_0 (Sun elevation angle above the orbital plane, see Fig. 1) dependent systematic errors observed in the orbit predictions of GPS-IIA, GPS-IIR and GLONASS-M satellites (Rodriguez-Solano et al, 2013). The β_0 angle varies with a period of one draconitic year, the maximum reachable values are given by the inclination of the satellite orbital plane plus the obliquity of the ecliptic (about 23.45°), i.e., $\pm 78.45^\circ$ for GPS and $\pm 88.25^\circ$ for GLONASS satellites. The reduction of β_0 systematic errors with the adjustable box-wing model only occurred outside eclipse seasons when the satellites are fully in nominal yaw attitude mode. During eclipse seasons when the satellites can perform yaw maneuvers the systematic errors were increased (especially for GPS-IIA satellites) with the adjustable box-wing model. Therefore, in Rodriguez-Solano et al (2013) we upgraded the adjustable box-wing model to accommodate non-nominal yaw attitude, especially the yaw maneuvers performed during eclipse seasons, and with it obtaining an important reduction of the orbit errors during eclipse seasons for GPS-IIA satellites. This was an important motivation to start this study, with the reasoning that if we achieved a reduction of the β_0 systematic errors in the orbits, we will most probably also achieve a reduction of the orbit errors at harmonics of the GPS draconitic year observed by Griffiths and Ray (2013). But we also suspected that the draconitic errors found in other GNSS derived geodetic products could be reduced since they were computed within the same GNSS solutions.

The description of the radiation pressure models and the main difference between them are given in Section 2. The reprocessing experiments realized to test the previ-

ous models and details on the power spectrum computation, widely used in this paper to analyze the errors at harmonics of the draconitic year, are described in Section 3. Finally, the GNSS geodetic products whose draconitic errors are analyzed in this study are the following: orbits (i.e. overlap errors, Section 4), geocenter Z -component (Section 5), Earth orientation parameters (Section 6) and station coordinates (Section 7).

2 Orbit models

2.1 CODE radiation pressure model

The CODE radiation pressure model is an empirical model to compensate the effect of solar radiation pressure on GPS and GLONASS satellites. The model was first introduced by Beutler et al (1994) where the extended orbit modeling techniques used by the Center for Orbit Determination in Europe (CODE) are described. Up to nine empirical acceleration parameters can be estimated in a Sun-fixed orthogonal frame (Fig. 1):

$$\begin{aligned} D(u) &= D_0 + D_C \cos u + D_S \sin u, \\ Y(u) &= Y_0 + Y_C \cos u + Y_S \sin u, \\ B(u) &= B_0 + B_C \cos u + B_S \sin u, \end{aligned} \quad (1)$$

where D points along the satellite-Sun direction, Y points along the solar panel beams (for nominal yaw attitude, explained in the next paragraph) and B completes the orthogonal frame. The main argument of the model is u , the argument of latitude of the satellite. This model is widely used within the IGS (International GNSS Service) community, in particular its 5-parameter version where only the D_0 , Y_0 , B_0 , B_C and B_S parameters are estimated. In this study we also use this last version of the model.

The nominal yaw-steering attitude (the yaw angle Ψ is shown in Fig. 1) of the GPS and GLONASS satellites is given by accomplishing two conditions at the same time: 1) the antennas should be pointing to the center of the Earth to transmit the navigation signals and 2) the solar panels should be pointing perpendicular to the Sun to keep a maximum power supply.

2.2 Adjustable box-wing model

The adjustable box-wing model (Rodriguez-Solano et al, 2012b) was created to compensate the effects of solar radiation pressure impacting on GPS satellites, using an intermediate approach between the physical/analytical models and the purely empirical models. The box-wing model is based on the physical interaction between solar radiation and satellite surfaces, simplifying the satellite to a box (satellite bus) and to a wing (solar panels). In addition, nine parameters can be adjusted (estimated) to fit best the GPS tracking data just as the CODE model does. The nine parameters are:

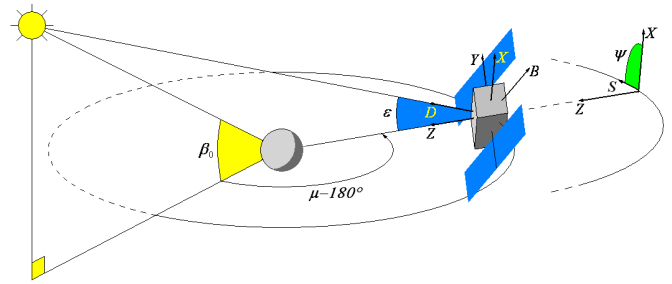


Fig. 1: Relative geometry of Sun, Earth and GPS satellites. Nominal yaw-steering attitude as a function of the position of the Sun in the orbital plane. Illustration of DYB (Sun-fixed) and XYZ (body-fixed) orthogonal frames.

1. solar panel scaling factor $(1 + \rho + \frac{2}{3}\delta)$,
2. solar panel rotation lag,
3. Y -bias acceleration (Y_0 of CODE model),
4. absorption plus diffusion $(\alpha + \delta)$ of $+X$ bus,
5. absorption plus diffusion $(\alpha + \delta)$ of $+Z$ bus,
6. absorption plus diffusion $(\alpha + \delta)$ of $-Z$ bus,
7. reflection coefficient (ρ) of $+X$ bus,
8. reflection coefficient (ρ) of $+Z$ bus,
9. reflection coefficient (ρ) of $-Z$ bus.

The partial derivatives of the acceleration w.r.t. the previous parameters are written analytically (for the case of nominal yaw attitude of the GPS satellites) in Rodriguez-Solano et al (2012b). The accelerations point towards the D and B directions for the first two parameters, if nominal yaw attitude is considered. The scaling factor of the solar panels just differs from D_0 in the units and the solar panel rotation lag is a novel parameter which compensates for a small lag of the solar panels when they follow the Sun, about 1.5 and 0.5 degrees respectively for the GPS-IIA and GPS-IIR satellites. Y_0 is identical to the same parameter of the CODE model. The last six parameters are the optical properties, divided into $\alpha + \delta$ and ρ , of the surfaces of satellite bus which are illuminated by the Sun under nominal yaw attitude conditions, namely the $+Z$, $+X$ and $-Z$ surfaces as shown in Fig. 1. For GLONASS satellites we tested adjustable box-wing models in Rodriguez-Solano et al (2013), which are actually cylinder-wing models for the GLONASS (old type) and GLONASS-M satellites.

Table 1: Solar radiation pressure and yaw attitude models selected for the eight years (2004-2011) reprocessing experiments.

# sol.	Solar radiation pressure	Yaw attitude
1	CODE 5-parameters	Nominal attitude law
2	Adjustable box-wing	Nominal attitude law
3	Adjustable box-wing	GPS-IIA: nominal yaw rates ¹ , Bar-Sever (1996) GPS-IIR: 0.20°/s yaw rate, Kouba (2009) GLONASS-M: 0.25°/s yaw rate, Dilssner et al (2011)

2.3 Yaw attitude models

During Sun-Earth eclipse seasons GPS and GLONASS satellites perform yaw maneuvers at orbit noon and orbit midnight, the first one happens in sunlight while the second one occurs in the shadow of the Earth. In particular, the GPS-II/IIA, GPS-IIR, GPS-IIF and GLONASS-M satellites perform these yaw maneuvers. Additionally, GPS-II/IIA satellites perform yaw maneuvers after shadow exit, usually called post-shadow maneuvers. Existing models describe precisely the yaw maneuvers performed by the GPS-II/IIA (Bar-Sever, 1996), GPS-IIR (Kouba, 2009), GPS-IIF (Dilssner, 2010) and GLONASS-M (Dilssner et al, 2011) satellites. These models (except the one of GPS-IIF satellites) have been implemented in a development version of the Bernese GNSS Software (Dach et al, 2007).

If the navigation antenna of the satellite has an offset w.r.t. the satellite rotation axis (which is the case for GPS-II/IIA, GPS-IIF and GLONASS-M satellites) and the yaw maneuvers are not correctly modeled, large errors in the GNSS observations are introduced. Besides these geometrical effects, the solar radiation pressure for the noon and post-shadow maneuvers will be mis-modeled if the yaw maneuvers are not properly taken into account. During shadow maneuvers, Earth radiation pressure still acts on the satellites and should also be properly modeled. In Rodriguez-Solano et al (2013) we upgraded the adjustable box-wing model to be able to work with non-nominal yaw attitude. However, the upgraded model does not have any longer an analytical expression and has to be computed numerically for any arbitrary direction of the Sun w.r.t. the satellite surfaces.

3 Data analysis

3.1 Reprocessing experiments

For this study, we extended the first three orbit solutions computed in Rodriguez-Solano et al (2013) from two years (2007-2008) to eight years (2004-2011). This extension of the solutions allows us to better detect the draconitic errors in the computed geodetic products. We have computed three GPS+GLONASS solutions of eight

years which differ only in the solar radiation pressure and yaw attitude models as described in Table 1. We started from GPS and GLONASS cleaned observations and followed the strategy presented by Fritsche et al (2013) with only minor differences described in detail in Rodriguez-Solano et al (2013). Together with the satellite orbits we have estimated the apparent geocenter coordinates, i.e., the offset between the instantaneous Earth's center of mass, as sensed by the satellites, and the reference frame origin (applying a no-net-translation condition). In Rodriguez-Solano et al (2013) we computed five solutions where the last two included the real yaw attitude of GPS-IIA satellites obtained from PPP phase residuals and a specific pitch attitude model for the solar panels of those satellites. The best orbit results were achieved with the last (fifth) solution, however, the largest improvements in the errors observed during eclipse seasons came with the Bar-Sever (1996) model with nominal yaw rates¹. This is the reason why we only extended the first three solutions of Rodriguez-Solano et al (2013) since the largest changes in the orbit errors occurred within these three first solutions. Therefore, if exchanging the solar radiation pressure and yaw attitude models has an impact on the draconitic errors observed in GNSS geodetic products, it should be observed within these three solutions.

3.2 Power spectrum

The power spectra, widely used in this paper to analyze the errors at harmonics of the draconitic year, are computed exactly as described in Rodriguez-Solano et al (2012a). The power spectra are based on the Fast Fourier Transform (FFT, Press et al, 1992) and where data is missing, zero padding was employed, since GPS-derived daily estimates are evenly spaced. Moreover, the units of the power spectrum are well-defined (e.g. mm²). Additionally, to compute the stacked (mean) power spectrum of the orbit overlap errors or of the stations coordinates a weighting according to the inverse of the variance was introduced to ensure that the noisier time

¹ftp://sideshow.jpl.nasa.gov/pub/GPS_yaw_attitude/nominal_yaw_rates

series have a lower contribution. Our time series have a length of $T_S = 2922$ days. This means that one can reliably distinguish between estimated frequencies that are separated by $\Delta f = 0.125$ cpy. This is in accordance with Eq. (41) of Rothacher et al (1999) which can be written as $\Delta f = 365.25/T_S$. Therefore, the 1st and 2nd draconitic harmonics at 1.04 and 2.08 cpy can be hardly distinguished from the annual and semiannual frequencies at 1 and 2 cpy. The separation of draconitic and annual harmonics starts to be reliable for the 3rd harmonic, where the separation of 0.12 cpy between harmonics almost reaches Δf . The separation between GPS and GLONASS draconitic harmonics starts to be reliable only for the 25th harmonic, i.e., as the respective frequencies are 26 and 25.875 cpy. Figures 2, 3, 4, 6 and 7 were created using the FFT approach with the number of tested frequencies equal to 4×2^{12} , where 12 is the next higher power of 2 of 2922, such that the frequency interval in the figures is 0.0223 cpy. For the Tables 2, 3, 4 and 5 the numerical values of the power spectra at the draconitic harmonics were extracted from the respective figures by using a simple interpolation at the desired frequency values.

4 Impact on the orbit overlap errors

The orbit overlap errors, are an indicator of internal orbit consistency. Our daily satellite arcs span from 00:00:00 until 24:00:00, therefore our orbit overlaps are simply computed by taking the difference between consecutive 1-day arcs at the midnight epoch. The daily orbit overlaps were computed for the eight years we have (2004-2011) and for all GPS and GLONASS satellites. We then separated the orbit overlaps by SVN (Space Vehicle Number) and computed the individual power spectrum for each satellite as described in Section 3.2. The individual power spectra were stacked separately for GPS and GLONASS satellites using a weighting with the inverse of the variance of the orbit overlap errors to create Fig. 2.

For GPS satellite orbits we find large systematic errors at harmonics of one GPS draconitic year as already reported by Griffiths and Ray (2013). As we have expected from the results of Rodriguez-Solano et al (2013) where we achieved significant reduction of the β_0 related orbit errors, the draconitic errors in the orbits also decrease with the new solar radiation pressure and attitude models. This can be seen in Fig 2 but Table 2 is much more conclusive, where it can be seen that there is a general reduction of the errors. Moreover, if solutions 1 and 3 are compared directly in Table 2, we find a reduction of the errors for all the draconitic harmonics and for all the components. With an average² reduction of 46%, 38% and 57% for the radial, along-track and cross-track components.

For GLONASS satellite orbits we find systematic er-

rors at harmonics of one GLONASS draconitic year, at least for the first five harmonics as shown in Fig. 2. Here we find a mixture of improvement and degradation in the errors when using the new solar radiation pressure and attitude models, see Table 2. We obtain an average² reduction of the errors of 5% and 39% for the along-track and cross-track components, while in the radial component the errors are increased in average by 16%. Mainly the cross-track component shows a general improvement, in all but the 1st harmonic which is slightly degraded. In Rodriguez-Solano et al (2013) the cross-track component was also the one with the highest improvements.

While the main focus of this paper is on the low draconitic harmonics, we consider important to include here also the power spectra of orbit overlap errors at higher frequencies (Fig. 3). In particular for GLONASS, there are some striking patterns in the power spectra of the orbits, like the clusters of peaks around 47 cpy, 94 cpy and 140 cpy. At the moment we do not have an explanation for these features but the first frequency is close to eight sidereal days or 45.8 cpy, the repeat period of the GLONASS ground tracks. Besides these features it is interesting to note in Fig. 3 that the power spectra are generally decreased when using the adjustable box-wing model, in particular for the cross-track component. From Table 2 one cannot affirm that the adjustable box-wing model brings a general improvement in the radial and along-track components of the GLONASS orbits, but this can be affirmed looking at Fig. 3. For GPS orbits most of the power concentrates at the low frequencies, besides the draconitic harmonics we find high peaks between 20 cpy and 50 cpy, most probably related to errors of the sub-daily EOP tide model as discussed by Griffiths and Ray (2013). Beyond 50 cpy there is only white noise, with just a small degradation in the radial component at very high frequencies when the adjustable box-wing model is used. For the other GNSS geodetic products analyzed in this paper, i.e., geocenter Z -component, Earth orientation parameters and stations coordinates, we did not find significant differences in the power spectra of the solutions given in Table 1 at high frequencies. Therefore, we did not include such figures in this paper.

²Over all the draconitic harmonics and weighted with the average values of solutions 1 and 3 such that small draconitic errors also have small contributions to the final average.

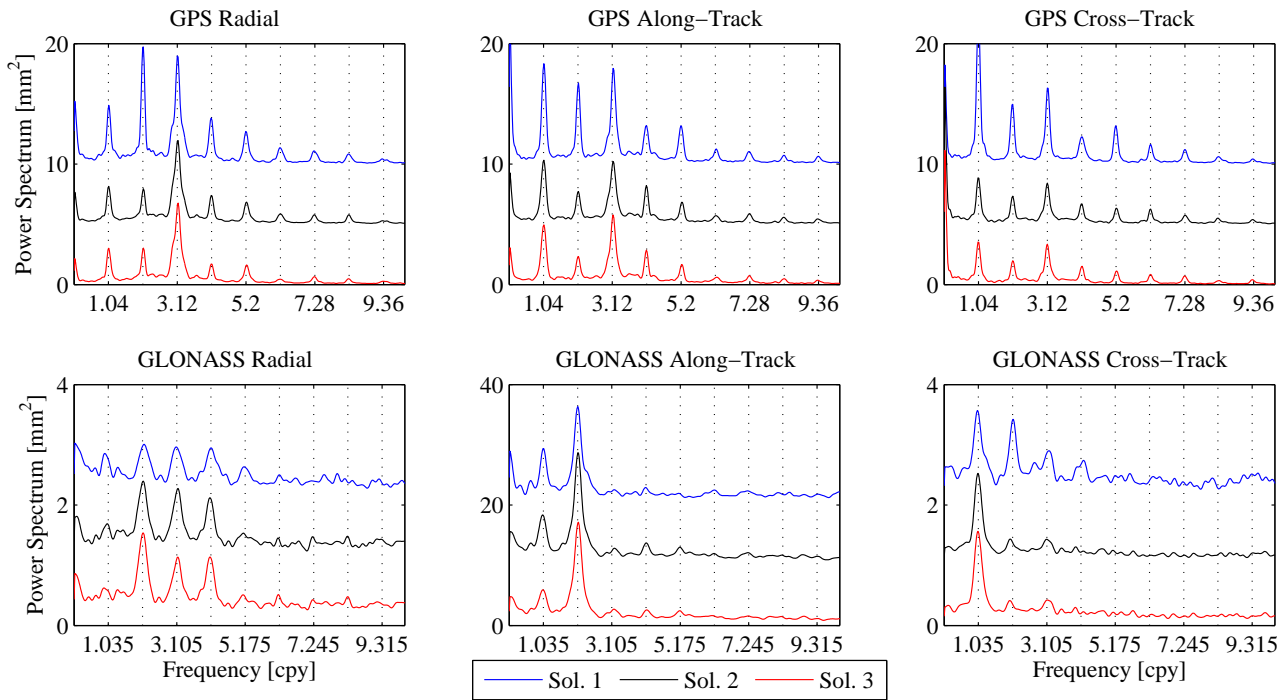


Fig. 2: Power spectrum of orbit overlap errors (stacked from all GPS and GLONASS satellites) for the three solutions given in Table 1 and separated in the radial, along-track and cross-track components. The power spectra of solutions 1 and 2 have been shifted along the vertical axes to make the details visible. The dotted vertical lines are at harmonics of 1.04 cycles per year for GPS and 1.035 cycles per year for GLONASS.

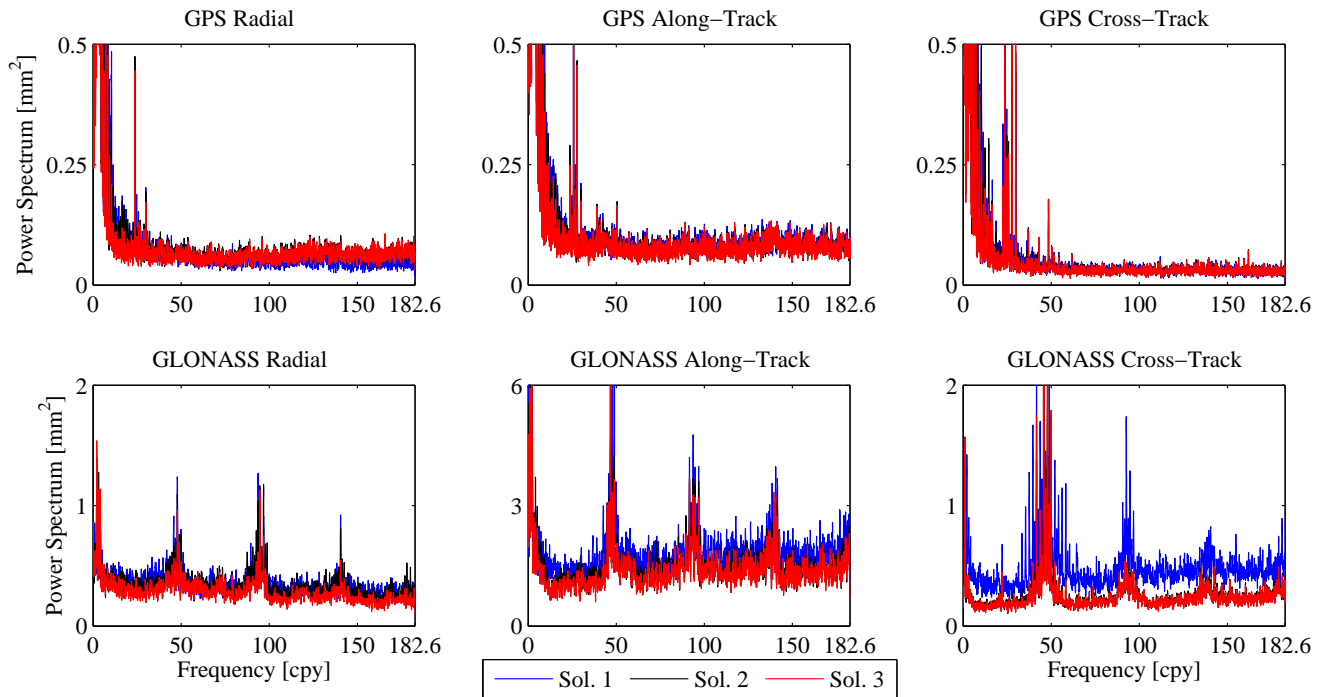


Fig. 3: Same as Fig. 2 but extended until the Nyquist frequency of 182.625 cpy. The power spectra of solutions 1 and 2 have not been shifted along the vertical axes as in Fig. 2.

Table 2: Numerical values [mm²] of the GPS (left) and GLONASS (right) orbit overlap errors power spectra (see Fig. 2) at harmonics of 1.04 and 1.035 cpy. Green indicates an improvement w.r.t. the previous solution while red indicates a degradation.

Comp.	Sol.	1.04	2.08	3.12	4.16	5.20	6.24	7.28	8.32	9.36	1.035	2.07	3.105	4.14	5.175
Radial	1	4.71	9.66	8.90	3.71	2.69	1.34	1.05	0.82	0.37	0.76	0.98	0.96	0.95	0.63
Radial	2	3.10	2.80	6.84	2.37	1.80	0.86	0.76	0.78	0.28	0.67	1.38	1.24	1.10	0.51
Radial	3	2.95	2.88	6.43	1.70	1.56	0.44	0.64	0.46	0.27	0.57	1.53	1.11	1.12	0.47
Along	1	8.14	6.53	7.12	3.11	3.17	1.18	1.00	0.73	0.64	9.37	16.29	2.28	2.89	1.84
Along	2	5.26	2.69	4.91	3.15	1.69	0.71	0.87	0.58	0.42	8.23	18.56	2.36	3.69	2.98
Along	3	4.90	2.31	5.46	2.79	1.55	0.56	0.72	0.48	0.34	5.88	16.90	2.43	2.55	2.43
Cross	1	12.03	4.80	6.24	2.25	3.13	1.62	1.20	0.59	0.39	1.54	1.41	0.86	0.68	0.49
Cross	2	3.84	2.28	3.41	1.69	1.31	1.26	0.74	0.43	0.36	1.51	0.38	0.43	0.22	0.22
Cross	3	3.51	1.95	3.34	1.48	1.09	0.83	0.70	0.32	0.34	1.55	0.35	0.42	0.20	0.20

5 Impact on the geocenter Z -component

The geocenter Z -component estimated with the CODE (5-parameter) radiation pressure model shows large variations that can be (visually) correlated with the β_0 angle of the different orbital planes as shown in Fig. 4. This correlation is particularly strong with the GLONASS β_0 angles in the last years of the time series. The power spectrum of the geocenter Z -component shows strong draconitic errors at odd harmonics of 1.04 cpy. We cannot make a distinction between the specific GPS and GLONASS draconitic errors as the fundamental frequencies of the harmonics (1.04 and 1.035 cpy) are very close to each other, see also Section 3.2. Exchanging the CODE (5-parameter) radiation pressure model by the adjustable box-wing model results in a significant reduction of the geocenter Z -component variations and of the associated draconitic errors (solutions 1 and 2 in Fig. 4 and Table 3). The possibility that the CODE model can cause these problems in the geocenter was already discussed by Meindl et al (2013) as follows:

“Having said that orbit parametrization plays an important role one might conclude that the problems encountered in this article are uniquely caused by the CODE orbit model (5), (6). This is not true, however: Alternative models, like, e.g., box-wing models, cannot live without model parameters, which have to be determined in the parameter estimation process. Our theory asks that each empirical acceleration standing behind such a free parameter has to be decomposed into the (R,S,W) -components-along the lines presented in Section 2.2. As soon as W -components with non-zero means over a revolution result, there is the danger of generating artifacts.”

We agree with the previous paragraph and indeed our adjustable box-wing model does have model parameters that have to be estimated in the orbit determination process as mentioned in Section 2.2 of this paper. However, those parameters with exception of D_0 and Y_0 are significantly different from the CODE model parameters. The D_0 acceleration has a non-zero mean in the W -component while Y_0 does not have one. The W -direction is identical to the cross-track direction. In the following we will analyze the box-wing model parameters which could have a W -component.

The solar panel rotation lag acceleration points in the B -direction (see Fig. 1) and has a main dependency on $\text{sign}(\dot{\epsilon})$, given in Eq. (15) of Rodriguez-Solano et al (2012b), which can be approximated as $\sin(\mu)$. Where μ (see Fig. 1) is the orbit angle formed between the spacecraft position vector and orbit midnight, growing with the satellite’s motion (Bar-Sever, 1996). According to Eq. (16) of Meindl et al (2013), the W -component of a constant B acceleration can be written as:

$$W_B = B \frac{-\sin 2\beta_0 \cos \mu}{2\sqrt{1 - \cos^2 \beta_0 \cos^2 \mu}}. \quad (2)$$

Multiplying the last equation with $\text{sign}(\dot{\epsilon})$ or $\sin(\mu)$ results in a twice-per-revolution term with zero mean acceleration. Meindl et al (2013) noted that the once-per-revolution empirical parameters in the Y -direction of the CODE model (Eq. 1) result in a superposition of a constant and a twice-per-revolution term in the W -component which can be very problematic for the geocenter estimation. However, in that paper it was not noted that it is the same case for the once-per-revolution empirical parameters in the B -direction of the CODE model (Eq. 1), which can perfectly generate a $\cos(\mu)$ term that multiplied with Eq. 2 also results in a superposition of a constant and a twice-per-revolution term. This coincides with the results of Rebischung et al (2013) who found that the simultaneous estimation of the D_0 , B_C and B_S from the CODE (5-parameter) radiation

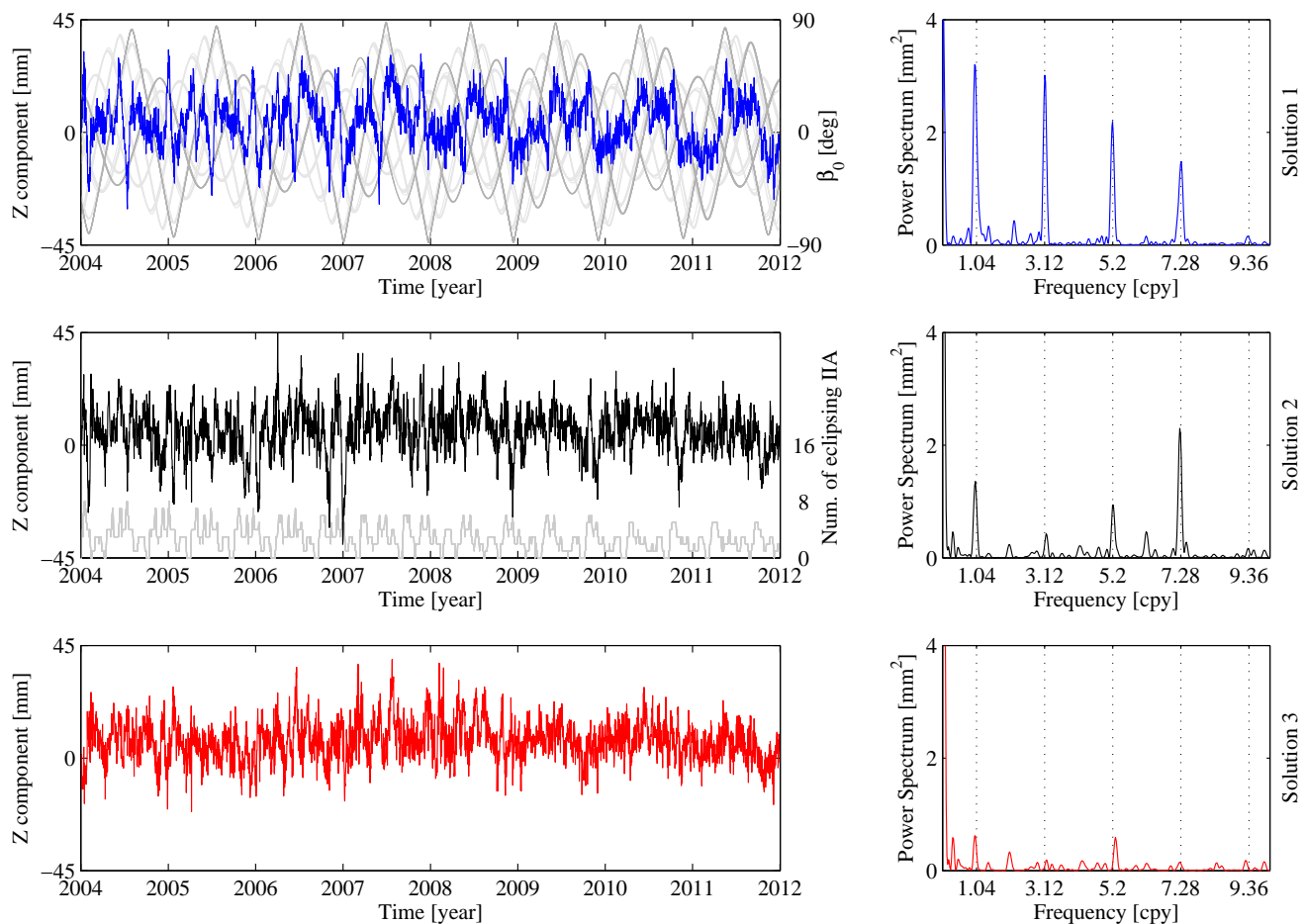


Fig. 4: Time series of the daily estimated Z -component geocenter for the three solutions given in Table 1. On the right, the power spectrum of the corresponding time series is shown. The dotted vertical lines are at harmonics of 1.04 cycles per year. In the background of the time series of solution 1, the Sun elevation angle above the orbital plane (β_0) of all GPS (light gray) and GLONASS (dark gray) satellites is displayed. In the background of the time series of solution 2, the number of GPS block II and IIA in eclipse season is displayed. During the time period from 2004 until 2011, a maximum number of 8 GPS block II and IIA satellites were simultaneously in eclipse season.

pressure model slightly increases the estimation problems of the geocenter Z -component.

The absorption plus diffusion parameters of the adjustable box-wing model show large correlations to other box-wing parameters if they are freely estimated. Therefore, as described in Rodriguez-Solano et al (2012b) those parameters are tightly constrained in the orbit determination process and consequently should have a minimal impact on the geocenter estimation. However, the reflection parameters are estimated with loose constrains. The $+Z$ and $-Z$ directions are parallel to the radial direction, such that the only parameter which could have a cross-track component is the one pointing along the $+X$ direction, see Fig. 1. This parameter has a main dependency on $\sin^2(\epsilon)$, given in Eq. (12) of Rodriguez-Solano

et al (2012b), which can be written as:

$$\sin^2 \epsilon = 1 - \cos^2 \beta_0 \cos^2 \mu. \quad (3)$$

The W -component of a constant X acceleration can be written as:

$$W_X = X \frac{\sin \beta}{\sqrt{1 - \cos^2 \beta_0 \cos^2 \mu}}. \quad (4)$$

Multiplying the last equation with $\sin^2(\epsilon)$ results in a twice-per-revolution term with non-zero mean acceleration.

Summarizing, the CODE (5-parameter) radiation pressure model has the D_0 , B_C and B_S parameters which could cause problems for the geocenter estima-

Table 3: Numerical values [mm^2] of the geocenter power spectrum (see Fig. 4) at odd harmonics of 1.04 cpy. Green indicates an improvement w.r.t. the previous solution while red indicates a degradation.

Comp.	# sol.	1.04	3.12	5.20	7.28	9.36
Z	1	2.30	2.97	2.14	1.45	0.13
Z	2	1.00	0.25	0.94	2.00	0.14
Z	3	0.37	0.08	0.13	0.13	0.02

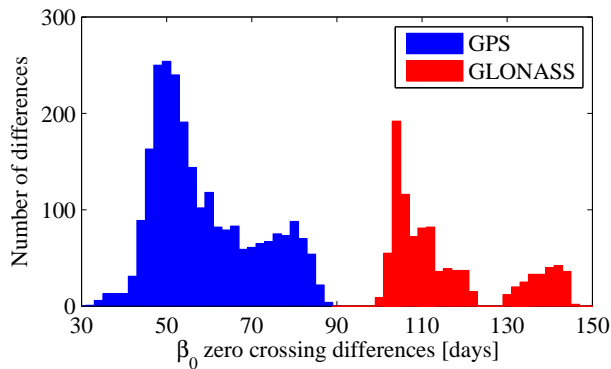


Fig. 5: Histogram of differences in days between β_0 zero crossing points ($\beta_0 = 0^\circ$, see also Fig. 4) of consecutive orbital planes during the time period 2004-2011, separately for GPS and GLONASS.

tion, while for the adjustable box-wing model the problematic parameters are the solar panel scaling factor and the reflection coefficient of the $+X$ bus surface. Therefore, according to the theory developed by Meindl et al (2013) the differences in the geocenter estimates between solutions 1 and 2 in Fig. 4 should mainly result from replacing the once-per-revolution B parameters by the $+X$ reflection parameter. Both type of parameters generate twice-per-revolution with non-zero mean cross-track accelerations. However, with the fundamental difference that the acceleration generated from the once-per-revolution parameters in B -direction is purely empirical while the acceleration due to $+X$ reflection results from the physical interaction between the Sun and the $+X$ surface. Moreover, with the adjustable box-wing model we obtained improvements in the cross-track components of the GPS orbits and especially of the GLONASS orbits as shown in Section 4. This parametrization difference is, from our point of view, the explanation of the improvement obtained in the geocenter Z -component estimation with the adjustable box-wing model.

We do not have an explanation about why the CODE radiation pressure model generates draconitic errors in the geocenter just at odd harmonics. However, we be-

lieve to have an explanation on the largest (7th) harmonic observed on solution 2, computed with the adjustable box-wing model with nominal yaw attitude. Solution 2 has mainly large orbit errors during eclipse seasons, which as mentioned in the Introduction happen twice per draconitic year. The GPS system, the one contributing the most to the geocenter computation as shown by Meindl et al (2013), has six orbital planes equally spaced along the equator. Thus one would intuitively expect the largest draconitic harmonic to be at the 6th harmonic, obviously this is not the case when looking at Fig. 4. Why the largest peak is at the 7th and not at the 6th harmonic may be explained through Fig. 5 which shows the histograms of differences in days between consecutive GPS orbital planes along the ecliptic (not the equator). The peak of this histogram is at about 50 days which would correspond to the 7th draconitic harmonic. Sun-Earth eclipses last at maximum one hour for a GPS satellite orbital revolution, and a satellite is in eclipse season around 73 days (average over 6 orbital planes) during one year. While these time periods seem small, the complete arc for an eclipsing satellite may be degraded. Moreover, the GPS consists of 6 different orbital planes, which increases the probability that for any day at least one GPS-II/IIA satellite is in eclipse season. This is shown in the background of the time series of solution 2 in Fig. 4. Moreover, one or few of the satellites with worse orbits than others can have a negative impact on a global GNSS solution and consequently on the geocenter estimation. As we would have expected, solution 3, which reduces the orbit errors during eclipse seasons mainly for GPS-IIA satellites, reduces very significantly the 7th draconitic harmonic when compared to the previous solution as shown in Fig. 4.

Finally, as in the case of the GPS orbits (Table 2), for the geocenter Z -component there is an overall reduction of the draconitic errors when the new solar radiation pressure and yaw attitude models are used. When comparing solutions 1 and 3 (Fig. 4 and Table 3) it can be observed that the errors almost disappear for all the draconitic harmonics, with an average² reduction of 92%.

6 Impact on the Earth orientation parameters

Seitz et al (2012) found draconitic harmonics in the Y -pole rate of GPS minus VLBI (Very Long Baseline Interferometry) time series. High peaks in the power spectrum were present at 50 and 70 days corresponding to the 7th and 5th harmonics of the GPS draconitic year. In the power spectrum of the X -pole rate the 5th and 7th peaks were also present but with a much lower magnitude. In this study we compared the GNSS-derived EOP (Earth Orientation Parameters) with external sources

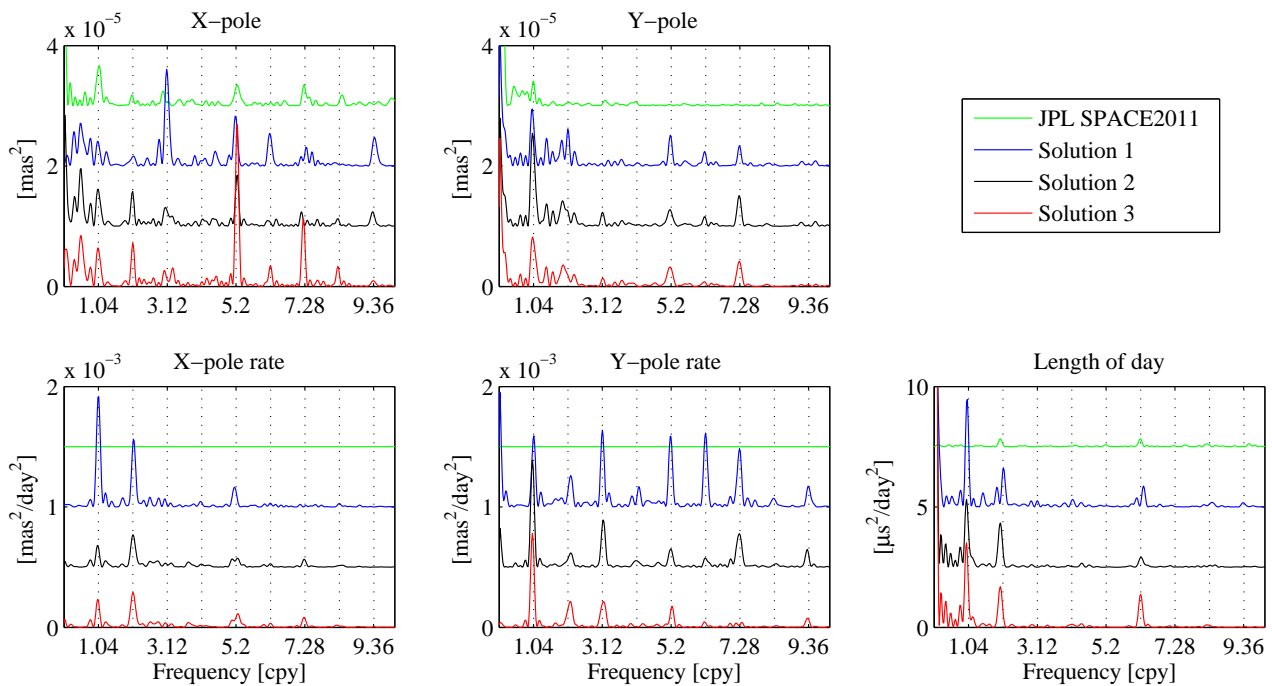


Fig. 6: Power spectrum of the Earth orientation parameters (minus IERS 08 C04 time series) for JPL SPACE2011 and the three solutions given in Table 1. The power spectra of JPL SPACE2011 and solutions 1 and 2 have been shifted along the vertical axes to make the details visible. The differences between JPL SPACE2011 and IERS 08 C04 are at the level of $10^{-7} \text{ mas}^2/\text{day}^2$ for the pole rates. The dotted vertical lines are at harmonics of 1.04 cycles per year. The power spectrum of UT1-UTC is not shown since in our GNSS solutions these values are fixed to IERS 08 C04 at the beginning of each day.

like the IERS 08 C04³ (International Earth Rotation and Reference Systems Service, Bizouard and Gambis, 2009) and the JPL SPACE2011⁴ (Jet Propulsion Laboratory, Ratcliff and Gross, 2013) time series, as the draconitic harmonics of the solutions alone were not clearly visible. When subtracting IERS 08 C04 or JPL SPACE2011 the draconitic harmonics become visible. However, the interpretation of the results is difficult as the IERS 08 C04 and JPL SPACE2011 time series contain GPS data which may also include draconitic errors. Moreover, the IGS Analysis Centers contributing to the EOP combinations use different solar radiation pressure models. A summary of the different models used within the IGS can be found in Froideval (2009).

Figure 6 shows the power spectra of the three solutions computed in this study (Table 1) minus the IERS 08 C04 time series. Additionally, the power spectrum of the JPL SPACE2011 minus IERS 08 C04 time series is displayed for comparison purposes. The power spectrum of the difference of these two external EOP time series sets a lower limit for the comparison of our solutions w.r.t. IERS 08 C04. Draconitic harmonics amplitudes

above this limit can be interpreted as significant (i.e. as an error in our solutions) while below or close to this limit the amplitudes can be interpreted as insignificant as they also exist between other EOP time series. Figure 6 shows that the draconitic errors in the X and Y pole as well as in the LOD (length of day) are generally close to this lower limit with some harmonics exceeding it. Table 4 shows a similar number of cases with improvements and degradations in the draconitic harmonics when comparing solutions 1 and 3 for the X and Y pole as well as for the LOD. We obtain an average² increase of the errors of 115% and 149% for the X-pole and LOD, while the errors in the Y-pole are reduced in average by 15%. The main contributor to the increase of the draconitic errors in the X-pole is the 5th harmonic while for the LOD it is the 6th harmonic. We do not have, at the moment, an explanation for the increase of the amplitudes of these particular harmonics. For the X and Y pole rates the draconitic harmonics are very significant, as shown in Fig. 6. Here the differences between JPL SPACE2011 and IERS 08 C04 are at the level of $10^{-7} \text{ mas}^2/\text{day}^2$, i.e., four orders of magnitude smaller than the differences between our solutions and IERS 08 C04. Table 4 shows that there are more cases

³<ftp://hpiers.obspm.fr/iers/eop/eopc04>

⁴<ftp://euler.jpl.nasa.gov/keof/combinations/2011>

Table 4: Numerical values of the Earth orientation parameters power spectra (w.r.t. IERS 08 C04, see Fig. 6) at significant harmonics of 1.04 cpy. The units are 10^{-5} mas² for pole values, 10^{-3} mas²/day² for pole rates and μ s²/day² for LOD. Green indicates a decrement w.r.t. the previous solution while red indicates an increment.

Component	# sol.	1.04	2.08	3.12	4.16	5.20	6.24	7.28	8.32	9.36
X-pole	1		0.16	1.55		0.81	0.51	0.20		0.44
X-pole	2		0.56	0.25		0.70	0.06	0.01		0.22
X-pole	3		0.71	0.11		2.25	0.34	0.80		0.09
X-pole rate	1	0.91	0.52			0.13		0.01		
X-pole rate	2	0.16	0.27			0.06		0.06		
X-pole rate	3	0.22	0.29			0.08		0.08		
Y-pole	1	0.72	0.60			0.48		0.32		
Y-pole	2	1.37	0.24			0.25		0.49		
Y-pole	3	0.76	0.18			0.30		0.41		
Y-pole rate	1	0.58	0.13	0.63	0.07	0.57	0.61	0.47	0.07	0.17
Y-pole rate	2	0.74	0.07	0.35	0.05	0.15	0.08	0.27	0.02	0.11
Y-pole rate	3	0.63	0.15	0.20	0.01	0.15	0.04	0.02	0.01	0.07
Length of day	1	3.04	1.52					0.11		
Length of day	2	1.55	0.77					0.40		
Length of day	3	1.64	0.73					1.35		

with improvements than degradations in the draconitic harmonics of the X and Y pole rates. With an average² reduction of the errors between solutions 1 and 3 of 24% and 50% for the X and Y pole rates.

We also computed the power spectra of the pole and pole-rates separately for prograde and retrograde motions (not shown) obtaining the highest differences to IERS 08 C04 at draconitic harmonics for the prograde motion rate. However, we decided to show here the pole and pole-rates for the X and Y components since the draconitic harmonics in the X -pole and Y -pole rate are much more dominant than in the Y -pole and X -pole rate, see Fig. 6 and Table 4. This asymmetry indicates that there is a relation with the distribution of GNSS ground stations over the Earth, as the X and Y components are given in an Earth-fixed system.

7 Impact on the station coordinates

The power spectra of GPS-derived station coordinates show spurious signals at harmonics of one GPS draconitic year as first noted by Ray et al (2008). At least until the 9th harmonic these spurious signals are visible as shown in the power spectra of our GNSS-derived station coordinates in Fig. 7. Rodriguez-Solano et al (2012a) obtained a reduction of 38% only in the 6th harmonic of the North component when introducing the Earth radiation pressure in the computation of GPS satellite orbits. In this study, the 6th harmonic of the North component is reduced (after subtracting a noise

floor of 0.00069 mm², see Table 5) by 32%⁵ when using the adjustable box-wing model for GPS and GLONASS satellites. Another 53%⁵ reduction (w.r.t. solution 2) is achieved with the upgraded version of the model based on non-nominal yaw attitude. In total, comparing solutions 1 and 3, a reduction of 68%⁵ is achieved for the 6th harmonic in the North component. However, in this study with the new radiation pressure and yaw attitude models not only this peak is reduced but we achieve a general reduction of the draconitic errors in the station coordinates as shown in Fig. 7. In fact, when comparing solutions 1 and 3 in Table 5, it can be observed that all the draconitic harmonics (except the 2nd harmonic in the North component) are reduced in the North, East and Height components. We obtain an average reduction over all the draconitic errors between solutions 1 and 3 of 41%⁵, 39%⁵ and 35%⁵ for the North, East and Height components after subtracting the approximate noise floors given in Table 5.

The impact of the new radiation pressure and yaw attitude models on the station coordinates can also be analyzed by looking at the time series of station coordinates. We did not look at the time series of individual ground tracking stations, but we computed the RMS of the differences of daily station coordinates (between one solution and the previous one) as a function of time as shown in Fig. 8. It can be noted that the adjustable box-wing model has a higher impact on the station coordinates (especially in the North and East

⁵This reduction may not be easily seen in Fig. 7 due to the logarithmic scale, but it can be computed from the numerical values given in Table 5.

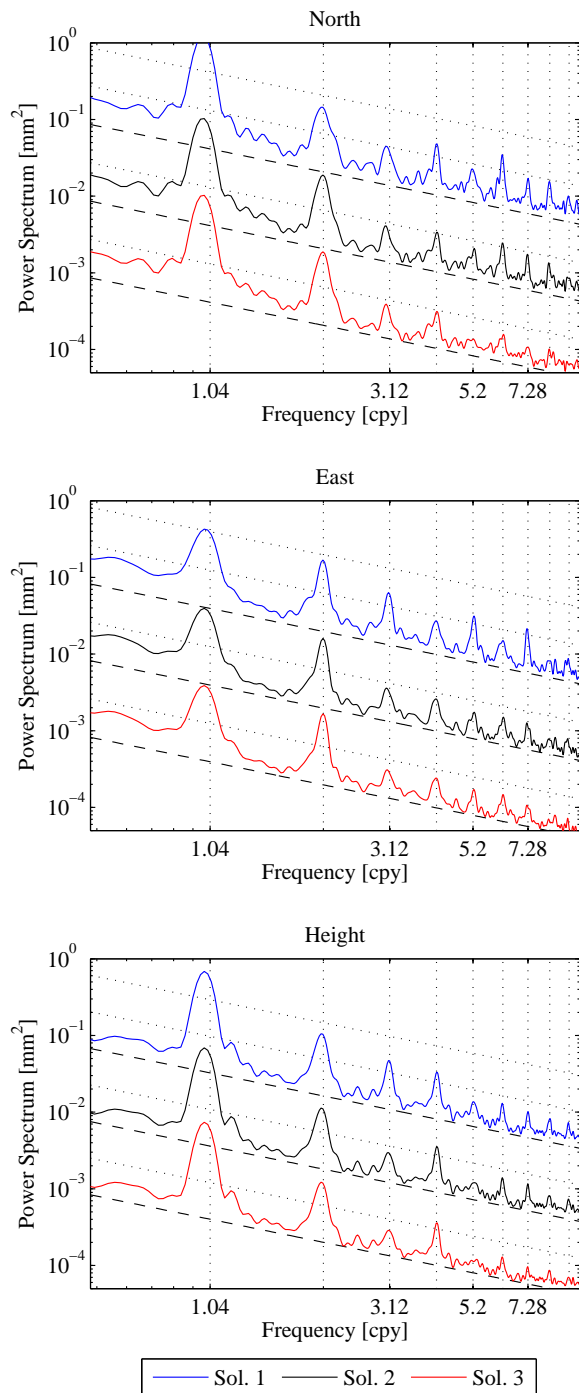


Fig. 7: Power spectrum of daily station coordinates (stacked from around 290 ground stations) for the three solutions given in Table 1 separately for the North, East and Height components. The power spectra of the solutions have been shifted along the vertical axes to make the details visible. The dotted vertical lines are at harmonics of 1.04 cycles per year. The sloped lines have a power law behavior of $1/f$ (i.e. flicker noise), the dashed lines represent approximate noise floors.

components) than its upgraded version for non-nominal yaw attitude. However, this last model causes a very systematic behavior, namely a nearly vanishing RMS difference when there are no GPS-II/IIA in eclipse seasons, see also Fig. 4. The RMS difference is not exactly zero since solution 3 includes the yaw bias for GPS-II/IIA satellites (Bar-Sever, 1996) which also acts outside of eclipse seasons, as well as specific yaw attitude models for eclipsing GPS-IIR and GLONASS-M satellites (Table 1). When GPS-II/IIA satellites are in eclipse season large differences appear in the station coordinates. Obviously one or few of the satellites with degraded orbits can have a negative impact on a global GNSS solution and consequently on the station coordinates.

8 Conclusions

Part of the draconitic errors found in GNSS geodetic products are definitely induced by orbit modeling deficiencies, in particular those related to the radiation pressure modeling. We have shown that by changing the radiation pressure models also the draconitic errors show important changes. By exchanging the CODE (5-parameter) radiation pressure model (Beutler et al, 1994) by our adjustable box-wing model (Rodriguez-Solano et al, 2012b) orbit related systematic errors with a β_0 (Sun elevation angle above the orbital plane) dependency are reduced outside eclipse seasons for GPS-IIA, GPS-IIR and GLONASS-M satellites as shown by Rodriguez-Solano et al (2013). However, the orbit errors during eclipse seasons are increased especially for GPS-IIA satellites if the yaw maneuvers of these satellites are not properly taken into account. In Rodriguez-Solano et al (2013) we upgraded the adjustable box-wing model to use non-nominal yaw attitude, i.e., to use the Bar-Sever (1996), Kouba (2009) and Dilssner et al (2011) yaw attitude models. With this an important improvement of the orbits (in particular for GPS-IIA satellites) was achieved during eclipse seasons. These improvements in the orbits, especially because related to the β_0 angle, were expected to reduce the draconitic errors observed in diverse GNSS geodetic products. In this study, we show that this is in fact the case. With the new radiation pressure models (Rodriguez-Solano et al, 2012b, 2013) we obtained a reduction of the draconitic errors in the orbits (overlap errors), in the geocenter Z -component, in the X and Y pole rates, and in the station coordinates. The draconitic errors for the X and Y pole as well as for the LOD are not that significant as for the pole rates and the results are not conclusive when using the new models. In Rodriguez-Solano et al (2013) we showed that there are still β_0 systematic errors present in the GPS and GLONASS orbits, even after using the new models. Therefore, a large potential to further reduce the draconitic errors in the GNSS geodetic products exists if the β_0 systematics in the orbits can be further

Table 5: Numerical values [mm²] of the station coordinates power spectra (see Fig. 7) at the harmonics of 1.04 cpy. Green indicates an improvement w.r.t. the previous solution while red indicates a degradation. Additionally, the value of the power law η/f (i.e. flicker noise) with $\eta = [0.0043, 0.0041, 0.0338]$ is included, representing approximate noise floors (dashed lines in Fig. 7) for the respective components.

Comp.	# sol.	1.04	2.08	3.12	4.16	5.20	6.24	7.28	8.32	9.36
North	1	0.08639	0.01413	0.00378	0.00479	0.00221	0.00328	0.00170	0.00152	0.00095
North	2	0.07365	0.01865	0.00296	0.00333	0.00187	0.00244	0.00166	0.00116	0.00085
North	3	0.07330	0.01858	0.00294	0.00309	0.00136	0.00152	0.00107	0.00097	0.00063
North	η/f	0.00413	0.00207	0.00138	0.00103	0.00083	0.00069	0.00059	0.00052	0.00046
East	1	0.03796	0.01655	0.00611	0.00269	0.00291	0.00150	0.00190	0.00082	0.00078
East	2	0.03300	0.01569	0.00310	0.00257	0.00163	0.00146	0.00112	0.00075	0.00063
East	3	0.03248	0.01636	0.00281	0.00240	0.00165	0.00146	0.00100	0.00065	0.00055
East	η/f	0.00394	0.00197	0.00131	0.00099	0.00079	0.00066	0.00056	0.00049	0.00044
Height	1	0.54979	0.10067	0.04660	0.03263	0.01362	0.01259	0.01012	0.00823	0.00674
Height	2	0.49564	0.09628	0.02588	0.03140	0.01073	0.01222	0.01033	0.00727	0.00639
Height	3	0.48429	0.09339	0.02298	0.02883	0.00920	0.01017	0.00765	0.00692	0.00561
Height	η/f	0.03250	0.01625	0.01083	0.00812	0.00650	0.00542	0.00464	0.00406	0.00361

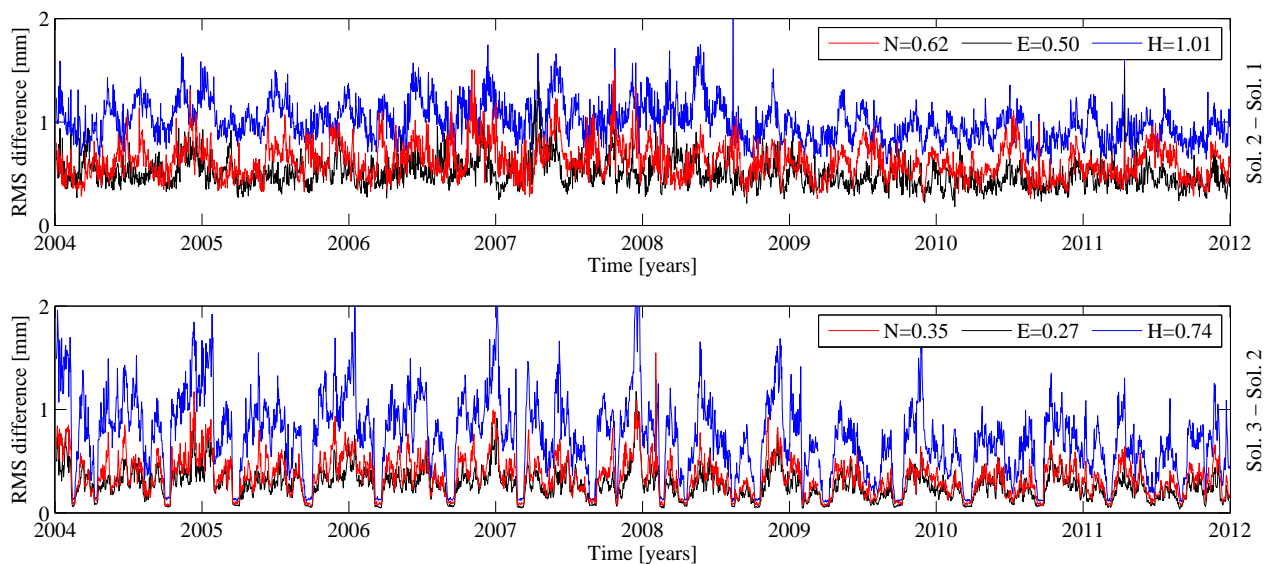


Fig. 8: RMS of differences of daily station coordinates (between one solution and the previous one) over all available stations. The mean RMS values [mm] for the 8 year period are given in the upper right corner of the plots for each component.

reduced. The draconitic errors observed in the geocenter Z -component tend to disappear with the new radiation pressure models and it can be concluded that the observed odd harmonics were introduced by the CODE 5-parameter model. However, we cannot conclude that only radiation pressure orbit modeling deficiencies contribute to the draconitic errors observed in the station coordinates, in the Earth rotation parameters or in the orbits themselves. Other error sources like multipath or mismodeling of sub-daily signals could be contribut-

ing to the observed draconitic errors. These other error sources cannot be ruled out by the results of this study.

Acknowledgements

This work has been funded by the DFG projects “LEO orbit modeling improvement and application for GNSS and DORIS LEO satellites” and “Geodätische und geodynamische Nutzung reprozessierter GPS-, GLONASS- und SLR-Daten”.

References

- Amiri-Simkooei AR (2007) Least-squares variance component estimation: theory and GPS applications. PhD thesis, Delf University of Technology, Publications on Geodesy 64, Netherlands Geodetic Commission, URL <http://www.ncg.knaw.nl/Publicaties/Geodesy/pdf/64AmiriSimkooei.pdf>
- Amiri-Simkooei AR (2013) On the nature of GPS draconitic year periodic pattern in multivariate position time series. *J Geophys Res* 118(5):2500–2511, DOI 10.1002/jgrb.50199
- Bar-Sever YE (1996) A new model for GPS yaw attitude. *J Geod* 70(11):714–723, DOI 10.1007/BF00867149
- Beutler G, Brockmann E, Gurtner W, Hugentobler U, Mervart L, Rothacher M, Verdun A (1994) Extended orbit modeling techniques at the CODE processing center of the International GPS Service for Geodynamics (IGS): theory and initial results. *Manuscr Geod* 19(6):367–386
- Bizouard C, Gambis D (2009) The Combined Solution C04 for Earth Orientation Parameters Consistent with International Reference Frame 2005. In: Drewes H (ed) *Geodetic Reference Frames*, IAG Symposia 134, Springer, pp 265–270, DOI 10.1007/978-3-642-00860-3_41
- Collilieux X, Altamini Z, Coulot D, Ray J, Sillard P (2007) Comparison of very long baseline interferometry, GPS, and satellite laser ranging height residuals from ITRF2005 using spectral and correlation methods. *J Geophys Res* 112(B12403), DOI 10.1029/2007JB004933
- Dach R, Hugentobler U, Fridez P, Meindl M (2007) Bernese GPS Software, Version 5.0. Astronomical Institute, University of Bern
- Dilssner F (2010) GPS IIF-1 Satellite Antenna Phase Center and Attitude Modeling. *Inside GNSS* 5(6):59–64, URL <http://www.insidegnss.com/node/2243>
- Dilssner F, Springer T, Gienger G, Dow J (2011) The GLONASS-M satellite yaw-attitude model. *Adv Space Res* 47(1):160–171, DOI 10.1016/j.asr.2010.09.007
- Fritsche M, Sosnica K, Rodriguez-Solano CJ, Steigenberger P, Wang K, Dietrich R, Dach R, Hugentobler U, Rothacher M (2013) Combined Reprocessing of GPS, GLONASS and SLR Observations. *J Geod*, submitted
- Froideval LO (2009) A Study of Solar Radiation Pressure Acting on GPS satellites. PhD thesis, The University of Texas at Austin, URL <http://repositories.lib.utexas.edu/handle/2152/6623>
- Griffiths J, Ray JR (2013) Sub-daily alias and draconitic errors in the IGS orbits. *GPS Solut* 17(3):413–422, DOI 10.1007/s10291-012-0289-1
- Hugentobler U, van der Marel H, Springer T (2006) Identification and mitigation of GNSS errors. In: Springer T, Gendt G, Dow JM (eds) *The International GNSS Service (IGS): "Perspectives and Visions for 2010 and beyond"*, IGS Workshop 2006
- King MA, Watson CS (2010) Long GPS coordinate time series: Multipath and geometry effects. *J Geophys Res* 115(B04403), DOI 10.1029/2009JB006543
- Kouba J (2009) A simplified yaw-attitude model for eclipsing GPS satellites. *GPS Solut* 13(1):1–12, DOI 10.1007/s10291-008-0092-1
- Meindl M (2011) Combined Analysis of Observations from Different Global Navigation Satellite Systems. PhD thesis, Astronomisches Institut der Universität Bern, Geodätisch-geophysikalische Arbeiten in der Schweiz, Vol. 83, URL <http://www.sgc.ethz.ch/sgc-volumes/sgk-83.pdf>
- Meindl M, Beutler G, Thaller D, Dach R, Jäggi A (2013) Geocenter coordinates estimated from GNSS data as viewed by perturbation theory. *Adv Space Res* 51(7):1047–1064, DOI 10.1016/j.asr.2012.10.026
- Ostini L (2012) Analysis and Quality Assessment of GNSS-Derived Parameter Time Series. PhD thesis, Astronomisches Institut der Universität Bern, URL http://www.bernese.unibe.ch/publist/2012/phd/diss_lo_4print.pdf
- Press W, Teukolsky S, Vetterling W, Flannery B (1992) *Numerical Recipes in Fortran 77: The Art of Scientific Computing*, 2nd edn. Cambridge University Press
- Ratcliff JT, Gross RS (2013) Combinations of Earth Orientation Measurements: SPACE2011, COMB2011 and POLE2011. JPL Publication 13-5, Jet Propulsion Laboratory, California Institute of Technology, URL <ftp://euler.jpl.nasa.gov/keof/combinations/2011/SpaceCombPole2011.pdf>
- Ray J, Altamini Z, Collilieux X, van Dam T (2008) Anomalous harmonics in the spectra of GPS position estimates. *GPS Solut* 12(1):55–64, DOI 10.1007/s10291-007-0067-7
- Rebischung P, Altamini Z, Springer T (2013) A collinearity diagnosis of the GNSS geocenter determination. *J Geod*, DOI 10.1007/s00190-013-0669-5
- Rodriguez-Solano CJ, Hugentobler U, Steigenberger P, Lutz S (2012a) Impact of Earth radiation pressure on GPS position estimates. *J Geod* 86(5):309–317, DOI 10.1007/s00190-011-0517-4
- Rodriguez-Solano CJ, Hugentobler U, Steigenberger P (2012b) Adjustable box-wing model for solar radiation pressure impacting GPS satellites. *Adv Space Res* 49(7):1113–1128, DOI 10.1016/j.asr.2012.01.016
- Rodriguez-Solano CJ, Hugentobler U, Steigenberger P, Allende-Alba G (2013) Improving the orbits of GPS block IIA satellites during eclipse seasons. *Adv Space Res* 52(8):1511–1529, DOI 10.1016/j.asr.2013.07.013
- Rothacher M, Beutler G, Herring TA, Weber R (1999)

- Estimation of nutation using the Global Positioning System. *J Geophys Res* 104(B3):4835–4859, DOI 10.1029/1998JB900078
- Santamaría-Gómez A, Bouin MN, Collilieux X, Wöppelmann G (2011) Correlated errors in GPS position time series: Implications for velocity estimates. *J Geophys Res* 116(B01405), DOI 10.1029/2010JB007701
- Seitz M, Angermann D, Bloßfeld M, Drewes H, Gerstl M (2012) The 2008 DGFI realization of the ITRS: DTRF2008. *J Geod* 86(12):1097–1123, DOI 10.1007/s00190-012-0567-2
- Tregoning P, Watson C (2009) Atmospheric effects and spurious signals in GPS analysis. *J Geophys Res* 114(B09403), DOI 10.1029/2009JB006344
- Tregoning P, Watson C (2011) Correction to “Atmospheric effects and spurious signals in GPS analysis”. *J Geophys Res* 116(B02412), DOI 10.1029/2010JB008157

Acknowledgements

First of all, I want to thank Urs Hugentobler for giving me the opportunity of pursuing the doctorate under his supervision. I also want to thank Oliver Montenbruck and Adrian Jäggi for being the reviewers of this dissertation. It is an honor that these three leading scientist are involved in this dissertation.

I thank the reviewers and editors in charge that contributed to the papers with their comments and suggestions, as well as the co-authors of the papers for the professional and constructive work.

I greatly appreciate the time Urs Hugentobler invested in our discussions related to issues of this dissertation or in more general discussions related to GNSS and satellite geodesy. I am very thankful for his guidance but also for giving me the freedom to follow my own research ideas. I also appreciate very much that he shared his deep knowledge of the Bernese GNSS Software with me. I also received a lot of help from Peter Steigenberger in many issues (implementation, usage and cluster computing) related to the Bernese GNSS Software. For this help and the time he invested, I am very thankful to Peter Steigenberger. The four years I spent at the Technische Universität München working closely with Urs Hugentobler and Peter Steigenberger were very productive and contributed very much to my professional development.

The last four years have been funded by two DFG (Deutsche Forschungsgemeinschaft) projects: “Geodätische und geodynamische Nutzung reprozessierter GPS-, GLONASS- und SLR-Daten” and “LEO orbit modeling improvement and application for GNSS and DORIS LEO satellites”. I thank the colleagues working in these two projects for the good collaboration during the last years.

I gratefully acknowledge the IGS (International GNSS Service) for providing the high quality GNSS tracking data needed for this dissertation, and especially the colleagues from the IGS analysis centers for the many valuable discussions.

Finalmente, le agradezco a mi esposa e hijo por su gran apoyo y paciencia, así como a mis padres y hermana por su permanente interés en mi educación. Mis logros, son sus logros.

Curriculum Vitae

Name: Carlos Javier Rodríguez Solano
 Geburtsdatum: 17. Mai 1983
 Nationalität: Costa Ricaner
 Familienstand: verheiratet, ein Kind

Ausbildung

10/2007 - 10/2009 Master Studiengang: Earth Oriented Space Science and Technology (ESPACE), Technische Universität München
 Master-Arbeit: "Impact of albedo modelling on GPS orbits"
 Abschluss: **Master of Science**, Note: 1,3

09/2001 - 03/2006 Bachelor Studiengang: Physikalische Ingenieurwissenschaften, Universidad Autónoma Metropolitana, Azcapotzalco, Mexiko Stadt
 Bachelor-Arbeit: "Propagación de ondas electromagnéticas en medios confinados y periódicos"
 Abschluss: **Physikingenieur**, Note: 9.82 (von 10)

01/1999 - 06/2001 Gymnasium "Dr. Alberto Zoebisch Sanchez", Pachuca, Hidalgo, Mexiko
 Note: 9.86 (von 10)

01/1998 - 12/1998 Gymnasium "John Dewey", San José, Costa Rica

08/1995 - 07/1997 Technisches Gymnasium No. 43 "Luis Enrique Erro", Mexiko Stadt

01/1995 - 07/1995 Grundschule "Fernando Brom Rojas", Mexiko Stadt

01/1990 - 12/1994 Grundschule "Conservatorio de Castella", Heredia, Costa Rica

Berufserfahrung

11/2009 - 02/2014 Wissenschaftlicher Mitarbeiter, Fachgebiet Satellitengeodäsie, Technische Universität München

09/2008 - 10/2008 Praktikum, Deutsches Geodätisches Forschungsinstitut, München

01/2007 - 09/2007 Physik Dozent, Instituto Tecnológico de Costa Rica, Cartago, Costa Rica

Auszeichnungen

- 11/2009 Auszeichnung für den besten Abschluss im ESPACE Jahrgang 2009, Technische Universität München
- 10/2007 - 09/2009 Alban Stipendium der Europäischen Union für den ESPACE Master Studiengang, Technische Universität München
- 05/2002 - 04/2005 Auszeichnungen für exzellente Ergebnisse in den Trimestern: 05/2002, 08/2002, 11/2002, 03/2003, 10/2003, 02/2004 und 04/2005, Universidad Autónoma Metropolitana, Azcapotzalco, Mexiko Stadt
- 06/2001 Auszeichnung für den besten Abschluss im Jahrgang 2001, Gymnasium "Dr. Alberto Zoebisch Sanchez", Pachuca, Hidalgo, Mexiko